AN EVALUATION OF THERMAL PLASMAS IN PYROMETALLURGY

PETER MALCOLM COWX

Doctor of Philosophy

THE UNIVERSITY OF ASTON IN BIRMINGHAM

SEPTEMBER 1988

The University of Aston in Birmingham

AN EVALUATION OF THERMAL PLASMAS IN PYROMETALLURGY

PETER MALCOLM COWX

Doctor of Philosophy

1988

The development of reliable, high powered plasma generators has resulted in many plasma processes being proposed as alternatives to existing pyrometallurgical technologies. Many plasma systems were shown to be technically and economically superior to existing technologies, but some of the plasma system advantages quoted in the literature were found to be impractical because of other system constraints. This work evaluates the advantages and disadvantages of plasma systems by reviewing thermal plasma characteristics, the generation of plasmas, the integration of plasmas with reactors and the plasma process economics.

To confirm the operating characteristics of the plasma system and their economics, a series of trials were conducted where chromite and steelplant baghouse dusts were smelted in the Tetronics' 2.0 MW transferred arc/open bath plasma reactor. Chromite smelting in the plasma furnace was technically superior to the conventional submerged arc furnace technology, but the economics were unfavourable because of the limited power available from the water-cooled plasma torch and the high electrical energy consumption. AOD dust smelting in the plasma furnace to recover Ni, Cr and Mo for recycling was shown to be technically and economically viable. Environmentally hazardous Electric Arc Furnace dusts were smelted to produce a non-toxic residue for disposal and to recover the contained zinc to an enriched zinc oxide product for recycling. The operation of the plasma furnace to produce zinc oxide is not economically viable compared to existing technologies, however it should be possible to condense the zinc vapour directly in a zinc splash condenser to increase the value of the product.

Because of the limited power available from plasma generators, plasma processes will be most suitable for treating high and medium value materials such as Au, Pt, Mo, Ni, Ti, V, Cr etc at small production rates and heating metals in tundishes and ladles where a "clean" energy source is required. The treatment of environmentally hazardous waste materials is a particularly interesting application because of the additional financial incentives brought about by the high disposal costs. Non-transferred arc plasma generators will be used for air and gas preheating in blast furnaces to reduce metallurgical coke consumptions.

Key words:
Thermal plasma, Transferred-arc plasma furnace, Ferrochrome smelting, Steelplant dust smelting.

ACKNOWLEDGEMENTS

The author gratefully acknowledges the help given by the following persons:

Mrs E Hodgman for typing and correcting much of this work without complaint.

The staff at Tetronics R&D for help in preparing the equipment, operating the furnace and for helpful discussions and suggestions, particularly Dr C.P. Heanley, Mr J.K. Williams, Mr D. Mills, Mr D. Beel, Mr G. Tanner, Mr D. Powell, Mr R. Dunlop, Mr W. Hannant, Mr E. Argent, Mr C. Jones, Mr O. Graham, Mr J. Farrow, Mr J. Lafford and Mr D. Page.

Dr S.M. Moser (Texasgulf Metals and Minerals), Mr J Wallein (Metallurg), Mr G. Hamakos (Hellenic Alloys) and Dr L. Gourtsoyannis (MIRTEC) for discussions on ferrochrome smelting.

Dr D. MacRae (Bethlehem Steel), Mr J. Hensler (Centre For Metal Production) and Dr J. Pargeter (IMS) for disussions on Electric Arc Furnace dust treatment.

Mr D. Freshcorn (Zinc Corporation of America) and Mr G. Walker (Commonwelth Smelting Limited) for discussions on zinc condensation.

Dr D. Engledow and Mr B. Roddis (British Steel Corporation) for discussions on Alloy Steel Dust Treatment.

Dr J.C. Billington and Dr S. Murphy (University of Aston in Birmingham) for their quidance, help and discussion throughout this work.

CONTENTS

TABLES

FIGURES

1.0 GENERAL INTRODUCTION

During the last twenty years, many thermal plasma systems have been proposed as alternatives to existing pyrometallurgical technologies for the smelting of ferroalloys, the melting of steels, the recovery of metals from by-products, etc. The interest in and development of thermal plasma technology was motivated by the availablity of high power, reliable plasma equipment and the potential technical advantages and cost savings that can be achieved by replacing conventional methods of generating thermal energy with plasma devices.

A review of the plasma process literature suggests that the technical advantages of plasma arc heating include:-

- high arc temperatures,
- high power densities,
- high enthalpy inputs,
- fast reaction rates,
- improved process control because the power input to the furnace is not constrained by the electrical resistivity of the materials being smelted or the combustion of fossil fuels,
- low thermal inertia,
- low exhaust gas volume,
- a range of feed material sizes can be smelted directly,
- a decreased environmental impact associated with the sealed furnace,
- low acoustic noise,
- independent control of furnace oxygen potential,
- increased metal recoveries,
- novel reaction chemistries resulting in reduced energy consumptions.

Potential cost savings arise because:-

- cheaper, fine raw materials can be utilized instead of lump ore or agglomerated fines,
- fine coal or coke breeze can sometimes be subsituted for expensive metallurgical coke as the reductant,
- the recovery of metals is often higher than conventional processes,
- high specific reactor throughputs reduce the reactor size and capital costs.

Many of the reviews are very optimistic in their claims for plasma systems because they do not consider the interfacing of the plasma generator with the reactor or furnace, the high cost of electrical energy compared to fossil fuel, the limited power available from individual plasma generators, the lower energy efficiency or the economics of plasma systems compared to other electrical and fossil fuel fired processes.

This work attempts to quantify the technical and economic advantages of thermal plasma systems by examining the properties of thermal plasmas, the various types of plasma generating devices, their interface with pyrometallurgical reactors and the commercial application of plasma systems. To obtain operating and economic data, tonnage quantities of chromite and steelplant dusts were smelted in the Tetronics Research and Development Company's (TRD) transferred arc plasma system and the results compared to existing processes.

Chromite smelting was examined as it had been suggested that the operating costs of the transferred arc plasma/open bath reactor may be up to 30% less than the conventional Submerged Arc Furnace (SAF) (1) because the plasma furnace can utilize readily available, cheap fine chromite concentrates or friable ores without the need for expensive agglomeration, coal or coke breeze can be used as the reductant rather than metallurgical coke, a greater range of slag compositions can be used and the feed rate and power input are independently controllable, improving furnace operation and chromium recovery to the ferroalloy. On the other hand, the unit energy consumption in the plasma furnace is likely to be greater than the SAF, unless the enthalpy and chemical energy of the exhaust gases are utilized for preheating and prereduction of the charge. The power inputs presently available from plasma furnaces are very much lower than SAF, restricting the size of the furnace and economies of scale.

Steelplant dust smelting was examined because there is a requirement for a low cost, on-site treatment process which would take the toxic dust direct from the steelplant baghouse, convert it into a non-hazardous residue for disposal and recover the contained metal values to defray the dust treatment costs.

Currently, the majority of steelplant dusts are dumped as landfill, but legislation is being introduced that will require steelplants to treat the dusts to render them non-toxic before disposal. In the USA, for example, the Environmental Protection Agency introduced legislation under the Resource Conservation and Recovery Act that classifies steelplant dusts as a hazardous waste because of the leachablity of the contained Pb, Cd, Cr, etc by ground water. This has resulted in steel companies having to pay £50-150/t for the dust to be dumped at a designated hazardous waste disposal site. In Germany, Japan and around the Chicago area in the USA, regional rotary kiln treatment facilities exist that can process the dust as a cheaper alternative to dumping, but this approach is impractical in other parts of the world because of the greater distances for transport and the lack of treatment facilities.

1.1 SCOPE OF WORK

The objective of this work was to review commercial plasma technologies and suggest the types of pyrometallurgical process where plasma technology can be most usefully employed. Chromite and steelplant dust smelting trials were conducted in the Tetronics' transferred arc/open bath reactor to provide data on the technical benefits of plasma reactors, their operating characteristics, the system design, reliablity, scale up criteria and operating and capital costs.

2.0 A LITERATURE SURVEY OF PLASMA SYSTEMS

To evaluate the technical and economic potential of plasma systems in pyrometallurgy, the properties of plasma arcs, methods of generating thermal plasmas and the interfacing of plasma generators with pyrometallurgical reactors are reviewed. In particular, reference is made to the most efficient way of operating the transferred arc/open slag bath reactor used in the experimental section of this work.

2.1 PROPERTIES OF PLASMA ARCS

2.1.1 Physical Properties of Plasma Arcs

Plasma can be defined as a gas of sufficient energy content that a significant fraction of the species present are ionized permitting the conduction of electrical energy. All gases are ionized at temperatures between 3000K and 30000K at atmospheric pressure to produce a mixture of electrons, positive ions and neutral species whose charges compensate each other to produce a quasi-neutral state. The degree of ionization is a function of temperature, pressure and ionization energy. Figure 1 (2) shows the increase in the number of gram moles/m^3 of Ar ions and electrons with increasing temperature at atmospheric pressure. Most thermal plasmas are created by electrons emitted from the cathode accelerating and colliding with atoms and molecules entrained in the arc.

Figure 2 (3) shows the computed temperature profile within the plasma arc. Temperatures can approach 15000K at the centre of the arc at the cathode spot and fall to about 4000K at the radial extremities of the arc. Because the plasma arc is very directional and stable, a hot spot will occur at the arc/melt interface unless the melt is stirred or the arc is moved.

The influence of temperature on the plasma gas electrical conductivity is seen in Figure 3 (4). Plasma gases start to become conductive at temperatures above 6000K, with the conductivity increases rapidly with temperature to a limiting value of about 10000 mhos/m at 20000K. Argon is often chosen as the plasma gas because it is conductive at low temperatures, facilitating arc ignition.

Figure 4 (2) shows the non-linear variation in plasma gas enthalpy with temperature. Polyatomic gases generally show larger enthalpies than monatomic gases because of the additional heat of dissociation. At a given temperature, hydrogen gives the highest enthalpy because of its high heat of dissociation and ionization, and should be used to increase the energy transfer efficiency from the arc to the melt. The high gas temperatures and enthalpies make thermal plasmas well suited to processes needing high temperatures and enthalpy transfer (melting, smelting and vaporisation).

Figure 5 (4) shows that the viscosity of common plasma gases increases with temperature up to 10000K and is approximately 10 times the value at room temperature. Because of the high plasma viscosities, gas diffusion and the introduction of particles into plasma stream is difficult unless a plasma torch specifically designed for injection is used.

2.1.2 Energy Transfer from the Plasma Arc.

Figure 6 shows the electrical potential (and energy distribution) in a thermal plasma arc at atmospheric pressure as a function of arc length. The factors affecting arc voltage and arc energy are reviewed to determine the most energy efficient operating conditions. The arc can be divided into three regions:- the cathode region, the arc column and the anode region or melt. The potential changes rapidly at the electrodes (the cathode and anode fall zones), but there is only a relatively small potential gradient in the arc column itself.

The Cathode Region

The cathode region may be considered as a thin electrical boundary layer overlying the electrode and separating it from the arc column. Electron emission at the cathode may be by thermionic emission or field emission. Thermionic emission occurs if the cathode (C, W, Ta or Rh) is heated to 3500-4000K. The voltage drop at the cathode depends upon the work function of the cathode material, but is typically 30-40V, accounting for 5 -10% of the energy dissipated in the plasma arc. Field emission of electrons occurs by arcs attaching to a cold cathode (typically copper) as single or multiple, rapidly moving, extremely small spots with very high current densities.

The Arc Column

The arc column is a high-temperature ionized gas stream generated predominantly by Joule heating. The voltage gradient along the arc column is typically 0.3-1kV/m and depends upon the plasma gas electrical conductivity, temperature, ionization potential, flowrate and whether extraneous gas or particulates enter the arc. Energy is mainly dissipated from the arc column by radiation and convection.

The Anode Region

The anode fall region is considered in detail because it provides the electrical connection between the high temperature arc and the low temperature anode or melt where the majority of the arc energy is liberated. Fauchais (5), Pfender (6) and Maske (1) have shown that the energy transfer from arcs at the anode surface is influenced by the mode of attachment of the arc to the anode. The arc may either be cathode dominated (diffusely attached and bell shaped) or anode dominated (severely constricted) as illustrated in Figure 7. Cathode dominated arcs are favoured by short arc lengths, high currents and easily ionized anode materials which enable the hot core of the plasma to reach the anode, eliminating the need for thermal ionization in the anode fall zone. Cathode dominated arcs are characterized by a well distributed heat flux, where 70-80% of the arc energy is transferred directly to the anode by convection, ion condensation and arc radiation. Anode dominated arcs seem to form with longer arc lengths, lower intensity arcs and where chemical reactions or surface evaporation are occurring at the anode surface. Independent, rapidly moving cathode and anode jets are formed which impinge with a turbulent, bulk expansion of the plasma column, a drastic increase in the the heat flux density at the anode and a reduction in the energy transfer efficiency because the macroscopic flow of gas is directed away from the anode. Current densities and heat fluxes at the anode range from 1-1000 MA/m^2 and 100-1000 MW/m^2 respectively, depending on the arc attachment mode.

Heat transfer models based on cathode dominated arcs suggest that the net heat flux at the anode, Qi may be expressed by (7):

$$Qi = Qcon + Qrad + Qa + Qe - Qrerad - Qrecon \qquad \text{eqn 1}$$

Qcon is the energy flux from convection and conduction from the plasma arc gases across the anode surface. The conductive and convective contribution is proportional to the mass of gas, the specific heat and the temperature difference between the bulk gas and the melt.

Qrad is the energy flux by radiation from the arc which can be established from the Stefan-Boltzmann equation.

Qa is the energy flux associated with the exothermic reassociation of the ionized particles and electrons in the plasma arc at the anode surface and is given by equation 2.

$$Qa = J(Va + W) \qquad \text{eqn 2}$$

where
Va = Anode fall voltage
W = Work function of melt
J = Current density at the arc melt interface.

Finkelburg (8) measured the anode fall voltage for high and low intensity arcs and demonstrated that the anode fall voltage increased as the current density at the anode increased. Polyatomic gases, with high ionization energies and high enthalpies at a given temperature, produce a higher anode fall voltage than monatomic gases. Slag melts have a higher work function than metallic melts, increasing the energy transfer to the melt.

Qe is the energy flux associated with transport of thermal energy by electrons (Thompson effect). Qe is proportional to the current density and electron temperature as given by equation 3.

$$Qe = 5Jk(aT_1-T_2)/2e \qquad \text{eqn 3}$$

where J = current density
e = electron charge
k = Stefan-Boltzmann constant
T_1 = Electron temperature
T_2 = Anode temperature
a = Ratio of electron to plasma temperature.

Under steady state conditions, the anode energy gain must be balanced by losses which consist of;

Qrecon, convection to the surrounding gas.

Qrerad, radiation from the hot anode spot to the reactor surroundings.

The major mechanisms of heat transfer to the anode are convection from the hot plasma gas, reassociation of ionized species and radiation from the arc. The relative proportions of the different heat transfer components are difficult to estimate because of the difficulty in measuring the arc temperature, arc emissivity, and whether the arc can be regarded as being optically thin (viz, no radiation is re-absorbed by the arc column). Stewart (9) measured the dissipation of energy from an arc generated between a water-cooled transferred arc plasma torch and a water-cooled calorimeter and concluded that up to 80% of the arc energy is liberated at the anode by convection and electron condensation. Bowman (10) and Stenkvist (11) determined mass, momentum and energy balances for DC graphite arcs which suggested that about 72% of the energy was transferred directly to the melt, predominantly by convection. Blackburn (12) found similar results for a free burning 10kA DC arc water-cooled plasma torch. Szekely et al (3, 13) developed an energy distribution model for DC transferred arcs based on magnetofluid dynamics, which showed that the dominant energy transfer mechanism at the anode is convection and reassociation of ionized species, with radiation being a minor component. Figure 8 shows a typical energy distribution from a DC arc.

All the studies suggest that the major energy transfer mechanism is convection and percentage of energy transferred to the melt or workpiece can be increased by:

- using the electrode in the negative polarity mode
- designing the electrode geometry to produce a well directed cathode dominated arc
- increasing the arc current
- decreasing the arc length to encourage a cathode dominated arc and decrease radiation losses
- using polyatomic gases rather than monatomic argon.

Unfortunately, the transfer of energy by convection to the molten bath is not particularly good, except in the region of high gas velocity close to the arc/melt interface. Two processes have been developed to increase the convective energy transfer from the plasma arc at the arc/melt interface: In the first a hollow, vertical DC graphite electrode is centrally located in a circular furnace and raw materials are fed down the electrode directly into the arc region to promote heat transfer and rapid reactions. In the second process, a water-cooled transferred arc torch is precessed so that the arc root describes a circle on the melt to more evenly distribute the energy.

The dissipation of radiation energy from a typical 0.3-0.5m long arc column is relatively small and does not cause excessive wear on the refractories. However, radiation from the hot melt or anode region to the furnace roof will cause some refractory wear unless the anode/melt is cooled by feeding materials into the hot zone or a dense opaque furnace atmosphere is generated.

2.1.3 Momentum Transfer from the Plasma Arc

A plasma column is subjected to a large negative pressure just below the cathode due to magnetohydrodynamic forces, expansion and cooling (approximating to a Joule-Thompson expansion), producing a low pressure region at the cathode/nozzle exit which entrains ions, gases and fine particles from the surroundings which can alter the plasma arc characteristics. Because of the high plasma arc momentum and velocity, a depression is produced at the arc/melt interface which has the effect of locally increasing the energy transfer to the melt and stirring the melt.

2.1.4 Bath Circulation and Temperature Profiles in the Transferred Arc Plasma/open Slag Bath Reactor.

Figure 9 (13) shows the circulation pattern in a melt heated by a transferred arc plasma torch. Circulation currents are produced by thermal gradients in the melt, the plasma arc momentum at the bath surface, electromagnetic forces induced in the bath by the passage of an electric current (Lorentz forces) and gas bubble driven circulation. Convection and gas driven circulation are the predominant mechanisms, overcoming the electromagnetically driven counterflow.

Figure 10 (13) shows the calculated temperature profiles in an arc furnace melt. A large temperature gradient exists close to the melt surface in the vicinity of the arc impingement zone, but rapidly falls away to an average bulk temperature aided by the strong convection currents. The presence of slag on the metal will reduce the melt circulation and increase thermal gradients. The arc can be mechanically moved over the melt surface or the melt can be gas stirred to reduce local overheating.

2.2 THERMAL PLASMA GENERATORS

The thermal plasmas described in this work are most commonly generated by passing an electric current between two or more electrodes in a gaseous atmosphere at high temperatures and atmospheric pressure, where the particle density and interparticle collisions are sufficiently numerous to produce a thermal equilibrium between electron and ion temperatures.

Several reviews of plasma technology (13-17) have been published describing the various commercial thermal plasma generators that have been developed. The shape, configuration and mode of operation of the generators are very varied, but can be broadly categorized into water-cooled non-transferred arc plasma torches, water-cooled transferred arc plasma torches and gas stabilized carbon electrodes.

2.2.1 Plasma Generator Design

Water-Cooled Non-Transferred Arc Plasma Torches

The non-transferred arc torch was developed by NASA in the 1960's as a means of heating gases for space re-entry vehicle studies, but is now used to heat gases which are then directed into the reaction zone of a shaft furnace or reactor for materials processing. The plasma arc is established between two or more water-cooled electrodes or segments within the torch and large volumes of gas are passed through the arc at high velocities.

Figure 11 illustrates some of the generator designs employed to enable these devices to operate at relatively high voltages (1.0-7.0kV) and moderate currents (1.0-3.0kA). Copper or copper alloys are used for the electrodes. Tangential injection of the gas or magnetic coils at one or both electrodes may be used to rotate the arc root to maximize energy transfer to the gas and protect the generator walls and electrodes from local overheating and erosion. AC and DC devices are used, although electrode wear and arc stablility are improved using a DC arc. Gases can be heated to temperatures in excess of 10000K, much hotter than conventional combustion techniques which are limited to about 3000K.

Water-cooled Transferred Arc Plasma Torches

The transferred-arc torch is an extension of TIG welding equipment developed in the 1950's. The plasma arc is established between a water-cooled electrode and the melt and the majority of the plasma arc energy is transferred directly to the melt at the arc-melt interface. Figure 12 illustrates some of the transferred arc torch designs available for operation up to 4.0 MW (0.1-0.7kV and 0.5-9.0kA). High power torches usually employ a water-cooled thoriated tungsten electrode surrounded by a water-cooled copper jacket to direct the plasma stabilising gas around the electrode and protect it from melt splashes. Alternative electrode materials include copper, tantalum and zirconium for use with oxidizing plasma gases. The diameter of the electrode depends on the current, electrode polarity and the materials of construction. AC and DC devices have been developed. AC devices have the advantage of not requiring a return electrode, but the power generated by each device is limited because of the higher heat load on the AC electrode, and a more complex and expensive power source is required to avoid arc extinction at the zero current point. DC devices can be used in the negative or positive polarity mode, but they are more efficient in the negative polarity mode because the majority of the energy is liberated at the arc-anode interface.

Carbon Electrodes

A plasma can be generated by establishing an arc between graphite electrodes or between the electrode and the melt. The plasma arc can be stablized by passing a suitable gas down a hole in the carbon electrode. Recent advances in the development of high power thyristor rectification has led to the installation of several DC carbon arc furnaces for steel scrap melting which use a single central hollow electrode and a return electrical connection in the furnace hearth. Advantages of the DC system over the conventional AC carbon arc furnace include improved energy transfer to the melt, reduced consumption of graphite electrodes, reduced electrical utility disturbance, less acoustic noise, higher operating currents for a given electrode diameter and less refractory wear. The requisite bottom electrode connection is a potential problem area requiring careful design to prevent melt outs.

2.2.2 Plasma Generator Power Rating

The power generated by a plasma device is dependent upon its operating current and voltage as illustrated in Figure 13 (18).

Water-cooled non-transferred arc devices can generate up to 5-6 MW of power at low currents (2kA) and high voltages (2-7kV), the maximum power output being constrained by the current limitation of about 2kA to avoid excessive electrode wear. Long arc lengths, multi-segment generators and high gas volumes are used to increase the plasma arc voltage and therefore the power. Multiple torches can be used in a reactor to increase the power input.

Water-cooled transferred arc devices can deliver up to 4-5 MW by operating at high currents (10kA), but relatively low voltages (500V). The arc current is ultimately limited by high electrode wear rates above 10kA, but improvements in the quality of electrode tungsten, the cathode design and the cathode cooling may allow increases in arc current. There is little scope for increasing the power by increasing the arc voltage because the voltage is independent of the plasma torch parameters, being controlled by the material being processed, the plasma gas and the arc length. Multiple torches may be used to increase the reactor power.

The maximum amperage that can be delivered by a graphite electrode is determined by the resistive heating in the electrode column which, in turn, depends upon the electrode diameter and the grade of graphite used. The power input from a DC electrode furnace is limited by the return electrode in the furnace hearth. Higher currents can be passed through a DC electrode of the same graphite quality and diameter as an AC electrode because the current is uniformly distributed over the electrode cross section rather than displaced to the outside of the electrode. Because the energy from the DC arc is liberated in a confined area in the centre of the furnace, incomplete melting of the scrap around the furnace sidewalls may result if the furnace diameter and power input are not carefully matched.

2.2.3 Plasma Generator Energy Efficiency

In the non-transferred arc torch, 15-30% of the electrical energy input to the torch appears in the electrode cooling water. Cooling losses in the transferred arc torch are 3-10% of the energy input because of the smaller torch size and the absence of anode cooling losses. Energy losses from graphite electrodes are small and associated with clamp and cable cooling.

Electrical system losses from DC systems are about 5% of the energy input and associated with the transformer and rectifier. Reactive wattless power factor correction can be fitted on a DC power source. AC system losses are also about 5% of the energy input and are associated with transformer and conductor losses.

The energy efficiency of the total plasma system will depend on the plasma generator and reactor design. Total energy losses of 10-25% are typical of transferred arc plasmas reactors where the radiation losses from the free burning arc and melt are high. Losses from shaft furnaces equipped with non-transferred arc generators are 15-30% of the energy input because of the extensive shaft cooling and the large plasma gas volumes that leave the reactor at close to the reaction temperature.

2.2.4 Plasma Generator Electrode Consumption and Reliability

Electrode wear rates are largely a function of current as shown in Figure 14 (18). For a given power output, the lowest rates of electrode erosion are associated with non-transferred arc devices which operate at high voltages and low currents, rather than transferred arc devices which operate at high currents and low voltages. However, the cost of replacing the simple transferred arc torch electrode tip will be less than the more complicated non-transferred arc torch electrodes. All water-cooled plasma torches are prone to premature catastrophic failure due to electrical insulation breakdown, localized arcing or burn through to the water passages. Graphite electrode wear depends on the current, electrode polarity, graphite quality, furnace environment and the electrode breakage rate. Graphite consumption for DC electrodes is slightly less than AC electrodes because of the reduction in surface oxidation and tip losses associated with the use of a single electrode rather than three electrodes.

2.2.5 Plasma Generator Gas Requirements

Water-cooled, non transferred arc devices are generally designed as gas heaters and require large gas flows of about $300m^3/MWh$ for efficient energy transfer, whereas transferred arc torches only require approximately $3m^3/MWh$ of argon. AC or DC graphite electrodes work satisfactorily without gas injection although, some benefits from arc stabilization and lower noise levels may be achieved by using gas injection.

2.2.6 Return Electrode Configurations

DC water-cooled and graphite transferred arc systems require a return electrode connection. This may be a second water-cooled or carbon electrode, an electrode built into the furnace refractories or a conductive refractory lining (19,20). Steel melting furnaces built by ASEA use conducting magnesia-carbon hearth refractories in contact with a copper plate in the furnace base which is connected to the return electrical cables. Furnaces built by Mannesman use steel pins built into the hearth ramming mass which are externally air-cooled.

2.3 INTERFACING OF THERMAL PLASMA GENERATORS WITH PYROMETALLURGICAL REACTORS

Plasma reactors can be broadly subdivided into non-transferred arc, transferred arc and carbon electrode reactors.

2.3.1 Interfacing of Non-Transferred Arc Plasma Generators with Reactors

Non-transferred arc plasma devices are generally used to superheat gas for injection into shaft furnaces. The advantages of the system include the replacement of metallurgical coke with electrical energy and injected coal fines, fine feed material can be utilized without agglomeration and higher reaction temperatures can be achieved. Several of the plasma heated shaft furnaces applications are described below.

Blast Furnace Air Superheating

Eight, 1.8 MW Aerospatiale arc heaters are fitted to the tuyeres of the Société du Ferro Manganese de Paris Outreau (SFPO) ferromanganese blast furnace to superheat the air blast from 1500K to 2000K (21). A reduction of 6% in metallurgical coke consumption and an improved manganese yield and furnace productivity are claimed. The process is only economically viable if low cost electrical energy is available, thus the SFPO plasma torches are only operated during the summer months when very cheap electrical energy is available.

Coal injection into blast furnaces is a common means of replacing the expensive metallurgical coke, but injection rates are limited to about 0.15 t of coal/t of hot metal because coal cools the furnace raceway. Coal injection rates of up to 0.3t coal/thm are predicted using oxygen injection or blast superheating. Cockerill, in conjuction with IRSID, have mounted six, 3.5 MW plasma arc heaters on the tuyeres of the Sambre iron blast furnace to superheat the blast air to 1800K (22) to permit high levels of coal injection. Six 1.9MW Aerospatiale torches have been installed on a blast furnace at Uckange with a target injection rate of 0.2 t coal/thm and cost savings of £1.8/thm.

Westinghouse have installed a plasma arc heater on a 0.6m diameter hot blast cupola melting cast iron borings (23). The operating costs are claimed to be £11/t of iron less than a conventional cupola because of the reduced coke consumption, readily available cheap cast iron borings can be melted without briquetting, metal temperature and composition control are improved, alloy losses and sulphur pickup are minimized and cupola productivity is increased by up to 50%. However, when the increased capital investment for the plasma equipment is included in the appraisal, the pig iron production costs are similar for the conventional and plasma cupolas.

It is suggested that the plasma heating of blast furnace air will be uneconomic, except in countries such as France, Sweden and Canada where electrical energy is cheap. In most of Europe and Japan, the economic performance of an oxygen/coal blast furnace injection system will be superior to the plasma/coal system.

The SKF Plasmadust Process for treating Steelplant Waste Dusts

In 1983, SKF (24) built the 24 MW "Scandust" plant shown in Figure 15 to process 70kt/annum of steelplant baghouse filter dusts. The oxidic dusts containing Cr, Ni, Mo, Zn and Pb oxides are blended with pulverized coal and fluxes and pneumatically injected into the raceway generated in the base of the coke filled shaft furnace by four 6MW plasma generators. The metal oxides are reduced to a ferroalloy containing Fe, Cr, Ni and Mo which is intermittently tapped from the furnace. Zinc and lead are vaporized and condensed from the exhaust gases in a lead venturi scrubber. The exhaust gases leaving the condenser are cleaned and burnt to supply hot water for district heating. The SKF Plasmadust process is claimed to be cheaper to operate than conventional smelting technologies because it can accept fine feed material directly and expensive metallurgical coke is partially replaced with electrical energy supplemented with fossil fuels. The capital investment for the plant was £27 million in 1985. The electrical energy intensive Plasmadust process is an expensive EAF dust treatment route, but in Sweden and countries where electrical energy is cheap compared to coke and where the excess hot water and gas generated by the plant can be sold for district heating, the economics of the Plasmadust system may compare favourably with existing technologies.

Gas synthesis

Chemishe Werke Hüls AG (25) developed an 8.5 MW DC plasma torch for the synthesis of acetylene. Saturated hydrocarbon and hydrogen gases are injected tangentially into a high temperature rotating arc column generated between two annular water-cooled steel electrodes and acetylene is recovered from the quenched products. Very high voltages (7kV) are achieved as a result of the very long vortex stabilised arcs obtained at high gas velocities. Hüls torches are to be used in a South African DRI plant for reforming synthesis gas produced by the gasification of bituminous coal

2.3.2. Interfacing of Water-cooled Transferred Arc Plasma Torches with Reactors

Transferred arc torches are usually interfaced with open bath reactors where the plasma arc energy is transferred directly from the electrode to the slag or metal bath.

Steel melting

One of the first DC water-cooled, transferred arc plasma torches was developed in 1962 by the Linde Company (26) for steel scrap melting, but they abandoned the concept after concluding that it was uneconomic compared to the EAF.

VEB Edelstahlwerke in Freital, East Germany developed a 4.0 MW DC, water-cooled, transferred arc torch for steel scrap melting applications and a 15 and 35 tonne multi-torch furnace are currently in operation. The Freital torch was developed further by Voest-Alpine in Austria, and a 45t, 5.8m diameter furnace was equipped with four 4.0 MW torches introduced laterally into the side of the furnace, as shown in Figure 16 (27). The scrap melt down rate was satisfactory when operating with high voltage, long arcs buried in the scrap, but at flat bath when the arc length was reduced to prevent refractory damage, the arc voltage and power input decreased, limiting the rate of steel temperature rise relative to a conventional EAF.

The production costs for the 45t Voest-Alpine plasma furnace and a similar size conventional arc furnace making low carbon, low alloy steels were compared and found to be about the same, but the individual cost make up was different. Torch maintenance costs were £2.5/t of steel compared to £3/t for graphite electrode consumption in the EAF, bottom electrode costs were about £2/t of steel more than the EAF, energy consumption was 615kWh/t compared to 580kWh/t for the EAF, refractory consumption was higher than the EAF, with hearth, wall and roof lives of about 308, 145 and 100 heats respectively, but metal yields were around 2% higher than the EAF. The Voest-Alpine plasma furnace ceased operation in 1987 because it was not economic compared to modern, large EAFs.

Krupp of West Germany developed a three phase AC plasma system using three 1.6MW plasma torches mounted vertically in the roof of the furnace to avoid the use of a vulnerable bottom electrode (28). A saving of 1.5 kg of graphite per tonne of steel compared to the conventional AC furnace operation is claimed. The energy losses associated with cooling three AC torches reduces the thermal efficiency of the system and the complex power source increases the capital cost of the system.

The advantages of water-cooled transferred arc plasma furnace for steel melting include increased steel and alloy yield associated with the sealed furnace construction and the argon atmosphere, steel quality is comparable with vacuum refined steels and there is no carbon contamination from the electrodes. Noise is suppressed below 60 dBA and the stable plasma arc eliminates the discontinuous shock loading and flicker on the power transmission mains. The disadvantages of the plasma furnace include the limited power available from the torches, the short electrode lives at high arc amperages, increased hearth maintenance with the DC system, increased costs associated with argon consumption and a more complex power source.

The use of plasma furnaces for carbon steel melting does not appear to be economically viable compared to the current 50-100MW UHP AC furnaces with energy consumptions of 350-450 kWh/t of steel using scrap preheating, foaming slags, oxygen/fuel injection and ladle steelmaking. Plasma melting of high alloy steels may be cost effective where savings of £10-15/t may be realised through improved alloy yields and product quality. However, if conventional arc furnaces were sealed and operated under an inert argon atmosphere there is no reason why the same improvements in yield and quality should not be realized.

Steel refining

Daido Steel in Japan (29) developed a Plasma-Induction-Furnace rated at 0.45 MW (2kA, 250 V) as an alternative to Vacuum Arc Remelting (VAR) and Vacuum Induction Melting (VIM). An induction coil is used to input energy and improve stirring, whilst the top heat from the plasma torch enables high basicity (high liquidus temperature) slags to be used for enhanced desulphurisation.

Steel heating in a ladle or tundish.

Nippon Steel Corporation installed a 2.0MW Tetronics' torch in a continuous caster tundish to maintain a constant casting temperature (30). The general arrangement of the tundish is shown in Figure 17. The advantages of plasma tundish heating are more controlled casting temperatures, improved steel cleanness and microstructure, avoidance of strand freeze offs, lower primary steelmaking vessel tapping temperatures and a reduction in steelmaking energy and refractory consumptions. The currently available transferred arc plasma torches are about the correct power for the majority of tundish applications, whereas they are rather too small for ladle heating applications. Plasma heating of tundishes is superior to induction heating because there is less stirring, energy can be put into the tundish immediately there is steel in the tundish and no major modifications to the tundish are required.

The recovery of Platinum Group Metals from Catalysts

Tetronics in conjunction with Texasgulf, developed a 2.0 MW DC plasma furnace for smelting automobile catalyst to recover platinum group metals (31). The catalyst is blended with lime to flux the alumina substrate and the feed blend is smelted at 1800K. An Fe-Pt alloy collects in the furnace hearth and is intermittently tapped. Figure 19 shows the general arrangement of the furnace. A platinum recovery of 95-98% is obtained from the plasma furnace compared to 80-85% from a conventional electric arc furnace or wet chemical processes.

2.3.3 Interfacing of Carbon Electrodes with Reactors.

In many applications, there is no need for the sophistication of a water-cooled electrode using expensive plasma gas and a simple graphite electrode can be substituted.

Steel Melting using DC Graphite Electrodes

In 1983, ASEA-Krupp in Avesta, Sweden (32), converted an 18 MVA conventional three phase AC arc furnace to a single electrode DC arc furnace to compare the AC and DC furnace operation. The bottom electrode was a copper plate next to the steel shell with steel pins passing up through the magnesia-carbon hearth refractories to contact the melt. The average bottom life was 83 heats. Electrode graphite consumption was 2.1kg/t of steel, which represented a saving of 2-3 kgs/t compared to the AC operation. The electrode graphite savings were offset by the slightly increased heat times, increased bottom maintenance and the adoption of a three basket charge which reduced operating efficiency. The energy consumption was not reported, but cost savings were less than £3/t of steel.

In 1985, Nucor in Darlington, S.Carolina (33), converted an existing AC furnace to a 28 tonne, 12MVA, DC arc furnace using a single 40cm diameter, 37kA electrode. The return electrode consists of steel pins passing through the rammed hearth refractory and attached to an air-cooled steel plate. Nucor estimate that the bottom electrode cost is about £1/tonne steel more than the conventional bottom, but the graphite electrode savings are about £3/tonne steel. The energy consumption for the DC furnace is 509kWh/tonne steel compared to 527kWh/tonne for the AC operation.

In 1986, Asea-Krupp installed a 16MVA DC furnace at Florida Steel's Tampa plant (33). The furnace uses magnesia-carbon hearth bricks in contact with a copper plate as the return electrode. Preliminary results suggest that electrode savings exceed the increased cost of bottom maintenance.

The largest DC furnace in operation is a 3 electrode, 75 tonne, 45MW furnace operated by Société Metallurgie D'Escault at Trith St. Leger in France (33). Each electrode is equipped with its own thyristor rectifier and transformer, supplying 40 kA to a 0.4m diameter electrode. Initial operating results include an electrode graphite consumption of 2.1kgs/tonne, an energy consumption of 500kWh/t of steel and reduced sidewall refractory costs.

The advantages of the single-electrode DC arc furnace include lower electrode graphite consumption than the comparable three-electrode AC furnace, a slight reduction in energy and refractory consumption, better temperature distribution due to the centrally located electrode and reduced power supply distortion. The single electrode design simplifies the furnace design because there are fewer electrode arms and fewer holes in the roof, reducing fugative emissions. The disadvantages of the DC furnace are the increased bottom maintenance and the inablity to scale up beyond about 50MW, limited by the integrity of the bottom electrode connection and the diameter of the electrode. It is unlikely that DC furnaces will bring major cost savings compared to modern UHP AC furnaces, but the conversion of small, low powered furnaces to DC may have benefits.

Fines Melting and Smelting using a DC Transferred Arc Hollow Graphite Electrode

ASEA introduced the concept of a hollow DC graphite electrode for feeding fine ores and concentrates directly to the centre of the transferred-arc plasma without the need for costly agglomeration. Figure 19 shows the 16 MVA system installed by Middelburg Steel and Alloys in 1983 for the combined remelting of ferrochromium metallic fines and reducing chromite ores to produce high carbon ferrochromium (34).

The advantages of the DC reactor compared to SAF for ferrochrome production include the freedom to select the slag composition without slag resistivity constraints, fine feed material can be used without agglomeration, fine coal or coke breeze can be used instead of metallurgical coke and the power input and feed rate are independently controllable, allowing rapid adjustment of the melt temperature and processing rate.

AC Arcs between Electrodes

Reactors have been developed where an "expanded plasma fireball" is produced by arcing between graphite electrodes. A 1MW unit is used by IONARC (35) for the rapid heating and dissociation of zircon sand to produce zirconia. Zircon sand is injected into the long plasma flame, quenched and the zirconia leached from the product.

2.3.4 A summary of the applications of Thermal Plasma Processes

It is unlikely that plasma processes will replace existing large scale conventional technologies, such as iron and steelmaking, because of the limited scale of operation and the high cost of electrical energy. The advantages of plasma may be better utilized in smaller scale operations producing high value materials, materials requiring high reaction temperatures, materials that cannot be treated easily by conventional technologies or where cheaper raw materials can be utilized. Specific applications may be cost effective where the cost of electrical energy is low compared to fossil fuels.

Non-transferred arc plasma torches have been fitted to shaft furnaces for the production of ferrochrome, ferromanganese and the treatment of steelplant dusts. The major advantages of the system are the replacement of metallurgical coke with cheap electrical energy and the ability to use cheap, fine feed materials directly. The general use of plasma to superheat gas in shaft furnaces does not appear to be economically viable, except when electrical energy is cheap, low cost raw materials can be utilized and the excess process gas can be used for district heating.

Water-cooled transferred-arc plasma torches have been used for steel scrap melting and steel heating in the continuous caster tundish. Carbon steel melting does not appear to be economically viable compared to UHP AC arc furnaces because of the limited power input and the small scale of operation, but plasma furnaces may have applications in high alloy steel melting where a smaller furnace size is required and increased alloy yields are important. Tundish heating is a good application for the water-cooled transferred arc plasma torch because carbon pickup from graphite electrodes must be avoided, low power inputs are required and the small torch can easily be fitted in the restricted space available on the tundish. In ferroalloy smelting applications, the operating cost of the water-cooled transferred plasma torch/open bath reactor will be greater than the SAF because of the limited scale of operation unless cheaper raw materials can be used and the high enthalpy and chemical energy content of the exhaust gas is recovered. Precious metals recovery from automobile catalyst is another application because only a small reactor is required and advantage can be taken of the high reaction temperatures and good metallurgical recoveries.

DC graphite arc furnaces are in operation producing steel and ferrochrome. Cost savings are associated with lower graphite electrode, refractory and energy consumptions compared to the AC arc steelmaking furnace. The bottom electrode life will eventually limit the power input to the furnace relative to the AC furnace.

Most of the literature reviews consider the application of a particular type of plasma generator and compare it to the existing technology. Very little work has been reported on the differences between the water-cooled non-transferred arc plasma reactor, the water-cooled transferred arc plasma reactor and the DC graphite transferred arc plasma furnace when used for the same pyrometallurgical application. In particular, the differences between the water-cooled transferred arc plasma torch and the DC graphite electrode at low power inputs need evaluating for ferroalloy smelting and steelplant dust recycling applications. The DC graphite electrode can deliver higher powers, has lower cooling losses, and has a more predictable operating life, but data is required on energy transfer, electrode consumption, plasma stabilizing gas requirements and the capital and operating costs of the two systems.

3.0 A LITERATURE REVIEW OF FERROCHROME SMELTING

This section of the work reviews the commercial chromite smelting technology and examines the theoretical aspects of chromite smelting to determine the potential advantages of plasma smelting.

3.1 FERROCHROME RAW MATERIALS

Chromite ores vary widely in composition but consist mainly of the spinel $FeO.Cr_2O_3$, where the FeO can be replaced by MgO and the Cr_2O_3 by Al_2O_3, ie $(Fe,Mg)O.(Cr,Al)_2O_3$.
Pure chromite spinel contains 67% Cr_2O_3 but metallurgical grade ores and concentrates vary considerably in composition:

	% OXIDE				
COUNTRY	Cr_2O_3	FeO	MgO	Al_2O_3	SiO_2
Albania	48.0	13.2	19.0	9.0	7.1
Finland	44.1	24.2	11.5	14.6	3.3
Greece	52.5	14.0	15.8	8.8	4.7
India	56.0	13.7	10.7	13.3	3.0
Philippines	52.0	14.8	15.3	12.0	3.8
S.Africa	52.0	17.6	12.0	12.6	2.0
Turkey	53.0	15.0	16.0	9.5	2.5
US. Montana	40.0	22.0	14.2	16.3	7.0
USSR	54.5	11.9	16.2	7.2	4.7
Zimbabwe	48.5	15.8	13.1	13.0	4.9

Chromite for SAF smelting must be in lump or agglomerated form because fines result in premature melting and crusting in the furnace shaft which reduces charge permeability, reduces furnace productivity and increases the particulate carry over with the exhaust gases. As high grade lumpy chromite ores are becoming scarce and expensive, pellets and briquettes are increasingly being used in the SAF. Fine chromite concentrates can be used directly in plasma furnaces, saving about £20/t on agglomeration costs.

Cheap coal or coke fines that are compatible with the process chemistry and kinetics can often be used in plasma furnaces, whereas expensive metallurgical coke is required in the SAF. The metallurgical coke should have a high electrical resistivity for power input, a high strength and a particle size of 0.05-0.20m to maintain a permeable charge and good furnace operation.

Fluxes such as limestone, dolomite and bauxite are added to the plasma furnace and SAF to produce a slag containing 25-35% MgO, 25-35% Al_2O_3 and 25-35% SiO_2. The exact slag composition depends on the furnace operating mode, the slag resistivity, liquidus temperature, viscosity and chromium recovery.

3.2 CHROMITE SMELTING TECHNOLOGY

3.2.1 Chromite Smelting in the SAF

The majority of ferrochrome is produced in the SAF, as shown in Figure 20. The furnace consists of a cylindrical, refractory lined shell which is non-tilting and tapped in a similar manner to a blast furnace. Consumable self-baking Söderberg electrodes are submerged in the charge and thermal energy is generated by local arcing and resistive heating of the coke and slag between the electrode tips. Mixed chromite, flux and coke are choke fed from overhead bunkers to the SAF shaft and are preheated and prereduced by the ascending hot CO rich exhaust gas as they descend towards the reaction zone. In the reaction zone the unreduced chromite dissolves in the slag and is reduced to ferrochrome containing 52-58% Cr, 25-40% Fe, 5-8% C and 0-6% Si and a slag containing 7-15% Cr_2O_3, 1-5% FeO, 30-34% MgO, 26-30% Al_2O_3, 27-32% SiO_2 and 1-3% CaO. The reaction zone is maintained at 2000K by controlling the power input, slag composition and liquidus temperature. The CO rich exhaust gas from the closed furnace is generally cleaned in a venturi scrubber, collected and used for in-plant heating.

The chromium recovery to the ferroalloy varies between 80 and 93% depending upon the chromite composition, particle size, slag chemistry and operating practice. The furnace energy consumption is 3.5-4.0 MWh/t of alloy (6.0-8.0 MWh/t contained Cr) and the coke consumption is 0.5-0.7t/t of alloy (0.8-1.2t/t contained Cr) (36). The SAF energy consumption can be decreased by utilizing the CO rich exhaust gases for preheating and prereducing the chromite.

Hokkanen (37) describes the Outokumpu Oy process where indurated pellets, flux and coke are blended and preheated in a rotary kiln fired by CO from the furnace. The SAF energy consumption is reduced to 2.65 MWh/t of alloy, but a further 0.2-0.3 MWh/t of alloy should be allowed for ancillaries and the kiln drive. Metallurgical coke consumption is reduced to 0.33t/t of alloy. In the Showa Denko Kabushiki process, green pellets of chromite, coke and flux fines are preheated in a travelling grate kiln and then prereduced in a rotary kiln fired by pulverized fuel before being charged hot to the SAF. 60-70% reduction of the Cr_2O_3 and FeO in the chromite is achieved. Further reduction is limited by the operating temperature of the kiln to avoid charge fusion and build up on the kiln walls. O'Shaughnessy (38) quotes a SAF energy consumption 2.0 MWh/t of alloy, but a further 0.3-0.4 MWh/t of alloy should be allowed for ancillaries. Reductant consumptions are 0.46t/t of coke fines in the pellets, 0.23t/t of coal in the prereducer and 0.18t/t of lumpy coke in the furnace.

Table 1 presents the estimated cost of smelting chromite in a modern 20MW submerged arc furnace located in the UK assuming a capital cost of £30m, a chromium recovery to the ferrochrome of 90% and a slag containing 30% MgO, 30% Al_2O_3, 30% SiO_2 and 3% Cr_2O_3 is produced. The total ferrochrome production cost for a UK based plant is approximately £691/t of contained chromium ($0.56/lb Cr). A similar plant located in S. Africa using Transvaal chromite concentrates has a production cost of approximately £482/t Cr ($0.38/lb Cr) because of the lower chromite, coke, energy and labour costs in S. Africa.

3.2.2. Chromite Smelting in Plasma Furnaces

Plasma smelting introduces the possibility of lowering the operating and capital costs by using cheap, fine ores and concentrates directly, using cheap coal and coke fines instead of metallurgical coke and using a wider range of slag chemistries to improve the alloy recovery. The plasma arc system allows the independent control of raw materials and power to the furnace, which together with the relatively short residence times in the furnace, means that a greater degree of control over the process is possible.

Middelburg Steel and Alloy

In 1984, MS&A converted a submerged arc furnace to a 14 MW DC open bath plasma furnace using a central hollow graphite electrode (32). The feed (a blend of chromite ore fines, coke and recycled ferrochrome fines) is fed down the hollow graphite electrode into the slag bath in the vicinity of the plasma arc. The furnace power is currently being increased to 28MW.

There is little published data on the furnace performance and economics but the energy consumption is thought to be higher than the SAF because the energy in the furnace exhaust gases is not utilized for counter-current heat exchange or prereduction of the raw materials and the sidewalls and roof are not shielded from the plasma arc radiation or the open melt. Table 2 presents the estimated costs of producing ferrochrome in a DC arc furnace in the UK using Turkish chromite concentrates. The total production cost of £663/t Cr ($0.54/lb Cr) are less than the SAF because the higher energy costs are offset by using fine chromite concentrates and coal instead of pellets and coke.

Swedechrome

In 1986, SKF commissioned the 70kt/annum, 48MW "Swedechrome" shaft furnace plant to produce high carbon ferrochrome from cheap chromite fines. The plant design is similar to the Plasmadust facility shown in Figure 15 (24) and consists of two 24MW coke filled shafts each heated by four 6MW non-transferred arc heaters. Coke in the shaft provides 30% of the reductant and the remainder is injected as coal into the plasma tail flame along with the chromite and fluxes. Chromium yields of 90% are achieved at energy consumptions of 5.2 MWh/t of ferrochrome. The capital cost of the plant was £50m in 1987. Table 2 presents the estimated ferrochrome production costs for a plant based in the UK using Turkish chromite concentrates. The total production cost is approximately £676/t Cr ($0.55/lb Cr). The economics of the plant depend upon using cheap chromite fines directly, replacing some of the metallurgical coke with coal and selling surplus energy to a local district heating scheme.

The Extended Arc Flash Reactor (EAFR)

The technical feasibility of producing ferrochrome from fine chromite in the 24kW plasma flash reactor was demonstrated by Pickles (39). Chromium recovery was 85-90% at an energy consumption of 9-33MWh/t of ferroalloy.

University of Minnesota

Maske (1) investigated the reduction of chromite in a 45kW DC transferred-arc/open bath reactor equipped with a hollow graphite electrode. Almost complete "in-bath" reduction of the chromite was achieved using fine chromite (<0.0025m) and fine reductant (<0.0025m), basic slags and short arc lengths. "In-flight" reduction of chromite was also investigated by injecting chromite into the plasma arc established between the plasma torch and a carbon or copper ring anode. It is claimed that up to 50% of the chromite was reducted "in-flight", but it is suggested that the majority of the "in-flight" reduction occurred as the chromite and reductant particles came into intimate contact on the sloping anode surface or in the hot collection chamber beneath the reactor. The degree of reduction increased when the cold copper anode was replaced with a larger, hot carbon anode and silica flux was added to the feed blend. The chromite probably dissolved in a liquid slag phase and was reduced by carbon particles entrained in the slag on the hot carbon anode surface.

3.2.3 Coal Based Chromite Smelting

The steel industry in Japan and Europe are developing a new generation of processes aimed at producing iron and ferroalloys using coal as the energy source rather than electricity. In Japan in particular, the conventional SAF-EAF-AOD route to stainless steel is becoming uneconomic because of the high cost of electrical energy (£50/MWh). In a review of coal based ironmaking, Smith and Corbett (40) identified three process types suitable for ferrochrome and stainless steel production:

Melting/Reduction Processes

Kawasaki (40) are producing stainless steel directly from blast furnace hot metal by injecting chromite, coal and oxygen into a Basic Oxygen Furnace (BOF) through submerged tuyeres. The energy for the chromite reduction is provided by the combustion of the coal in the bath and by post combustion of CO using a top lance. Nippon Steel (40) are developing a process based on pre-reduction of chromite in a fluidized bed and reduction and melting in a top and bottom blown converter.

Chromite reduction in a BOF is probably cost effective in Japan where electrical energy is expensive and there is excess hot metal and converter capacity available. In Europe, stainless steel scrap is the cheapest source of Cr/Ni units, therefore, the economics are dependent upon maximizing the use of stainless steel scrap by the EAF-AOD route. The BF/BOF route only consumes about 30% scrap and cannot use all the stainless scrap arising.

Coke Bed Reactor Processes

Kawasaki (40) are developing a coke bed melter-gasifier coupled to a fluidized bed pre-reduction. Pre-reduced chromite, pulverized coal, oxygen and hot blast air are injected into a coke-filled shaft through two-stage tuyeres. The pre-reduced chromite is smelted by the heat liberated by the oxy/coal combustion in the shaft. The smelter exhaust gases are taken from the top of the shaft and used to pre-reduce the chromite in a separate vessel. Kawasaki are further developing the process to use 100% coal by replacing the coke-filled shaft with a fluidized bed of coal.

Prereduction/EAF Melting

Nippon steel (40) are developing a process where chromite pellets are completely reduced in a rotary kiln and fed directly to an EAF making stainless steel. All the energy for chromite reduction is provided by fossil fuel and electrical energy consumption is kept to the minimum required for melting and gangue separation.

No data on the economics of coal based chromite smelting are available.

3.2.4 Chromite Smelting Costs

The SAF is an economic and technically proven method of producing charge grade ferrochrome. Further economies can be realised by preheating and partial reduction of the chromite prior to smelting using the Outokumpu or Showa Denko processes which reduce the electrical energy and coke consumptions. New technologies will only be economically competitive with the SAF if they can utilize cheaper raw materials, have a higher chromium recovery to the alloy, consume less electrical energy or use a cheaper energy source.

The estimated cost of smelting Turkish chromite in an Outokumpu SAF, an SKF plasma furnace and an MS&A hollow graphite electrode plasma furnace located in the UK are presented in Tables 1 and 2 and summarized below:

UK MS&A plasma furnace	£663/t Cr
UK SKF Plasma furnace	£676/t Cr
UK Outokumpu SAF	£691/t Cr
S. African SAF	£482/t Cr
Ferrochrome selling price	£700-800/t Cr

The production costs of the MS&A and SKF plasma processes located in the UK are marginally less than the equivalent SAF because the cheap chromite fines and coal used offset the lower energy consumption of the SAF. Energy and reductant costs in all processes could be reduced if the chromite concentrates are pre-reduced before feeding to the furnaces using a rotary kiln or hearth. Because all demonstrated pre-reduction technologies require an agglomerated or lumpy feed, the advantage of being able to use chromite concentrates directly in the plasma furnaces is lost. The economics of the SKF plasma process rely on selling excess energy to local district heating schemes, but this may not be possible, or desirable, in all locations. S. African operations will have the lowest cost because of the availability of cheap chromite, energy and manpower and the weak Rand.

3.3 THEORETICAL ASPECTS OF CHROMITE SMELTING

Considerable theoretical work has been carried out on chromite smelting in the SAF with reference to the reduction reaction mechanism, the smelting temperature, slag chemistry and the distribution of the elements between the condensed phases and this is reviewed in order to compare the operation of the SAF and plasma furnace.

3.3.1 The Chromite Reduction Reaction Mechanism

An understanding of the chromite reduction reaction mechanism is necessary to optimize the furnace operating parameters, feed material particle size, reductant type and reactivity, slag chemistry, reaction temperature etc. The reduction of chromite occurs in at least four stages;

- Solid state reduction of chromite by carbon and CO.
- Dissolution of chromite in the slag phase.
- The reduction of the dissolved chromium oxide by solid C, C dissolved in the ferroalloy or CO.
- Reduction of solid chromite by C dissolved in the ferroalloy.

Barzca (41) showed that the initial reduction of chromite in the SAF shaft takes place by solid state reaction between chromite and carbon. The reaction rate was controlled by the diffusion of the reactant species, which was a function of particle size, chromite composition and mineralogy. CO was found not to be an effective reducing agent, although Downing (42) suggests that this was probably due to the impure gas used in the experimentation. Downing (42) went on to show that the rate determining step in the solid state reduction was the CO regeneration reaction between CO_2 and C at the carbon surface.

Where solid state reduction occurs, it is primarily ferrous ions diffusing out of the chromite spinel to be reduced to iron or carbides. The ferrous ions are replaced by magnesium ions which diffuse into the chromite to form the altered spinel, $MgO.Cr_2O_3$.

Urquart (43) and Wederpohl (44) studied the reduction of chromite in the slag phase and found that the major rate limiting step was the dissolution of chromite into the primary slag prior to reduction. Muan (45) investigated the ferrochrome slag-metal equilibria and showed that very reducing conditions enhanced the dissolution of chromite in the molten slag by the formation of the more soluble oxide, CrO. Fukagawa et al (46), Kadarmetov (47) and Kouroki (48) all showed that the chromite reduction rate was initially controlled by the dissolution of the chromite in the slag. They suggest that the "FeO" in the chromite is preferentially reduced and the resultant "Cr_2O_3" forms the altered spinel, $MgO.Cr_2O_3$, which has a limited solubility. Decreasing the MgO content or increasing the silica content of the slag was shown to increase the reaction rate because the solubility of chromium oxide increased, presumably because the MgO activity in the slag was reduced. The addition of CaO also increased the rate of chromite reduction because of the enhanced solubility of $MgO.Cr_2O_3$ spinel in the $MgO-CaO-Cr_2O_3$ system

There is considerable discussion on the carbonaceous reductant species responsible for chromite/chromium oxide reduction. Solid carbon, carbon dissolved in the metal and CO are all thought to play an important role in the chromite reduction. Kouroki (48) suggests that the carbon suspended in the slag is the most important carbon source for the reduction of dissolved chromium oxide because the slag volume and interfacial area is relatively large compared to the carbon saturated metal. In the SAF, lumpy refractory chromite and agglomerates can pass unreacted through the slag layer to the metal where they are reduced by the carbon dissolved in the alloy. Barmin (49), Sevinc (50), Suzuki (51) and Fruehan (52) simulated this reaction by rotating solid Cr_2O_3 pellets in a liquid iron-carbon bath. Barmin (49) found that the process was chemical reaction rate controlled, Sevinc (50) and Suzuki (51) concluded that the reduction rate was determined by the oxygen transport in the melt and Fruehan (52) found that the rate was determined by carbon transport in the melt. Kawakami (53) investigated the reduction of chromite by injecting it into a carbon saturated iron melt and concluded from the behavior of the silicon, that the rate determining step was the transport of oxygen, either from the ore-melt interface to the bulk, or from the bulk to the bubble-melt interface where CO was evolved.

In summary, the dissolution of the $MgO.Cr_2O_3$ spinel formed after the solid state reduction of the iron oxide and the diffusion of reactants in the slag and metal phases constitute the rate limiting steps in chromite reduction in the SAF. It is, therefore, important to employ slags that have a high solubility for the $MgO.Cr_2O_3$ spinel and a low viscosity, ie slags with a low MgO activity containing about 30% SiO_2, 30% MgO and 30% Al_2O_3 or, if practicable, slags containing CaO.

Figure 21 illustrates the possible reaction mechanism in the open bath plasma reactor. There will be little solid state chromite reduction as the feed blend falls through the furnace atmosphere. The inability of the fine chromite and coal particles to penetrate through the slag layer to the carbon saturated ferroalloy would suggest that the majority of the chromite reduction occurs in the slag phase. The carbothermic reduction of the metal oxides dissolved in the slag may occur via particulate carbon, CO and carbon dissolved in the metal phase, but it is suggested that the majority of the reduction proceeds via the gaseous intermediates CO and CO_2. CO bubbles form on carbon particles floating in the slag and the reaction between CO and the metal oxides occurs at the bubble-melt interface. The CO_2 generated at the interface reacts with C to renew the CO via the Boudouard reaction. The transport of oxide from the slag bulk to the bubble melt-interface, the reaction between the CO and the metal oxide and the regeneration of the CO via the Boudouard reaction will determine the reduction rate. Good mixing, reactive reductants and low viscosity slags containing CaO that "wet" the reductant and have a high solubility for the $MgO.Cr_2O_3$ spinel should be employed to ensure rapid reaction rates and good chromium recoveries.

3.3.2 The Chromite Smelting Temperature

The typical chromite smelting temperature of 1900K is determined by the thermodynamic stability of the oxides, mass and heat transfer, metal and slag liquidus temperatures and the minimization of energy and refractory consumptions.

The reduction of the chromium oxide in the SAF proceeds in several stages. Solid state reduction of chromite with carbon and CO to form Cr_3C_2 containing 13.3% C begins at 1423K, according to equation 4.

$Cr_2O_3 + 13/3C = 2/3Cr_3C_2 + 3CO$ eqn 4

As the chromite descends the furnace shaft towards the reaction zone, the more stable lower carbide Cr_7C_3 containing 9.0% C forms at 1523K.

$Cr_2O_3 + 27/7C = 2/7Cr_7C_3 + 3CO$

eqn 5

At 1873K, $Cr_{23}C_6$ containing 5.7% C becomes the stable chromium carbide.

$Cr_2O_3 + 81/23C = 2/23Cr_{23}C_6 + 3CO$

eqn 6

At temperatures above 2100K, chromium metal forms.

$Cr_2O_3 + 3C = 2Cr + 3CO$

eqn 7

Thus, as the reaction temperature increases, the stable chromium carbide contains less carbon. In practice, the chromite reduction temperature will be somewhat different from the temperatures indicated above because the reduction temperature depends on the composition and characteristics of the chromite used, the simultaneous reduction of iron oxide lowers the concentration and activity of the chromium, the Cr_2O_3 is chemically combined in the chromite and the gangue oxides in the chromite lower the Cr_2O_3 activity. Lisniak (54) found that chromites with a high Fe:Cr ratio or a high SiO_2 content began to reduce at 1000K and were nearly completely reduced at 1500K, whereas chromites with a low Fe:Cr ratio or high MgO or Al_2O_3 content were only reduced at temperatures approaching 1700K.

Figure 22 shows the Cr-Fe-C liquidus diagram derived by Griffing (55). The liquidus temperature of a typical ferrochrome containing 6-8% C and 50-55% Cr is 1850K.

The reactor temperature must be limited to prevent excessive refractory wear and the carbothermic reduction of unwanted species. SiO_2, MgO and CaO start to be reduced if the melt temperature exceeds 2000K.

REACTION	REDUCTION TEMPERATURE, K	
$SiO_2 + 2C = [Si] + 2CO$	1813	eqn 8
$SiO_2 + C = SiO_v + CO$	2100	eqn 9
$MgO + C = Mg_v + CO$	2100	eqn 10
$CaO + 3C = (CaC_2) + CO$	2198	eqn 11
$CaO + C = Ca_v + CO$	2423	eqn 12
$1/3Al_2O_3 + C = 2/3[Al] + CO$	2273	eqn 13
$2/3Al_2O_3 + 3C = 1/3[Al_4C_3] + 2CO$	2170	eqn 14

where
[ ] denotes solution in the metal phase
( ) denotes solution in the slag phase
$_v$ denotes the vapour phase

The solid burden in the SAF condenses and recycles much of the vapourized species, whereas the vapour will escape from the open bath plasma reactor.

3.3.3 Distribution of Elements between the Condensed Phases in Chromite Smelting

Chromium

At the typical reaction temperature of 1850-2000K, chromite is reduced to a Cr-Fe-C alloy according to reaction 15.

$$Cr_2O_3 + 3C = 2[Cr] + 3CO \qquad \text{eqn 15}$$

where

$\Delta G^\circ = 818046 - 540.1T$ J/mole (56)

therefore

$$-42718/T + 28.2 = 2\log a_{Cr} + 3\log P_{CO} - \log a_{Cr_2O_3} - 3\log a_C \qquad \text{eqn 16}$$

$$a_{Cr_2O_3} = N_{Cr_2O_3} . \gamma_{Cr_2O_3} \qquad \text{eqn 17}$$

$$N Cr_2O_3 = \text{mass\% } Cr_2O_3/1.6 \text{ Mol Wt} \qquad \text{eqn 18}$$

therefore

$$-42718/T + 28.2 = 2\log a_{Cr} + 3\log P_{CO} - 3\log a_C - \log \text{mass\% } Cr_2O_3 + \log 1.6 \text{ Mol Wt} - \log \gamma_{Cr_2O_3} \qquad \text{eqn 19}$$

P_{CO} is the partial pressure of CO, a_C, a_{Cr}, $a_{Cr_2O_3}$ are the activities of the species referred to the pure solid state, N is the mole fraction of the species, γ is the Raoultian activity coefficient, Mol Wt. is the molecular weight of the species (Cr_2O_3) and 1.6 is the approximate number of moles of slag oxides in a 100g of slag. The CO partial pressure will be approximately 1 atm. Healy (57) calculated the carbon activity in Cr-Fe-C alloys using carbon saturation data and obtained the activity coefficients of Cr and Fe from the carbon activity coefficient by the Gibbs-Schumann integration method. Figure 23 shows that for a Fe-Cr-C alloy containing 55% Cr, 35% Fe and 5% C at 1873-2000K, the activities of Cr, Fe and C are 0.1, 0.35 and 0.35 respectively. There is little published data on the activity coefficient of chrome oxide in $CaO-MgO-Al_2O_3-SiO_2$ slags under reducing conditions, most data referring to the refining of stainless steels. Maun (45) determined the activity-composition relationship of chrome oxide in the system CaO-"CrO"-SiO_2 under reducing conditions and showed that it is similar to the CaO-"FeO"-SiO_2 system and almost ideal. Substituting the values into equation 19, the mass% chromium oxide in equilibrium with a Fe-Cr-C alloy can be found from equation 20.

$$-42718/T + 26.5 = -\log \text{mass\%}\ Cr_2O_3 \qquad \text{eqn 20}$$

The equilibrium chromium oxide content of the slag should be negligible throughout the temperature range of interest. In practice, the recovery of chromium is controlled by the reaction kinetics, slag composition, slag viscosity, slag volume and the amount of metallic inclusions entrained in the slag.

Rowley (58) and Dresler (59) reported typical chromium losses in S. African SAF slags of 7.5% as dissolved Cr_2O_3 and 7.0% as metallic inclusions. Dresler (59) and Thomas (60) developed a chromite smelting model which predicts a decrease in Cr recovery to the alloy with decreasing Cr_2O_3 content in the ore/concentrate because lean ores generate a high slag volume and, therefore, higher chromium losses. Dresler (59) and Hamakos (61) suggest that the chromium recovery to the alloy increases with increasing MgO/Al_2O_3 ratio in the slag because of the lower slag volume and more complete dissolution of Cr_2O_3 in the slag with decreasing slag viscosity. Fukagawa et al (46), Kadarmetov (47) and Kouroki (48), on the other hand, suggest that concentrates with a low MgO/Al_2O_3 ratio should reduce more easily because the activity of MgO will be lower, promoting the reduction of the $MgO.Cr_2O_3$ spinel in the chromite. Figure 24 illustrates the relationship between Cr recovery and the Cr_2O_3 in the concentrate for two MgO/Al_2O_3 ratios in the slag. Figure 25 shows that high Cr_2O_3/FeO ratios in the chromite decrease the chromium recovery, probably because the chromites are more refractory and difficult to reduce.

Plasma furnace slags should be lower in chromium oxide than SAF slags because the slag composition can be chosen independently of slag resistivity. Pickles (39) reported 4.2% Cr_2O_3 in the EAFR slags, Maske (1) found the Cr_2O_3 in a DC graphite electrode furnace slag was 3-4% when smelting very fine chromites and reductants. Kouroki (48) reported 2-5% Cr_2O_3 in transferred arc plasma furnace slags.

Carbon

Before the introduction of the AOD process, the SAF had been operated to produce a high carbon ferrochrome with a carbon content of <5%. Lumpy refractory ores and a slag MgO/Al_2O_3 ratio of unity were used to retard the reaction of chromium oxide with carbon until the feed reached the high temperature reaction zone. The decarburization of high carbon Fe-Cr-C alloys in the AOD with a minimal chromium oxidation loss opened up the market for a higher carbon or charge grade ferrochrome and the acceptance of processes that produced a carbon saturated alloy.

The carbon content of the ferrochrome is controlled by the reaction temperature, the ore composition and physical properties and the process route. Ores high in iron oxide produce a high carbon ferrochrome because iron oxide is readily reduced to a high carbon complex carbide $(Cr,Fe)_7C_3$, the activity of the chromium carbide is lowered and the low temperature reduction of Cr_2O_3 is promoted. Kadarmetov (47) showed that a lower carbon ferrochrome (<5% C) is more readily obtainable in the SAF by using a dense, low iron oxide content, lumpy ore with a high melting point which penetrates the slag to form a viscous chromic oxide rich layer above the ferrochrome, decarburizing the alloy droplets as they pass through the layer. Downing (62) showed that high carbon alloys were produced from fine ores or agglomerates with a high surface to volume ratio and low viscosity slags with magnesia/alumina ratios >1 and silica contents >35% because they promote rapid dissolution of the ore in the slag, rapid reaction rates and lower reaction temperatures. The alloy carbon content from the transferred arc plasma furnace should be higher than the SAF because fine feed material is used, the reaction temperature is lower and there will be little "decarburization" of the ferrochrome by a chrome oxide rich slag.

Silica

Some silica will be reduced during chromite smelting because the stablity of silica is similar to chromite. Silica reduction will increase with increasing melt temperature, acid slags and easy to reduce ores.

Phosphorus

Phosphorus removal from the alloy in the SAF is difficult under high temperature, reducing conditions with siliceous slags. Robiette (36) reported that 60-80% of phosphorus charged to the SAF reports to the alloy, 10-20% to the slag and 10-20% to the gas phase and, therefore, low P raw materials must be selected to achieve low phosphorus alloys. Chipman (63) found that Si increased the activity coefficient of P. Pickles (39) reported P recoveries of <60% to the ferrochrome in the EAPR due to the formation of phosphorus vapour which was swept from the reactor. A limited degree of dephosphorization may be possible in the transferred arc plasma furnace by using basic slags, lower temperatures and good slag-metal stirring.

Sulphur

60-80% of the sulphur in the raw materials charged to the SAF reports to the ferrochrome (36). Sulphur can be minimized by using low sulphur raw materials (<0.5% S), a high melt temperature and if possible, a basic slag. C and Si increase the activity coefficient of sulphur and decrease the sulphur content of the alloy, whereas Cr decreases the activity coefficient of sulphur (64). Pickles (39) reported the removal of S as volatile SiS under very reducing conditions in the EAFR.

3.3.4 Slag Compositions in Chromite Smelting

The slag composition used in the SAF is a compromise determined by the slag liquidus temperature, slag viscosity, slag resistivity, slag volume, chromium recovery and furnace operating practice. Because the power input and feed rate are independent in the plasma furnace, there will be no slag resistivity constraints.

Slag Liquidus Temperature

The slag liquidus temperature in the choke fed SAF controls the slag and metal temperatures, because once the solid charge has fused, it rapidly drops away from the area of intense heat between the electrodes and settles in the furnace bottom where it is difficult to raise the alloy or slag temperature by increasing the energy input or retention time. The slag liquidus temperature must be maintained at 100-200K in excess of the alloy liquidus temperature (1850-1900K) to ensure that the alloy is sufficiently superheated for tapping. In the open bath of the transferred-arc plasma furnace, the melt temperature can be controlled directly by the energy input rate and the slag liquidus temperature can be approximately the same as the alloy liquidus temperature. The slag liquidus temperature for the $CaO-MgO-Al_2O_3-SiO_2$ system of interest has been investigated by Osborn (65) and is shown in Figure 26. Examining the SiO_2, MgO and Al_2O_3 contents of the chromites presented in section 3.1, it is seen that slags produced from the reduction of Finnish, Indian and US chromites lie to the right of the $MgO.Al_2O_3$ field, those from S.African and Zimbabwe lie in the centre of the field and those from Albania, Greece, Turkey and the USSR lie in the MgO field. In SAF smelting, SiO2, MgO or Al_2O_3 fluxes are added to produce a slag which lies in the centre of the $MgO.Al_2O_3$ field with a liquidus temperature of about 2000K. For plasma smelting, a slag with liquidus temperature of 1870K and a composition nearer the Cordierite field is aimed for.

Slag Resistivity

In the SAF, thermal energy is generated by resistive heating of the charge between the electrode tips, therefore a high slag (and coke) resistivity is required for maximum furnace productivity. Johnston (66) showed that the slag resistivity generally increases with increasing silica content, decreasing lime and decreasing magnesia/alumina ratios. Slag resistivity is not an important criteria in the transferred-arc plasma furnace because the energy is liberated at the arc/melt interface. Slags with a high magnesia/alumina ratio or a high lime content can be used to decrease the slag viscosity and increase the chromium oxide activity.

Slag Viscosity

Low viscosity slags are required for rapid heat and mass transfer and phase separation in both the SAF and the plasma furnace. Johnston (66), Machin (67), Lyutikov (68) and Rennie (69) investigated the viscosity of slags in the system $CaO-Al_2O_3-MgO-SiO_2$ at temperatures between 1573 and 2000K and found that the viscosity decreased rapidly with increasing MgO and CaO content, but Cr_2O_3 increased the slag viscosity. Unlike the SAF, the open bath plasma furnace can use low viscosity slags containing MgO and CaO because there is no restriction on slag resistivity. Figure 27 shows the viscosity in the systems of interest.

Alloy Composition

The slag composition has an indirect effect on the carbon content of the alloy in the SAF because the slag liquidus temperature determines the reaction temperature and the alloy carbon content. Slags high in magnesia or low in silica will have a high liquidus temperature, promoting high reaction temperatures and low carbon contents. Slags containing calcium oxide produce high carbon content alloys because the formation of calcium carbide aids the transfer of carbon to the alloy, basic slags wet the carbon particles and calcium oxide lowers the slag viscosity. Basic slags will aid the desulphurization and dephosphorization of the ferrochrome.

Chromium Recovery

Many workers (1,36,45,48,70) have reported higher chromium recoveries for alloys smelted under basic slags. Muan (45) showed that the chromium content of slags decreased from 7% to 1.5% as the slag basicity ($\%\ CaO + \%\ MgO/\%\ SiO_2$) increased from 0.5 to 1.6. Kouroki (48) found that a minimum chrome oxide in the slag of 2% was associated with slags containing 8-15% CaO and 35-40% SiO_2. Increasing the calcium oxide content of the slag decreases the chromium oxide content, but will increase the slag volume and may reduce the chromium recovery to the ferroalloy.

Furnace Operating Practice

In S. African furnace operation, where chromite concentrates and coke are relatively cheap and furnace productivity is the primary objective, the furnaces are operated with a slag MgO/Al_2O_3 ratio of around unity to maximize the slag resistivity and power input to the furnace at the expense of chromium yield. S. African chromite concentrates have a natural MgO/Al_2O_3 ratio of approximately unity, therefore the minimum of flux additions are required. Typically, 10-20% of the chromium charged to the SAF is retained in this slag as dissolved oxide or suspended metallic droplets and the metallic content of the slag is often recovered in a crushing and gravity separation circuit. In European operations the SAF is operated with slag MgO/Al_2O_3 ratios of 1.3-2.0 to maximize chromium yield. The natural MgO/Al_2O_3 ratio in European chromites is 1.6-2.0. Typically 3-8% of the chromium is retained in the slag as dissolved Cr_2O_3.

3.4 SUMMARY OF CHROMITE SMELTING

The SAF is an economic and technically proven process for the production of high carbon ferrochrome with scope for further cost reduction by external preheating and prereduction of the chromite. The plasma reactor has potential for cost savings because it can use fine chromite ores and coals directly instead of lumpy chromite/pellets and coke, and the chromium recovery to the ferroalloy may be marginally improved because of the greater flexibility in slag composition. The energy consumption in the plasma reactor will be higher than the SAF unless external pre-heating and pre-reduction of the chromite is practised. Scale up of plasma furnaces using water-cooled electrodes is limited by the size of the available electrodes (5MW), but this can be overcome by using hollow graphite electrodes. The plasma furnace feed blend should be configured to produce a slag containing >30% silica and a high magnesia/alumina ratio for maximum chromium recovery to the alloy. A furnace operating temperature of 1900K is required to promote the reduction reactions and exceed the alloy liquidus temperature whilst minimizing energy consumption, refractory wear and the reduction of gangue oxides.

3.5 CHROMITE SMELTING OBJECTIVES

To quantify the plasma furnace operation and evaluate the process economics, a chromite smelting trial was conducted to examine:-

- The energy consumption.
- The ablity to smelt fine chromite directly using coal as a reductant.
- The effect of slag composition and operating parameters on chromium and the element distributions between the condensed phases
- Reactor availability, including plasma torch and refractory life.
- The process economics, including operating and capital costs.

4.0 A LITERATURE REVIEW OF STEELPLANT DUST TREATMENT

Steelplant baghouse dusts contain appreciable quantities of recoverable iron, chromium, nickel, zinc, lead, cadmium, etc. In many countries steelplant dusts are classified as hazardous wastes because the contained lead, cadmium and chromium can be leached from the dust into ground water if the dust is dumped in an open landfill, and enter the food production chain. The high cost of disposal in secure landfill sites has been a major incentive to develop new treatment technologies, especially if the zinc and lead can be recovered to an enriched oxide or preferably a condensed metal to offset the treatment costs. In Europe, where the environmental lobby is less strong, the value of the recoverable chromium, nickel and zinc from alloy steel dusts has initiated process development.

4.1 STEELPLANT DUST CHARACTERISATION

During the scrap melt down and refining stages in the Electric Arc Furnace (EAF), Argon Oxygen Decarburization converter (AOD) or Basic Oxygen Furnace (BOF), 1-2% of the steel charge is converted to an extremely fine fume which is collected in baghouse filters, scrubbers etc. The dust is produced by a combination of metal vaporization in the high temperature arc-melt interface, metal atomization through oxygen jet-melt interactions and volatilization of the high vapour pressure species from the scrap charge. An appreciation of the variability in quantity, chemical composition and physical properties of EAF fume may be obtained from various surveys (71-75). Table 3 presents some typical European and US steel dust analyses and production rates. Dusts from carbon steel production are rich in ZnO and PbO because of the use of galvanized scrap and other zinc bearing materials in the charge. Dusts from alloy and stainless steel production contain Cr_2O_3, NiO and MoO_3 roughly in proportion to the grade of steel being melted. CaO varies considerably, depending upon the lime charging and injection practice. Fluorine results from fluorspar additions made to the EAF slag. Chlorine originates from road salt and plastics in the scrap. Alkalies arise from road salt. The average dust generation rate from EAF plants is 1-2% of steel production capacity, but this is expected to increase as zinc usage in automobiles increases.

4.2 CONVENTIONAL DUST TREATMENT PROCESSES

Dust treatment technologies can be divided into regional processes or on-site processes. Regional processes, where the dust is transported to a central facility, include the ISF shaft furnace, the Horsehead rotary kiln, the Inmetco rotary hearth, SKF Scandust and the Zinc Corporation of America flame reactor. Table 4 presents the estimated costs of a 76500 t/y regional facility. On-site processes, where the dust is treated at the point of origin, include recycling to the EAF, the Cebedeau caustic leach process and the Chemfix encapsulation process. Table 5 presents the estimated costs for a 5500 t/y on-site facility. Table 6 presents the estimated costs of smelting alloy dusts at Scandust to recover an alloy pig iron.

The Imperial Smelting Lead/Zinc Blast Furnace Regional Process

The Imperial Smelting Lead/Zinc Blast Furnace (76) can process EAF dusts containing ZnO, PbO and halogens. The dust is blended with zinc ores and fed to a sinter strand to agglomerate the dust and volatilize the majority of the halogens, PbO and CdO. The sinter is charged with preheated coke to the blast furnace where the ZnO is reduced and volatilized and leaves the furnace top with the exhaust gas stream. The zinc is condensed in a lead splash condenser and separated from the lead by liquation in a cooling launder. Lead bullion and an iron oxide rich slag are intermittently tapped from the furnace hearth. Both Commonwealth Smelting Limited in England and Metallgesellshaft in W. Germany incorporate EAF dust in their ISF charge. There are no ISFs in N. America.

Process advantages:
- Can accept a wide variety of feed materials.
- Zinc and lead are recovered as metals.
- Known technology.
- There is an existing infrastructure to sell the zinc, lead and any toxic residues.

Process disadvantages:
- High capital cost.
- Large throughput required for economies of scale.
- Environmental problems associated with the sinter plant and lead splash condenser.

The Electrothermic Furnace Regional Process

In the Zinc Corporation of America (St Joe) electrothermic zinc shaft furnace (77), the zinc bearing sinter and coke are resistively heated by an electric current passing between graphite electrodes located at the top and bottom of the shaft. Zinc vapour leaves the furnace through a vapour ring and is condensed in a zinc splash condenser. The furnace can only accept limited quantities of EAF dusts because the halogen and lead content of the dusts cannot be completely eliminated in the sinter plant and cause zinc condenser operating problems (78). ZCA are developing a caustic leach pretreatment step to reduce the halogen and lead levels in the feed derived from EAF dust, but the cost of the leach step is significant, often exceeding the value of the contained zinc in the dust.

Process advantages:
- Pure zinc product.
- Known technology.

Process disadvantages:
- High capital cost.
- Complicated process.
- Only feed materials containing low lead and halogen contents can be processed.
- Environmental problems associated with the sinter plant.

Waelz Kiln Regional Process

EAF dusts and other zinc containing materials are pelletized, mixed with coke and fed to a rotary kiln where reduction and volatilization of the ZnO, PbO and CdO occurs at 1500K. The Zn, Pb/PbO and CdO vapour is reoxidised in the kiln atmosphere, cooled and collected in a baghouse filter as an enriched oxide containing 50-60% ZnO, 5-7% PbO and 0-1% CdO. The FeO and any alloy oxides in the dust are partially reduced and discarded with the solid slag. As the operating temperature of the kiln must be kept below 1500K to avoid the formation of accretions on the lining, only 85-90% of the ZnO, PbO and CdO are recovered from the steelplant dust. The Waelz kiln process is operated by Horsehead Industries in Palmerton and Calumet City, USA (79) and by Berzelius (80) in Duisburg, West Germany at processing capacities of 380kt/y and 50kt/y respectively.

In the Berzelius operation, excess coal and sand are added to the charge to control the physical characteristics of the slag and assure complete reduction, adding appreciably to the fuel costs. The enriched oxide product from the kiln is used as a feed for their ISF furnace. In the Horsehead operation, the majority of crude zinc oxide is reheated to 1400K in a second kiln to drive off the Pb, Cd and halogen impurities before it is used as a feed for the ZCA electrothermic smelter. Horsehead Industries currently charge £44/t plus transportation costs for processing EAF dust containing in excess of 20% ZnO. An additional £2.2/t is charged for every 1% ZnO below 20%. The low treatment costs of the Horsehead plant reflect the low kiln operating costs and the fully amortized plant. Horsehead Industries recently bought the ZCA electrothermic smelter and now control the market for the production and consumption of impure zinc oxide in the USA.

Process Advantages:
- Known technology.
- Low operating costs.

Process disadvantages:
- Relatively low ZnO recovery.
- High capital cost.
- A large throughput is required for the kiln to be economical.
- The ZnO product must be further treated to remove halogens.
- The economics are very sensitive to the zinc price.

Economics:

Capital cost (76500t/y)	£17m
Estimated operating cost	£50/t dust
ZnO revenue	£57/t dust
Reported treatment charge	£44/t dust

The HTR Regional Process

The "HTR" Process (Himezi Tekko Rifain KK) operated by N.K.K. (81) is a modification of the Waelz kiln which reduces the kiln operating costs by replacing some of the coal by auxiliary fuel and utilizing a higher reaction temperature of 1700K to selectively reduce the ZnO, leaving the FeO in the slag.

As a result, the metallization of FeO is reduced to less than 5%, the ZnO recovery to the enriched oxide is increased to about 90%, the reductant consumption is reduced from 0.24 to 0.1 t/t of dust and the production rate is increased by 85%.

Process Advantages:
- Low operating costs.
- High ZnO recovery.

Process disadvantages:
- Oil is required to supplement the coal.
- The ZnO product must be further treated to remove halogens.
- The economics are very sensitive to the zinc price.

Economics:

Capital cost (76500t/y)	£10m
Estimated operating cost	£39/t dust
ZnO revenue	£61/t dust
Reported treatment charge	£39/t dust

Sumitomo Kiln Regional Process

To improve the recovery of the zinc and lead, Sumitomo (82) developed a double kiln process, where the steelmaking dust is pre-reduced in the first kiln at low temperatures to avoid kiln accretions and in the second kiln, the temperature is raised and the liquidus temperature of the materials adjusted to produce a molten charge. No data on operating and capital costs or slag/residue toxicity are available.

The Inmetco (Demag) Regional Process

Inmetco operate a rotary hearth-submerged arc furnace plant for the treatment of 45000 t/y of alloy steel dust and millscale (83). Dust, coke breeze and fluxes are blended and pelletized with water and the green pellets are heated and prereduced at 1523K using oxy-fuel burners in a rotary hearth furnace. The NiO, MoO_3, CuO and Fe_2O_3 are almost completely reduced but the Cr_2O_3 is only partially reduced. The ZnO, PbO, alkalies and halogens are volatilized and recovered as an enriched oxide in a wet scrubber. The partially reduced pellets are smelted in a submerged arc furnace to produce a ferroalloy pig.

Inmetco currently charge a treatment fee of £190/tonne ($320/t) of dust, excluding transport, but return the recovered ferroalloy to the steel company. Trials have been carried out to recycle the preduced pellets directly to the EAF, but these were unsuccessful because the pellets reoxidized on cooling, resulting in low metallic yields and increased silicon reductant and energy consumption in the EAF.

Process Advantages:
- The process is suitable for on-site or regional processing.
- A wide range of steel mill wastes can be processed.
- Ni, Cr, and Mo are recovered as a recycleable pig iron.

Process Disadvantages:
- Zinc is recovered as an impure oxide.
- Capital intensive, especially for small tonnages.

Economics:

Capital cost	not known
Estimated operating cost	£120/t dust
Reported treatment charge	£190/t dust

The SKF Plasmadust Regional Process

The Scandust plant built by SKF (24) in Sweden was commissioned in 1984 to treat 70kt/y of EAF and AOD dust. Figure 15 shows the main features of the plant. The dust is washed, filtered, micropelletized and blended with powdered fluxes and coal. The feed is pneumatically injected into the raceway created in front of the plasma generators in the base of the coke filled shaft furnace. The ferroalloy and slag produced collect in the furnace hearth and are intermittently tapped. The exhaust gas containing 68% CO, 18% H_2, 5% N_2, 7% Zn and 1% Pb leaves the furnace top at 1375K and passes through a hot cyclone into a lead spray condenser. Zinc is absorbed by the lead and separated by cooling and liquation. Reported ferroalloy recoveries are 83% Cr, 83% Ni and 95% Mo, but one pass zinc recoveries are <70% because of hard metal and dross formation in the condenser associated with halogens and particulate matter carry over from the furnace.

The capital cost of the 70kt/y regional processing plant was £27m in 1984. The extensive feed preparation, zinc condensation and gas handling facilities were responsible for a major part of the capital cost. Operating costs are estimated to be about £117/t for EAF dust and £128/t for AOD dust, somewhat higher than alternative regional processes because of the high electrical energy consumption, metallurgical coke as well as coal is consumed and the process is labour intensive. The high capital and operating costs are partially offset by producing an alloy pig iron from the AOD dust, metallic zinc from the EAF dust and the sale of excess energy (hot water) to local users.

It is considered that the SKF Plasmadust process is only viable for EAF dusts in geographic areas where electrical energy is cheap, excess process energy can be sold to adjacent facilities and a high processing fee can be charged. The processing of alloy steel dusts is more economically viable because the product value is greater. In December 1987, SKF stopped treating EAF dust because of the poor economics of zinc recovery, although it is thought that some zinc condenser problems also remained to be solved. SKF are now operating the furnace only on AOD dusts, but as there are only approximately 40kt/y of AOD dust arising in Europe, the furnace must be operating at less than its breakeven tonnage.

Process advantages:
- Zinc can be condensed directly from the exhaust gases.
- Cr, Ni and Mo can be recovered from AOD dusts as a ferroalloy.
- The excess process gas can be sold to offset the high energy costs.
- A variety of steelplant arisings can be treated.

Process disadvantages:
- High energy costs.
- High capital costs.
- A large production capacity is required to achieve economies of scale.

Economics of EAF dust processing:-

Capital cost	£27m (1984)
Estimated operating cost	£117/t dust
Zn, Pb and energy revenue	£134/t dust
Reported treatment charge	£65-100/t dust

Economics of Alloy dust processing:-

Capital cost	£27m (1984)
Estimated operating cost	£128/t dust
Reported treatment charge	£200/t dust

Flash Reactor Regional Process

The Zinc Company of America (St Joe) have been operating a 15kt/y pilot plant facility since 1984 (84). Fine coal is pneumatically injected into a water-cooled burner and combusted with oxygen-enriched air under fuel rich conditions at 2000K to produce a reducing gas. EAF dust is injected into the hot gas stream where the oxides are reduced to form Zn, Pb and Cd vapour and an iron oxide rich slag. The slag is separated from the reactor gases in a horizontal cyclone at the base of the vertical reactor tube. The reactor gases are combusted, cooled with excess air and an impure ZnO is recovered in a baghouse filter. The large exhaust gas volume associated with fossil fuel combustion results in a large carry over of feed material, contaminating the ZnO product. The ZnO product must be treated to remove the halogens and lead before it can be incorporated in the sinter feed for the Electrothermic process. The combustion of carbon to simultaneously provide energy and reducing gas limits the flexibility of the system.

Process advantages:
- Low capital cost.
- Can be scaled up.

Process disadvantages:
- Produces an impure ZnO product which requires further treatment.
- Feed must be very fine.
- Impure product
- Oxygen enrichment of the flame is required.
- Inflexible Redox potential

Economics:

Capital cost	£1.5m in 1984
Operating costs	not known
ZnO revenue	£58/t dust
Reported treatment charge	£120-180/t dust

Direct Recycle to the EAF

Direct recycling of EAF dust to the arc furnace, as green pellets or briquettes mixed in with the scrap charge has been shown to concentrate the zinc and lead into a secondary fume containing in excess of 60% ZnO (85-88). However, the dust, pellets and briquettes generate clouds of lead-containing fugative emissions on charging to the arc furnace with the scrap. Armco (89) in the USA investigated pneumatic injection of the dust into the melt in an attempt to overcome the fugative emissions problem. Both processes have been abandoned because the EAF energy consumption is increased by 2-5% due to the reduction of the contained oxides, vaporization of the lead and zinc and decomposition of the carbonates. Steel quality deteriorated because of the pickup of tramp elements, Cu, Sn, As, Te etc,

Process Advantages:
- Simple technology
- Low capital cost
- Low operating costs.

Process Disadvantages:
- A low value enriched ZnO is produced.
- Green pellets break up on storage due to lime hydration.
- Increased EAF energy consumption.
- Increase in the tramp element level in the steel.

Economics:

Capital cost	£0.4m
Operating costs	£10-35/t dust
Revenue	£65/t dust

Hydrometallurgical On-site Processes

Conventional zinc electrowinning technology cannot be applied to EAF dust because the iron consumes large quantities of acid and the halogens adversely affect the cell operation. In 1986, Cebedau (90) installed a 12kt/y caustic electrolytic process where the zinc and lead are dissolved in caustic soda, the lead is cemented out with zinc powder and the zinc is electrowon on special cathodes to produce a high quality zinc powder. Not all the zinc ferrite is dissolved in the process, leaving a potentially toxic waste material for disposal.

Process advantages:
- Recovery of pure zinc.

Process disadvantages:
- Potential environmental problems with residues.
- High energy cost.
- Complex technology.

Process economics:

Capital cost	£1.8m (1985)
Reported operating cost	£95/t dust
Revenue	£105/t dust
Treatment charge	not known

On-site Chemical Treatment

EAF dust is treated at the steelplant with, or encapsulated in, a second phase to lower its surface area, reduce its permeability and decrease the leach rates of the toxic substances. Asphalt, silicates, pozzolanic and portland cements have been used as chemical fixation and stabilizing agents to produce a non-permeable agglomerate and encourage ion-exchange of heavy metals with the aluminosilicate matrix of the cementitious solidification agent. The process requires a low capital outlay for the feed and materials blending system and the low operating costs of £15-30/t cover additives, labour and product disposal (91). Chemfix are currently quoting a treatment charge of <£75/t including transport and product disposal.

Process advantages:
- Low capital and operating costs

Process disadvantages:
- Not a long term environmental solution.

Process economics:

Capital cost	£0.33m
Estimated operating costs	£15/t dust
Revenue	£0/t dust
Reported treatment charge	£75/t dust

4.2.1 A Summary of Dust Treatment Technologies

Recycling the dust to the EAF is apparently the cheapest option because the process uses existing equipment. However, the process complicates the EAF operation, contributes to steel quality problems, generates a low value enriched oxide product which requires transportation and further processing, and is generally disliked by the furnace operators. Regional rotary kiln facilities offer a cheap dust treatment route because they have low operating costs, large throughputs and the existing plants are fully amortized, but there are liabilities and costs associated with transporting the feed and disposing of the enriched oxide product and slag. In the USA, the market for impure ZnO is limited and controlled by Horsehead Resources/ZCA.

There would appear to be a need for a small scale, economic, on-site process that can recover metallic zinc and ferroalloys directly form the dust, thereby removing any environmental problems associated with the transport of the dust or the enriched ZnO product and securing a market for the product.

4.3 THEORETICAL ASPECTS OF STEELPLANT DUST SMELTING

This section of the work attempts to identify the least cost smelting route to produce a non-toxic slag and to maximize the recovery of Zn to an enriched oxide (or a condensed metal) and Cr, Ni and Mo to a ferroalloy. The reaction mechanism, the reduction potential (as measured by the CO_2/CO ratio and reaction temperature), slag chemistry and the smelting energy requirements are examined.

4.3.1 The Reduction Reaction Mechanism

Studies (92-98) of slag fuming furnaces have established that the reduction of ZnO etc from liquid slag by solid carbon occurs, for the most part, via the gaseous intermediates CO and CO_2 according to equation 21.

$$(ZnO) + CO = Zn_v + CO_2 \qquad \text{eqn 21}$$

FeO may also reduce ZnO, giving ferric ions, which in turn are reduced by CO. Bell (92), Kellogg (93) and Grant (94) developed thermodynamic models for the carbothermic reduction and fuming of ZnO from lead blast furnace slags which accounted relatively well for the observed fuming behaviour. Quarm (95) and later Richards and Brimacombe (96), disputed the attainment of thermodynamic equilibrium and concluded that the process was kinetically controlled by the diffusion of ZnO and Fe_2O_3 through the slag to the reaction site. Sannikov (97) and Yakovenko (98) also found diffusion of ZnO and Fe_2O_3 in electric furnace fuming of zinc slags to be the rate limiting step. It has been noted (99) that the addition of small quantities of strong surface active agents increased the kinetics of zinc fuming by decreasing the surface tension of the melt and accelerating the wetting of the carbon reductant particles.

It is suggested that the carbothermic reduction of metal oxides in steelplant dusts proceeds via the gaseous intermediates CO and CO_2. The CO_2 reacts with C to renew the CO via the Boudouard reaction. It is unlikely that the rate determining step will be the slag-gas chemical reaction, but the rate will be determined by the transport of reactants in the slag and gas phases and the regeneration of the CO via the Boudouard reaction. Consequently, such factors as melt temperature, feed particle size, reductant reactivity, slag viscosity and melt stirring will affect the overall reaction rate.

4.3.2 The Reduction Potential required for Smelting Steelplant Dust

The reduction potential as measured by the CO_2/CO ratio and reaction temperature are determined by:

- The thermodynamic stability of the metal oxides.
- The product purity.
- The prevention of ZnO formation during condensation of the zinc vapour.
- The selective reduction of ZnO, leaving the FeO in the slag.

The furnace operating temperature of about 1773K is also determined by:

- Metal and slag liquidus temperatures
- Slag viscosity.
- Refractory wear rate.

The CO_2/CO ratio and temperature required for the reduction of an EAF dust containing 25% ZnO, 3% PbO, 40% FeO, 5% MnO and 1% Cr_2O_3 to produce a slag containing less than 1.0% Cr_2O_3, 0.1% PbO and 0.1% CdO is presented in Figure 28.

The CO_2/CO Ratio and Temperature for ZnO Reduction

The ZnO activity in the slag in equilibrium with a given CO_2/CO ratio and zinc partial pressure is given by equation 22.

$$ZnO + CO = Zn_v + CO_2 \qquad \text{eqn 21}$$

where
$\Delta G^\circ = 178235 - 111.3T$ J/mole (56)

therefore

$$\log P_{CO_2} - \log P_{CO} = -9312/T + 5.81 - \log P_{Zn} + \log a_{ZnO} \qquad \text{eqn 22}$$

now

$$P_{total} = 1 \text{ atmosphere} = P_{Zn} + P_{CO} + P_{CO_2} \qquad \text{eqn 23}$$

$$aZnO = NZnO.\gamma_{ZnO} \qquad \text{eqn 24}$$

$$NZnO = \text{mass\% } ZnO/1.6 \text{ Mol Wt} \qquad \text{eqn 25}$$

therefore

$$\log P_{CO_2} - \log P_{CO} = -9312/T + 3.69 - \log P_{Zn} + \log\gamma_{ZnO} + \log\text{mass\% } ZnO \qquad \text{eqn 26}$$

The equilibrium mass % ZnO in the slag can be calculated knowing the zinc vapour partial pressure, the zinc oxide activity coefficient, the gas analysis and the reaction temperature. From mass balance considerations, the zinc partial pressure generated from a dust containing 25% ZnO is approximately 0.2 atmospheres. The ZnO activity data for the $CaO-SiO_2-FeO-ZnO$ system of interest were determined for slag composition ranges and temperatures typical of lead and lead-zinc blast furnace practice, ie 20-40 mole % FeO, 20-50 mole % SiO_2, 10-40 mole % CaO and 0-10 mole % ZnO at 1400-1700K.

The early work of Bell et al (92) and Okuner et al (101) calculated ZnO activities based on observed zinc elimination rates during slag fuming, however Quarm (95) concluded that equilibrium was not attained in the slag fuming furnace and, therefore, these results are not considered. Lebed et al (102) used a vapour pressure measurement technique under reduced pressure to determine ZnO activities. The validity of the technique is questionable, therefore the data was discarded. Davenport (103) calculated the ZnO activity relative to pure liquid ZnO rather than pure solid ZnO, the standard state used by most investigators. Reyes and Gaskell (104) pointed out the inaccuracies in the free energy of fusion of ZnO, making the conversion of the data to the solid standard state of limited use for this work. Ashuma et al (105) used a gas equilibrium technique for slags in the $FeO-Fe_2O_3-CaO-SiO_2$ system containing 0-20 % ZnO at 1373K and showed that the zinc oxide activity coefficient increased with increasing slag basicity. Richards (106) determined the ZnO activity in the system $FeO-CaO-SiO_2$ containing 0.2 mole % ZnO at 1473K using a gas equilibrium technique and found the activity coefficients of both FeO and ZnO increased with increasing slag basicity. The activity of ZnO could be represented by a regular solution formula involving interaction constants for each of the constituent binary systems over the limited composition and temperature range considered. Filipovska (107) measured FeO and ZnO activities in the system $FeO-CaO-SiO_2$ at 1525K using an EMF technique. The activity coefficients of ZnO and FeO were shown to increase with increasing slag basicity and Al_2O_3 content and a correlation expression was derived to predict the effect of slag composition on ZnO and FeO activity coefficients. Levin (108) used a gas equilibrium technique for the determination of ZnO activity at 1573K in the system $FeO-CaO-SiO_2$ containing 1-5 mole % ZnO. Although their data analysis technique was unclear, the zinc oxide activity coefficient was shown to increase with increasing slag basicity. Reyes and Gaskell (104) used a transpiration technique to determine ZnO activities in the system $CaO-Al_2O_3-SiO_2$ containing 1-5 mole % ZnO at temperatures between 1673 and 1823K and showed that the ZnO activity coefficient increased with increasing slag basicity and temperature. Figure 29 summarizes the zinc oxide activity coefficient data in the system $CaO-SiO_2-FeO$ at various temperatures. (104-108). Because of the limited data, no quantative relationship between ZnO activity and slag composition and temperature could be produced, however, several general trends were observed:-

- Isoactivity coefficient contours run parallel to the liquidus isotherms.
- The activity coefficient increases with increasing slag basicity.
- The activity coefficient decreases with increasing temperature.

For slags produced from smelting EAF dusts at 1723K, the ZnO activity coefficient increases from 0.5 for low FeO contents, to about 1.0 for slags containing >20 mass% FeO.

Curve A in Figure 28 shows the CO_2/CO ratio and temperature required to achieve 0.5 mass % ZnO in the slag when PZn = 0.2 and $\gamma ZnO = 1$. At the suggested reaction temperature of 1723K, a CO_2/CO ratio of <0.05 is required to reduce the mass % ZnO in the slag to 0.5% . Increasing the reaction temperature decreases the % ZnO in the slag, increasing the PZn by using a dust richer in ZnO increases the % ZnO in the slag and increasing the slag basicity reduces the % ZnO in the slag.

The CO_2/CO Ratio and Temperature for FeO Reduction

In the smelting of carbon steel dusts, the majority of the ZnO can be reduced from the slag without reducing the FeO by careful control of the CO_2/CO ratio and temperature. The CO_2/CO ratio in equilibrium with iron oxide and metallic iron according to reaction 27 is given by equation 28.

$$FeO + CO = [Fe] + CO_2 \qquad \text{eqn 27}$$

where

$\Delta G^\circ = -43600 + 38T$ J/mole (56)

and

$$\log P_{CO_2} - \log P_{CO} = 2277/T - 1.985 + \log a_{FeO} - \log a_{Fe} \qquad \text{eqn 28}$$

At a constant temperature, the limiting CO_2/CO ratio on the point of reduction of FeO to metallic Fe can be calculated from a knowledge of the FeO activity in the slag and the Fe activity in the metal phase. Figure 30 shows the FeO activity in the system $CaO-SiO_2-FeO$ (109). In a typical slag containing 40 mass% Fe_2O_3, 10% CaO, 10% SiO_2 etc, aFeO is approximately 0.5.

In iron-carbon melts, the Fe activity approximates to unity at low concentrations of carbon.

Curve B in Figure 28 shows the limiting CO_2/CO ratio and temperature to avoid the reduction of FeO. For the selective reduction of ZnO, the CO_2/CO ratio and temperature must be above Curve B (FeO reduction) but below Curve A (ZnO reduction). Decreasing the Fe_2O_3 content of the dust lowers the CO_2/CO ratio for selective reduction, enabling more ZnO to be reduced.

The CO_2/CO Ratio and Temperature for Cr_2O_3 Reduction

In the smelting of steelplant dusts, the "Cr_2O_3" content of the slag must be reduced to less than about 1% to meet the slag toxicity test requirements. The CO_2/CO ratio in equilibrium with chrome oxide and chromium, according to reaction 29, is given by equation 30.

$$1/3Cr_2O_3 + CO = [2/3Cr] + CO_2 \qquad \text{eqn. 29}$$

where

$\Delta G^{\circ} = 104068 + 12.3T$ J/mole (56)

and

$$\log P_{CO_2} - \log P_{CO} = -5437/T - 0.64 + 1/3\log a_{Cr_2O_3} - 2/3\log a_{Cr} \qquad \text{eqn 30}$$

The CO_2/CO ratio to reduce the chromium in the slag to less than 1% can be calculated from a knowledge of the temperature, the chromium activity and the chromium oxide activity in the slag. The activity coefficient of Cr dissolved in Fe has been measured by Hadrys et al (110) and found to have a constant value of 0.02 for melts containing up to 30 mass% Cr. Wellbeloved (111) determined chromium oxide activities in $CaO-SiO_2-MgO$ and $CaO-SiO_2-Al_2O_3$ slags respectively, but the scatter in the data does not allow any meaningful relationship to be derived, therefore, the chrome oxide activity coefficient is asssumed to be unity.

Curve C in Figure 28 shows the CO_2/CO ratio and temperature to achieve less than 1 mass% Cr_2O_3 in the slag when aCr2O3 = 0.004 and aCr = 0.0002. At 1723K, the limiting CO_2/CO ratio is 0.004 for dusts containing less than 1% Cr_2O_3 and 0.001 for alloy dusts containing 10-20% Cr_2O_3.

Thus it is not possible to selectively reduce ZnO from high Cr_2O_3 content dusts whilst producing a slag containing <1% Cr_2O_3.

The CO_2/CO Ratio and Temperature for PbO Reduction

In the smelting of EAF dusts, the "PbO" content of the discard slag must be reduced to <0.1% to meet the slag toxicity requirements. The CO_2/CO ratio in equilibrium with lead oxide and Pb vapour according to reaction 31 is given by equation 32.

$$PbO + CO = Pb_v + CO_2 \qquad \text{eqn 31}$$

where

$$\Delta G^\circ = -59356 - 20.9T \text{ J/mole (56)}$$

and

$$\log P_{CO_2} - \log P_{PCO} = 3101/T + 1.09 - \log P_{Pb} + \log a_{PbO} \qquad \text{eqn 32}$$

The CO_2/CO ratio to reduce the PbO in the slag to less than 0.1% can be calculated from a knowledge of the temperature, the partial pressure of the lead vapour and the activity of the PbO in the slag. The lead partial pressure generated from the carbothermic reduction a dust containing 5% PbO is approximately 0.02 atmospheres. Little work has been done on PbO activity in low ZnO CaO-SiO_2-FeO slags in the temperature range of interest. The majority of the data relates to high ZnO content lead blast furnace slag compositions at 1300-1500K. Richardson (112) and Meyer (113) found that the PbO activity coefficient increased from 0.4 to 1.2 as the CaO/SiO_2 ratio increased from 0.5 to 1.0 for slags containing 50% FeO at 1573K.

Curve D in Figure 28 shows that the limiting CO_2/CO ratio and temperature to reduce the mass% PbO in the slag to <0.1% will be about 10 at 1723K for a dust containing 5 mass% PbO.

CO_2/CO Ratio in Equilibrium with solid Carbon

The maximum degree of carbothermic reduction of metallic oxides will be defined by the CO_2/CO ratio in equilibrium with solid carbon at a given temperature. The CO_2/CO ratio in equilibrium with excess solid carbon according to reaction 33 is given by equation 34.

$$C + CO_2 = 2CO$$

eqn 33

where
$\Delta G^\circ = 170544 - 173.4T$ J/mole (56)

thus
$$\log P_{CO_2} - \log P_{CO} = 8910/T - 9.06 + \log P_{CO} - \log a_C$$

eqn 34

The activity of carbon in equilibrium with excess solid carbon will be unity. The partial pressure of CO generated from the carbothermic reduction of a typical steelplant dust containing 25 mass% ZnO, 30 mass% FeO, 5 mass% PbO, etc, will be about 0.6 atmospheres.

Curve E in Figure 28 shows the limiting CO_2/CO ratio in equilibrium with excess carbon where aC = 1 and PCO = 0.6. Gas compositions above the curve are stable, but convert to CO_2 and C below the curve. The minimum CO_2/CO ratio that is possible at 1723K is about 0.0001.

The CO_2/CO Ratio for Zinc Condensation and the Avoidance of ZnO Formation

The CO_2/CO ratio and temperature of the gas stream leaving the furnace (and entering a zinc condenser) must be carefully controlled to prevent premature zinc condensation and the reoxidation of zinc vapour, which would block the exhaust duct and form a dross in the condenser, reducing the zinc recovery. Curve F represents the saturated vapour pressure of zinc given by equation 35 (56).

$$\log P_{Zn} \text{ (mm Hg)} = - 6620/T - 1.255\log T + 12.34$$

eqn 35

For a zinc partial pressure of 0.2 atm, zinc condensation commences at 1000K. To condense the majority of the zinc vapour, it is necessary to decrease the zinc partial pressure to <0.01 atm by cooling the gas to at least 860K. In practice, it is necessary to cool the gas to 750K because of supercooling effects.

If complete chemical equilibrium were maintained on cooling the $Zn/CO/CO_2$ gas, the zinc vapour would reoxidize to form ZnO according to reactions 21 and 33.

$$ZnO + CO = Zn_v + CO_2 \qquad \text{eqn 21}$$

$$C + CO_2 = 2CO \qquad \text{eqn 33}$$

The reversion of reaction 33 is kinetically slow and C and CO_2 formation can be avoided by fast cooling. Reaction 21 is very fast and unless the gas is rapidly quenched, the CO_2 in the gas will react with an equivalent amount of Zn vapour to form ZnO. The conditions necessary to minimize the ZnO formation are illustrated in Figure 28. Curve G shows the CO_2/CO ratio in equilibrium with pure solid ZnO ($aZnO = 1$) at a zinc partial pressure of 0.2 atm. ZnO formation will commence on slow cooling the gas when the $Zn/CO_2/CO$ gas composition intersects Curve G (assuming the CO does not revert to CO_2 and C). To avoid ZnO formation on slow cooling the $Zn/CO_2/CO$ vapour to the condenser outlet temperature of 860K, the CO_2/CO ratio in the furnace must be maintained at <0.001. If the $Zn/CO_2/CO$ vapour can be quenched at a rate faster than the Zn vapour oxidation rate, then the acceptable gas composition will be limited by the intersection of the gas temperature and Curve G. For example, for a gas entering the condenser at 1273K, the CO_2/CO ratio should be <0.1 to avoid ZnO formation. The theoretical evaluation suggests that it should be possible to condense zinc from the $Zn/CO/CO_2$ vapour produced during selective reduction, provided the gas temperature entering the condenser is in excess of 1273K, the CO_2/CO ratio is less than 0.1 and the gas is rapidly quenched.

In practice, the back reaction to form ZnO is accelerated in the presence of H_2, H_2O, S and nucleation sites, therefore low volatile, low sulphur coals or preferably coke should be used as the reductant, and the feed should be dry and agglomerated to reduce feed carry-over.

4.3.3 Slag Composition

The slag composition is determined by:

- The slag liquidus temperature.
- The slag viscosity.
- The product purity. S, F, Cl, Na, K, etc may be partially retained in basic slags.

Slag Liquidus Temperature

The slag composition should aim to produce a slag liquidus temperature of <1723K, about 50K below the furnace operating temperature. Slags from EAF dusts generally have compositions which fall in a liquidus temperature trough extending from $CaO.SiO_2$ to the FeO corner of the $CaO-SiO_2-FeO$ system shown in Figure 31 (65). Slags from selectively reduced dusts contain around 20-30 mass% CaO, 20-30 mass% SiO_2 and 40-60 mass% FeO and have liquidus temperatures around 1500K, whereas slags from totally reduced dusts containing <5% FeO have liquidus temperatures around 1723K. A sand flux addition must be made to dusts containing more than 15% CaO.

Slag Viscosity

The slag composition should be configured to produce a slag viscosity of <5 centipoise at the furnace operating temperature of 1773K. The data on slag viscosities are too extensive to review in detail, but in general, viscosity increases rapidly with increasing silica for all concentrations more acid than 2RO.SiO2 (114-120). Al_2O_3 increases the viscosity in basic slags containing <33% SiO_2 by substituting for SiO_2 in the silicate network (115). CaO reduces the slag viscosity by breaking the silicate lattice. As CaO additions also increase the slag liquidus temperature, there will be an increase in viscosity if the slag liquidus/solidus temperature approaches the furnace operating temperature. MgO and FeO behave in a similar manner to CaO (122). ZnO additions up to 10% have been shown to decrease the slag viscosity (121-123). Figure 32 shows the slag viscosity in the $CaO-SiO_2-FeO-Al_2O_3$ system at 1673K will be <5 centipoises for the composition range of interest, but to minimize the slag viscosity, it is advantageous to use a slag composition high in CaO, FeO or MgO concommitant with a low slag liquidus temperature and volume.

Partition of Species Between The Phases

The reduction of ZnO, PbO, Cr_2O_3 etc from the slag phase increases with increasing slag basicity because the oxide activity coefficients increase with basicity.

The vapourization of alkalies should be minimized because they contaminate the ZnO product. Fukatake (124) investigated the vaporization of potassium from carbon saturated iron blast furnace slags and demonstrated that the potassium capacity of slags increased as temperature and basicity decreased (the activity coefficient of K_2O decreases with decreasing slag basicity). Dietzel (125) found that the vaporization of alkalies is enhanced in the presence of water vapour because of the formation of volatile alkali hydroxides.

The vapourization of halogens should be minimized because they contaminate the product and cause dross formation in the exhaust system and condenser. Schwertfeger (126) studied the vaporization losses of fluorine from CaO-SiO2-CaF_2 slags at 1900K and found that fluorine ions in the slag reacted with silica, alumina and water vapour to form the volatile species SiF_4, AlF_3, HF and to a lesser extent, CaF_2. Shinmei (127) measured the equilibrium SiF_4 pressure over CaO-CaF_2-SiO_2 melts at 1773K and found that the SiF_4 pressure decreased with increasing slag basicity (decreasing SiO_2 activity). The St Joe (78), Sumitomo (82), Inmetco (83) and Miike (128) smelters all found that the majority of the Cl, Na and K in the feed is volatilized and reported to the Zn/ZnO product, but a proportion of the F can be retained in the slag by using high slag basicities.

Refractory Consumption

Corrosion of the magnesia refractory lining in the plasma furnace can be minimized by operating with magnesia saturated slags with high CaO/SiO_2 ratios and low FeO contents.

4.3.4 Energy and Reductant Consumption for Steelplant Dust Smelting

The energy and reductant requirements for dust smelting will depend upon the dust analysis and the reduction potential used. Using the energy balance model presented in Appendix 1, the selective and total reduction of Tremorfa dust containing 35% ZnO and 33% Fe_2O_3 can be compared.

ITEM	SELECTIVE REDUCTION	TOTAL REDUCTION
Final % ZnO in slag	2.6	0.02
Final % FeO in slag	59.0	0.04
Nett energy, MWh/t dust	1.052	1.341
Reductant, t/t dust	0.078	0.18
CO_2/CO ratio	0.17	0.001
PZn, atm	0.30	0.2
Gas volume, m^3/t dust	305.0	486.0

Selective reduction can be used to reduce the majority of the zinc oxide, leaving the FeO unreduced in the slag, decreasing the energy consumption, reductant consumption and exhaust gas volume compared to the total reduction mode. The smaller exhaust gas volume results a higher partial pressure of zinc vapour and less entrainment of particulate matter, improving the zinc condenser efficiency and reducing product contamination.

4.4 SUMMARY OF STEELPLANT DUST SMELTING

None of the existing technologies that recover ZnO produce an enriched ZnO product that meets the ZnO specification imposed by Horsehead or Metallgeselschafts without calcining or leaching the oxide to remove impurities. The value of the zinc oxide product and the market outlet will be limited, imposing financial restrictions on these processes.

Apart from the ISF, the Plasmadust regional process is the only process which is designed to treat EAF dust and produce zinc metal directly. This overcomes the zinc oxide marketing problem, but the Plasmadust process suffers from high capital and operating costs and the zinc condenser operating problems have not been fully resolved.

The transferred arc plasma/open bath reactor appears to be a potential method of smelting steelplant dusts to produce a non-toxic slag, to recover zinc as an enriched zinc oxide or a condensed zinc metal and to recover alloy oxides to a ferroalloy for recycling. For the plasma furnace to be a viable dust treatment process, the treatment charge must be equivalent to the lowest cost alternative technology, ie the rotary kiln at about £50/t dust plus transport costs. To keep the energy and reductant costs to a minimum, EAF dusts should be smelted in the selective reduction mode at about 1723K with a CO_2/CO ratio <0.1, recovering the majority of the ZnO, but leaving the FeO in a non-toxic slag. Dusts containing alloy oxides must be totally reduced to recover the alloy elements and produce a non-toxic slag. Zinc metal may be condensed directly from the $Zn/CO_2/CO$ gas generated by selective reduction, provided the zinc condenser quenches the gas very rapidly. At slower quench rates, the furnace must be operated in the total reduction mode to generate a CO_2/CO ratio of <0.001 to minimize zinc vapour reoxidation. The halogen, alkali and lead contaminants in the dust are likely to be a problem in both the zinc oxide and zinc metal product routes. Slags with a % CaO/% SiO_2 of 1.0-1.2 should be used to maximize the metal oxide activities, minimize viscosity, retain halogens in the slag and minimize refractory corrosion.

4.5 STEELPLANT DUST SMELTING TESTWORK OBJECTIVES

To confirm the plasma process operating parameters, a series of trials was planned to examine:

- The CO_2/CO ratio, slag chemistry and operating temperature required to produce a non-toxic slag and recover the majority of the metal values.
- The effect of steelplant dust analysis, operating temperature, CO_2/CO ratio and slag chemistry on the purity of the enriched baghouse dust.
- The feasibility of condensing the zinc/lead vapour directly to a liquid product.
- The performance and availability of the plasma torch, furnace and ancillary equipment.
- The total processing costs.

5.0 EQUIPMENT

The plasma furnace and ancillaries used in the experimental section of the testwork consist of:

- The raw materials blending and feed system.
- The 2.0MW plasma furnace.
- The exhaust gas system.
- The plasma torch.
- The power source
- The instrumentation.

5.1 THE FEED SYSTEM

5.1.1 Feed Blending

The raw materials were stockpiled and crudely homogenised using a front end loader and sieved through a 0.006m vibrating screen to remove oversize particles. Preweighed raw materials, reductant and fluxes were loaded into a 0.4t capacity ribbon blender mounted on load cells (accuracy +/- 0.01t). After mixing, the blend was discharged into a bottom discharge bag, check weighed and conveyed to the furnace hopper. This system, although labour intensive, allowed for an accurate control of the feed batching and could accommodate rapid changes in the feed recipe as a trial progressed.

5.1.2 Feed Rate Control

The original furnace feeder consisted of a 0.5m diameter mass flow hopper fitted with a manually controlled variable speed plough feeder and mounted on load cells adjacent to the furnace. This system worked well for chromite, but EAF dusts bridged in the hopper and fed very erratically. The hopper was modified to accept a vertical screw agitator, fluidizing air pads and mechanical vibrators in an attempt to avoid bridging, but all proved to be unsuccessful and the plough feeder was replaced with a screw discharge feeder. The 200kg capacity screw feeder was equipped with six variable speed 0.05m diameter screws in the hopper base. Feedback signals from the hopper load cells controlled the screw speed and discharge rate.

This system gave a constant, controllable feed rate but was very labour intensive because it required frequent refills. The small feeder was replaced by a larger live bottom hopper mounted on a 1.0t weighbridge fitted with a twin 0.15m diameter variable speed screw discharge. The feed rate was monitored by integrating the hopper load cell output over 2 minute intervals to give a feed rate accuracy of +/-0.02t/hour.

5.1.3 Feed Transfer from the Hopper to the Furnace

Three 0.075m diameter horizontal screw conveyors were originally used to transfer the feed material from the feeder to the feed ports in the furnace roof. Screw conveyors were used because they are robust in the furnace environment and can be partially sealed to the furnace roof and the feed hopper to prevent the escape of furnace gases. This design was satisfactory for chromite, but caused extensive delays with EAF dust because the feed ports in the furnace roof sintered up with condensed zinc/zinc oxide that was difficult to remove. The three 0.075m diameter feed transfer screws were replaced with two 0.15m diameter screws discharging into two 0.15m diameter ports modified to accept disposable alumina feed port liner tubes which could be rapidly replaced if they sintered up. The feed ports were located 0.5m from the centre line of the furnace so that the feed materials fell into the hot arc/melt interface area to improve energy transfer to the melt.

5.2 THE FURNACE

5.2.1 Furnace Dimensions

Figure 33 shows a schematic layout of the plasma furnace. The furnace internal diameter of 1.5m was based on a "rule of thumb" power density of 1.0 MW/m² of hearth area obtained from considerations of the reaction kinetics, energy transfer, refractory wear rates and the bath volume for a realistic tapping interval. Figure 34 shows the relationship between furnace power and diameter for commercial DC furnace operation. AC UHP steelmaking furnaces using extensive water cooling have a power density of approximately 2.0MW/m² and SAF have a power density of around 0.5MW/m². The refractory life of the UHP arc furnace is around 2-4 weeks whereas the SAF refractory lining lasts up to 5 years.

A hearth-to-roof height of 1.4m was chosen so that with a typical melt depth of 0.2m and an arc length of 0.3-0.4m, the distance from the roof to the torch tip and the melt would be sufficient to protect the roof from the plasma arc and melt radiation.

5.2.2 Furnace Refractory Lining

The working refractory lining of lower sidewalls consisted of 0.23m thick high fired pitch impregnated magnesia bricks (Steetley MTB), chosen for their resistance to slag attack. The annulus between the cold face of the brick and the steel shell was rammed with high conductivity carbon paste to increase the thermal conductivity of the lining and reduce the refractory corrosion rate. The upper sidewall working lining was constructed from 0.18m thick high fired magnesia-chrome bricks (Steetley MC6), chosen for their resistance to thermal spalling. The annulus between the cold face of the brick and the furnace shell was filled with insulating concrete. The working lining of the hearth was 0.23m of high fired pitch impregnated magnesia bricks laid on end to prevent them floating out of the hearth. High grade, low iron firebrick was used as a backing lining to the magnesia bricks.

5.2.3 Roof Design

The original arched brick roof was constructed from 0.23m thick magnesia-chrome crowns and incorporated a central hole for the plasma torch and six feed entry holes. Although the refractory performance was good, difficulty was experienced in sealing the plasma torch and feed tubes into the roof and it was expensive and time consuming to rebuild. A water-cooled roof panel lined with 0.15m of cast tabular alumina was constructed and has been used successfully with minimum maintenance.

5.2.4 Anode Design

A central, air-cooled steel billet, 0.06*0.06m in cross section and 1.0m long, was built into the furnace hearth refractories to establish the return electrical connection required for the DC transferred-arc mode of operation. A molten heel of metal was maintained in the furnace at all times to avoid overheating the anode.

5.2.5 Molten Product Handling

The taphole of the static furnace was located 0.05m above the hearth to retain a metal heel in contact with the anode to maintain an electrical circuit. The taphole was opened with a conventional oxygen lance and closed with taphole clay. Molten slag and metal were intermittently tapped into refractory lined boxes. After cooling, the slag and metal were separated and weighed.

5.3 THE EXHAUST GAS SYSTEM

5.3.1 The Exhaust Duct

A single horizontal, refractory lined exhaust port located in the upper furnace sidewalls conveyed the gases to a refractory lined combustion chamber.

5.3.2 The Combustion Chamber

The furnace exhaust gases containing carbon monoxide and metal vapours were combusted and cooled to 600K with excess air in a vertical, refractory-lined combustion chamber. The combustion and cooling air flow was controlled by a damper immediately in front of the 70kW induced draught fan.

5.3.3 The Cyclone

A cyclone was installed ahead of the baghouse in an attempt to reduce the dust burden on the baghouse, but proved to be an ineffective dust collector because of the very small dust particle size and the low gas velocities.

5.3.4 The Baghouse Filter

Combusted gases were cleaned in two independently controlled Morley baghouse filters, each equipped with 96m^2 of woven stainless steel fibre filter envelopes capable of operating at 700K. Each baghouse could be isolated using dampers in the inlet and outlet ducting for off-line cleaning by reverse air jets. Several filter bags split during the early trials. The incidence of failure was reduced by locating a restraining cage around the envelope to restrict its flexure during the rigorous reverse jet cleaning cycle.

5.4 THE PLASMA TORCH

The plasma torch consisted of a water-cooled thoriated tungsten cathode surrounded by a water-cooled copper nozzle assembly to direct the plasma gas over the cathode tip. The torch was mounted in a service frame to facilitate its accurate positioning on the furnace roof and to enable it to be withdrawn to alter the arc length. The torch passed through a spherical water-cooled bearing seal in the furnace roof to allow it to precess through a variable angle. Power and cooling water connections between the torch and the service manifold were made via water-cooled flexible copper braids.

Figure 35 shows the original torch design and the modifications made during this work to improve its operating life to over 70 hours.

5.4.1 The Cathode

The thoriated tungsten tip was silver soldered into a water-cooled copper conductor tube. Electrical connection from the busbars to the conductor tube was made via twin flexible water-cooled copper braids. Electrical insulation between the cathode and the nozzle was achieved using a silica glass tube at the front (hot) end of the conductor tube and a PVC tube at the rear end.

5.4.1 The Cathode Material

Thermionic emission of electrons occurs when a suitable cathode material is heated to 3500-4000K at current densities greater than 1 MA/m². The current density at the cathode tip is given by the Richardson-Dushman equation:-

$$J = aT^2e^{-eW/kT} \qquad \text{eqn 36}$$

where

J = current density (A/m²)

a = constant (6 MA/m²K²)

T = temperature (K)

e = electron charge ($1.6*10^{-19}$ C)

W = thermionic work function (V)

k = Boltzmann constant ($1.38*10^{-9}$J/K)

Figure 36 shows the work function of cathode materials at their boiling point, with the required current densities for thermionic emission superimposed (17). Most materials except C, Ta, Rh or W are vapours at the temperatures needed to achieve current densities of >10 MA/m². Tungsten is usually doped with 2% thoria, yttria, ceria or lanthia to reduce the work function and the operating temperature of the emitting surface. Tungsten doped with thoria is most commonly used because of the availablity of good quality material in the size range necessary for high current operation.

5.4.2 Cathode geometry

The cathode tip diameter for water-cooled thoriated tungsten is obtained from the limiting current density of approximately 30 MA/m² specified by the Plansee (129). A 5kA cathode has a diameter of 0.014m.

The tungsten cathode length to maintain the arc terminus spot at slightly below the tungsten melting point to aid thermionic emission is calculated from the approximate relationship:

$$l = fd^2/A \qquad \text{eqn 37}$$

where
l = cathode tip length (m)
f = tip heating function for thoriated tungsten (0.3 MA/m)
d = diameter of cathode (m)
A = cathode current (A)

A 5kA cathode will be 0.013m long.

The cathode tip is pointed and projects 0.003m in front of the nozzle front face to encourage the central attachment of the arc and to aid starting. The whole cathode assembly can be moved forward relative to the nozzle to maintain the gas annulus geometry as the tungsten tip erodes. Choosing the correct tip geometry for a given current is important because if a tip that is too long for the required current is used it will run hot and erode rapidly, destroying the cathode/nozzle geometry. If the tip is too short it will run cold and crack, giving a short cathode life.

5.4.3 Cathode Cooling

The high heat fluxes encountered at the cathode (and nozzle) demand that special attention should be paid to the heat transfer to the cooling water. At low heat fluxes, heat transfer occurs by conventional axial flow non-boiling convective heat transfer. As the heat flux increases, nucleate boiling occurs when bubbles form at the cooled surface, even though the bulk water temperature is well below its boiling point. Nucleate boiling is usually accompanied by a marked increase in the heat transfer coefficient as long as provision is made to sweep the bubbles away from the cooled surface to prevent the formation of an insulating steam film. Above a critical heat flux, film boiling occurs where the cooled surface is covered by a continuous steam film and the water no longer makes contact with the cooled surface, resulting in a much lower heat transfer coefficient and a rapid rise in the temperature of the cooled surface, leading to failure by burnout. For a high critical heat flux, the coolant should have a low vapour mass fraction, a low bulk temperature, a high pressure, a high velocity and a high convective heat transfer coefficient (130-135). By causing the the coolant flow to turn on a small radius at the cooled surface, a centripetal acceleration can be imparted to the flow which sweeps away the low density bubbles from the cooled surface, further increasing the the critical heat flux. Figure 37 (130) shows the heat flux against film temperature drop for various water velocities.

In the initial trials cathode failure by burnout occurred after 30 hours at 3kA, therefore the heat flux, water velocity and pressure at the cathode tip were calculated to determine the heat transfer mechanism. The power dissipated to the cathode cooling water arises from the Joule heating of the conductor tube, Joule heating of the flexible water-cooled copper cables and heating of the tungsten tip itself.

Total Power Dissipated in the Cathode Assembly

Water flow rate = 0.000175 m^3/s
Inlet temperature = 285.2K
Outlet temperature = 296.6K
Power dissipated = 8.4 kW

Power Dissipation due to Joule Heating in the Copper Conductor Tube

Internal diameter of tube = 0.01255m
External diameter of tube = 0.01905m
Length of tube = 1.4m
Cross sectional area of tube = 0.000161m
Resistivity at 373K = $0.022*10^{-6}$ ohms.m
Resistance at 373K = $194.7*10^{-6}$ ohms
Heat generated at 3kA = 1.75 kW

Power Dissipation due to Joule Heating in the Water-cooled Flexible Copper Braids Connecting the Plasma Torch to The Busbars

Cross sectional area of braid = 0.0000731 m^2
Length of twin braids = 1.40 m
Resistivity of braids at 373K = $0.0174*10^{-6}$ ohms.m
Resistance of braids at 373K = $333*10^{-6}$ ohms
Heat generated at 3kA = 3.0 kW

Power dissipated in the Tungsten Tip

Power dissipated = 8.4 - 1.75 - 3.0 = 3.65 kW
Diameter of tip = 0.019 m
Power density at tip = 12.8 MW/m^2

Water Velocity at Tungsten Tip

Gap between flow divider tube and tip = 0.002 m
Internal diameter of divider tube = 0.0075 m
Area of water passage = 0.0000471 m^2
Water flow = 0.000175 m^3/s
Water velocity = 3.7 m/s

Water pressure at Tip

Water pressure = 3.5 bar

Assessment of Cooling Efficiency

The boiling point of water at 3.5 atms pressure was 411K and the return water temperature was 296.6K, giving a maximum allowable temperature drop across the film of 114.4K before the onset of film boiling. From Figure 37, with a water velocity of 3.7 m/s and a film temperature drop of 114.4K, the maximum heat flux that can be dissipated by water is 2.0 MW/m^2. The measured heat flux was 12.8 MW/m^2. Therefore, cathode failure was almost certainly due to film boiling and burnout. A dedicated high pressure coolant pump was installed to increase the cathode coolant flow and pressure and the gap between the divider tube and the tip was reduced to 0.0015m to increase the water velocity. The heat flux and water velocities for the new arrangement were:-.

Coolant flow	= 0.00037 m^3/s
Coolant velocity	= 10.4 m/s
Coolant pressure at tungsten tip	= 7 bar
Coolant boiling point	= 441K
Maximum temperature drop across film	= 150K

From Figure 37, the maximum theoretical heat flux that can be dissipated by the water is now 9.0 MW/m^2 compared to the measured heat flux 12.8 MW/m^2. The improved water flow increased the cathode tip life from about 30 hours to 70 hours. Further improvements in the cathode life may be achievable by further increasing the water pressure, flow and the cooled surface area of the tungsten tip.

5.4.4 The Nozzle

The nozzle directs the plasma gas around the cathode tip, protects the tip from splashes and provides a return electrical connection for the high frequency starting discharge during arc initiation. The 0.05m diameter nozzle was manufactured from a series of concentric copper tubes welded into a copper end piece. Oxygen free, high conductivity copper was used for the end face because it combined high thermal and electrical conductivity with ease of construction at a reasonable price.

5.4.5 Nozzle Cooling

The initial nozzle design failed after approximately 30 hours of operation by burnout at the inner edge of the nozzle orifice, therefore an examination of the heat flux and cooling design was carried out.

Heat Flux on Nozzle Tip

To estimate the heat flux on the critical nozzle tip alone, the plasma arc was run onto a piece of hot carbon in a cold furnace.

Inlet water temperature = 295K
Outlet water temperature = 305K
Water flow rate = 0.00087 m^3/s
Power absorbed = 36.4 kW
Surface area of coolant passage = 0.00083m^2
Power density = 43.9 MW/m^2

Water Velocity at Nozzle Tip

Cross sectional area of coolant passage = 0.00026m^2
Water flow rate = 0.00087 m^3/s
Water velocity = 3.33m/s

Coolant Pressure at Nozzle Tip

Coolant pressure at nozzle tip = 3.5 bar

Assessment of Cooling Efficiency

Boiling point of water at 3.5 bar = 411K
Return water temperature = 305K
Temperature drop across film = 106K

From Figure 37, the maximum heat flux that can be dissipated for a film temperature of 106K and a water velocity of 3.33m/s is 2.0MW/m^2 compared to a measured heat flux of 44.9MW/m^2. The nozzle coolant passages were modified to increase the surface area presented to the coolant, the passage gaps were reduced to increase the coolant velocity and a larger capacity, higher pressure coolant pump was installed. The following results were obtained:

Inlet water temperature = 295K
Outlet water temperature = 299K
Flow rate = 0.002m^3/s
Power absorbed at nozzle tip = 35kW
Surface area of coolant passage = 0.0017m^2
Measured power density = 20.5MW/m^2
Cross sectional area of coolant passage at nozzle tip = 0.00019m^2
Water velocity = 10.5 m/sec
Coolant pressure at nozzle tip = 7 bar
Boiling point of water at 7 bar = 441K
Maximum temperature drop across film = 142K
Critical power density = 10MW/m^2

Although the measured power density of 20.5MW/m^2 still exceeded the critical power density of 10MW/m^2, the modifications to the nozzle tip increased its life from 30 hours to about 70 hours.

5.4.6 Plasma Gas

Argon gas was passed through the annulus formed between the nozzle and the cathode to produce an electrically conductive ionized gas stream to stabilize the arc, to protect the cathode from attack by the furnace atmosphere, slag and metal splashes and to cool the cathode by the endothermic dissociation of the gas. The required gas flow rate was 0.0004-0.0006 m^3/s of argon per 1kA.

5.4.7 Torch Movement

The plasma arc length (and voltage) could be altered by withdrawing the torch through a water-cooled spherical bearing assembly mounted in the furnace roof. The torch precessed at a variable angle of 0-15 degrees from the vertical axis and at a rotational speed of 30 rpm to distribute the plasma arc energy evenly over the melt surface. With the torch fully lowered, the arc length (to the hearth) was 0.4m and the precession circle diameter was 0.5m. With the torch fully raised, the arc length increased to 1.0m and the precession circle diameter decreased to 0.2m.

5.5 THE PLASMA POWER SOURCE

The D.C. power source was a fully phase controlled, 24 pulse thyristor rectifier unit in 2 bridge pairs which could be connected in series or parallel for high voltage or high current operation. Off-load tap changing on the primary winding of the transformer was used to set the open circuit voltage near to the voltage requirement for the particular process to maximize the power factor. Because the plasma arc has a very low inductance, short circuit protection and ripple control was provided by a series DC reactance.

The plasma arc was initiated by a high-frequency, high-voltage spark between the cathode tip and the nozzle. The subsequent 200A pilot arc produced between the cathode and the front face of the nozzle was transferred directly to the melt or to a temporary hand held carbon electrode held 0.05m below the plasma torch and subsequently lowered to the melt surface. Arc initiation, power source control and protection circuits were controlled by a programmable logic computer (PLC).

To detect unwanted current leakage paths and protect the torch from destructive 'side arcs', the torch frame, furnace roof, furnace shell and anode were all electrically isolated from each other and earthed via individual current detecting transformers which tripped the power source if the leakage current exceeded a set value, typically 200A.

5.6 INSTRUMENTATION

Arc Characteristics

The plasma Arc amperes were measured to an accuracy of +/-2% at 3kA by a current transformer located in the anode cabling. The anode amps were intermittently checked using a hand held "clip on" ammeter. The "plasma arc" voltage was measured to an accuracy of +/-2.5% at 300V. The "plasma arc" power was calculated by the PLC by multiplying the instantaneous arc amps and volts. Because of the slight fluctuations in the arc amps and volts, the kW recording was subject to an instantaneous error of +/-5% at 1 MW. The energy consumed was calculated to an accuracy of +/- 5% by integrating the power input over a time base.

Argon Gas Consumption

The consumption of argon plasma gas was monitored and controlled using calibrated rotameters.

Water Cooling

All return water flows were monitored using rotameters to an accuracy of +/-5%. Matched pairs of Cu-constantan thermocouples were located in the flow and return of every cooling water circuit to compute temperature differentials. The Cu-constantan thermocouples and associated chart recorder were calibrated before and after each trial using a mercury-in-glass thermometer. Accuracies of the matched pairs of thermocouples was +/-0.5K. Water flow, pressure and temperature alarms interfaced with the PLC to shut down the power source in the event of a water circuit malfunction.

Thermocouples

Pt-Pt/13% Rh thermocouples were located in the refractories to monitor the condition of the side walls at the slag line, the roof, and the anode. The thermocouples were generally located in groups of three to measure a temperature profile across the refractories and predict a hot face temperature and refractory thickness. Cu-constantan thermocouples were welded to the steel shell to monitor the shell temperature for computation of convective and radiation heat losses. Chromel-Alumel thermocouples were positioned in the exhaust gas and baghouse system to monitor the exhaust gas temperature. A port in the furnace sidewalls was provided for the measurement of the bath temperature using a Land disposable Pt-Pt/13% Rh immersion thermocouple. The accuracy of the Pt-Pt/13% Rh and the Chromel-Alumel thermocouples was reported as +/-2K by the manufacturer and their resolution on the chart recorders was +/-5K.

Furnace pressure

A pressure transducer mounted on the inspection port door monitored the furnace pressure. A slightly positive furnace pressure (+0.001 bar) was maintained by varying the position of the butterfly valve immediately in front of the induced draught fan.

Raw Materials And Product Weights

All raw materials and product were weighed on a weighbridge to an accuracy of +/-2% The weighbridge was calibrated before and after the trials.

6.0 EXPERIMENTAL PROCEDURE

6.1 EXPERIMENTAL PLAN

Four trials of one week duration were conducted:

In trial week A, 15 t of chromite concentrates were smelted to produce a charge grade carbon ferrochrome.

In trial week B, alloy steel dust was smelted to recover the Cr, Ni and Mo to a ferroalloy for recycling to the arc furnace.

In trial week C, a low ZnO content EAF dust from Templeborough Steel and a medium ZnO content dust from Sheerness steel were smelted under totally reducing conditions to produce a non-toxic slag and recover the zinc and lead values to an enriched zinc oxide baghouse dust.

In trial week D, high ZnO content EAF dusts from Tremorfa Steel and Irish Steel were smelted under selectively reducing conditions to produce a non-toxic slag and recover the zinc and lead values to an enriched zinc oxide baghouse dust.

The dusts were selected to include a range of ZnO, PbO, Cr_2O_3 and CaO contents to determine the effect of dust composition on slag toxicity, product analyses, energy consumption, furnace operation and treatment economics.

6.2 RAW MATERIALS

The majority of the chromite and dusts were smelted in the "as received" form. A proportion of the Irish steel and Sheerness EAF dusts were pelletized with approximately 10% moisture in a concrete mixer. No binders were necessary to produce green pellets up to 0.01m in diameter which would support a 0.025t load. Drying the pellets at 400K in a gas fired rotary drier increased the pellet strength to 0.075t breaking load. Pellets were sieved through a 0.002m screen and the undersize returned to the pelletizer. Feeder tests showed that passing the pellets through the furnace feed system produced about 10% of <0.002m material.

An anthracitic coal containing 81% fixed carbon, 9% ash and 10% volatile matter was chosen as the reductant because of its high reactivity, low ash and low sulphur contents. The coal contained 5% moisture and had a particle size of <0.05m. Silica sand containing 98% SiO_2 and lime containing 96% CaO were used as fluxes.

The blend of chromite or steelplant dust, reductant and fluxes was calculated using the mass and energy balance model presented in Appendix 1. In the chromite smelting trial (A), the effect of slag composition and degree of reduction on chromium recovery were investigated by varying the sand/chromite and the anthracite/chromite ratios. In the steelplant dust trials (B, C and D), the coal addition was varied to determine the effect of degree of reduction on product analyses, slag toxicity and smelting energy consumption.

6.3 FURNACE OPERATION

The furnace refractories were dried out and preheated to 1100K at 20K/h using a 100kW natural gas burner. After soaking, the gas burner was replaced by the plasma torch arcing to a coke bed and the furnace was brought up to the operating temperature of 1700K over 24 hours. Once thermal equilibrium was attained, the energy losses from furnace were determined by measuring the total energy input and comparing it to the total energy losses from the various parts of the furnace. Feeding was started at a low rate of 0.1t/hour and gradually increased to the desired rate over several hours.

The primary operating aim was the maintenance of a constant melt temperature, high uninterrupted feed rates and a minimum power input so that meaningful mass and energy balance data could be obtained. For each feed blend, a feed rate-power input relationship based on the smelting energy requirements of the feed material and the steady state energy losses from the furnace was generated by the thermodynamic mass and energy balance model. As the feed rate varied, the operator adjusted the power input (arc current) to maintain a constant melt temperature. The accuracy of the feed rate-power input relationship was checked by measuring melt temperature over a time period and observing any deviations from the predicted value.

The energy losses were periodically checked by measuring the total energy input to the furnace to maintain the bath at a constant temperature and/or measuring the total water-cooling, convective and radiation losses from the shell.

During trial week A, feed was processed between 06-00 and 22-00 hours only because of shortage of manpower. Between 22-00 and 06-00 hours the furnace was maintained at 1700K using a carbon electrode arcing to the bath. In subsequent trials, the furnace was operated continuously, 24 hours per day. Tap temperatures were generally in the range 1723-1798K when continuous, uninterrupted feeding was practised, but processing delays upset the energy balance predictions and often resulted in temperature excursions. The feed rate to the furnace varied between 0.2-0.7t/hour and was limited by the capacity of the baghouse. The furnace was tapped when approximately 1t of feed had been consumed.

The feed ports in the furnace roof occasionally blocked up with sintered feed and required rodding out at least once per shift. In the event of a plasma torch failure, the power and feed were immediately stopped, maximum suction applied to the furnace and the torch removed. Exchanging the torch took about 30 minutes.

The furnace pressure was kept slightly positive to minimize the ingress of air by adjusting the baghouse fan damper. The baghouse inlet gas temperature was maintained at 400-650K by altering the position of the dilution air damper in the base of the combustion chamber. The two baghouses were operated with one on-line and one off-line for cleaning and were emptied and sampled every time the furnace was tapped. The horizontal exhaust duct from the furnace to the combustion chamber was rodded on every shift to remove the build up of loose slag and ZnO. During trial week D, the exhaust duct was completely blocked by a foaming slag, requiring the furnace to be brought off-line for several days for a clean out. Several of the filter envelopes in the baghouse ruptured during the trials, allowing dust to escape to the downstream scrubbing tower.

6.4 SAMPLING

The raw materials were sampled by taking approximately twenty 0.5kg grab samples from the homogenized pile of raw materials, mixing the resultant conglomerate sample and splitting it down in successive stages to 0.2kg. The lack of perfect homogenization of the feed and the grab sampling of the pile introduced an unquantified error into the analytical results. Four spoon samples of metal and slag were taken at intervals from each tapping stream and composited. For the EPA toxicity test, a representative 0.2t bulk sample was taken from the cooled tap slag and reduced to 0.002t. The baghouse dust from each tap was sampled by taking four tube samples from the dust receiving hopper. The furnace exhaust gases were sampled from the exhaust duct immediately after the furnace using a stainless steel probe and a vacuum pump to transfer the sample to a gas burette for analysis by gas chromatography. Zinc often condensed inside the probe and blocked it before a sufficient volume of sample could be obtained.

Full analyses of all raw materials and condensed products were carried out on a historical basis by the British Steel Corporation, Swinden Laboratories using X-ray fluoroscopy for oxides, Leco combustion in oxygen for C and S and atomic absorption for CdO, PbO and halogens. The Environmental Protection Agencies Toxicity Tests (EPTox) were made by the Bethlehem Steel Corporations' Homer Research Laboratories in Bethlehem, USA.

6.5 DATA COLLECTION

The weight of feed material consumed per tap was determined from the loss in weight of the furnace feed hopper and by counting the number of bags of preweighed feed that were consumed. Approximately 2% of the feed material was lost as spillage in bag handling, loading to the feed system and clearing blockages in the feed conveyors. At the end of a trial, the feed system was emptied and the residual feed subtracted from the total consumed. The metal, slag and baghouse dust weights were recorded on an individual tap basis to an accuracy of +/-2%. Emptying the slag/metal boxes resulted in an estimated spillage of 2% of the contents weight. At the end of a trial, the furnace roof was removed and a crude estimate of the residual slag and metal in the furnace was made by drilling and measuring the heel. The duct work and baghouse filter were cleaned down as far as practically possible, but it was conceivable that as much as 5% of the total baghouse dust was unrecovered. The estimated trial mass balance accuracy is +/-10%.

All significant changes in operating variables, events and delays longer than 2 minutes in duration were recorded in a log book. A data logger printed out the plasma arc current, voltage, power, kWh, feed rate and cumulative feed weight consumed, at 2 minute intervals.

An energy balance was calculated around the furnace at 30 minute intervals by measuring the total power input, the water flows to all cooling circuits, the inlet and outlet temperatures of the coolant water and the temperature of the furnace shell. In the initial trials, the thermocouples and chart recorder were accurate to +/-1K, but high resolution thermocouples and a digital thermocouple readout were used in the later trials to improve the accuracy and resolution to +/-0.2K.

The dimensions of the refractory working lining were measured before and after each trial to determine the rate of refractory corrosion.

7.0 RESULTS

The results for the chromite, alloy dust and EAF dust smelting trials are broadly categorised into;

- raw material analyses
- metal analyses
- slag analyses
- baghouse dust analyses
- plant operation
- mass balance
- energy consumption

7.1 CHROMITE SMELTING RESULTS

7.1.1 Raw Materials

The chromite raw materials analyses are given in Table 7 and the feed blends used are given in Table 8. Taps A/1 to A/16 examined the effect of slag composition on chromium recovery by varying the sand/chromite ratio from 0.14 to 0.18. Taps A/17 to A/21 examined the effect of degree of reduction on chromium recovery to the ferroalloy by varying the anthracite/chromite ratio from 0.24 to 0.31.

7.1.2 Ferrochrome Metal Analyses

Ferroalloy, slag and baghouse dust samples were analysed by the BSC Swinden laboratories and the results are presented in Table 8. Selected samples were analysed by the London and Scandanavian Metallurgical Co., Ltd (LSM) and these results are given in Table 9. The chromium analyses from BSC were generally 2-3% higher than the LSM results, but no explanation for the difference is offered, as the laboratories used a similar analytical technique. The reported alloy silicon, carbon, phosphorus and sulphur contents from both laboratories were in acceptable agreement.

If taps A/1 to A/5, where the ferrochrome was diluted by the metal heel remaining from a previous trial are ignored, an acceptable charge grade ferrochrome containing 50-57% Cr, 6.0-7.1% C, 1-4% Si, 0.03-0.04% P and 0.03-0.08% S was produced.

Figure 38 shows that, although the alloy chromium content varied between 49.6% and 57.2% (BSC analyses), there was no significant relationship between alloy chromium content and the tapping temperature or the anthracite/chromite ratio. An increase in alloy chromium content might be expected with increasing reductant addition as more Cr_2O_3 was reduced from the slag, but the relationship was probably masked by the increase in alloy silicon content.

Figure 39 shows the increase in the alloy silicon content from <1% to 4.6% as the tap temperature increased from 1700K to 1950K and the anthracite/chromite ratio increased from 0.27 to 0.31. The sand/chromite ratio in the blend had no significant effect on alloy silicon content. The increase in alloy silicon content with increasing temperature and reductant is to be expected because SiO_2 has a similar free energy of reduction to Cr_2O_3.

Figure 40 shows the slight decrease in ferroalloy carbon content from 7.1% to 6.7% as the melt temperature increased from 1700K to 1950K. The alloy carbon content was independent of the anthracite/chromite ratio and the silica/chromite ratio. It is not apparent from the limited results whether the decrease in carbon content with increasing temperature was due to dilution by the increasing silicon content of the ferroalloy (see figure 39) or to the increasing thermodynamic stability of lower carbon chromium carbides with increasing temperature.

Figure 41 illustrates the decrease in alloy sulphur content from about 0.06% S to 0.04% S as the slag basicity ($CaO+MgO/SiO_2$) increased from 0.8 to 1.3. The alloy sulphur content appears to decrease with increasing anthracite/chromite ratio and tapping temperature, but this is probably a reflection of the higher slag basicity associated with the reduction of silica from the slag.

The ferrochrome phosphorus content of 0.03-0.04% was independent of anthracite/chromite ratio, slag basicity and tap temperature over the range examined. To meet the alloy phosphorus specification, low phosphorus content reductant and fluxes must be selected.

7.1.3 Ferrochrome Slag Analyses

The ferrochrome slag analyses presented in Table 9 ranged from 23-36% SiO_2, 4-8% CaO, 21-37% MgO, 22-34% Al_2O_3, 1-5% FeO and 2-10% Cr_2O_3 and are shown superimposed on the SiO_2-MgO-Al_2O_3 liquidus diagram in Figure 26. There was considerable variation in slag chemistry in Taps A/4 to A/12, despite the constant sand/chromite and reductant/chromite ratios because of variations in the melt temperature, SiO_2 reduction and MgO pickup from the refractory lining.

Taps A/1, A/3, A/3, A/13 and A/14 with a high anthracite/chromite ratio of 0.31 and a low sand/chromite ratio of 0.14 were difficult to tap because of a high slag liquidus temperature associated with a low slag SiO_2 content. The tapping problem was resolved by increasing the sand/chromite ratio from 0.14 to 0.16-0.18 to increase the slag SiO_2 content to30% and decrease the slag liquidus temperature to 1700K. For a constant sand/chromite ratio of 0.185 in Taps A/16 to A/21, the SiO_2 in the slag decreased from 36-38% to 26-28% as the anthracite/chromite ratio increased from 0.24 to 0.31 and more silica was carbothermically reduced from the slag.

Figure 42 shows the expected decrease in the chromium oxide in the slag as the anthracite/chromite ratio increased. Increasing the sand/chromite ratio marginally decreased the chromium oxide content in the slag, probably by decreasing the slag liquidus temperature and enhancing the chromite dissolution. Figure 43 shows the decrease in chromium oxide content with increasing slag MgO/Al_2O_3 ratio, probably as a result of the decreased slag viscosity. The variation in MgO/Al_2O_3 ratio was not deliberate, but a result of MgO pickup from the furnace refractories.

It was difficult to determine the independent effect of process variables on, for example, the chromium oxide content of the slag because most variables were interdependent. Increasing the tap temperature increases the driving force for the reaction, but also increases the amount of silica reduced and the slag basicity. Increasing the tap temperature also increases the amount of MgO corroded from the refractory lining and increases the MgO/Al_2O_3 ratio.

7.1.4 Ferrochrome Baghouse Dust Composition

The baghouse dust contained 4% Cr_2O_3, which represents an acceptable loss of <1% Cr_2O_3 charged to the furnace. The dust was enriched in SiO_2 and MgO relative to the feed composition because SiO_2 and MgO are probably reduced to the volatile subspecies SiO and Mg at the elevated temperatures and reducing conditions existing in the melt.

OXIDE	THEORETICAL ANALYSIS mass%	ACTUAL ANALYSIS mass%
SiO_2	21.6	24.8-30.8
CaO	3.7	4.5- 4.5
MgO	11.9	39.3-41.0
Al_2O_3	11.8	3.1- 4.1
Fe_2O_3	18.8	4.7- 4.7
Cr_2O_3	29.2	3.9- 4.6

7.1.5 Gas Analysis

Gas sampling was difficult because the sampling point in the exhaust duct continually blocked up, making it impossible to obtain good samples. The average of 4 results was 50% CO, 5.8% CO_2, 24% H_2, 20% N_2 and 0.2% O_2, suggesting that air was leaking into the system. The high H_2 content of the gas was produced from the volatile matter content of the coal and the reaction between H_2O in the feed and carbon.

7.1.6 Chromite Smelting Mass Balance

Table 10 shows the distribution of oxides between the condensed phases after estimating the weight of the initial metal heel to be 0.6t +/-0.3t (95% Fe, 0% Cr) and the final heel to be 0.7t +/-0.3t (28% Fe, 54% Cr). A total of 14.9t of chromite was consumed producing 6.4t of alloy, 9.1t of slag and 0.8t of baghouse dust. Single tap mass balances were not calculated because the retention of metal and slag in the furnace from one tap to the next and the experimental nature of the trial made them relatively meaningless. A completely closed trial mass balance was not possible because the exhaust gas mass was not measured.

91.4% of the chromium in the feed reported to the alloy, 8.2% to the slag and 0.7% to the baghouse dust, giving an acceptable accountability of 100.3%. The chromium recovery to the alloy improved to 93% during taps A/5-A/11 with constant operating conditions at an anthracite/chromite ratio of >0.3 and a sand/chromite ratio of >0.16.

90.9% of the iron charged to the furnace reported to the alloy, 6.1% to the slag and 1.2% to the baghouse dust, giving an acceptable trial accountability of 98.2%.

8.3% of the silica was reduced to silicon and dissolved in the alloy, 7.1% reported to the baghouse dust and 84.4% reported to the slag, giving a trial accountability of 99.8%. Allowance must be made for the SiO_2 losses from the slag when calculating the charge composition, otherwise high liquidus temperature slags will be produced.

The high MgO accountablity of 140% was a result of the corrosion of approximately 1.2t of MgO refractory by the siliceous slag. 16.7% of the MgO charged to the furnace reported to the baghouse dust, probably by the reduction of MgO in the slag to Mg vapour, which was reoxidized in the combustion chamber and collected in the baghouse. The carbothermic reduction of MgO and SiO_2 from the slag alters the slag composition and significantly increases both the reductant and energy consumptions.

7.1.7 Furnace Operation

The furnace operating parameters for individual taps are summarized in Table 11. Blend feed rates were limited to 0.35-0.4t/hr by the power available from the power source (0.64MW at 1.6kA and 400V) and the capacity of the baghouse filter. The overall feed processing time was 96 hours out of a possible 106 hours, representing a process availablity of 93% which is good for a small pilot plant operation and would suggest that high availablities can be expected in a commercial design. Delays were mainly due to power source thermal overloads, feeder blockages, torch failures, tapping difficulties and roof refractory maintenance. 5 torch failures occurred due to local overheating of the cathode and nozzle tips and short circuit arcing between the nozzle and the furnace refractories. The torch design was modified to increase the water velocity at the torch tip and high pressure water pumps were installed as described in section 5.4.

Short circuit arcing was reduced by improving the torch head bearing insulation and operating at shorter arc lengths and lower arc voltages.

Difficulties in tapping the high liquidus temperature slag experienced at the beginning of the trial were overcome by increasing the power input and increasing the sand/chromite ratio to lower the slag liquidus temperature.

Tapping temperatures were variable and generally lower than the desired 1873K because the furnace was under-powered at the beginning of the trial when its operating characteristics were being determined. The non-continuous, 16 hours/day furnace operation led to significant departures from thermal equilibrium, especially at the beginning of each day.

7.1.8 Refractory Life

Mass balance and visual observations suggest that 1.1-1.2t of refractory were corroded from the slag line region during the testwork, corresponding to nearly 10% of the original refractory mass or 50% of the slag line refractory mass. This was an extremely high refractory consumption compared to conventional submerged arc furnaces, which have a refractory life of about 5 years. Factors contributing to the refractory wear were the small furnace size, the absence of any protective feed/frozen slag banks near the sidewalls and the use of mag-chrome refractories with a siliceous slag. Carbon, mag-carbon or straight magnesia refractories in a larger furnace shell and cooling at the slag line may be a superior refractory system. The feed ports in the furnace roof should be moved out towards the sidewalls to encourage the formation of a bank of unreacted feed against the sidewalls.

7.1.9 Chromite Smelting Energy Balance

The gross energy consumption for each tap is given in Table 11 and Figure 44. The average gross energy consumption was 6.96MWh/t of alloy, but there is a very wide scatter in the data because of variable feed rates, delays and difficulty in allocating the weight of alloy tapped to a particular tap. If the second period of the trial (Taps A/13-A/21), when the furnace operation was smoother and the operating delays were less frequent is considered, the average energy consumption drops to about 6.48MWh/t of alloy.

The average energy losses from the furnace were 160kW and are itemized in Table 12. The energy losses are high because of the small unit size, the water-cooled electrode and the fully exposed roof and sidewalls.

7.1.10 Summary of Chromite Smelting Results

An in-specification charge grade ferrochrome containing 52-54% Cr, 6-7% C, 1-3% Si, <0.04% S and <0.04% P was produced by smelting chromite concentrate in the transferred-arc plasma furnace.

Fine chromite concentrates were smelted directly without any furnace operating problems or excessive feed carry over with the exhaust gases. Anthracitic coal was successfully used as the reductant.

Chromium partitioned 87-93% to the ferroalloy, 4-6% to the slag and 1% to the baghouse dust.

For maximum Cr recovery to the ferrochrome, an anthracite/chromite ratio of 0.31, a sand/chromite ratio of >0.16 and a magnesia/alumina ratio of >1.6 is required.

The gross smelting energy consumption was 6.5-7.0MWh/t of alloy, suggesting a commercial value as low as 4.5MWh/t with dry feed.

Furnace processing availablity was 93% of the time available, suggesting an availability of around 95% for a commercial plant. Plasma torch life was improved from 30 hours to 70 hours by increasing the water flow to the nozzle and cathode and redesigning the torch water passages. Refractory corrosion of the magnesia chrome bricks at the slag line was severe.

7.2 STEELPLANT DUST SMELTING RESULTS

7.2.1 Dust Analyses

Table 13 presents the composition of the five dusts used in the smelting trials. To determine the variation in analytical results between laboratories, an identical dust sample was distributed to 5 independent laboratories and the results are listed below:

LABORATORY	DUST COMPOSITION, %		
	ZnO	PbO	Fe_2O_3
BSC	31.1	4.9	31.1
ARMCO	30.5	5.1	34.4
INLAND	29.9	5.1	37.9
LTV	30.7	5.3	40.7
St. JOE	32.9	5.4	40.8

The variation in iron oxide analysis has implications on reductant consumption, energy consumption and process costings. Further analyses and a comparison of analytical techniques is suggested to highlight the source of error.

To determine the day to day variation in dust analyses from a given steelplant plant, eight Tremorfa dusts samples were analysed and the results are presented in Table 14. The variation in the iron and zinc oxide content of the dust is sufficient to cause fluctuations in the slag ZnO and FeO content for a given reductant and energy. The peak in the dust fluorine content would cause dross formation problems in a zinc condenser.

7.2.2 Feed Composition

The feed compositions used in the trials are presented in Tables 15-17. The coal addition to the alloy steel dust was maintained at the stoichiometric requirement to totally reduce all the alloy oxides to a ferroalloy. The coal addition to the EAF dusts was varied between 0.1 and 0.25t/t to investigate the merits of selective reduction of the ZnO, leaving the FeO in the slag. A small silica flux addition was blended with the dusts to produce a CaO/SiO_2 ratio of 0.8-1.0, a slag liquidus temperature of 1723K and a slag viscosity of <5 centipoise.

7.2.3 Metal Analyses

The total carbothermic reduction of the AOD dust produced 0.45t of ferroalloy/t of dust smelted. The ferroalloy contained 58-68% Fe, 17-22% Cr, 5-7% Ni, 2.0-2.5% Mo, 4-6% C, 0-4% Si, 0.04-0.1% S and 0.05-0.075% P, which was in reasonable agreement with the model prediction of 58% Fe, 21% Cr, 5.5% Ni, 2.4% Mo and 4.3% C, calculated assuming 100% recovery of the metal oxides to the ferroalloy.

The iron alloy produced from the reduction of the EAF dusts contained 95.0-97.0% Fe, 0.5-3.0% C, 0.1-2.0% Si, 0.1-0.7% S, 0.2-0.7% P and 0.5-1.0% Cu. The carbon level in the iron was lower than blast furnace pig iron because of the higher oxygen potential in the slag associated with the selective reduction of ZnO. Both the carbon and sulphur in the iron increased as the coal adition increased. The majority of the phosphorus, copper and tramp elements in the dust were recovered to the iron, reducing its value as scrap for recycling to the EAF.

7.2.4 Slag Analyses

The slag analyses produced from smelting steelplant dust are shown superimposed on the $CaO-SiO_2-FeO$ liquidus diagram in Figure 31. Slag analyses were consistent with the dust composition and reductant addition rate except for the early slags in Trial C, where the high chromium oxide content was a result of pickup from the chromium rich metal heel remaining in the furnace after treating alloy steel dust.

The Effect of Degree of Reduction on Slag Composition

The effect of coal addition on the residual ZnO, Cr_2O_3 and FeO content in the slag is illustrated in Figures 45, 46 and 47 respectively. In the total reduction mode (using a stoichiometric coal addition), the residual FeO, ZnO, Cr_2O_3, PbO and CdO in the slag were reduced to <0.5%, <0.2%, <1.0%, <0.2% and <0.2% respectively. In the selective reduction mode using a coal addition rate of around 0.15t/t dust, the ZnO, PbO and CdO in the slag were reduced to <1.0%, <0.2% and <0.2% respectively, leaving about 2% Cr_2O_3 and 30-50% FeO unreduced in the slag. Because very little chromium oxide is reduced in the selective reduction mode, steelplant dust containing >0.5% chromium oxide must be smelted under more reducing conditions to produce a non-toxic slag containing <1% chromium oxide.

Slags containing around 50% FeO were prone to foaming, but this could be avoided by adjusting the reductant addition to maintain <50% FeO in the slag or increasing the slag temperature.

The Effect of Slag Basicity on the Residual ZnO in the Slag

No relationship between slag CaO/SiO_2 ratio and the ZnO, PbO and CdO content of the slag could be determined because the metal oxide content of the slag was <0.2%,the detection limit of the XRF analysis technique. Slag basicity will have a more pronounced effect at lower melt temperatures where the changes in the zinc oxide activity coefficient with slag compostion are larger.

7.2.5 Baghouse Dust Analyses produced from Smelting Steelplant Dusts

Smelting ZnO rich EAF dusts produced a baghouse dust containing 60-75% ZnO, 5-10% PbO, 3-6% K_2O, 3-6% Na_2O, 5-10% Cl and 5-10% F, whereas smelting alloy steel dusts produced a baghouse dust containing 34-54% ZnO, 4-6% PbO, 5-17% Fe_2O_3, 1-3% Cr_2O_3 and 2-3% K_2O.

The Effect of Steelplant Dust Composition on Baghouse Dust Analysis

The majority of the ZnO, PbO, CdO, K_2O, Na_2O, F and Cl in the steelplant dusts were reduced, volatilized, reoxidized and recovered to the baghouse dust, limiting the ZnO content of the baghouse dust to about 80% by contamination. Figure 48 shows that the % ZnO in the baghouse dust increased as the % ZnO in the steelplant dust increased because of the mass concentration effect and dusts high in zinc oxide (low in iron oxide) produce a smaller gas volume than dusts with a low zinc (high iron oxide) content, reducing the particulate carry over. The same effect is seen in Figure 49, where the iron oxide in the baghouse dust increased with increasing iron oxide content in the steelplant dust.

The Effect of the Degree of Reduction of the Steelplant Dust on the Baghouse Dust Analysis

Figures 50 and 51 show the slight decrease in ZnO and the rapid increase in the Fe_2O_3 content of the baghouse dust with increasing coal addition rate. The sudden increase in the iron oxide content of the baghouse dust with near stoichiometric reductant additions to the steelplant dust may be due to the increased feed carry over with larger exhaust gas volume and the formation of iron vapour or a volatile complex species under the hot, reducing conditions at the arc/melt interface.

The increase in gangue oxides carried over to the baghouse with increasing coal addition is probably a result of the increased exhaust gas volume and the reduction and volatilization of SiO_2 and MgO at the high temperature plasma arc/slag interface. Insufficient data was available to determine the independent effect of feed rate (and therefore exhaust gas velocity) on the degree of feed carry over.

The Effect of Agglomerating the Steelplant Dust on Baghouse Dust Analysis

There was no apparent difference in the % ZnO and % Fe_2O_3 in the baghouse dust produced from a limited number of taps using Sheerness dust or pellets. The lack of benefit from agglomeration may be due to the pellets degrading in passage through the screw feeders to the furnace, or disintegrating on entering the furnace through thermal shock and rapid expansion.

7.2.6 Slag Toxicity

The results of the EPA Toxicity Test are compared to the 6 times the drinking water standard in Table 18. All the slags tested passed the EPTT test. Pb and Cd in the leachate were below the detection limits of the analyser, but the Cr levels were variable and did not relate to the "Cr_2O_3" levels in the slag. The leaching characteristics of the slag require further investigation, but are probably affected by the slag chemistry, mineralogy, cooling rate and particle size.

7.2.7 Steelplant Dusts Mass Balance and Distribution of Elements Between the Condensed Phases

Table 19 presents the distribution of the oxides between the condensed phases. The total accountablity of the oxides was only 90%, probably because of spillages and losses from the feed blending and product handling system, unrecovered dust from the inaccessible sections of the exhaust gas ductwork and baghouse filters, several ruptured baghouse filter envelopes and retained Fe, Cr, Ni in the metallic heel below the furnace taphole level.

The recovery of the Fe_2O_3, Cr_2O_3, NiO and MoO_3 from the alloy steel dust to the ferroalloy was 90.7%, 84%, 94% and 86% respectively. Less than 5% of the alloy oxides reported to the slag and baghouse dust, suggesting that recoveries to the ferroalloy in a commercial operation with a sealed feed and product handling system may exceed 95%.

The recovery of ZnO, CdO and PbO from the EAF dust to the baghouse dust was about 90%. Less than 0.2% ZnO, PbO and CdO were retained in the slag phase, suggesting that in a prolonged steady state operation, the recoveries to the baghouse filter should approach 99.0%.

7.2.8 Equipment Operation and Availablity

The tap to tap time, feed processing time and power on time are presented on a tap-to-tap basis in Tables 20-22 and are summarized below:

TRIAL No	FEED AVAILABLITY %	PLASMA AVAILABLITY %
B Alloy dust	74	85
C EAF dust	71	96
D EAF dust	81	87

The Feed System Operation

The feed processing availablity during the trials averaged 75%, which considering the development nature of the trials and the difficult handling properties of the dust, is a reasonable result. Delays were mainly associated with the poor flow characteristics and sintering of the EAF and Alloy steel dusts in the feed system. Problems with EAF and Alloy steel dusts bridging in the furnace feed hopper were reduced by building a larger feed hopper incorporating a "live bottom" with large diameter screws and a horizontal agitator to keep the dust in motion. Transfer screw blockages were overcome by increasing the diameter and torque of the transfer screws, sieving the feed to remove oversize particles, modifying the screw flight at the feed discharge end to prevent feed compaction against the end face of the screw casing and water-cooling the end face of the screw casing adjacent to the furnace feed port to prevent feed sintering. The roof feed ports were increased in size and fitted with a disposable refractory liner to reduce the impact of accretion build up.

The Exhaust System

The horizontal exhaust duct between the furnace and the combustion chamber required cleaning about every 8 hours to remove dry drop-out material and slag splash. During the selective reduction of the Templeborough dust, a foaming slag flowed into the duct and almost completely blocked it, resulting in an extended delay to clear the duct. A roof mounted exhaust is recommended to reduce the effect of slag splash and to facilitate the rebricking of the furnace sidewalls. An expansion box or drop out chamber in the exhaust duct to remove the coarser particles should be considered. The high level of dust and slag carry over would probably cause excessive dross build up if a zinc condenser was built into the exhaust system. The cyclone used in the Sheerness and Templeborough dust trials captured relatively little of the dust, but acted as a heat exchanger, lowering the gas temperature entering the baghouse. Problems were encountered with the baghouse during the early trials when the reverse jet air pressure was set too low to dislodge the filter cake from the filter envelopes. The large pressure drop across the baghouse resulted in a lack of suction and low cooling air flows to the combustion chamber. Increasing the air pressure cleaned the envelopes but caused them to split along the seam until a restraining cage was fitted to limit their flexing. Throughout the trials, the baghouse has been one of the major factors limiting furnace productivity.

The Plasma System

The plasma torch operated at around 1MW (3kA, 350V) during the trials. The individual torch lives, in hours, are detailed below:

12, 37, 14, >15, 10, >50, 24, 12, 31, 43, >5, 11, 61, 2, >34

The >34 hours signifies that the torch was still serviceable at the end of a trial. Torch life was limited by the rapid erosion of the nozzle front face, probably by stray arcs running continuously from the cathode to the nozzle to the furnace roof and up the sintered feed in the feed ports to the earthed steel roof.

The stray arcs were consistent with the detection of current in the steel shell and the large number of earth leakage trips which occurred, especially when the furnace was working under a positive pressure. These trips were usually stopped by cleaning the conductive deposits from the torch, feed and the exhaust ports and by doubling the gas flow to the torch. Despite the short torch life, the plasma system availablity was 85-95% of the time available. Modifying the water passages in the torch nozzle and increasing the water cooling pump capacity increased the torch life to around 70 hours in later trials. Coating the nozzle with an insulating refractory, enamel, boron nitride etc may reduce the arcing from the nozzle. Alternatively, the front face of the nozzle could be coated with tungsten or molybdenum to reduce the arc erosion rate.

7.2.9 Plasma Arc Characteristics

The plasma arc voltage was 330-380V at 2.5kA-3kA with an arc length 0.3m when feeding steelplant dust. All the steelplant dusts gave approximately the same arc voltage for a given arc length and current. Increasing the arc length increased the arc voltage, but also increased the potential for short circuit arcing between the nozzle and the roof, resulting in a water leak from the torch.

7.2.10 Energy Consumption

The gross energy consumption and the energy losses for the individual taps are presented in Tables 20-22 and shown in Figure 52. The gross smelting energy consumptions ranged from 1.5 to 5.0 MWh/t dust. The overriding effect of the speed of working masked any correlation between gross energy consumption and coal addition or dust analysis. At a feed rate of 1t/hour, the gross energy consumption should be about 1.5MWh/t of dust for selective reduction and 1.7MWh/t of dust for total reduction.

The furnace losses ranged from 0.20-0.29MW because of variations in the melt temperature and build up of feed on the furnace walls. The three dominant losses were the sidewall cooling sprays, the water-cooled roof panel and the plasma torch. At a power input of 1.0 MW, with total losses of 0.29 MW, the conversion of electrical energy to useful thermal energy was about 71%.

7.2.11 Summary Of The Steelplant Dusts Results

Five different dust compositions were smelted under different degrees of reduction.

Total reduction of the alloy steel dust recovered the majority of the alloy elements to a saleable ferroalloy.

Selective reduction of the EAF dust was a viable means of eliminating the majority of the ZnO, CdO and PbO from the slag to produce a non-toxic slag.

Dusts containing >0.5% Cr_2O_3 must be totally reduced to meet the slag toxicity test requirements.

A baghouse dust containing 85% ZnO and PbO was produced from steelplant dusts containing >15% ZnO.

Agglomerating the feed had little effect upon the ZnO baghouse dust quality.

The impurity content in the ZnO baghouse dust increased with increasing degrees of reduction and Fe_2O_3 content in the steelplant dust. The majority of the halogens and alkalies in the dust reported to baghouse dust.

Accountablity of the oxides to the condensed phases was only 90% because of losses from the system. In excess of 85% of the Cr, Ni and Mo units in the Alloy steel dust were recovered to a ferroalloy.

Plant availablity was initially poor due to problems with the plasma torch, feed system and baghouses. As the trials progressed and modifications were made to the equipment the availablity improved to 80%.

The minimum total energy requirement for the reduction of EAF or alloy steel dust was about 1.5 MWh/t at a feed rate of 1.0 t/hour. Feed composition and partial reduction of the dust had no measurable effect on the energy consumption.

8.0 DISCUSSION

The section examines the metallurgical results of the testwork, the design of the open bath plasma reactor and evaluates the economics of smelting chromites and steelplant dusts. Finally, an assessment of the potential of plasma processes is presented.

8.1 CHROMITE SMELTING IN THE TRANSFERRED ARC/OPEN BATH REACTOR

8.1.1 Raw Materials

The transferred arc/open bath plasma reactor was successfully used to smelt fine chromite concentrates to produce charge grade ferrochrome without any significant furnace operating problems or feed carry over with the exhaust gases. The ability to smelt fines directly supports the results of the small scale plasma smelting testwork of Maske (1) and Barcza (41), and the commercial experience of the MS&A DC graphite electrode plasma furnace (32) and the SKF non-transferred arc plasma furnace (24). The use of chromite concentrates rather than pellets or briquettes represents a cost saving of £15-25/t of chromite.

Fine anthracite was used as the reducing agent in the plasma furnace rather than the more expensive lumpy metallurgical coke required by the SAF. Any reactive coal compatible with the process chemistry should be acceptable, but a coal with low ash, low volatile matter, low phophorus and low sulphur contents is preferred. 0.31t of coal/t chromite (0.74t of coal/t ferrochrome) was required to achieve <5% residual chromium oxide in the plasma furnace slag. More coal than the model prediction of 0.3t of coal/t chromite was required because of the unexpected reduction of silica and magnesia. The conventional SAF only uses <0.28t metallurgical coke/t chromite (0.73t coke/t ferrochrome) because the coke contains a higher fixed carbon content than coal and there is some pre-reduction of the chromite by ascending CO gas.

Middelburg Steel and Alloy

In 1984, MS&A converted a submerged arc furnace to a 14 MW DC open bath plasma furnace using a central hollow graphite electrode (32). The feed (a blend of chromite ore fines, coke and recycled ferrochrome fines) is fed down the hollow graphite electrode into the slag bath in the vicinity of the plasma arc. The furnace power is currently being increased to 28MW.

There is little published data on the furnace performance and economics but the energy consumption is thought to be higher than the SAF because the energy in the furnace exhaust gases is not utilized for counter-current heat exchange or prereduction of the raw materials and the sidewalls and roof are not shielded from the plasma arc radiation or the open melt. Table 2 presents the estimated costs of producing ferrochrome in a DC arc furnace in the UK using Turkish chromite concentrates. The total production cost of £663/t Cr ($0.54/lb Cr) are less than the SAF because the higher energy costs are offset by using fine chromite concentrates and coal instead of pellets and coke.

Swedechrome

In 1986, SKF commissioned the 70kt/annum, 48MW "Swedechrome" shaft furnace plant to produce high carbon ferrochrome from cheap chromite fines. The plant design is similar to the Plasmadust facility shown in Figure 15 (24) and consists of two 24MW coke filled shafts each heated by four 6MW non-transferred arc heaters. Coke in the shaft provides 30% of the reductant and the remainder is injected as coal into the plasma tail flame along with the chromite and fluxes. Chromium yields of 90% are achieved at energy consumptions of 5.2 MWh/t of ferrochrome. The capital cost of the plant was £50m in 1987. Table 2 presents the estimated ferrochrome production costs for a plant based in the UK using Turkish chromite concentrates. The total production cost is approximately £676/t Cr ($0.55/lb Cr). The economics of the plant depend upon using cheap chromite fines directly, replacing some of the metallurgical coke with coal and selling surplus energy to a local district heating scheme.

The Extended Arc Flash Reactor (EAFR)

The technical feasibility of producing ferrochrome from fine chromite in the 24kW plasma flash reactor was demonstrated by Pickles (39). Chromium recovery was 85-90% at an energy consumption of 9-33MWh/t of ferroalloy.

University of Minnesota

Maske (1) investigated the reduction of chromite in a 45kW DC transferred-arc/open bath reactor equipped with a hollow graphite electrode. Almost complete "in-bath" reduction of the chromite was achieved using fine chromite (<0.0025m) and fine reductant (<0.0025m), basic slags and short arc lengths. "In-flight" reduction of chromite was also investigated by injecting chromite into the plasma arc established between the plasma torch and a carbon or copper ring anode. It is claimed that up to 50% of the chromite was reducted "in-flight", but it is suggested that the majority of the "in-flight" reduction occurred as the chromite and reductant particles came into intimate contact on the sloping anode surface or in the hot collection chamber beneath the reactor. The degree of reduction increased when the cold copper anode was replaced with a larger, hot carbon anode and silica flux was added to the feed blend. The chromite probably dissolved in a liquid slag phase and was reduced by carbon particles entrained in the slag on the hot carbon anode surface.

3.2.3 Coal Based Chromite Smelting

The steel industry in Japan and Europe are developing a new generation of processes aimed at producing iron and ferroalloys using coal as the energy source rather than electricity. In Japan in particular, the conventional SAF-EAF-AOD route to stainless steel is becoming uneconomic because of the high cost of electrical energy (£50/MWh). In a review of coal based ironmaking, Smith and Corbett (40) identified three process types suitable for ferrochrome and stainless steel production:

Melting/Reduction Processes

Kawasaki (40) are producing stainless steel directly from blast furnace hot metal by injecting chromite, coal and oxygen into a Basic Oxygen Furnace (BOF) through submerged tuyeres. The energy for the chromite reduction is provided by the combustion of the coal in the bath and by post combustion of CO using a top lance. Nippon Steel (40) are developing a process based on pre-reduction of chromite in a fluidized bed and reduction and melting in a top and bottom blown converter.

Chromite reduction in a BOF is probably cost effective in Japan where electrical energy is expensive and there is excess hot metal and converter capacity available. In Europe, stainless steel scrap is the cheapest source of Cr/Ni units, therefore, the economics are dependent upon maximizing the use of stainless steel scrap by the EAF-AOD route. The BF/BOF route only consumes about 30% scrap and cannot use all the stainless scrap arising.

Coke Bed Reactor Processes

Kawasaki (40) are developing a coke bed melter-gasifier coupled to a fluidized bed pre-reduction. Pre-reduced chromite, pulverized coal, oxygen and hot blast air are injected into a coke-filled shaft through two-stage tuyeres. The pre-reduced chromite is smelted by the heat liberated by the oxy/coal combustion in the shaft. The smelter exhaust gases are taken from the top of the shaft and used to pre-reduce the chromite in a separate vessel. Kawasaki are further developing the process to use 100% coal by replacing the coke-filled shaft with a fluidized bed of coal.

Prereduction/EAF Melting

Nippon steel (40) are developing a process where chromite pellets are completely reduced in a rotary kiln and fed directly to an EAF making stainless steel. All the energy for chromite reduction is provided by fossil fuel and electrical energy consumption is kept to the minimum required for melting and gangue separation.

No data on the economics of coal based chromite smelting are available.

3.2.4 Chromite Smelting Costs

The SAF is an economic and technically proven method of producing charge grade ferrochrome. Further economies can be realised by preheating and partial reduction of the chromite prior to smelting using the Outokumpu or Showa Denko processes which reduce the electrical energy and coke consumptions. New technologies will only be economically competitive with the SAF if they can utilize cheaper raw materials, have a higher chromium recovery to the alloy, consume less electrical energy or use a cheaper energy source.

The estimated cost of smelting Turkish chromite in an Outokumpu SAF, an SKF plasma furnace and an MS&A hollow graphite electrode plasma furnace located in the UK are presented in Tables 1 and 2 and summarized below:

UK MS&A plasma furnace	£663/t Cr
UK SKF Plasma furnace	£676/t Cr
UK Outokumpu SAF	£691/t Cr
S. African SAF	£482/t Cr
Ferrochrome selling price	£700-800/t Cr

The production costs of the MS&A and SKF plasma processes located in the UK are marginally less than the equivalent SAF because the cheap chromite fines and coal used offset the lower energy consumption of the SAF. Energy and reductant costs in all processes could be reduced if the chromite concentrates are pre-reduced before feeding to the furnaces using a rotary kiln or hearth. Because all demonstrated pre-reduction technologies require an agglomerated or lumpy feed, the advantage of being able to use chromite concentrates directly in the plasma furnaces is lost. The economics of the SKF plasma process rely on selling excess energy to local district heating schemes, but this may not be possible, or desirable, in all locations. S. African operations will have the lowest cost because of the availability of cheap chromite, energy and manpower and the weak Rand.

3.3 THEORETICAL ASPECTS OF CHROMITE SMELTING

Considerable theoretical work has been carried out on chromite smelting in the SAF with reference to the reduction reaction mechanism, the smelting temperature, slag chemistry and the distribution of the elements between the condensed phases and this is reviewed in order to compare the operation of the SAF and plasma furnace.

3.3.1 The Chromite Reduction Reaction Mechanism

An understanding of the chromite reduction reaction mechanism is necessary to optimize the furnace operating parameters, feed material particle size, reductant type and reactivity, slag chemistry, reaction temperature etc. The reduction of chromite occurs in at least four stages;

- Solid state reduction of chromite by carbon and CO.
- Dissolution of chromite in the slag phase.
- The reduction of the dissolved chromium oxide by solid C, C dissolved in the ferroalloy or CO.
- Reduction of solid chromite by C dissolved in the ferroalloy.

Barzca (41) showed that the initial reduction of chromite in the SAF shaft takes place by solid state reaction between chromite and carbon. The reaction rate was controlled by the diffusion of the reactant species, which was a function of particle size, chromite composition and mineralogy. CO was found not to be an effective reducing agent, although Downing (42) suggests that this was probably due to the impure gas used in the experimentation. Downing (42) went on to show that the rate determining step in the solid state reduction was the CO regeneration reaction between CO_2 and C at the carbon surface.

Where solid state reduction occurs, it is primarily ferrous ions diffusing out of the chromite spinel to be reduced to iron or carbides. The ferrous ions are replaced by magnesium ions which diffuse into the chromite to form the altered spinel, $MgO.Cr_2O_3$.

Urquart (43) and Wederpohl (44) studied the reduction of chromite in the slag phase and found that the major rate limiting step was the dissolution of chromite into the primary slag prior to reduction. Muan (45) investigated the ferrochrome slag-metal equilibria and showed that very reducing conditions enhanced the dissolution of chromite in the molten slag by the formation of the more soluble oxide, CrO. Fukagawa et al (46), Kadarmetov (47) and Kouroki (48) all showed that the chromite reduction rate was initially controlled by the dissolution of the chromite in the slag. They suggest that the "FeO" in the chromite is preferentially reduced and the resultant "Cr_2O_3" forms the altered spinel, $MgO.Cr_2O_3$, which has a limited solubility. Decreasing the MgO content or increasing the silica content of the slag was shown to increase the reaction rate because the solubility of chromium oxide increased, presumably because the MgO activity in the slag was reduced. The addition of CaO also increased the rate of chromite reduction because of the enhanced solubility of $MgO.Cr_2O_3$ spinel in the $MgO-CaO-Cr_2O_3$ system

There is considerable discussion on the carbonaceous reductant species responsible for chromite/chromium oxide reduction. Solid carbon, carbon dissolved in the metal and CO are all thought to play an important role in the chromite reduction. Kouroki (48) suggests that the carbon suspended in the slag is the most important carbon source for the reduction of dissolved chromium oxide because the slag volume and interfacial area is relatively large compared to the carbon saturated metal. In the SAF, lumpy refractory chromite and agglomerates can pass unreacted through the slag layer to the metal where they are reduced by the carbon dissolved in the alloy. Barmin (49), Sevinc (50), Suzuki (51) and Fruehan (52) simulated this reaction by rotating solid Cr_2O_3 pellets in a liquid iron-carbon bath. Barmin (49) found that the process was chemical reaction rate controlled, Sevinc (50) and Suzuki (51) concluded that the reduction rate was determined by the oxygen transport in the melt and Fruehan (52) found that the rate was determined by carbon transport in the melt. Kawakami (53) investigated the reduction of chromite by injecting it into a carbon saturated iron melt and concluded from the behavior of the silicon, that the rate determining step was the transport of oxygen, either from the ore-melt interface to the bulk, or from the bulk to the bubble-melt interface where CO was evolved.

In summary, the dissolution of the $MgO.Cr_2O_3$ spinel formed after the solid state reduction of the iron oxide and the diffusion of reactants in the slag and metal phases constitute the rate limiting steps in chromite reduction in the SAF. It is, therefore, important to employ slags that have a high solubility for the $MgO.Cr_2O_3$ spinel and a low viscosity, ie slags with a low MgO activity containing about 30% SiO_2, 30% MgO and 30% Al_2O_3 or, if practicable, slags containing CaO.

Figure 21 illustrates the possible reaction mechanism in the open bath plasma reactor. There will be little solid state chromite reduction as the feed blend falls through the furnace atmosphere. The inability of the fine chromite and coal particles to penetrate through the slag layer to the carbon saturated ferroalloy would suggest that the majority of the chromite reduction occurs in the slag phase. The carbothermic reduction of the metal oxides dissolved in the slag may occur via particulate carbon, CO and carbon dissolved in the metal phase, but it is suggested that the majority of the reduction proceeds via the gaseous intermediates CO and CO_2. CO bubbles form on carbon particles floating in the slag and the reaction between CO and the metal oxides occurs at the bubble-melt interface. The CO_2 generated at the interface reacts with C to renew the CO via the Boudouard reaction. The transport of oxide from the slag bulk to the bubble melt-interface, the reaction between the CO and the metal oxide and the regeneration of the CO via the Boudouard reaction will determine the reduction rate. Good mixing, reactive reductants and low viscosity slags containing CaO that "wet" the reductant and have a high solubility for the $MgO.Cr_2O_3$ spinel should be employed to ensure rapid reaction rates and good chromium recoveries.

3.3.2 The Chromite Smelting Temperature

The typical chromite smelting temperature of 1900K is determined by the thermodynamic stability of the oxides, mass and heat transfer, metal and slag liquidus temperatures and the minimization of energy and refractory consumptions.

The reduction of the chromium oxide in the SAF proceeds in several stages. Solid state reduction of chromite with carbon and CO to form Cr_3C_2 containing 13.3% C begins at 1423K, according to equation 4.

$Cr_2O_3 + 13/3C = 2/3Cr_3C_2 + 3CO$ eqn 4

As the chromite descends the furnace shaft towards the reaction zone, the more stable lower carbide Cr_7C_3 containing 9.0% C forms at 1523K.

$Cr_2O_3 + 27/7C = 2/7Cr_7C_3 + 3CO$

eqn 5

At 1873K, $Cr_{23}C_6$ containing 5.7% C becomes the stable chromium carbide.

$Cr_2O_3 + 81/23C = 2/23Cr_{23}C_6 + 3CO$

eqn 6

At temperatures above 2100K, chromium metal forms.

$Cr_2O_3 + 3C = 2Cr + 3CO$

eqn 7

Thus, as the reaction temperature increases, the stable chromium carbide contains less carbon. In practice, the chromite reduction temperature will be somewhat different from the temperatures indicated above because the reduction temperature depends on the composition and characteristics of the chromite used, the simultaneous reduction of iron oxide lowers the concentration and activity of the chromium, the Cr_2O_3 is chemically combined in the chromite and the gangue oxides in the chromite lower the Cr_2O_3 activity. Lisniak (54) found that chromites with a high Fe:Cr ratio or a high SiO_2 content began to reduce at 1000K and were nearly completely reduced at 1500K, whereas chromites with a low Fe:Cr ratio or high MgO or Al_2O_3 content were only reduced at temperatures approaching 1700K.

Figure 22 shows the Cr-Fe-C liquidus diagram derived by Griffing (55). The liquidus temperature of a typical ferrochrome containing 6-8% C and 50-55% Cr is 1850K.

The reactor temperature must be limited to prevent excessive refractory wear and the carbothermic reduction of unwanted species. SiO_2, MgO and CaO start to be reduced if the melt temperature exceeds 2000K.

REACTION	REDUCTION TEMPERATURE, K	
$SiO_2 + 2C = [Si] + 2CO$	1813	eqn 8
$SiO_2 + C = SiO_v + CO$	2100	eqn 9
$MgO + C = Mg_v + CO$	2100	eqn 10
$CaO + 3C = (CaC_2) + CO$	2198	eqn 11
$CaO + C = Ca_v + CO$	2423	eqn 12
$1/3Al_2O_3 + C = 2/3[Al] + CO$	2273	eqn 13
$2/3Al_2O_3 + 3C = 1/3[Al_4C_3] + 2CO$	2170	eqn 14

where
[ ] denotes solution in the metal phase
( ) denotes solution in the slag phase
$_v$ denotes the vapour phase

The solid burden in the SAF condenses and recycles much of the vapourized species, whereas the vapour will escape from the open bath plasma reactor.

3.3.3 Distribution of Elements between the Condensed Phases in Chromite Smelting

Chromium

At the typical reaction temperature of 1850-2000K, chromite is reduced to a Cr-Fe-C alloy according to reaction 15.

$$Cr_2O_3 + 3C = 2[Cr] + 3CO$$

eqn 15

where

$\Delta G^\circ = 818046 - 540.1T$ J/mole (56)

therefore

$$-42718/T + 28.2 = 2\log a_{Cr} + 3\log P_{CO} - \log a_{Cr_2O_3} - 3\log a_C \qquad \text{eqn 16}$$

$$a_{Cr_2O_3} = N_{Cr_2O_3} \cdot y_{Cr_2O_3} \qquad \text{eqn 17}$$

$$NCr_2O_3 = \text{mass\% } Cr_2O_3/1.6 \text{ Mol Wt} \qquad \text{eqn 18}$$

therefore

$$-42718/T + 28.2 = 2\log a_{Cr} + 3\log P_{CO} - 3\log a_C - \log\text{mass\% } Cr_2O_3 + \log 1.6 \text{ Mol Wt} - \log y_{Cr_2O_3} \qquad \text{eqn 19}$$

P_{CO} is the partial pressure of CO, a_C, a_{Cr}, $a_{Cr_2O_3}$ are the activities of the species referred to the pure solid state, N is the mole fraction of the species, y is the Raoultian activity coefficient, Mol Wt. is the molecular weight of the species (Cr_2O_3) and 1.6 is the approximate number of moles of slag oxides in a 100g of slag. The CO partial pressure will be approximately 1 atm. Healy (57) calculated the carbon activity in Cr-Fe-C alloys using carbon saturation data and obtained the activity coefficients of Cr and Fe from the carbon activity coefficient by the Gibbs-Schumann integration method. Figure 23 shows that for a Fe-Cr-C alloy containing 55% Cr, 35% Fe and 5% C at 1873-2000K, the activities of Cr, Fe and C are 0.1, 0.35 and 0.35 respectively. There is little published data on the activity coefficient of chrome oxide in CaO-MgO-Al_2O_3-SiO_2 slags under reducing conditions, most data referring to the refining of stainless steels. Maun (45) determined the activity-composition relationship of chrome oxide in the system CaO-"CrO"-SiO_2 under reducing conditions and showed that it is similar to the CaO-"FeO"-SiO_2 system and almost ideal. Substituting the values into equation 19, the mass% chromium oxide in equilibrium with a Fe-Cr-C alloy can be found from equation 20.

$$-42718/T + 26.5 = -\log \text{mass\%}\ Cr_2O_3$$

eqn 20

The equilibrium chromium oxide content of the slag should be negligible throughout the temperature range of interest. In practice, the recovery of chromium is controlled by the reaction kinetics, slag composition, slag viscosity, slag volume and the amount of metallic inclusions entrained in the slag.

Rowley (58) and Dresler (59) reported typical chromium losses in S. African SAF slags of 7.5% as dissolved Cr_2O_3 and 7.0% as metallic inclusions. Dresler (59) and Thomas (60) developed a chromite smelting model which predicts a decrease in Cr recovery to the alloy with decreasing Cr_2O_3 content in the ore/concentrate because lean ores generate a high slag volume and, therefore, higher chromium losses. Dresler (59) and Hamakos (61) suggest that the chromium recovery to the alloy increases with increasing MgO/Al_2O_3 ratio in the slag because of the lower slag volume and more complete dissolution of Cr_2O_3 in the slag with decreasing slag viscosity. Fukagawa et al (46), Kadarmetov (47) and Kouroki (48), on the other hand, suggest that concentrates with a low MgO/Al_2O_3 ratio should reduce more easily because the activity of MgO will be lower, promoting the reduction of the $MgO.Cr_2O_3$ spinel in the chromite. Figure 24 illustrates the relationship between Cr recovery and the Cr_2O_3 in the concentrate for two MgO/Al_2O_3 ratios in the slag. Figure 25 shows that high Cr_2O_3/FeO ratios in the chromite decrease the chromium recovery, probably because the chromites are more refractory and difficult to reduce.

Plasma furnace slags should be lower in chromium oxide than SAF slags because the slag composition can be chosen independently of slag resistivity. Pickles (39) reported 4.2% Cr_2O_3 in the EAFR slags, Maske (1) found the Cr_2O_3 in a DC graphite electrode furnace slag was 3-4% when smelting very fine chromites and reductants. Kouroki (48) reported 2-5% Cr_2O_3 in transferred arc plasma furnace slags.

Carbon

Before the introduction of the AOD process, the SAF had been operated to produce a high carbon ferrochrome with a carbon content of <5%. Lumpy refractory ores and a slag MgO/Al_2O_3 ratio of unity were used to retard the reaction of chromium oxide with carbon until the feed reached the high temperature reaction zone. The decarburization of high carbon Fe-Cr-C alloys in the AOD with a minimal chromium oxidation loss opened up the market for a higher carbon or charge grade ferrochrome and the acceptance of processes that produced a carbon saturated alloy.

The carbon content of the ferrochrome is controlled by the reaction temperature, the ore composition and physical properties and the process route. Ores high in iron oxide produce a high carbon ferrochrome because iron oxide is readily reduced to a high carbon complex carbide $(Cr,Fe)_7C_3$, the activity of the chromium carbide is lowered and the low temperature reduction of Cr_2O_3 is promoted. Kadarmetov (47) showed that a lower carbon ferrochrome (<5% C) is more readily obtainable in the SAF by using a dense, low iron oxide content, lumpy ore with a high melting point which penetrates the slag to form a viscous chromic oxide rich layer above the ferrochrome, decarburizing the alloy droplets as they pass through the layer. Downing (62) showed that high carbon alloys were produced from fine ores or agglomerates with a high surface to volume ratio and low viscosity slags with magnesia/alumina ratios >1 and silica contents >35% because they promote rapid dissolution of the ore in the slag, rapid reaction rates and lower reaction temperatures. The alloy carbon content from the transferred arc plasma furnace should be higher than the SAF because fine feed material is used, the reaction temperature is lower and there will be little "decarburization" of the ferrochrome by a chrome oxide rich slag.

Silica

Some silica will be reduced during chromite smelting because the stablity of silica is similar to chromite. Silica reduction will increase with increasing melt temperature, acid slags and easy to reduce ores.

Phosphorus

Phosphorus removal from the alloy in the SAF is difficult under high temperature, reducing conditions with siliceous slags. Robiette (36) reported that 60-80% of phosphorus charged to the SAF reports to the alloy, 10-20% to the slag and 10-20% to the gas phase and, therefore, low P raw materials must be selected to achieve low phosphorus alloys. Chipman (63) found that Si increased the activity coefficient of P. Pickles (39) reported P recoveries of <60% to the ferrochrome in the EAPR due to the formation of phosphorus vapour which was swept from the reactor. A limited degree of dephosphorization may be possible in the transferred arc plasma furnace by using basic slags, lower temperatures and good slag-metal stirring.

Sulphur

60-80% of the sulphur in the raw materials charged to the SAF reports to the ferrochrome (36). Sulphur can be minimized by using low sulphur raw materials (<0.5% S), a high melt temperature and if possible, a basic slag. C and Si increase the activity coefficient of sulphur and decrease the sulphur content of the alloy, whereas Cr decreases the activity coefficient of sulphur (64). Pickles (39) reported the removal of S as volatile SiS under very reducing conditions in the EAFR.

3.3.4 Slag Compositions in Chromite Smelting

The slag composition used in the SAF is a compromise determined by the slag liquidus temperature, slag viscosity, slag resistivity, slag volume, chromium recovery and furnace operating practice. Because the power input and feed rate are independent in the plasma furnace, there will be no slag resistivity constraints.

Slag Liquidus Temperature

The slag liquidus temperature in the choke fed SAF controls the slag and metal temperatures, because once the solid charge has fused, it rapidly drops away from the area of intense heat between the electrodes and settles in the furnace bottom where it is difficult to raise the alloy or slag temperature by increasing the energy input or retention time. The slag liquidus temperature must be maintained at 100-200K in excess of the alloy liquidus temperature (1850-1900K) to ensure that the alloy is sufficiently superheated for tapping. In the open bath of the transferred-arc plasma furnace, the melt temperature can be controlled directly by the energy input rate and the slag liquidus temperature can be approximately the same as the alloy liquidus temperature. The slag liquidus temperature for the $CaO-MgO-Al_2O_3-SiO_2$ system of interest has been investigated by Osborn (65) and is shown in Figure 26. Examining the SiO_2, MgO and Al_2O_3 contents of the chromites presented in section 3.1, it is seen that slags produced from the reduction of Finnish, Indian and US chromites lie to the right of the $MgO.Al_2O_3$ field, those from S.African and Zimbabwe lie in the centre of the field and those from Albania, Greece, Turkey and the USSR lie in the MgO field. In SAF smelting, SiO2, MgO or Al_2O_3 fluxes are added to produce a slag which lies in the centre of the $MgO.Al_2O_3$ field with a liquidus temperature of about 2000K. For plasma smelting, a slag with liquidus temperature of 1870K and a composition nearer the Cordierite field is aimed for.

Slag Resistivity

In the SAF, thermal energy is generated by resistive heating of the charge between the electrode tips, therefore a high slag (and coke) resistivity is required for maximum furnace productivity. Johnston (66) showed that the slag resistivity generally increases with increasing silica content, decreasing lime and decreasing magnesia/alumina ratios. Slag resistivity is not an important criteria in the transferred-arc plasma furnace because the energy is liberated at the arc/melt interface. Slags with a high magnesia/alumina ratio or a high lime content can be used to decrease the slag viscosity and increase the chromium oxide activity.

Slag Viscosity

Low viscosity slags are required for rapid heat and mass transfer and phase separation in both the SAF and the plasma furnace. Johnston (66), Machin (67), Lyutikov (68) and Rennie (69) investigated the viscosity of slags in the system $CaO-Al_2O_3-MgO-SiO_2$ at temperatures between 1573 and 2000K and found that the viscosity decreased rapidly with increasing MgO and CaO content, but Cr_2O_3 increased the slag viscosity. Unlike the SAF, the open bath plasma furnace can use low viscosity slags containing MgO and CaO because there is no restriction on slag resistivity. Figure 27 shows the viscosity in the systems of interest.

Alloy Composition

The slag composition has an indirect effect on the carbon content of the alloy in the SAF because the slag liquidus temperature determines the reaction temperature and the alloy carbon content. Slags high in magnesia or low in silica will have a high liquidus temperature, promoting high reaction temperatures and low carbon contents. Slags containing calcium oxide produce high carbon content alloys because the formation of calcium carbide aids the transfer of carbon to the alloy, basic slags wet the carbon particles and calcium oxide lowers the slag viscosity. Basic slags will aid the desulphurization and dephosphorization of the ferrochrome.

Chromium Recovery

Many workers (1,36,45,48,70) have reported higher chromium recoveries for alloys smelted under basic slags. Muan (45) showed that the chromium content of slags decreased from 7% to 1.5% as the slag basicity ($\%\ CaO + \%\ MgO / \%\ SiO_2$) increased from 0.5 to 1.6. Kouroki (48) found that a minimum chrome oxide in the slag of 2% was associated with slags containing 8-15% CaO and 35-40% SiO_2. Increasing the calcium oxide content of the slag decreases the chromium oxide content, but will increase the slag volume and may reduce the chromium recovery to the ferroalloy.

Furnace Operating Practice

In S. African furnace operation, where chromite concentrates and coke are relatively cheap and furnace productivity is the primary objective, the furnaces are operated with a slag MgO/Al_2O_3 ratio of around unity to maximize the slag resistivity and power input to the furnace at the expense of chromium yield. S. African chromite concentrates have a natural MgO/Al_2O_3 ratio of approximately unity, therefore the minimum of flux additions are required. Typically, 10-20% of the chromium charged to the SAF is retained in this slag as dissolved oxide or suspended metallic droplets and the metallic content of the slag is often recovered in a crushing and gravity separation circuit. In European operations the SAF is operated with slag MgO/Al_2O_3 ratios of 1.3-2.0 to maximize chromium yield. The natural MgO/Al_2O_3 ratio in European chromites is 1.6-2.0. Typically 3-8% of the chromium is retained in the slag as dissolved Cr_2O_3.

3.4 SUMMARY OF CHROMITE SMELTING

The SAF is an economic and technically proven process for the production of high carbon ferrochrome with scope for further cost reduction by external preheating and prereduction of the chromite. The plasma reactor has potential for cost savings because it can use fine chromite ores and coals directly instead of lumpy chromite/pellets and coke, and the chromium recovery to the ferroalloy may be marginally improved because of the greater flexibility in slag composition. The energy consumption in the plasma reactor will be higher than the SAF unless external pre-heating and pre-reduction of the chromite is practised. Scale up of plasma furnaces using water-cooled electrodes is limited by the size of the available electrodes (5MW), but this can be overcome by using hollow graphite electrodes. The plasma furnace feed blend should be configured to produce a slag containing >30% silica and a high magnesia/alumina ratio for maximum chromium recovery to the alloy. A furnace operating temperature of 1900K is required to promote the reduction reactions and exceed the alloy liquidus temperature whilst minimizing energy consumption, refractory wear and the reduction of gangue oxides.

3.5 CHROMITE SMELTING OBJECTIVES

To quantify the plasma furnace operation and evaluate the process economics, a chromite smelting trial was conducted to examine:-

- The energy consumption.
- The ablity to smelt fine chromite directly using coal as a reductant.
- The effect of slag composition and operating parameters on chromium and the element distributions between the condensed phases
- Reactor availability, including plasma torch and refractory life.
- The process economics, including operating and capital costs.

4.0 A LITERATURE REVIEW OF STEELPLANT DUST TREATMENT

Steelplant baghouse dusts contain appreciable quantities of recoverable iron, chromium, nickel, zinc, lead, cadmium, etc. In many countries steelplant dusts are classified as hazardous wastes because the contained lead, cadmium and chromium can be leached from the dust into ground water if the dust is dumped in an open landfill, and enter the food production chain. The high cost of disposal in secure landfill sites has been a major incentive to develop new treatment technologies, especially if the zinc and lead can be recovered to an enriched oxide or preferably a condensed metal to offset the treatment costs. In Europe, where the environmental lobby is less strong, the value of the recoverable chromium, nickel and zinc from alloy steel dusts has initiated process development.

4.1 STEELPLANT DUST CHARACTERISATION

During the scrap melt down and refining stages in the Electric Arc Furnace (EAF), Argon Oxygen Decarburization converter (AOD) or Basic Oxygen Furnace (BOF), 1-2% of the steel charge is converted to an extremely fine fume which is collected in baghouse filters, scrubbers etc. The dust is produced by a combination of metal vaporization in the high temperature arc-melt interface, metal atomization through oxygen jet-melt interactions and volatilization of the high vapour pressure species from the scrap charge. An appreciation of the variability in quantity, chemical composition and physical properties of EAF fume may be obtained from various surveys (71-75). Table 3 presents some typical European and US steel dust analyses and production rates. Dusts from carbon steel production are rich in ZnO and PbO because of the use of galvanized scrap and other zinc bearing materials in the charge. Dusts from alloy and stainless steel production contain Cr_2O_3, NiO and MoO_3 roughly in proportion to the grade of steel being melted. CaO varies considerably, depending upon the lime charging and injection practice. Fluorine results from fluorspar additions made to the EAF slag. Chlorine originates from road salt and plastics in the scrap. Alkalies arise from road salt. The average dust generation rate from EAF plants is 1-2% of steel production capacity, but this is expected to increase as zinc usage in automobiles increases.

4.2 CONVENTIONAL DUST TREATMENT PROCESSES

Dust treatment technologies can be divided into regional processes or on-site processes. Regional processes, where the dust is transported to a central facility, include the ISF shaft furnace, the Horsehead rotary kiln, the Inmetco rotary hearth, SKF Scandust and the Zinc Corporation of America flame reactor. Table 4 presents the estimated costs of a 76500 t/y regional facility. On-site processes, where the dust is treated at the point of origin, include recycling to the EAF, the Cebedeau caustic leach process and the Chemfix encapsulation process. Table 5 presents the estimated costs for a 5500 t/y on-site facility. Table 6 presents the estimated costs of smelting alloy dusts at Scandust to recover an alloy pig iron.

The Imperial Smelting Lead/Zinc Blast Furnace Regional Process

The Imperial Smelting Lead/Zinc Blast Furnace (76) can process EAF dusts containing ZnO, PbO and halogens. The dust is blended with zinc ores and fed to a sinter strand to agglomerate the dust and volatilize the majority of the halogens, PbO and CdO. The sinter is charged with preheated coke to the blast furnace where the ZnO is reduced and volatilized and leaves the furnace top with the exhaust gas stream. The zinc is condensed in a lead splash condenser and separated from the lead by liquation in a cooling launder. Lead bullion and an iron oxide rich slag are intermittently tapped from the furnace hearth. Both Commonwealth Smelting Limited in England and Metallgesellshaft in W. Germany incorporate EAF dust in their ISF charge. There are no ISFs in N. America.

Process advantages:
- Can accept a wide variety of feed materials.
- Zinc and lead are recovered as metals.
- Known technology.
- There is an existing infrastructure to sell the zinc, lead and any toxic residues.

Process disadvantages:
- High capital cost.
- Large throughput required for economies of scale.
- Environmental problems associated with the sinter plant and lead splash condenser.

The Electrothermic Furnace Regional Process

In the Zinc Corporation of America (St Joe) electrothermic zinc shaft furnace (77), the zinc bearing sinter and coke are resistively heated by an electric current passing between graphite electrodes located at the top and bottom of the shaft. Zinc vapour leaves the furnace through a vapour ring and is condensed in a zinc splash condenser. The furnace can only accept limited quantities of EAF dusts because the halogen and lead content of the dusts cannot be completely eliminated in the sinter plant and cause zinc condenser operating problems (78). ZCA are developing a caustic leach pretreatment step to reduce the halogen and lead levels in the feed derived from EAF dust, but the cost of the leach step is significant, often exceeding the value of the contained zinc in the dust.

Process advantages:
- Pure zinc product.
- Known technology.

Process disadvantages:
- High capital cost.
- Complicated process.
- Only feed materials containing low lead and halogen contents can be processed.
- Environmental problems associated with the sinter plant.

Waelz Kiln Regional Process

EAF dusts and other zinc containing materials are pelletized, mixed with coke and fed to a rotary kiln where reduction and volatilization of the ZnO, PbO and CdO occurs at 1500K. The Zn, Pb/PbO and CdO vapour is reoxidised in the kiln atmosphere, cooled and collected in a baghouse filter as an enriched oxide containing 50-60% ZnO, 5-7% PbO and 0-1% CdO. The FeO and any alloy oxides in the dust are partially reduced and discarded with the solid slag. As the operating temperature of the kiln must be kept below 1500K to avoid the formation of accretions on the lining, only 85-90% of the ZnO, PbO and CdO are recovered from the steelplant dust. The Waelz kiln process is operated by Horsehead Industries in Palmerton and Calumet City, USA (79) and by Berzelius (80) in Duisburg, West Germany at processing capacities of 380kt/y and 50kt/y respectively.

In the Berzelius operation, excess coal and sand are added to the charge to control the physical characteristics of the slag and assure complete reduction, adding appreciably to the fuel costs. The enriched oxide product from the kiln is used as a feed for their ISF furnace. In the Horsehead operation, the majority of crude zinc oxide is reheated to 1400K in a second kiln to drive off the Pb, Cd and halogen impurities before it is used as a feed for the ZCA electrothermic smelter. Horsehead Industries currently charge £44/t plus transportation costs for processing EAF dust containing in excess of 20% ZnO. An additional £2.2/t is charged for every 1% ZnO below 20%. The low treatment costs of the Horsehead plant reflect the low kiln operating costs and the fully amortized plant. Horsehead Industries recently bought the ZCA electrothermic smelter and now control the market for the production and consumption of impure zinc oxide in the USA.

Process Advantages:
- Known technology.
- Low operating costs.

Process disadvantages:
- Relatively low ZnO recovery.
- High capital cost.
- A large throughput is required for the kiln to be economical.
- The ZnO product must be further treated to remove halogens.
- The economics are very sensitive to the zinc price.

Economics:

Capital cost (76500t/y)	£17m
Estimated operating cost	£50/t dust
ZnO revenue	£57/t dust
Reported treatment charge	£44/t dust

The HTR Regional Process

The "HTR" Process (Himezi Tekko Rifain KK) operated by N.K.K. (81) is a modification of the Waelz kiln which reduces the kiln operating costs by replacing some of the coal by auxiliary fuel and utilizing a higher reaction temperature of 1700K to selectively reduce the ZnO, leaving the FeO in the slag.

As a result, the metallization of FeO is reduced to less than 5%, the ZnO recovery to the enriched oxide is increased to about 90%, the reductant consumption is reduced from 0.24 to 0.1 t/t of dust and the production rate is increased by 85%.

Process Advantages:

- Low operating costs.
- High ZnO recovery.

Process disadvantages:

- Oil is required to supplement the coal.
- The ZnO product must be further treated to remove halogens.
- The economics are very sensitive to the zinc price.

Economics:

Capital cost (76500t/y)	£10m
Estimated operating cost	£39/t dust
ZnO revenue	£61/t dust
Reported treatment charge	£39/t dust

Sumitomo Kiln Regional Process

To improve the recovery of the zinc and lead, Sumitomo (82) developed a double kiln process, where the steelmaking dust is pre-reduced in the first kiln at low temperatures to avoid kiln accretions and in the second kiln, the temperature is raised and the liquidus temperature of the materials adjusted to produce a molten charge. No data on operating and capital costs or slag/residue toxicity are available.

The Inmetco (Demag) Regional Process

Inmetco operate a rotary hearth-submerged arc furnace plant for the treatment of 45000 t/y of alloy steel dust and millscale (83). Dust, coke breeze and fluxes are blended and pelletized with water and the green pellets are heated and prereduced at 1523K using oxy-fuel burners in a rotary hearth furnace. The NiO, MoO_3, CuO and Fe_2O_3 are almost completely reduced but the Cr_2O_3 is only partially reduced. The ZnO, PbO, alkalies and halogens are volatilized and recovered as an enriched oxide in a wet scrubber. The partially reduced pellets are smelted in a submerged arc furnace to produce a ferroalloy pig.

Inmetco currently charge a treatment fee of £190/tonne ($320/t) of dust, excluding transport, but return the recovered ferroalloy to the steel company. Trials have been carried out to recycle the preduced pellets directly to the EAF, but these were unsuccessful because the pellets reoxidized on cooling, resulting in low metallic yields and increased silicon reductant and energy consumption in the EAF.

Process Advantages:

- The process is suitable for on-site or regional processing.
- A wide range of steel mill wastes can be processed.
- Ni, Cr, and Mo are recovered as a recycleable pig iron.

Process Disadvantages:

- Zinc is recovered as an impure oxide.
- Capital intensive, especially for small tonnages.

Economics:

Capital cost	not known
Estimated operating cost	£120/t dust
Reported treatment charge	£190/t dust

The SKF Plasmadust Regional Process

The Scandust plant built by SKF (24) in Sweden was commissioned in 1984 to treat 70kt/y of EAF and AOD dust. Figure 15 shows the main features of the plant. The dust is washed, filtered, micropelletized and blended with powdered fluxes and coal. The feed is pneumatically injected into the raceway created in front of the plasma generators in the base of the coke filled shaft furnace. The ferroalloy and slag produced collect in the furnace hearth and are intermittently tapped. The exhaust gas containing 68% CO, 18% H_2, 5% N_2, 7% Zn and 1% Pb leaves the furnace top at 1375K and passes through a hot cyclone into a lead spray condenser. Zinc is absorbed by the lead and separated by cooling and liquation. Reported ferroalloy recoveries are 83% Cr, 83% Ni and 95% Mo, but one pass zinc recoveries are <70% because of hard metal and dross formation in the condenser associated with halogens and particulate matter carry over from the furnace.

The capital cost of the 70kt/y regional processing plant was £27m in 1984. The extensive feed preparation, zinc condensation and gas handling facilities were responsible for a major part of the capital cost. Operating costs are estimated to be about £117/t for EAF dust and £128/t for AOD dust, somewhat higher than alternative regional processes because of the high electrical energy consumption, metallurgical coke as well as coal is consumed and the process is labour intensive. The high capital and operating costs are partially offset by producing an alloy pig iron from the AOD dust, metallic zinc from the EAF dust and the sale of excess energy (hot water) to local users.

It is considered that the SKF Plasmadust process is only viable for EAF dusts in geographic areas where electrical energy is cheap, excess process energy can be sold to adjacent facilities and a high processing fee can be charged. The processing of alloy steel dusts is more economically viable because the product value is greater. In December 1987, SKF stopped treating EAF dust because of the poor economics of zinc recovery, although it is thought that some zinc condenser problems also remained to be solved. SKF are now operating the furnace only on AOD dusts, but as there are only approximately 40kt/y of AOD dust arising in Europe, the furnace must be operating at less than its breakeven tonnage.

Process advantages:
- Zinc can be condensed directly from the exhaust gases.
- Cr, Ni and Mo can be recovered from AOD dusts as a ferroalloy.
- The excess process gas can be sold to offset the high energy costs.
- A variety of steelplant arisings can be treated.

Process disadvantages:
- High energy costs.
- High capital costs.
- A large production capacity is required to achieve economies of scale.

Economics of EAF dust processing:-

Capital cost	£27m (1984)
Estimated operating cost	£117/t dust
Zn, Pb and energy revenue	£134/t dust
Reported treatment charge	£65-100/t dust

Economics of Alloy dust processing:-

Capital cost	£27m (1984)
Estimated operating cost	£128/t dust
Reported treatment charge	£200/t dust

Flash Reactor Regional Process

The Zinc Company of America (St Joe) have been operating a 15kt/y pilot plant facility since 1984 (84). Fine coal is pneumatically injected into a water-cooled burner and combusted with oxygen-enriched air under fuel rich conditions at 2000K to produce a reducing gas. EAF dust is injected into the hot gas stream where the oxides are reduced to form Zn, Pb and Cd vapour and an iron oxide rich slag. The slag is separated from the reactor gases in a horizontal cyclone at the base of the vertical reactor tube. The reactor gases are combusted, cooled with excess air and an impure ZnO is recovered in a baghouse filter. The large exhaust gas volume associated with fossil fuel combustion results in a large carry over of feed material, contaminating the ZnO product. The ZnO product must be treated to remove the halogens and lead before it can be incorporated in the sinter feed for the Electrothermic process. The combustion of carbon to simultaneously provide energy and reducing gas limits the flexibility of the system.

Process advantages:
- Low capital cost.
- Can be scaled up.

Process disadvantages:
- Produces an impure ZnO product which requires further treatment.
- Feed must be very fine.
- Impure product
- Oxygen enrichment of the flame is required.
- Inflexible Redox potential

Economics:

Capital cost	£1.5m in 1984
Operating costs	not known
ZnO revenue	£58/t dust
Reported treatment charge	£120-180/t dust

Direct Recycle to the EAF

Direct recycling of EAF dust to the arc furnace, as green pellets or briquettes mixed in with the scrap charge has been shown to concentrate the zinc and lead into a secondary fume containing in excess of 60% ZnO (85-88). However, the dust, pellets and briquettes generate clouds of lead-containing fugative emissions on charging to the arc furnace with the scrap. Armco (89) in the USA investigated pneumatic injection of the dust into the melt in an attempt to overcome the fugative emissions problem. Both processes have been abandoned because the EAF energy consumption is increased by 2-5% due to the reduction of the contained oxides, vaporization of the lead and zinc and decomposition of the carbonates. Steel quality deteriorated because of the pickup of tramp elements, Cu, Sn, As, Te etc,

Process Advantages:
- Simple technology
- Low capital cost
- Low operating costs.

Process Disadvantages:
- A low value enriched ZnO is produced.
- Green pellets break up on storage due to lime hydration.
- Increased EAF energy consumption.
- Increase in the tramp element level in the steel.

Economics:

Capital cost	£0.4m
Operating costs	£10-35/t dust
Revenue	£65/t dust

Hydrometallurgical On-site Processes

Conventional zinc electrowinning technology cannot be applied to EAF dust because the iron consumes large quantities of acid and the halogens adversely affect the cell operation. In 1986, Cebedau (90) installed a 12kt/y caustic electrolytic process where the zinc and lead are dissolved in caustic soda, the lead is cemented out with zinc powder and the zinc is electrowon on special cathodes to produce a high quality zinc powder. Not all the zinc ferrite is dissolved in the process, leaving a potentially toxic waste material for disposal.

Process advantages:

- Recovery of pure zinc.

Process disadvantages:

- Potential environmental problems with residues.
- High energy cost.
- Complex technology.

Process economics:

Capital cost	£1.8m (1985)
Reported operating cost	£95/t dust
Revenue	£105/t dust
Treatment charge	not known

On-site Chemical Treatment

EAF dust is treated at the steelplant with, or encapsulated in, a second phase to lower its surface area, reduce its permeability and decrease the leach rates of the toxic substances. Asphalt, silicates, pozzolanic and portland cements have been used as chemical fixation and stabilizing agents to produce a non-permeable agglomerate and encourage ion-exchange of heavy metals with the aluminosilicate matrix of the cementitious solidification agent. The process requires a low capital outlay for the feed and materials blending system and the low operating costs of £15-30/t cover additives, labour and product disposal (91). Chemfix are currently quoting a treatment charge of <£75/t including transport and product disposal.

Process advantages:

- Low capital and operating costs

Process disadvantages:

- Not a long term environmental solution.

Process economics:

Capital cost	£0.33m
Estimated operating costs	£15/t dust
Revenue	£0/t dust
Reported treatment charge	£75/t dust

4.2.1 A Summary of Dust Treatment Technologies

Recycling the dust to the EAF is apparently the cheapest option because the process uses existing equipment. However, the process complicates the EAF operation, contributes to steel quality problems, generates a low value enriched oxide product which requires transportation and further processing, and is generally disliked by the furnace operators. Regional rotary kiln facilities offer a cheap dust treatment route because they have low operating costs, large throughputs and the existing plants are fully amortized, but there are liabilities and costs associated with transporting the feed and disposing of the enriched oxide product and slag. In the USA, the market for impure ZnO is limited and controlled by Horsehead Resources/ZCA.

There would appear to be a need for a small scale, economic, on-site process that can recover metallic zinc and ferroalloys directly form the dust, thereby removing any environmental problems associated with the transport of the dust or the enriched ZnO product and securing a market for the product.

4.3 THEORETICAL ASPECTS OF STEELPLANT DUST SMELTING

This section of the work attempts to identify the least cost smelting route to produce a non-toxic slag and to maximize the recovery of Zn to an enriched oxide (or a condensed metal) and Cr, Ni and Mo to a ferroalloy. The reaction mechanism, the reduction potential (as measured by the CO_2/CO ratio and reaction temperature), slag chemistry and the smelting energy requirements are examined.

4.3.1 The Reduction Reaction Mechanism

Studies (92-98) of slag fuming furnaces have established that the reduction of ZnO etc from liquid slag by solid carbon occurs, for the most part, via the gaseous intermediates CO and CO_2 according to equation 21.

$$(ZnO) + CO = Zn_v + CO_2 \qquad \text{eqn 21}$$

FeO may also reduce ZnO, giving ferric ions, which in turn are reduced by CO. Bell (92), Kellogg (93) and Grant (94) developed thermodynamic models for the carbothermic reduction and fuming of ZnO from lead blast furnace slags which accounted relatively well for the observed fuming behaviour. Quarm (95) and later Richards and Brimacombe (96), disputed the attainment of thermodynamic equilibrium and concluded that the process was kinetically controlled by the diffusion of ZnO and Fe_2O_3 through the slag to the reaction site. Sannikov (97) and Yakovenko (98) also found diffusion of ZnO and Fe_2O_3 in electric furnace fuming of zinc slags to be the rate limiting step. It has been noted (99) that the addition of small quantities of strong surface active agents increased the kinetics of zinc fuming by decreasing the surface tension of the melt and accelerating the wetting of the carbon reductant particles.

It is suggested that the carbothermic reduction of metal oxides in steelplant dusts proceeds via the gaseous intermediates CO and CO_2. The CO_2 reacts with C to renew the CO via the Boudouard reaction. It is unlikely that the rate determining step will be the slag-gas chemical reaction, but the rate will be determined by the transport of reactants in the slag and gas phases and the regeneration of the CO via the Boudouard reaction. Consequently, such factors as melt temperature, feed particle size, reductant reactivity, slag viscosity and melt stirring will affect the overall reaction rate.

4.3.2 The Reduction Potential required for Smelting Steelplant Dust

The reduction potential as measured by the CO_2/CO ratio and reaction temperature are determined by:
- The thermodynamic stability of the metal oxides.
- The product purity.
- The prevention of ZnO formation during condensation of the zinc vapour.
- The selective reduction of ZnO, leaving the FeO in the slag.

The furnace operating temperature of about 1773K is also determined by:
- Metal and slag liquidus temperatures
- Slag viscosity.
- Refractory wear rate.

The CO_2/CO ratio and temperature required for the reduction of an EAF dust containing 25% ZnO, 3% PbO, 40% FeO, 5% MnO and 1% Cr_2O_3 to produce a slag containing less than 1.0% Cr_2O_3, 0.1% PbO and 0.1% CdO is presented in Figure 28.

The CO_2/CO Ratio and Temperature for ZnO Reduction

The ZnO activity in the slag in equilibrium with a given CO_2/CO ratio and zinc partial pressure is given by equation 22.

$$ZnO + CO = Zn_v + CO_2 \qquad \text{eqn 21}$$

where

$\Delta G^\circ = 178235 - 111.3T$ J/mole (56)

therefore

$$\log P_{CO_2} - \log P_{CO} = - 9312/T + 5.81 - \log P_{Zn} + \log a_{ZnO} \qquad \text{eqn 22}$$

now

$$P_{total} = 1 \text{ atmosphere} = P_{Zn} + P_{CO} + P_{CO_2} \qquad \text{eqn 23}$$

$$aZnO = NZnO.\gamma_{ZnO} \qquad \text{eqn 24}$$

$$NZnO = \text{mass\% ZnO}/1.6 \text{ Mol Wt} \qquad \text{eqn 25}$$

therefore

$$\log P_{CO_2} - \log P_{CO} = - 9312/T + 3.69 - \log P_{Zn} + \log \gamma_{ZnO} + \log \text{mass\% ZnO} \qquad \text{eqn 26}$$

The equilibrium mass % ZnO in the slag can be calculated knowing the zinc vapour partial pressure, the zinc oxide activity coefficient, the gas analysis and the reaction temperature. From mass balance considerations, the zinc partial pressure generated from a dust containing 25% ZnO is approximately 0.2 atmospheres. The ZnO activity data for the $CaO-SiO_2-FeO-ZnO$ system of interest were determined for slag composition ranges and temperatures typical of lead and lead-zinc blast furnace practice, ie 20-40 mole % FeO, 20-50 mole % SiO_2, 10-40 mole % CaO and 0-10 mole % ZnO at 1400-1700K.

The early work of Bell et al (92) and Okuner et al (101) calculated ZnO activities based on observed zinc elimination rates during slag fuming, however Quarm (95) concluded that equilibrium was not attained in the slag fuming furnace and, therefore, these results are not considered. Lebed et al (102) used a vapour pressure measurement technique under reduced pressure to determine ZnO activities. The validity of the technique is questionable, therefore the data was discarded. Davenport (103) calculated the ZnO activity relative to pure liquid ZnO rather than pure solid ZnO, the standard state used by most investigators. Reyes and Gaskell (104) pointed out the inaccuracies in the free energy of fusion of ZnO, making the conversion of the data to the solid standard state of limited use for this work. Ashuma et al (105) used a gas equilibrium technique for slags in the $FeO-Fe_2O_3-CaO-SiO_2$ system containing 0-20 % ZnO at 1373K and showed that the zinc oxide activity coefficient increased with increasing slag basicity. Richards (106) determined the ZnO activity in the system $FeO-CaO-SiO_2$ containing 0.2 mole % ZnO at 1473K using a gas equilibrium technique and found the activity coefficients of both FeO and ZnO increased with increasing slag basicity. The activity of ZnO could be represented by a regular solution formula involving interaction constants for each of the constituent binary systems over the limited composition and temperature range considered. Filipovska (107) measured FeO and ZnO activities in the system $FeO-CaO-SiO_2$ at 1525K using an EMF technique. The activity coefficients of ZnO and FeO were shown to increase with increasing slag basicity and Al_2O_3 content and a correlation expression was derived to predict the effect of slag composition on ZnO and FeO activity coefficients. Levin (108) used a gas equilibrium technique for the determination of ZnO activity at 1573K in the system $FeO-CaO-SiO_2$ containing 1-5 mole % ZnO. Although their data analysis technique was unclear, the zinc oxide activity coefficient was shown to increase with increasing slag basicity. Reyes and Gaskell (104) used a transpiration technique to determine ZnO activities in the system $CaO-Al_2O_3-SiO_2$ containing 1-5 mole % ZnO at temperatures between 1673 and 1823K and showed that the ZnO activity coefficient increased with increasing slag basicity and temperature. Figure 29 summarizes the zinc oxide activity coefficient data in the system $CaO-SiO_2-FeO$ at various temperatures. (104-108). Because of the limited data, no quantative relationship between ZnO activity and slag composition and temperature could be produced, however, several general trends were observed:-

- Isoactivity coefficient contours run parallel to the liquidus isotherms.
- The activity coefficient increases with increasing slag basicity.
- The activity coefficient decreases with increasing temperature.

For slags produced from smelting EAF dusts at 1723K, the ZnO activity coefficient increases from 0.5 for low FeO contents, to about 1.0 for slags containing >20 mass% FeO.

Curve A in Figure 28 shows the CO_2/CO ratio and temperature required to achieve 0.5 mass % ZnO in the slag when PZn = 0.2 and $\gamma ZnO = 1$. At the suggested reaction temperature of 1723K, a CO_2/CO ratio of <0.05 is required to reduce the mass % ZnO in the slag to 0.5% . Increasing the reaction temperature decreases the % ZnO in the slag, increasing the PZn by using a dust richer in ZnO increases the % ZnO in the slag and increasing the slag basicity reduces the % ZnO in the slag.

The CO_2/CO Ratio and Temperature for FeO Reduction

In the smelting of carbon steel dusts, the majority of the ZnO can be reduced from the slag without reducing the FeO by careful control of the CO_2/CO ratio and temperature. The CO_2/CO ratio in equilibrium with iron oxide and metallic iron according to reaction 27 is given by equation 28.

$$FeO + CO = [Fe] + CO_2 \qquad \text{eqn 27}$$

where

$\Delta G^{\circ} = -43600 + 38T$ J/mole (56)

and

$$\log P_{CO_2} - \log P_{CO} = 2277/T - 1.985 + \log a_{FeO} - \log a_{Fe} \qquad \text{eqn 28}$$

At a constant temperature, the limiting CO_2/CO ratio on the point of reduction of FeO to metallic Fe can be calculated from a knowledge of the FeO activity in the slag and the Fe activity in the metal phase. Figure 30 shows the FeO activity in the system $CaO-SiO_2-FeO$ (109). In a typical slag containing 40 mass% Fe_2O_3, 10% CaO, 10% SiO_2 etc, aFeO is approximately 0.5.

In iron-carbon melts, the Fe activity approximates to unity at low concentrations of carbon.

Curve B in Figure 28 shows the limiting CO_2/CO ratio and temperature to avoid the reduction of FeO. For the selective reduction of ZnO, the CO_2/CO ratio and temperature must be above Curve B (FeO reduction) but below Curve A (ZnO reduction). Decreasing the Fe_2O_3 content of the dust lowers the CO_2/CO ratio for selective reduction, enabling more ZnO to be reduced.

The CO_2/CO Ratio and Temperature for Cr_2O_3 Reduction

In the smelting of steelplant dusts, the "Cr_2O_3" content of the slag must be reduced to less than about 1% to meet the slag toxicity test requirements. The CO_2/CO ratio in equilibrium with chrome oxide and chromium, according to reaction 29, is given by equation 30.

$$1/3Cr_2O_3 + CO = [2/3Cr] + CO_2 \qquad \text{eqn. 29}$$

where
$\Delta G^\circ = 104068 + 12.3T$ J/mole (56)

and

$$\log P_{CO_2} - \log P_{CO} = -5437/T - 0.64 + 1/3\log a_{Cr_2O_3} - 2/3\log a_{Cr} \qquad \text{eqn 30}$$

The CO_2/CO ratio to reduce the chromium in the slag to less than 1% can be calculated from a knowledge of the temperature, the chromium activity and the chromium oxide activity in the slag. The activity coefficient of Cr dissolved in Fe has been measured by Hadrys et al (110) and found to have a constant value of 0.02 for melts containing up to 30 mass% Cr. Wellbeloved (111) determined chromium oxide activities in $CaO-SiO_2-MgO$ and $CaO-SiO_2-Al_2O_3$ slags respectively, but the scatter in the data does not allow any meaningful relationship to be derived, therefore, the chrome oxide activity coefficient is asssumed to be unity.

Curve C in Figure 28 shows the CO_2/CO ratio and temperature to achieve less than 1 mass% Cr_2O_3 in the slag when aCr2O3 = 0.004 and aCr = 0.0002. At 1723K, the limiting CO_2/CO ratio is 0.004 for dusts containing less than 1% Cr_2O_3 and 0.001 for alloy dusts containing 10-20% Cr_2O_3.

Thus it is not possible to selectively reduce ZnO from high Cr_2O_3 content dusts whilst producing a slag containing <1% Cr_2O_3.

The CO_2/CO Ratio and Temperature for PbO Reduction

In the smelting of EAF dusts, the "PbO" content of the discard slag must be reduced to <0.1% to meet the slag toxicity requirements. The CO_2/CO ratio in equilibrium with lead oxide and Pb vapour according to reaction 31 is given by equation 32.

$$PbO + CO = Pb_v + CO_2 \qquad \text{eqn 31}$$

where
$\Delta G^\circ = - 59356 - 20.9T$ J/mole (56)

and

$$\log P_{CO_2} - \log P_{PCO} = 3101/T + 1.09 - \log P_{Pb} + \log a_{PbO} \qquad \text{eqn 32}$$

The CO_2/CO ratio to reduce the PbO in the slag to less than 0.1% can be calculated from a knowledge of the temperature, the partial pressure of the lead vapour and the activity of the PbO in the slag. The lead partial pressure generated from the carbothermic reduction a dust containing 5% PbO is approximately 0.02 atmospheres. Little work has been done on PbO activity in low ZnO CaO-SiO_2-FeO slags in the temperature range of interest. The majority of the data relates to high ZnO content lead blast furnace slag compositions at 1300-1500K. Richardson (112) and Meyer (113) found that the PbO activity coefficient increased from 0.4 to 1.2 as the CaO/SiO_2 ratio increased from 0.5 to 1.0 for slags containing 50% FeO at 1573K.

Curve D in Figure 28 shows that the limiting CO_2/CO ratio and temperature to reduce the mass% PbO in the slag to <0.1% will be about 10 at 1723K for a dust containing 5 mass% PbO.

CO_2/CO Ratio in Equilibrium with solid Carbon

The maximum degree of carbothermic reduction of metallic oxides will be defined by the CO_2/CO ratio in equilibrium with solid carbon at a given temperature. The CO_2/CO ratio in equilibrium with excess solid carbon according to reaction 33 is given by equation 34.

$C + CO_2 = 2CO$

eqn 33

where
$\Delta G^\circ = 170544 - 173.4T$ J/mole (56)

thus
$\log P_{CO_2} - \log P_{CO} = 8910/T - 9.06 + \log P_{CO} - \log a_C$

eqn 34

The activity of carbon in equilibrium with excess solid carbon will be unity. The partial pressure of CO generated from the carbothermic reduction of a typical steelplant dust containing 25 mass% ZnO, 30 mass% FeO, 5 mass% PbO, etc, will be about 0.6 atmospheres.

Curve E in Figure 28 shows the limiting CO_2/CO ratio in equilibrium with excess carbon where aC = 1 and PCO = 0.6. Gas compositions above the curve are stable, but convert to CO_2 and C below the curve. The minimum CO_2/CO ratio that is possible at 1723K is about 0.0001.

The CO_2/CO Ratio for Zinc Condensation and the Avoidance of ZnO Formation

The CO_2/CO ratio and temperature of the gas stream leaving the furnace (and entering a zinc condenser) must be carefully controlled to prevent premature zinc condensation and the reoxidation of zinc vapour, which would block the exhaust duct and form a dross in the condenser, reducing the zinc recovery. Curve F represents the saturated vapour pressure of zinc given by equation 35 (56).

$\log P_{Zn}$ (mm Hg) $= - 6620/T - 1.255\log T + 12.34$

eqn 35

For a zinc partial pressure of 0.2 atm, zinc condensation commences at 1000K. To condense the majority of the zinc vapour, it is necessary to decrease the zinc partial pressure to <0.01 atm by cooling the gas to at least 860K. In practice, it is necessary to cool the gas to 750K because of supercooling effects.

If complete chemical equilibrium were maintained on cooling the $Zn/CO/CO_2$ gas, the zinc vapour would reoxidize to form ZnO according to reactions 21 and 33.

$$ZnO + CO = Zn_v + CO_2 \qquad \text{eqn 21}$$

$$C + CO_2 = 2CO \qquad \text{eqn 33}$$

The reversion of reaction 33 is kinetically slow and C and CO_2 formation can be avoided by fast cooling. Reaction 21 is very fast and unless the gas is rapidly quenched, the CO_2 in the gas will react with an equivalent amount of Zn vapour to form ZnO. The conditions necessary to minimize the ZnO formation are illustrated in Figure 28. Curve G shows the CO_2/CO ratio in equilibrium with pure solid ZnO ($a_{ZnO} = 1$) at a zinc partial pressure of 0.2 atm. ZnO formation will commence on slow cooling the gas when the $Zn/CO_2/CO$ gas composition intersects Curve G (assuming the CO does not revert to CO_2 and C). To avoid ZnO formation on slow cooling the $Zn/CO_2/CO$ vapour to the condenser outlet temperature of 860K, the CO_2/CO ratio in the furnace must be maintained at <0.001. If the $Zn/CO_2/CO$ vapour can be quenched at a rate faster than the Zn vapour oxidation rate, then the acceptable gas composition will be limited by the intersection of the gas temperature and Curve G. For example, for a gas entering the condenser at 1273K, the CO_2/CO ratio should be <0.1 to avoid ZnO formation. The theoretical evaluation suggests that it should be possible to condense zinc from the $Zn/CO/CO_2$ vapour produced during selective reduction, provided the gas temperature entering the condenser is in excess of 1273K, the CO_2/CO ratio is less than 0.1 and the gas is rapidly quenched.

In practice, the back reaction to form ZnO is accelerated in the presence of H_2, H_2O, S and nucleation sites, therefore low volatile, low sulphur coals or preferably coke should be used as the reductant, and the feed should be dry and agglomerated to reduce feed carry-over.

4.3.3 Slag Composition

The slag composition is determined by:

- The slag liquidus temperature.
- The slag viscosity.
- The product purity. S, F, Cl, Na, K, etc may be partially retained in basic slags.

Slag Liquidus Temperature

The slag composition should aim to produce a slag liquidus temperature of <1723K, about 50K below the furnace operating temperature. Slags from EAF dusts generally have compositions which fall in a liquidus temperature trough extending from $CaO.SiO_2$ to the FeO corner of the $CaO-SiO_2-FeO$ system shown in Figure 31 (65). Slags from selectively reduced dusts contain around 20-30 mass% CaO, 20-30 mass% SiO_2 and 40-60 mass% FeO and have liquidus temperatures around 1500K, whereas slags from totally reduced dusts containing <5% FeO have liquidus temperatures around 1723K. A sand flux addition must be made to dusts containing more than 15% CaO.

Slag Viscosity

The slag composition should be configured to produce a slag viscosity of <5 centipoise at the furnace operating temperature of 1773K. The data on slag viscosities are too extensive to review in detail, but in general, viscosity increases rapidly with increasing silica for all concentrations more acid than 2RO.SiO2 (114-120). Al_2O_3 increases the viscosity in basic slags containing <33% SiO_2 by substituting for SiO_2 in the silicate network (115). CaO reduces the slag viscosity by breaking the silicate lattice. As CaO additions also increase the slag liquidus temperature, there will be an increase in viscosity if the slag liquidus/solidus temperature approaches the furnace operating temperature. MgO and FeO behave in a similar manner to CaO (122). ZnO additions up to 10% have been shown to decrease the slag viscosity (121-123). Figure 32 shows the slag viscosity in the $CaO-SiO_2-FeO-Al_2O_3$ system at 1673K will be <5 centipoises for the composition range of interest, but to minimize the slag viscosity, it is advantageous to use a slag composition high in CaO, FeO or MgO concommitant with a low slag liquidus temperature and volume.

Partition of Species Between The Phases

The reduction of ZnO, PbO, Cr_2O_3 etc from the slag phase increases with increasing slag basicity because the oxide activity coefficients increase with basicity.

The vapourization of alkalies should be minimized because they contaminate the ZnO product. Fukatake (124) investigated the vaporization of potassium from carbon saturated iron blast furnace slags and demonstrated that the potassium capacity of slags increased as temperature and basicity decreased (the activity coefficient of K_2O decreases with decreasing slag basicity). Dietzel (125) found that the vaporization of alkalies is enhanced in the presence of water vapour because of the formation of volatile alkali hydroxides.

The vapourization of halogens should be minimized because they contaminate the product and cause dross formation in the exhaust system and condenser. Schwertfeger (126) studied the vaporization losses of fluorine from CaO-SiO2-CaF_2 slags at 1900K and found that fluorine ions in the slag reacted with silica, alumina and water vapour to form the volatile species SiF_4, AlF_3, HF and to a lesser extent, CaF_2. Shinmei (127) measured the equilibrium SiF_4 pressure over CaO-CaF_2-SiO_2 melts at 1773K and found that the SiF_4 pressure decreased with increasing slag basicity (decreasing SiO_2 activity). The St Joe (78), Sumitomo (82), Inmetco (83) and Miike (128) smelters all found that the majority of the Cl, Na and K in the feed is volatilized and reported to the Zn/ZnO product, but a proportion of the F can be retained in the slag by using high slag basicities.

Refractory Consumption

Corrosion of the magnesia refractory lining in the plasma furnace can be minimized by operating with magnesia saturated slags with high CaO/SiO_2 ratios and low FeO contents.

4.3.4 Energy and Reductant Consumption for Steelplant Dust Smelting

The energy and reductant requirements for dust smelting will depend upon the dust analysis and the reduction potential used. Using the energy balance model presented in Appendix 1, the selective and total reduction of Tremorfa dust containing 35% ZnO and 33% Fe_2O_3 can be compared.

ITEM	SELECTIVE REDUCTION	TOTAL REDUCTION
Final % ZnO in slag	2.6	0.02
Final % FeO in slag	59.0	0.04
Nett energy, MWh/t dust	1.052	1.341
Reductant, t/t dust	0.078	0.18
CO_2/CO ratio	0.17	0.001
PZn, atm	0.30	0.2
Gas volume, m^3/t dust	305.0	486.0

Selective reduction can be used to reduce the majority of the zinc oxide, leaving the FeO unreduced in the slag, decreasing the energy consumption, reductant consumption and exhaust gas volume compared to the total reduction mode. The smaller exhaust gas volume results a higher partial pressure of zinc vapour and less entrainment of particulate matter, improving the zinc condenser efficiency and reducing product contamination.

4.4 SUMMARY OF STEELPLANT DUST SMELTING

None of the existing technologies that recover ZnO produce an enriched ZnO product that meets the ZnO specification imposed by Horsehead or Metallgeselschafts without calcining or leaching the oxide to remove impurities. The value of the zinc oxide product and the market outlet will be limited, imposing financial restrictions on these processes.

Apart from the ISF, the Plasmadust regional process is the only process which is designed to treat EAF dust and produce zinc metal directly. This overcomes the zinc oxide marketing problem, but the Plasmadust process suffers from high capital and operating costs and the zinc condenser operating problems have not been fully resolved.

The transferred arc plasma/open bath reactor appears to be a potential method of smelting steelplant dusts to produce a non-toxic slag, to recover zinc as an enriched zinc oxide or a condensed zinc metal and to recover alloy oxides to a ferroalloy for recycling. For the plasma furnace to be a viable dust treatment process, the treatment charge must be equivalent to the lowest cost alternative technology, ie the rotary kiln at about £50/t dust plus transport costs. To keep the energy and reductant costs to a minimum, EAF dusts should be smelted in the selective reduction mode at about 1723K with a CO_2/CO ratio <0.1, recovering the majority of the ZnO, but leaving the FeO in a non-toxic slag. Dusts containing alloy oxides must be totally reduced to recover the alloy elements and produce a non-toxic slag. Zinc metal may be condensed directly from the $Zn/CO_2/CO$ gas generated by selective reduction, provided the zinc condenser quenches the gas very rapidly. At slower quench rates, the furnace must be operated in the total reduction mode to generate a CO_2/CO ratio of <0.001 to minimize zinc vapour reoxidation. The halogen, alkali and lead contaminants in the dust are likely to be a problem in both the zinc oxide and zinc metal product routes. Slags with a % CaO/% SiO_2 of 1.0-1.2 should be used to maximize the metal oxide activities, minimize viscosity, retain halogens in the slag and minimize refractory corrosion.

4.5 STEELPLANT DUST SMELTING TESTWORK OBJECTIVES

To confirm the plasma process operating parameters, a series of trials was planned to examine:

- The CO_2/CO ratio, slag chemistry and operating temperature required to produce a non-toxic slag and recover the majority of the metal values.
- The effect of steelplant dust analysis, operating temperature, CO_2/CO ratio and slag chemistry on the purity of the enriched baghouse dust.
- The feasibility of condensing the zinc/lead vapour directly to a liquid product.
- The performance and availability of the plasma torch, furnace and ancillary equipment.
- The total processing costs.

5.0 EQUIPMENT

The plasma furnace and ancillaries used in the experimental section of the testwork consist of:

- The raw materials blending and feed system.
- The 2.0MW plasma furnace.
- The exhaust gas system.
- The plasma torch.
- The power source
- The instrumentation.

5.1 THE FEED SYSTEM

5.1.1 Feed Blending

The raw materials were stockpiled and crudely homogenised using a front end loader and sieved through a 0.006m vibrating screen to remove oversize particles. Preweighed raw materials, reductant and fluxes were loaded into a 0.4t capacity ribbon blender mounted on load cells (accuracy +/- 0.01t). After mixing, the blend was discharged into a bottom discharge bag, check weighed and conveyed to the furnace hopper. This system, although labour intensive, allowed for an accurate control of the feed batching and could accommodate rapid changes in the feed recipe as a trial progressed.

5.1.2 Feed Rate Control

The original furnace feeder consisted of a 0.5m diameter mass flow hopper fitted with a manually controlled variable speed plough feeder and mounted on load cells adjacent to the furnace. This system worked well for chromite, but EAF dusts bridged in the hopper and fed very erratically. The hopper was modified to accept a vertical screw agitator, fluidizing air pads and mechanical vibrators in an attempt to avoid bridging, but all proved to be unsuccessful and the plough feeder was replaced with a screw discharge feeder. The 200kg capacity screw feeder was equipped with six variable speed 0.05m diameter screws in the hopper base. Feedback signals from the hopper load cells controlled the screw speed and discharge rate.

This system gave a constant, controllable feed rate but was very labour intensive because it required frequent refills. The small feeder was replaced by a larger live bottom hopper mounted on a 1.0t weighbridge fitted with a twin 0.15m diameter variable speed screw discharge. The feed rate was monitored by integrating the hopper load cell output over 2 minute intervals to give a feed rate accuracy of +/-0.02t/hour.

5.1.3 Feed Transfer from the Hopper to the Furnace

Three 0.075m diameter horizontal screw conveyors were originally used to transfer the feed material from the feeder to the feed ports in the furnace roof. Screw conveyors were used because they are robust in the furnace environment and can be partially sealed to the furnace roof and the feed hopper to prevent the escape of furnace gases. This design was satisfactory for chromite, but caused extensive delays with EAF dust because the feed ports in the furnace roof sintered up with condensed zinc/zinc oxide that was difficult to remove. The three 0.075m diameter feed transfer screws were replaced with two 0.15m diameter screws discharging into two 0.15m diameter ports modified to accept disposable alumina feed port liner tubes which could be rapidly replaced if they sintered up. The feed ports were located 0.5m from the centre line of the furnace so that the feed materials fell into the hot arc/melt interface area to improve energy transfer to the melt.

5.2 THE FURNACE

5.2.1 Furnace Dimensions

Figure 33 shows a schematic layout of the plasma furnace. The furnace internal diameter of 1.5m was based on a "rule of thumb" power density of 1.0 MW/m² of hearth area obtained from considerations of the reaction kinetics, energy transfer, refractory wear rates and the bath volume for a realistic tapping interval. Figure 34 shows the relationship between furnace power and diameter for commercial DC furnace operation. AC UHP steelmaking furnaces using extensive water cooling have a power density of approximately 2.0MW/m² and SAF have a power density of around 0.5MW/m². The refractory life of the UHP arc furnace is around 2-4 weeks whereas the SAF refractory lining lasts up to 5 years.

A hearth-to-roof height of 1.4m was chosen so that with a typical melt depth of 0.2m and an arc length of 0.3-0.4m, the distance from the roof to the torch tip and the melt would be sufficient to protect the roof from the plasma arc and melt radiation.

5.2.2 Furnace Refractory Lining

The working refractory lining of lower sidewalls consisted of 0.23m thick high fired pitch impregnated magnesia bricks (Steetley MTB), chosen for their resistance to slag attack. The annulus between the cold face of the brick and the steel shell was rammed with high conductivity carbon paste to increase the thermal conductivity of the lining and reduce the refractory corrosion rate. The upper sidewall working lining was constructed from 0.18m thick high fired magnesia-chrome bricks (Steetley MC6), chosen for their resistance to thermal spalling. The annulus between the cold face of the brick and the furnace shell was filled with insulating concrete. The working lining of the hearth was 0.23m of high fired pitch impregnated magnesia bricks laid on end to prevent them floating out of the hearth. High grade, low iron firebrick was used as a backing lining to the magnesia bricks.

5.2.3 Roof Design

The original arched brick roof was constructed from 0.23m thick magnesia-chrome crowns and incorporated a central hole for the plasma torch and six feed entry holes. Although the refractory performance was good, difficulty was experienced in sealing the plasma torch and feed tubes into the roof and it was expensive and time consuming to rebuild. A water-cooled roof panel lined with 0.15m of cast tabular alumina was constructed and has been used successfully with minimum maintenance.

5.2.4 Anode Design

A central, air-cooled steel billet, 0.06*0.06m in cross section and 1.0m long, was built into the furnace hearth refractories to establish the return electrical connection required for the DC transferred-arc mode of operation. A molten heel of metal was maintained in the furnace at all times to avoid overheating the anode.

5.2.5 Molten Product Handling

The taphole of the static furnace was located 0.05m above the hearth to retain a metal heel in contact with the anode to maintain an electrical circuit. The taphole was opened with a conventional oxygen lance and closed with taphole clay. Molten slag and metal were intermittently tapped into refractory lined boxes. After cooling, the slag and metal were separated and weighed.

5.3 THE EXHAUST GAS SYSTEM

5.3.1 The Exhaust Duct

A single horizontal, refractory lined exhaust port located in the upper furnace sidewalls conveyed the gases to a refractory lined combustion chamber.

5.3.2 The Combustion Chamber

The furnace exhaust gases containing carbon monoxide and metal vapours were combusted and cooled to 600K with excess air in a vertical, refractory-lined combustion chamber. The combustion and cooling air flow was controlled by a damper immediately in front of the 70kW induced draught fan.

5.3.3 The Cyclone

A cyclone was installed ahead of the baghouse in an attempt to reduce the dust burden on the baghouse, but proved to be an ineffective dust collector because of the very small dust particle size and the low gas velocities.

5.3.4 The Baghouse Filter

Combusted gases were cleaned in two independently controlled Morley baghouse filters, each equipped with 96m^2 of woven stainless steel fibre filter envelopes capable of operating at 700K. Each baghouse could be isolated using dampers in the inlet and outlet ducting for off-line cleaning by reverse air jets. Several filter bags split during the early trials. The incidence of failure was reduced by locating a restraining cage around the envelope to restrict its flexure during the rigorous reverse jet cleaning cycle.

5.4 THE PLASMA TORCH

The plasma torch consisted of a water-cooled thoriated tungsten cathode surrounded by a water-cooled copper nozzle assembly to direct the plasma gas over the cathode tip. The torch was mounted in a service frame to facilitate its accurate positioning on the furnace roof and to enable it to be withdrawn to alter the arc length. The torch passed through a spherical water-cooled bearing seal in the furnace roof to allow it to precess through a variable angle. Power and cooling water connections between the torch and the service manifold were made via water-cooled flexible copper braids.

Figure 35 shows the original torch design and the modifications made during this work to improve its operating life to over 70 hours.

5.4.1 The Cathode

The thoriated tungsten tip was silver soldered into a water-cooled copper conductor tube. Electrical connection from the busbars to the conductor tube was made via twin flexible water-cooled copper braids. Electrical insulation between the cathode and the nozzle was achieved using a silica glass tube at the front (hot) end of the conductor tube and a PVC tube at the rear end.

5.4.1 The Cathode Material

Thermionic emission of electrons occurs when a suitable cathode material is heated to 3500-4000K at current densities greater than 1 MA/m^2. The current density at the cathode tip is given by the Richardson-Dushman equation:-

$$J = aT^2e^{-eW/kT} \qquad \text{eqn 36}$$

where
J = current density (A/m^2)
a = constant (6 MA/m^2K^2)
T = temperature (K)
e = electron charge ($1.6*10^{-19}$ C)
W = thermionic work function (V)
k = Boltzmann constant ($1.38*10^{-9}J/K$)

Figure 36 shows the work function of cathode materials at their boiling point, with the required current densities for thermionic emission superimposed (17). Most materials except C, Ta, Rh or W are vapours at the temperatures needed to achieve current densities of >10 MA/m². Tungsten is usually doped with 2% thoria, yttria, ceria or lanthia to reduce the work function and the operating temperature of the emitting surface. Tungsten doped with thoria is most commonly used because of the availablity of good quality material in the size range necessary for high current operation.

5.4.2 Cathode geometry

The cathode tip diameter for water-cooled thoriated tungsten is obtained from the limiting current density of approximately 30 MA/m² specified by the Plansee (129). A 5kA cathode has a diameter of 0.014m.

The tungsten cathode length to maintain the arc terminus spot at slightly below the tungsten melting point to aid thermionic emission is calculated from the approximate relationship:

$$l = fd^2/A \qquad \text{eqn 37}$$

where

l = cathode tip length (m)
f = tip heating function for thoriated tungsten (0.3 MA/m)
d = diameter of cathode (m)
A = cathode current (A)

A 5kA cathode will be 0.013m long.

The cathode tip is pointed and projects 0.003m in front of the nozzle front face to encourage the central attachment of the arc and to aid starting. The whole cathode assembly can be moved forward relative to the nozzle to maintain the gas annulus geometry as the tungsten tip erodes. Choosing the correct tip geometry for a given current is important because if a tip that is too long for the required current is used it will run hot and erode rapidly, destroying the cathode/nozzle geometry. If the tip is too short it will run cold and crack, giving a short cathode life.

5.4.3 Cathode Cooling

The high heat fluxes encountered at the cathode (and nozzle) demand that special attention should be paid to the heat transfer to the cooling water. At low heat fluxes, heat transfer occurs by conventional axial flow non-boiling convective heat transfer. As the heat flux increases, nucleate boiling occurs when bubbles form at the cooled surface, even though the bulk water temperature is well below its boiling point. Nucleate boiling is usually accompanied by a marked increase in the heat transfer coefficient as long as provision is made to sweep the bubbles away from the cooled surface to prevent the formation of an insulating steam film. Above a critical heat flux, film boiling occurs where the cooled surface is covered by a continuous steam film and the water no longer makes contact with the cooled surface, resulting in a much lower heat transfer coefficient and a rapid rise in the temperature of the cooled surface, leading to failure by burnout. For a high critical heat flux, the coolant should have a low vapour mass fraction, a low bulk temperature, a high pressure, a high velocity and a high convective heat transfer coefficient (130-135). By causing the the coolant flow to turn on a small radius at the cooled surface, a centripetal acceleration can be imparted to the flow which sweeps away the low density bubbles from the cooled surface, further increasing the the critical heat flux. Figure 37 (130) shows the heat flux against film temperature drop for various water velocities.

In the initial trials cathode failure by burnout occurred after 30 hours at 3kA, therefore the heat flux, water velocity and pressure at the cathode tip were calculated to determine the heat transfer mechanism. The power dissipated to the cathode cooling water arises from the Joule heating of the conductor tube, Joule heating of the flexible water-cooled copper cables and heating of the tungsten tip itself.

Total Power Dissipated in the Cathode Assembly

Water flow rate = $0.000175\ m^3/s$
Inlet temperature = 285.2K
Outlet temperature = 296.6K
Power dissipated = 8.4 kW

Power Dissipation due to Joule Heating in the Copper Conductor Tube

Internal diameter of tube = 0.01255m
External diameter of tube = 0.01905m
Length of tube = 1.4m
Cross sectional area of tube = 0.000161m
Resistivity at 373K = $0.022*10^{-6}$ ohms.m
Resistance at 373K = $194.7*10^{-6}$ ohms
Heat generated at 3kA = 1.75 kW

Power Dissipation due to Joule Heating in the Water-cooled Flexible Copper Braids Connecting the Plasma Torch to The Busbars

Cross sectional area of braid = $0.0000731\ m^2$
Length of twin braids = 1.40 m
Resistivity of braids at 373K = $0.0174*10^{-6}$ ohms.m
Resistance of braids at 373K = $333*10^{-6}$ ohms
Heat generated at 3kA = 3.0 kW

Power dissipated in the Tungsten Tip

Power dissipated = 8.4 - 1.75 - 3.0 = 3.65 kW
Diameter of tip = 0.019 m
Power density at tip = $12.8\ MW/m^2$

Water Velocity at Tungsten Tip

Gap between flow divider tube and tip = 0.002 m
Internal diameter of divider tube = 0.0075 m
Area of water passage = $0.0000471\ m^2$
Water flow = $0.000175\ m^3/s$
Water velocity = 3.7 m/s

Water pressure at Tip

Water pressure = 3.5 bar

Assessment of Cooling Efficiency

The boiling point of water at 3.5 atms pressure was 411K and the return water temperature was 296.6K, giving a maximum allowable temperature drop across the film of 114.4K before the onset of film boiling. From Figure 37, with a water velocity of 3.7 m/s and a film temperature drop of 114.4K, the maximum heat flux that can be dissipated by water is 2.0 MW/m^2. The measured heat flux was 12.8 MW/m^2. Therefore, cathode failure was almost certainly due to film boiling and burnout. A dedicated high pressure coolant pump was installed to increase the cathode coolant flow and pressure and the gap between the divider tube and the tip was reduced to 0.0015m to increase the water velocity. The heat flux and water velocities for the new arrangement were:-.

Coolant flow = 0.00037 m^3/s
Coolant velocity = 10.4 m/s
Coolant pressure at tungsten tip = 7 bar
Coolant boiling point = 441K
Maximum temperature drop across film = 150K

From Figure 37, the maximum theoretical heat flux that can be dissipated by the water is now 9.0 MW/m^2 compared to the measured heat flux 12.8 MW/m^2. The improved water flow increased the cathode tip life from about 30 hours to 70 hours. Further improvements in the cathode life may be achievable by further increasing the water pressure, flow and the cooled surface area of the tungsten tip.

5.4.4 The Nozzle

The nozzle directs the plasma gas around the cathode tip, protects the tip from splashes and provides a return electrical connection for the high frequency starting discharge during arc initiation. The 0.05m diameter nozzle was manufactured from a series of concentric copper tubes welded into a copper end piece. Oxygen free, high conductivity copper was used for the end face because it combined high thermal and electrical conductivity with ease of construction at a reasonable price.

5.4.5 Nozzle Cooling

The initial nozzle design failed after approximately 30 hours of operation by burnout at the inner edge of the nozzle orifice, therefore an examination of the heat flux and cooling design was carried out.

Heat Flux on Nozzle Tip

To estimate the heat flux on the critical nozzle tip alone, the plasma arc was run onto a piece of hot carbon in a cold furnace.

Inlet water temperature = 295K
Outlet water temperature = 305K
Water flow rate = 0.00087 m^3/s
Power absorbed = 36.4 kW
Surface area of coolant passage = 0.00083m^2
Power density = 43.9 MW/m^2

Water Velocity at Nozzle Tip

Cross sectional area of coolant passage = 0.00026m^2
Water flow rate = 0.00087 m^3/s
Water velocity = 3.33m/s

Coolant Pressure at Nozzle Tip

Coolant pressure at nozzle tip = 3.5 bar

Assessment of Cooling Efficiency

Boiling point of water at 3.5 bar = 411K
Return water temperature = 305K
Temperature drop across film = 106K

From Figure 37, the maximum heat flux that can be dissipated for a film temperature of 106K and a water velocity of 3.33m/s is 2.0MW/m^2 compared to a measured heat flux of 44.9MW/m^2. The nozzle coolant passages were modified to increase the surface area presented to the coolant, the passage gaps were reduced to increase the coolant velocity and a larger capacity, higher pressure coolant pump was installed. The following results were obtained:

Inlet water temperature = 295K
Outlet water temperature = 299K
Flow rate = 0.002m^3/s
Power absorbed at nozzle tip = 35kW
Surface area of coolant passage = 0.0017m^2
Measured power density = 20.5MW/m^2
Cross sectional area of coolant passage at nozzle tip = 0.00019m^2
Water velocity = 10.5 m/sec
Coolant pressure at nozzle tip = 7 bar
Boiling point of water at 7 bar = 441K
Maximum temperature drop across film = 142K
Critical power density = 10MW/m^2

Although the measured power density of 20.5MW/m^2 still exceeded the critical power density of 10MW/m^2, the modifications to the nozzle tip increased its life from 30 hours to about 70 hours.

5.4.6 Plasma Gas

Argon gas was passed through the annulus formed between the nozzle and the cathode to produce an electrically conductive ionized gas stream to stabilize the arc, to protect the cathode from attack by the furnace atmosphere, slag and metal splashes and to cool the cathode by the endothermic dissociation of the gas. The required gas flow rate was 0.0004-0.0006 m^3/s of argon per 1kA.

5.4.7 Torch Movement

The plasma arc length (and voltage) could be altered by withdrawing the torch through a water-cooled spherical bearing assembly mounted in the furnace roof. The torch precessed at a variable angle of 0-15 degrees from the vertical axis and at a rotational speed of 30 rpm to distribute the plasma arc energy evenly over the melt surface. With the torch fully lowered, the arc length (to the hearth) was 0.4m and the precession circle diameter was 0.5m. With the torch fully raised, the arc length increased to 1.0m and the precession circle diameter decreased to 0.2m.

5.5 THE PLASMA POWER SOURCE

The D.C. power source was a fully phase controlled, 24 pulse thyristor rectifier unit in 2 bridge pairs which could be connected in series or parallel for high voltage or high current operation. Off-load tap changing on the primary winding of the transformer was used to set the open circuit voltage near to the voltage requirement for the particular process to maximize the power factor. Because the plasma arc has a very low inductance, short circuit protection and ripple control was provided by a series DC reactance.

The plasma arc was initiated by a high-frequency, high-voltage spark between the cathode tip and the nozzle. The subsequent 200A pilot arc produced between the cathode and the front face of the nozzle was transferred directly to the melt or to a temporary hand held carbon electrode held 0.05m below the plasma torch and subsequently lowered to the melt surface. Arc initiation, power source control and protection circuits were controlled by a programmable logic computer (PLC).

To detect unwanted current leakage paths and protect the torch from destructive 'side arcs', the torch frame, furnace roof, furnace shell and anode were all electrically isolated from each other and earthed via individual current detecting transformers which tripped the power source if the leakage current exceeded a set value, typically 200A.

5.6 INSTRUMENTATION

Arc Characteristics

The plasma Arc amperes were measured to an accuracy of +/- 2% at 3kA by a current transformer located in the anode cabling. The anode amps were intermittently checked using a hand held "clip on" ammeter. The "plasma arc" voltage was measured to an accuracy of +/-2.5% at 300V. The "plasma arc" power was calculated by the PLC by multiplying the instantaneous arc amps and volts. Because of the slight fluctuations in the arc amps and volts, the kW recording was subject to an instantaneous error of +/-5% at 1 MW. The energy consumed was calculated to an accuracy of +/- 5% by integrating the power input over a time base.

Argon Gas Consumption

The consumption of argon plasma gas was monitored and controlled using calibrated rotameters.

Water Cooling

All return water flows were monitored using rotameters to an accuracy of +/-5%. Matched pairs of Cu-constantan thermocouples were located in the flow and return of every cooling water circuit to compute temperature differentials. The Cu-constantan thermocouples and associated chart recorder were calibrated before and after each trial using a mercury-in-glass thermometer. Accuracies of the matched pairs of thermocouples was +/-0.5K. Water flow, pressure and temperature alarms interfaced with the PLC to shut down the power source in the event of a water circuit malfunction.

Thermocouples

Pt-Pt/13% Rh thermocouples were located in the refractories to monitor the condition of the side walls at the slag line, the roof, and the anode. The thermocouples were generally located in groups of three to measure a temperature profile across the refractories and predict a hot face temperature and refractory thickness. Cu-constantan thermocouples were welded to the steel shell to monitor the shell temperature for computation of convective and radiation heat losses. Chromel-Alumel thermocouples were positioned in the exhaust gas and baghouse system to monitor the exhaust gas temperature. A port in the furnace sidewalls was provided for the measurement of the bath temperature using a Land disposable Pt-Pt/13% Rh immersion thermocouple. The accuracy of the Pt-Pt/13% Rh and the Chromel-Alumel thermocouples was reported as +/-2K by the manufacturer and their resolution on the chart recorders was +/-5K.

Furnace pressure

A pressure transducer mounted on the inspection port door monitored the furnace pressure. A slightly positive furnace pressure (+0.001 bar) was maintained by varying the position of the butterfly valve immediately in front of the induced draught fan.

Raw Materials And Product Weights

All raw materials and product were weighed on a weighbridge to an accuracy of +/-2% The weighbridge was calibrated before and after the trials.

6.0 EXPERIMENTAL PROCEDURE

6.1 EXPERIMENTAL PLAN

Four trials of one week duration were conducted:

In trial week A, 15 t of chromite concentrates were smelted to produce a charge grade carbon ferrochrome.

In trial week B, alloy steel dust was smelted to recover the Cr, Ni and Mo to a ferroalloy for recycling to the arc furnace.

In trial week C, a low ZnO content EAF dust from Templeborough Steel and a medium ZnO content dust from Sheerness steel were smelted under totally reducing conditions to produce a non-toxic slag and recover the zinc and lead values to an enriched zinc oxide baghouse dust.

In trial week D, high ZnO content EAF dusts from Tremorfa Steel and Irish Steel were smelted under selectively reducing conditions to produce a non-toxic slag and recover the zinc and lead values to an enriched zinc oxide baghouse dust.

The dusts were selected to include a range of ZnO, PbO, Cr_2O_3 and CaO contents to determine the effect of dust composition on slag toxicity, product analyses, energy consumption, furnace operation and treatment economics.

6.2 RAW MATERIALS

The majority of the chromite and dusts were smelted in the "as received" form. A proportion of the Irish steel and Sheerness EAF dusts were pelletized with approximately 10% moisture in a concrete mixer. No binders were necessary to produce green pellets up to 0.01m in diameter which would support a 0.025t load. Drying the pellets at 400K in a gas fired rotary drier increased the pellet strength to 0.075t breaking load. Pellets were sieved through a 0.002m screen and the undersize returned to the pelletizer. Feeder tests showed that passing the pellets through the furnace feed system produced about 10% of <0.002m material.

An anthracitic coal containing 81% fixed carbon, 9% ash and 10% volatile matter was chosen as the reductant because of its high reactivity, low ash and low sulphur contents. The coal contained 5% moisture and had a particle size of <0.05m. Silica sand containing 98% SiO_2 and lime containing 96% CaO were used as fluxes.

The blend of chromite or steelplant dust, reductant and fluxes was calculated using the mass and energy balance model presented in Appendix 1. In the chromite smelting trial (A), the effect of slag composition and degree of reduction on chromium recovery were investigated by varying the sand/chromite and the anthracite/chromite ratios. In the steelplant dust trials (B, C and D), the coal addition was varied to determine the effect of degree of reduction on product analyses, slag toxicity and smelting energy consumption.

6.3 FURNACE OPERATION

The furnace refractories were dried out and preheated to 1100K at 20K/h using a 100kW natural gas burner. After soaking, the gas burner was replaced by the plasma torch arcing to a coke bed and the furnace was brought up to the operating temperature of 1700K over 24 hours. Once thermal equilibrium was attained, the energy losses from furnace were determined by measuring the total energy input and comparing it to the total energy losses from the various parts of the furnace. Feeding was started at a low rate of 0.1t/hour and gradually increased to the desired rate over several hours.

The primary operating aim was the maintenance of a constant melt temperature, high uninterrupted feed rates and a minimum power input so that meaningful mass and energy balance data could be obtained. For each feed blend, a feed rate-power input relationship based on the smelting energy requirements of the feed material and the steady state energy losses from the furnace was generated by the thermodynamic mass and energy balance model. As the feed rate varied, the operator adjusted the power input (arc current) to maintain a constant melt temperature. The accuracy of the feed rate-power input relationship was checked by measuring melt temperature over a time period and observing any deviations from the predicted value.

The energy losses were periodically checked by measuring the total energy input to the furnace to maintain the bath at a constant temperature and/or measuring the total water-cooling, convective and radiation losses from the shell.

During trial week A, feed was processed between 06-00 and 22-00 hours only because of shortage of manpower. Between 22-00 and 06-00 hours the furnace was maintained at 1700K using a carbon electrode arcing to the bath. In subsequent trials, the furnace was operated continuously, 24 hours per day. Tap temperatures were generally in the range 1723-1798K when continuous, uninterrupted feeding was practised, but processing delays upset the energy balance predictions and often resulted in temperature excursions. The feed rate to the furnace varied between 0.2-0.7t/hour and was limited by the capacity of the baghouse. The furnace was tapped when approximately 1t of feed had been consumed.

The feed ports in the furnace roof occasionally blocked up with sintered feed and required rodding out at least once per shift. In the event of a plasma torch failure, the power and feed were immediately stopped, maximum suction applied to the furnace and the torch removed. Exchanging the torch took about 30 minutes.

The furnace pressure was kept slightly positive to minimize the ingress of air by adjusting the baghouse fan damper. The baghouse inlet gas temperature was maintained at 400-650K by altering the position of the dilution air damper in the base of the combustion chamber. The two baghouses were operated with one on-line and one off-line for cleaning and were emptied and sampled every time the furnace was tapped. The horizontal exhaust duct from the furnace to the combustion chamber was rodded on every shift to remove the build up of loose slag and ZnO. During trial week D, the exhaust duct was completely blocked by a foaming slag, requiring the furnace to be brought off-line for several days for a clean out. Several of the filter envelopes in the baghouse ruptured during the trials, allowing dust to escape to the downstream scrubbing tower.

6.4 SAMPLING

The raw materials were sampled by taking approximately twenty 0.5kg grab samples from the homogenized pile of raw materials, mixing the resultant conglomerate sample and splitting it down in successive stages to 0.2kg. The lack of perfect homogenization of the feed and the grab sampling of the pile introduced an unquantified error into the analytical results. Four spoon samples of metal and slag were taken at intervals from each tapping stream and composited. For the EPA toxicity test, a representative 0.2t bulk sample was taken from the cooled tap slag and reduced to 0.002t. The baghouse dust from each tap was sampled by taking four tube samples from the dust receiving hopper. The furnace exhaust gases were sampled from the exhaust duct immediately after the furnace using a stainless steel probe and a vacuum pump to transfer the sample to a gas burette for analysis by gas chromatography. Zinc often condensed inside the probe and blocked it before a sufficient volume of sample could be obtained.

Full analyses of all raw materials and condensed products were carried out on a historical basis by the British Steel Corporation, Swinden Laboratories using X-ray fluoroscopy for oxides, Leco combustion in oxygen for C and S and atomic absorption for CdO, PbO and halogens. The Environmental Protection Agencies Toxicity Tests (EPTox) were made by the Bethlehem Steel Corporations' Homer Research Laboratories in Bethlehem, USA.

6.5 DATA COLLECTION

The weight of feed material consumed per tap was determined from the loss in weight of the furnace feed hopper and by counting the number of bags of preweighed feed that were consumed. Approximately 2% of the feed material was lost as spillage in bag handling, loading to the feed system and clearing blockages in the feed conveyors. At the end of a trial, the feed system was emptied and the residual feed subtracted from the total consumed. The metal, slag and baghouse dust weights were recorded on an individual tap basis to an accuracy of +/-2%. Emptying the slag/metal boxes resulted in an estimated spillage of 2% of the contents weight. At the end of a trial, the furnace roof was removed and a crude estimate of the residual slag and metal in the furnace was made by drilling and measuring the heel. The duct work and baghouse filter were cleaned down as far as practically possible, but it was conceivable that as much as 5% of the total baghouse dust was unrecovered. The estimated trial mass balance accuracy is +/-10%.

All significant changes in operating variables, events and delays longer than 2 minutes in duration were recorded in a log book. A data logger printed out the plasma arc current, voltage, power, kWh, feed rate and cumulative feed weight consumed, at 2 minute intervals.

An energy balance was calculated around the furnace at 30 minute intervals by measuring the total power input, the water flows to all cooling circuits, the inlet and outlet temperatures of the coolant water and the temperature of the furnace shell. In the initial trials, the thermocouples and chart recorder were accurate to +/-1K, but high resolution thermocouples and a digital thermocouple readout were used in the later trials to improve the accuracy and resolution to +/-0.2K.

The dimensions of the refractory working lining were measured before and after each trial to determine the rate of refractory corrosion.

7.0 RESULTS

The results for the chromite, alloy dust and EAF dust smelting trials are broadly categorised into;

- raw material analyses
- metal analyses
- slag analyses
- baghouse dust analyses
- plant operation
- mass balance
- energy consumption

7.1 CHROMITE SMELTING RESULTS

7.1.1 Raw Materials

The chromite raw materials analyses are given in Table 7 and the feed blends used are given in Table 8. Taps A/1 to A/16 examined the effect of slag composition on chromium recovery by varying the sand/chromite ratio from 0.14 to 0.18. Taps A/17 to A/21 examined the effect of degree of reduction on chromium recovery to the ferroalloy by varying the anthracite/chromite ratio from 0.24 to 0.31.

7.1.2 Ferrochrome Metal Analyses

Ferroalloy, slag and baghouse dust samples were analysed by the BSC Swinden laboratories and the results are presented in Table 8. Selected samples were analysed by the London and Scandanavian Metallurgical Co., Ltd (LSM) and these results are given in Table 9. The chromium analyses from BSC were generally 2-3% higher than the LSM results, but no explanation for the difference is offered, as the laboratories used a similar analytical technique. The reported alloy silicon, carbon, phosphorus and sulphur contents from both laboratories were in acceptable agreement.

If taps A/1 to A/5, where the ferrochrome was diluted by the metal heel remaining from a previous trial are ignored, an acceptable charge grade ferrochrome containing 50-57% Cr, 6.0-7.1% C, 1-4% Si, 0.03-0.04% P and 0.03-0.08% S was produced.

Figure 38 shows that, although the alloy chromium content varied between 49.6% and 57.2% (BSC analyses), there was no significant relationship between alloy chromium content and the tapping temperature or the anthracite/chromite ratio. An increase in alloy chromium content might be expected with increasing reductant addition as more Cr_2O_3 was reduced from the slag, but the relationship was probably masked by the increase in alloy silicon content.

Figure 39 shows the increase in the alloy silicon content from <1% to 4.6% as the tap temperature increased from 1700K to 1950K and the anthracite/chromite ratio increased from 0.27 to 0.31. The sand/chromite ratio in the blend had no significant effect on alloy silicon content. The increase in alloy silicon content with increasing temperature and reductant is to be expected because SiO_2 has a similar free energy of reduction to Cr_2O_3.

Figure 40 shows the slight decrease in ferroalloy carbon content from 7.1% to 6.7% as the melt temperature increased from 1700K to 1950K. The alloy carbon content was independent of the anthracite/chromite ratio and the silica/chromite ratio. It is not apparent from the limited results whether the decrease in carbon content with increasing temperature was due to dilution by the increasing silicon content of the ferroalloy (see figure 39) or to the increasing thermodynamic stability of lower carbon chromium carbides with increasing temperature.

Figure 41 illustrates the decrease in alloy sulphur content from about 0.06% S to 0.04% S as the slag basicity ($CaO+MgO/SiO_2$) increased from 0.8 to 1.3. The alloy sulphur content appears to decrease with increasing anthracite/chromite ratio and tapping temperature, but this is probably a reflection of the higher slag basicity associated with the reduction of silica from the slag.

The ferrochrome phosphorus content of 0.03-0.04% was independent of anthracite/chromite ratio, slag basicity and tap temperature over the range examined. To meet the alloy phosphorus specification, low phosphorus content reductant and fluxes must be selected.

7.1.3 Ferrochrome Slag Analyses

The ferrochrome slag analyses presented in Table 9 ranged from 23-36% SiO_2, 4-8% CaO, 21-37% MgO, 22-34% Al_2O_3, 1-5% FeO and 2-10% Cr_2O_3 and are shown superimposed on the SiO_2-MgO-Al_2O_3 liquidus diagram in Figure 26. There was considerable variation in slag chemistry in Taps A/4 to A/12, despite the constant sand/chromite and reductant/chromite ratios because of variations in the melt temperature, SiO_2 reduction and MgO pickup from the refractory lining.

Taps A/1, A/3, A/3, A/13 and A/14 with a high anthracite/chromite ratio of 0.31 and a low sand/chromite ratio of 0.14 were difficult to tap because of a high slag liquidus temperature associated with a low slag SiO_2 content. The tapping problem was resolved by increasing the sand/chromite ratio from 0:14 to 0.16-0.18 to increase the slag SiO_2 content to30% and decrease the slag liquidus temperature to 1700K. For a constant sand/chromite ratio of 0.185 in Taps A/16 to A/21, the SiO_2 in the slag decreased from 36-38% to 26-28% as the anthracite/chromite ratio increased from 0.24 to 0.31 and more silica was carbothermically reduced from the slag.

Figure 42 shows the expected decrease in the chromium oxide in the slag as the anthracite/chromite ratio increased. Increasing the sand/chromite ratio marginally decreased the chromium oxide content in the slag, probably by decreasing the slag liquidus temperature and enhancing the chromite dissolution. Figure 43 shows the decrease in chromium oxide content with increasing slag MgO/Al_2O_3 ratio, probably as a result of the decreased slag viscosity. The variation in MgO/Al_2O_3 ratio was not deliberate, but a result of MgO pickup from the furnace refractories.

It was difficult to determine the independent effect of process variables on, for example, the chromium oxide content of the slag because most variables were interdependent. Increasing the tap temperature increases the driving force for the reaction, but also increases the amount of silica reduced and the slag basicity. Increasing the tap temperature also increases the amount of MgO corroded from the refractory lining and increases the MgO/Al_2O_3 ratio.

7.1.4 Ferrochrome Baghouse Dust Composition

The baghouse dust contained 4% Cr_2O_3, which represents an acceptable loss of <1% Cr_2O_3 charged to the furnace. The dust was enriched in SiO_2 and MgO relative to the feed composition because SiO_2 and MgO are probably reduced to the volatile subspecies SiO and Mg at the elevated temperatures and reducing conditions existing in the melt.

OXIDE	THEORETICAL ANALYSIS mass%	ACTUAL ANALYSIS mass%
SiO_2	21.6	24.8-30.8
CaO	3.7	4.5- 4.5
MgO	11.9	39.3-41.0
Al_2O_3	11.8	3.1- 4.1
Fe_2O_3	18.8	4.7- 4.7
Cr_2O_3	29.2	3.9- 4.6

7.1.5 Gas Analysis

Gas sampling was difficult because the sampling point in the exhaust duct continually blocked up, making it impossible to obtain good samples. The average of 4 results was 50% CO, 5.8% CO_2, 24% H_2, 20% N_2 and 0.2% O_2, suggesting that air was leaking into the system. The high H_2 content of the gas was produced from the volatile matter content of the coal and the reaction between H_2O in the feed and carbon.

7.1.6 Chromite Smelting Mass Balance

Table 10 shows the distribution of oxides between the condensed phases after estimating the weight of the initial metal heel to be 0.6t +/-0.3t (95% Fe, 0% Cr) and the final heel to be 0.7t +/-0.3t (28% Fe, 54% Cr). A total of 14.9t of chromite was consumed producing 6.4t of alloy, 9.1t of slag and 0.8t of baghouse dust. Single tap mass balances were not calculated because the retention of metal and slag in the furnace from one tap to the next and the experimental nature of the trial made them relatively meaningless. A completely closed trial mass balance was not possible because the exhaust gas mass was not measured.

91.4% of the chromium in the feed reported to the alloy, 8.2% to the slag and 0.7% to the baghouse dust, giving an acceptable accountability of 100.3%. The chromium recovery to the alloy improved to 93% during taps A/5-A/11 with constant operating conditions at an anthracite/chromite ratio of >0.3 and a sand/chromite ratio of >0.16.

90.9% of the iron charged to the furnace reported to the alloy, 6.1% to the slag and 1.2% to the baghouse dust, giving an acceptable trial accountability of 98.2%.

8.3% of the silica was reduced to silicon and dissolved in the alloy, 7.1% reported to the baghouse dust and 84.4% reported to the slag, giving a trial accountability of 99.8%. Allowance must be made for the SiO_2 losses from the slag when calculating the charge composition, otherwise high liquidus temperature slags will be produced.

The high MgO accountablity of 140% was a result of the corrosion of approximately 1.2t of MgO refractory by the siliceous slag. 16.7% of the MgO charged to the furnace reported to the baghouse dust, probably by the reduction of MgO in the slag to Mg vapour, which was reoxidized in the combustion chamber and collected in the baghouse. The carbothermic reduction of MgO and SiO_2 from the slag alters the slag composition and significantly increases both the reductant and energy consumptions.

7.1.7 Furnace Operation

The furnace operating parameters for individual taps are summarized in Table 11. Blend feed rates were limited to 0.35-0.4t/hr by the power available from the power source (0.64MW at 1.6kA and 400V) and the capacity of the baghouse filter. The overall feed processing time was 96 hours out of a possible 106 hours, representing a process availablity of 93% which is good for a small pilot plant operation and would suggest that high availablities can be expected in a commercial design. Delays were mainly due to power source thermal overloads, feeder blockages, torch failures, tapping difficulties and roof refractory maintenance. 5 torch failures occurred due to local overheating of the cathode and nozzle tips and short circuit arcing between the nozzle and the furnace refractories. The torch design was modified to increase the water velocity at the torch tip and high pressure water pumps were installed as described in section 5.4.

Short circuit arcing was reduced by improving the torch head bearing insulation and operating at shorter arc lengths and lower arc voltages.

Difficulties in tapping the high liquidus temperature slag experienced at the beginning of the trial were overcome by increasing the power input and increasing the sand/chromite ratio to lower the slag liquidus temperature.

Tapping temperatures were variable and generally lower than the desired 1873K because the furnace was under-powered at the beginning of the trial when its operating characteristics were being determined. The non-continuous, 16 hours/day furnace operation led to significant departures from thermal equilibrium, especially at the beginning of each day.

7.1.8 Refractory Life

Mass balance and visual observations suggest that 1.1-1.2t of refractory were corroded from the slag line region during the testwork, corresponding to nearly 10% of the original refractory mass or 50% of the slag line refractory mass. This was an extremely high refractory consumption compared to conventional submerged arc furnaces, which have a refractory life of about 5 years. Factors contributing to the refractory wear were the small furnace size, the absence of any protective feed/frozen slag banks near the sidewalls and the use of mag-chrome refractories with a siliceous slag. Carbon, mag-carbon or straight magnesia refractories in a larger furnace shell and cooling at the slag line may be a superior refractory system. The feed ports in the furnace roof should be moved out towards the sidewalls to encourage the formation of a bank of unreacted feed against the sidewalls.

7.1.9 Chromite Smelting Energy Balance

The gross energy consumption for each tap is given in Table 11 and Figure 44. The average gross energy consumption was 6.96MWh/t of alloy, but there is a very wide scatter in the data because of variable feed rates, delays and difficulty in allocating the weight of alloy tapped to a particular tap. If the second period of the trial (Taps A/13-A/21), when the furnace operation was smoother and the operating delays were less frequent is considered, the average energy consumption drops to about 6.48MWh/t of alloy.

The average energy losses from the furnace were 160kW and are itemized in Table 12. The energy losses are high because of the small unit size, the water-cooled electrode and the fully exposed roof and sidewalls.

7.1.10 Summary of Chromite Smelting Results

An in-specification charge grade ferrochrome containing 52-54% Cr, 6-7% C, 1-3% Si, <0.04% S and <0.04% P was produced by smelting chromite concentrate in the transferred-arc plasma furnace.

Fine chromite concentrates were smelted directly without any furnace operating problems or excessive feed carry over with the exhaust gases. Anthracitic coal was successfully used as the reductant.

Chromium partitioned 87-93% to the ferroalloy, 4-6% to the slag and 1% to the baghouse dust.

For maximum Cr recovery to the ferrochrome, an anthracite/chromite ratio of 0.31, a sand/chromite ratio of >0.16 and a magnesia/alumina ratio of >1.6 is required.

The gross smelting energy consumption was 6.5-7.0MWh/t of alloy, suggesting a commercial value as low as 4.5MWh/t with dry feed.

Furnace processing availablity was 93% of the time available, suggesting an availability of around 95% for a commercial plant. Plasma torch life was improved from 30 hours to 70 hours by increasing the water flow to the nozzle and cathode and redesigning the torch water passages. Refractory corrosion of the magnesia chrome bricks at the slag line was severe.

7.2 STEELPLANT DUST SMELTING RESULTS

7.2.1 Dust Analyses

Table 13 presents the composition of the five dusts used in the smelting trials. To determine the variation in analytical results between laboratories, an identical dust sample was distributed to 5 independent laboratories and the results are listed below:

LABORATORY	DUST COMPOSITION, %		
	ZnO	PbO	Fe_2O_3
BSC	31.1	4.9	31.1
ARMCO	30.5	5.1	34.4
INLAND	29.9	5.1	37.9
LTV	30.7	5.3	40.7
St. JOE	32.9	5.4	40.8

The variation in iron oxide analysis has implications on reductant consumption, energy consumption and process costings. Further analyses and a comparison of analytical techniques is suggested to highlight the source of error.

To determine the day to day variation in dust analyses from a given steelplant plant, eight Tremorfa dusts samples were analysed and the results are presented in Table 14. The variation in the iron and zinc oxide content of the dust is sufficient to cause fluctuations in the slag ZnO and FeO content for a given reductant and energy. The peak in the dust fluorine content would cause dross formation problems in a zinc condenser.

7.2.2 Feed Composition

The feed compositions used in the trials are presented in Tables 15-17. The coal addition to the alloy steel dust was maintained at the stoichiometric requirement to totally reduce all the alloy oxides to a ferroalloy. The coal addition to the EAF dusts was varied between 0.1 and 0.25t/t to investigate the merits of selective reduction of the ZnO, leaving the FeO in the slag. A small silica flux addition was blended with the dusts to produce a CaO/SiO_2 ratio of 0.8-1.0, a slag liquidus temperature of 1723K and a slag viscosity of <5 centipoise.

7.2.3 Metal Analyses

The total carbothermic reduction of the AOD dust produced 0.45t of ferroalloy/t of dust smelted. The ferroalloy contained 58-68% Fe, 17-22% Cr, 5-7% Ni, 2.0-2.5% Mo, 4-6% C, 0-4% Si, 0.04-0.1% S and 0.05-0.075% P, which was in reasonable agreement with the model prediction of 58% Fe, 21% Cr, 5.5% Ni, 2.4% Mo and 4.3% C, calculated assuming 100% recovery of the metal oxides to the ferroalloy.

The iron alloy produced from the reduction of the EAF dusts contained 95.0-97.0% Fe, 0.5-3.0% C, 0.1-2.0% Si, 0.1-0.7% S, 0.2-0.7% P and 0.5-1.0% Cu. The carbon level in the iron was lower than blast furnace pig iron because of the higher oxygen potential in the slag associated with the selective reduction of ZnO. Both the carbon and sulphur in the iron increased as the coal adition increased. The majority of the phosphorus, copper and tramp elements in the dust were recovered to the iron, reducing its value as scrap for recycling to the EAF.

7.2.4 Slag Analyses

The slag analyses produced from smelting steelplant dust are shown superimposed on the $CaO-SiO_2-FeO$ liquidus diagram in Figure 31. Slag analyses were consistent with the dust composition and reductant addition rate except for the early slags in Trial C, where the high chromium oxide content was a result of pickup from the chromium rich metal heel remaining in the furnace after treating alloy steel dust.

The Effect of Degree of Reduction on Slag Composition

The effect of coal addition on the residual ZnO, Cr_2O_3 and FeO content in the slag is illustrated in Figures 45, 46 and 47 respectively. In the total reduction mode (using a stoichiometric coal addition), the residual FeO, ZnO, Cr_2O_3, PbO and CdO in the slag were reduced to <0.5%, <0.2%, <1.0%, <0.2% and <0.2% respectively. In the selective reduction mode using a coal addition rate of around 0.15t/t dust, the ZnO, PbO and CdO in the slag were reduced to <1.0%, <0.2% and <0.2% respectively, leaving about 2% Cr_2O_3 and 30-50% FeO unreduced in the slag. Because very little chromium oxide is reduced in the selective reduction mode, steelplant dust containing >0.5% chromium oxide must be smelted under more reducing conditions to produce a non-toxic slag containing <1% chromium oxide.

Slags containing around 50% FeO were prone to foaming, but this could be avoided by adjusting the reductant addition to maintain <50% FeO in the slag or increasing the slag temperature.

The Effect of Slag Basicity on the Residual ZnO in the Slag

No relationship between slag CaO/SiO_2 ratio and the ZnO, PbO and CdO content of the slag could be determined because the metal oxide content of the slag was <0.2%,the detection limit of the XRF analysis technique. Slag basicity will have a more pronounced effect at lower melt temperatures where the changes in the zinc oxide activity coefficient with slag compostion are larger.

7.2.5 Baghouse Dust Analyses produced from Smelting Steelplant Dusts

Smelting ZnO rich EAF dusts produced a baghouse dust containing 60-75% ZnO, 5-10% PbO, 3-6% K_2O, 3-6% Na_2O, 5-10% Cl and 5-10% F, whereas smelting alloy steel dusts produced a baghouse dust containing 34-54% ZnO, 4-6% PbO, 5-17% Fe_2O_3, 1-3% Cr_2O_3 and 2-3% K_2O.

The Effect of Steelplant Dust Composition on Baghouse Dust Analysis

The majority of the ZnO, PbO, CdO, K_2O, Na_2O, F and Cl in the steelplant dusts were reduced, volatilized, reoxidized and recovered to the baghouse dust, limiting the ZnO content of the baghouse dust to about 80% by contamination. Figure 48 shows that the % ZnO in the baghouse dust increased as the % ZnO in the steelplant dust increased because of the mass concentration effect and dusts high in zinc oxide (low in iron oxide) produce a smaller gas volume than dusts with a low zinc (high iron oxide) content, reducing the particulate carry over. The same effect is seen in Figure 49, where the iron oxide in the baghouse dust increased with increasing iron oxide content in the steelplant dust.

The Effect of the Degree of Reduction of the Steelplant Dust on the Baghouse Dust Analysis

Figures 50 and 51 show the slight decrease in ZnO and the rapid increase in the Fe_2O_3 content of the baghouse dust with increasing coal addition rate. The sudden increase in the iron oxide content of the baghouse dust with near stoichiometric reductant additions to the steelplant dust may be due to the increased feed carry over with larger exhaust gas volume and the formation of iron vapour or a volatile complex species under the hot, reducing conditions at the arc/melt interface.

The increase in gangue oxides carried over to the baghouse with increasing coal addition is probably a result of the increased exhaust gas volume and the reduction and volatilization of SiO_2 and MgO at the high temperature plasma arc/slag interface. Insufficient data was available to determine the independent effect of feed rate (and therefore exhaust gas velocity) on the degree of feed carry over.

The Effect of Agglomerating the Steelplant Dust on Baghouse Dust Analysis

There was no apparent difference in the % ZnO and % Fe_2O_3 in the baghouse dust produced from a limited number of taps using Sheerness dust or pellets. The lack of benefit from agglomeration may be due to the pellets degrading in passage through the screw feeders to the furnace, or disintegrating on entering the furnace through thermal shock and rapid expansion.

7.2.6 Slag Toxicity

The results of the EPA Toxicity Test are compared to the 6 times the drinking water standard in Table 18. All the slags tested passed the EPTT test. Pb and Cd in the leachate were below the detection limits of the analyser, but the Cr levels were variable and did not relate to the "Cr_2O_3" levels in the slag. The leaching characteristics of the slag require further investigation, but are probably affected by the slag chemistry, mineralogy, cooling rate and particle size.

7.2.7 Steelplant Dusts Mass Balance and Distribution of Elements Between the Condensed Phases

Table 19 presents the distribution of the oxides between the condensed phases. The total accountablity of the oxides was only 90%, probably because of spillages and losses from the feed blending and product handling system, unrecovered dust from the inaccessible sections of the exhaust gas ductwork and baghouse filters, several ruptured baghouse filter envelopes and retained Fe, Cr, Ni in the metallic heel below the furnace taphole level.

The recovery of the Fe_2O_3, Cr_2O_3, NiO and MoO_3 from the alloy steel dust to the ferroalloy was 90.7%, 84%, 94% and 86% respectively. Less than 5% of the alloy oxides reported to the slag and baghouse dust, suggesting that recoveries to the ferroalloy in a commercial operation with a sealed feed and product handling system may exceed 95%.

The recovery of ZnO, CdO and PbO from the EAF dust to the baghouse dust was about 90%. Less than 0.2% ZnO, PbO and CdO were retained in the slag phase, suggesting that in a prolonged steady state operation, the recoveries to the baghouse filter should approach 99.0%.

7.2.8 Equipment Operation and Availablity

The tap to tap time, feed processing time and power on time are presented on a tap-to-tap basis in Tables 20-22 and are summarized below:

TRIAL No	FEED AVAILABLITY %	PLASMA AVAILABLITY %
B Alloy dust	74	85
C EAF dust	71	96
D EAF dust	81	87

The Feed System Operation

The feed processing availablity during the trials averaged 75%, which considering the development nature of the trials and the difficult handling properties of the dust, is a reasonable result. Delays were mainly associated with the poor flow characteristics and sintering of the EAF and Alloy steel dusts in the feed system. Problems with EAF and Alloy steel dusts bridging in the furnace feed hopper were reduced by building a larger feed hopper incorporating a "live bottom" with large diameter screws and a horizontal agitator to keep the dust in motion. Transfer screw blockages were overcome by increasing the diameter and torque of the transfer screws, sieving the feed to remove oversize particles, modifying the screw flight at the feed discharge end to prevent feed compaction against the end face of the screw casing and water-cooling the end face of the screw casing adjacent to the furnace feed port to prevent feed sintering. The roof feed ports were increased in size and fitted with a disposable refractory liner to reduce the impact of accretion build up.

The Exhaust System

The horizontal exhaust duct between the furnace and the combustion chamber required cleaning about every 8 hours to remove dry drop-out material and slag splash. During the selective reduction of the Templeborough dust, a foaming slag flowed into the duct and almost completely blocked it, resulting in an extended delay to clear the duct. A roof mounted exhaust is recommended to reduce the effect of slag splash and to facilitate the rebricking of the furnace sidewalls. An expansion box or drop out chamber in the exhaust duct to remove the coarser particles should be considered. The high level of dust and slag carry over would probably cause excessive dross build up if a zinc condenser was built into the exhaust system. The cyclone used in the Sheerness and Templeborough dust trials captured relatively little of the dust, but acted as a heat exchanger, lowering the gas temperature entering the baghouse. Problems were encountered with the baghouse during the early trials when the reverse jet air pressure was set too low to dislodge the filter cake from the filter envelopes. The large pressure drop across the baghouse resulted in a lack of suction and low cooling air flows to the combustion chamber. Increasing the air pressure cleaned the envelopes but caused them to split along the seam until a restraining cage was fitted to limit their flexing. Throughout the trials, the baghouse has been one of the major factors limiting furnace productivity.

The Plasma System

The plasma torch operated at around 1MW (3kA, 350V) during the trials. The individual torch lives, in hours, are detailed below:

12, 37, 14, >15, 10, >50, 24, 12, 31, 43, >5, 11, 61, 2, >34

The >34 hours signifies that the torch was still serviceable at the end of a trial. Torch life was limited by the rapid erosion of the nozzle front face, probably by stray arcs running continuously from the cathode to the nozzle to the furnace roof and up the sintered feed in the feed ports to the earthed steel roof.

The stray arcs were consistent with the detection of current in the steel shell and the large number of earth leakage trips which occurred, especially when the furnace was working under a positive pressure. These trips were usually stopped by cleaning the conductive deposits from the torch, feed and the exhaust ports and by doubling the gas flow to the torch. Despite the short torch life, the plasma system availablity was 85-95% of the time available. Modifying the water passages in the torch nozzle and increasing the water cooling pump capacity increased the torch life to around 70 hours in later trials. Coating the nozzle with an insulating refractory, enamel, boron nitride etc may reduce the arcing from the nozzle. Alternatively, the front face of the nozzle could be coated with tungsten or molybdenum to reduce the arc erosion rate.

7.2.9 Plasma Arc Characteristics

The plasma arc voltage was 330-380V at 2.5kA-3kA with an arc length 0.3m when feeding steelplant dust. All the steelplant dusts gave approximately the same arc voltage for a given arc length and current. Increasing the arc length increased the arc voltage, but also increased the potential for short circuit arcing between the nozzle and the roof, resulting in a water leak from the torch.

7.2.10 Energy Consumption

The gross energy consumption and the energy losses for the individual taps are presented in Tables 20-22 and shown in Figure 52. The gross smelting energy consumptions ranged from 1.5 to 5.0 MWh/t dust. The overriding effect of the speed of working masked any correlation between gross energy consumption and coal addition or dust analysis. At a feed rate of 1t/hour, the gross energy consumption should be about 1.5MWh/t of dust for selective reduction and 1.7MWh/t of dust for total reduction.

The furnace losses ranged from 0.20-0.29MW because of variations in the melt temperature and build up of feed on the furnace walls. The three dominant losses were the sidewall cooling sprays, the water-cooled roof panel and the plasma torch. At a power input of 1.0 MW, with total losses of 0.29 MW, the conversion of electrical energy to useful thermal energy was about 71%.

7.2.11 Summary Of The Steelplant Dusts Results

Five different dust compositions were smelted under different degrees of reduction.

Total reduction of the alloy steel dust recovered the majority of the alloy elements to a saleable ferroalloy.

Selective reduction of the EAF dust was a viable means of eliminating the majority of the ZnO, CdO and PbO from the slag to produce a non-toxic slag.

Dusts containing >0.5% Cr_2O_3 must be totally reduced to meet the slag toxicity test requirements.

A baghouse dust containing 85% ZnO and PbO was produced from steelplant dusts containing >15% ZnO.

Agglomerating the feed had little effect upon the ZnO baghouse dust quality.

The impurity content in the ZnO baghouse dust increased with increasing degrees of reduction and Fe_2O_3 content in the steelplant dust. The majority of the halogens and alkalies in the dust reported to baghouse dust.

Accountablity of the oxides to the condensed phases was only 90% because of losses from the system. In excess of 85% of the Cr, Ni and Mo units in the Alloy steel dust were recovered to a ferroalloy.

Plant availablity was initially poor due to problems with the plasma torch, feed system and baghouses. As the trials progressed and modifications were made to the equipment the availablity improved to 80%.

The minimum total energy requirement for the reduction of EAF or alloy steel dust was about 1.5 MWh/t at a feed rate of 1.0 t/hour. Feed composition and partial reduction of the dust had no measurable effect on the energy consumption.

8.0 DISCUSSION

The section examines the metallurgical results of the testwork, the design of the open bath plasma reactor and evaluates the economics of smelting chromites and steelplant dusts. Finally, an assessment of the potential of plasma processes is presented.

8.1 CHROMITE SMELTING IN THE TRANSFERRED ARC/OPEN BATH REACTOR

8.1.1 Raw Materials

The transferred arc/open bath plasma reactor was successfully used to smelt fine chromite concentrates to produce charge grade ferrochrome without any significant furnace operating problems or feed carry over with the exhaust gases. The ability to smelt fines directly supports the results of the small scale plasma smelting testwork of Maske (1) and Barcza (41), and the commercial experience of the MS&A DC graphite electrode plasma furnace (32) and the SKF non-transferred arc plasma furnace (24). The use of chromite concentrates rather than pellets or briquettes represents a cost saving of £15-25/t of chromite.

Fine anthracite was used as the reducing agent in the plasma furnace rather than the more expensive lumpy metallurgical coke required by the SAF. Any reactive coal compatible with the process chemistry should be acceptable, but a coal with low ash, low volatile matter, low phophorus and low sulphur contents is preferred. 0.31t of coal/t chromite (0.74t of coal/t ferrochrome) was required to achieve <5% residual chromium oxide in the plasma furnace slag. More coal than the model prediction of 0.3t of coal/t chromite was required because of the unexpected reduction of silica and magnesia. The conventional SAF only uses <0.28t metallurgical coke/t chromite (0.73t coke/t ferrochrome) because the coke contains a higher fixed carbon content than coal and there is some pre-reduction of the chromite by ascending CO gas.

Metallurgical coke consumption in the SAF can be further reduced to around 0.18t coke/ chromite by pre-reducing the chromite in the Showa Denko Kabushiki or similar process (38). The increased reductant consumption in the plasma furnace offsets some of the cost savings associated with using coal instead of coke, but a cost saving of £5-15/t of chromite smelted should be realized compared to the SAF.

A sand consumption of 0.16t of sand/t chromite (0.38t of sand/t ferrochrome) was required to produce a workable slag containing >30% SiO_2. More sand than the model prediction of 0.13t sand/t chromite was required because some of the SiO_2 was reduced to Si and SiO. The SAF uses a smaller quantity of the more expensive lumpy quartz because a higher slag liquidus temperature is required. Rather than using silica as the flux in the plasma furnace, it may be advantageous to use lime, as this will increase the chrome oxide activity, reduce the slag viscosity and may reduce the S and P content of the ferroalloy.

8.1.2 Ferrochrome Analysis

The ferrochrome produced from the plasma furnace contained 50-56% Cr, 6.0-7.1% C, 1.0-4.0% Si, 0.03-0.04% P and 0.03-0.08% S compared to the ASTM charge grade specification of 52-58% Cr, 6-8% C, <6% Si, <0.03% P and <0.04% S.

The 50-56% Cr content of the ferrochrome from the plasma furnace was slightly less than the model prediction of 55% Cr because the model considers equilibrium conditions only, whereas deviations from equilibrium due to kinetic constraints are experienced in practice. Ferrochrome produced in the SKF Swedechrome plasma furnace from a similar chromite contained 52-54% Cr (24). Thomas (60) predicted a slightly lower ferrochrome chromium content of 51% for a similar chromite smelted in an SAF because of the lower Cr recovery.

The Si in the plasma furnace ferrochrome increased from 1% to 4% with increasing coal/chromite ratio and operating temperature. Ferrochrome from the SAF contains 3-8% Si, reflecting the higher operating temperatures. Silicon contents of >10% in the ferrochrome are predicted from equilibrium considerations, but the lack of equilibrium in the silica reduction reaction is commonly observed, particularly in iron blast furnace practice.

The carbon content of the ferrochrome tapped from the transferred arc plasma furnace at 1900K was 6.5–7.3% C, compared to 6.0–8.0% C from the SKF plasma furnace tapped at 1973K and 5.0–6.0% C from the SAF tapped at 1973K. The ferrochrome carbon content from both types of plasma furnace approximates to a carbon saturated alloy (7.5% C for ferrochrome containing 50–55% Cr at 1900K) and is higher than that from the SAF probably because the fine chromite is rapidly dissolved and reduced from the slag phase and there is no refining of the alloy by the viscous, chromium oxide rich slag layer or chromite lumps that penetrate through the slag to the alloy that Kadarmetov (47) has shown exist in the SAF. Hamakos (61) and Downing (62) also suggest that excessive chromite fines in the SAF charge result in a higher ferrochrome carbon content. These results differ from Urquarts' (43) hypothesis that the ferrochrome alloy carbon content decreases with increasing reaction temperature because the stable chromium carbide carbon content decreases with increasing temperature. There is little possiblity of producing a lower carbon content alloy directly in the plasma furnace

The S in the ferrochrome was just within the alloy specification limit of 0.04%. Increasing the slag basicity by decreasing the silica addition to the blend decreased the alloy sulphur content at a given temperature. Increasing the operating temperature decreased the alloy sulphur content because desulphurization is thermodynamically more favourable and more silica was reduced from the slag increasing the slag basicity, the silicon content of the alloy and the activity coefficient of sulphur in the alloy (64). Sulphur is not a major concern in stainless steel making because the AOD is an excellent desulphurizing unit.

The ferrochrome phosphorus content approached the specification limit of 0.03%. As in all reduction processes, the majority of the phosphorus in the charge reported to the metal phase. To meet the specification limits, low phosphorus reductant and fluxes must be used. The enhanced dephosphorization experienced by Pickles (39) in the small scale 24kW Extended Arc Plasma Reactor was probably a result of good metal/slag stirring, elevated temperatures at the plasma arc/slag interface and some loss of phosphorus as vapour.

As over 70% of the charge grade ferrochrome produced is consumed in the AOD, it is appropriate to consider the value in use of the alloy in the AOD and how it relates to the alloy analysis. Because only the chromium units in the ferrochrome are paid for, EAF-AOD operators prefer an alloy with a chromium content towards the bottom end of the alloy specification range and therefore an iron content towards the top end of the range, because the iron represent a cheap source of relatively pure iron units. A high Si content is preferred because the oxidation of Si in the AOD vessel is highly exothermic, requires little extra oxygen and argon and does not increase the refining time appreciably, allowing additional coolant scrap to be melted. A low C in the ferrochrome is preferred because the decarburization reaction is less exothermic than silicon oxidation and increases the processing time. There should be no problems with alloy sulphur because the AOD is an excellent desulphurizer, but the P should be as low as possible. The plasma furnace produces a ferrochrome with a lower silicon and higher carbon content than the SAF, resulting in a slightly lower value in use to the steelmaker.

8.1.3 Slag Composition

A minumum of 3-5% chromium oxide in the plasma furnace slag was obtained by utilizing a slag containing >30% SiO_2 and a MgO/Al_2O_3 ratio of >1.2. Kadarmetov (47) and Kouroki (48) found that the minimum residual chromium oxide content was associated with slags containing >30% SiO_2 because the dissolution and reduction of the chromite was enhanced by lowering the slag liquidus temperature and the MgO activity. The decrease in the slag chromium oxide content with increasing MgO/Al_2O_3 ratio was probably a result of the decrease in slag viscosity and an increase in the chromium oxide activity coefficient, which is contrary to the findings of Fukagawa (46), Kadarmetov (47) and Kouroki (48) who reported a decrease in chromium oxide solubility in slag and its subsequent reduction as the MgO activity increased.

The slag analysis from the Swedechrome (24) plasma furnace is very similar to the transferred arc plasma furnace. SAF slags generally contain around 30% SiO_2 and a MgO/Al_2O_3 ratio of 1.0-1.2 in order to increase the slag liquidus temperature and electrical resistivity, resulting in an increased residual chromium oxide content of between 5% and 10% in the slag.

The chromium oxide contents of all the furnace slags are much higher than the model prediction of 0.001%, probably because of the lack of equilibrium and a small amount of alloy prill entrainment.

8.1.4 Chromite Smelting Temperature

An indicated melt temperature of 1873K gave a satisfactory furnace operation, fast reaction rates and good chromium recovery, provided the silica content of the slag was >30% to maintain a fluid slag. The plasma furnace melt temperature could be easily increased by increasing the power input for a given feed rate, but this resulted in a higher alloy silicon content, increased refractory corrosion and enhanced reduction, volatilization and loss of silica and magnesia from the slag, ie no advantage could be taken of the higher operating temperatures offered by the plasma furnace.

8.1.5 Chromium Recovery

91.4% of the chromium charged to the plasma furnace was recovered to the ferrochrome, compared to 87-90% for the same chromite in an SAF (136) and 91.3% in the Swedechrome plasma furnace (24). Continuous plasma furnace operation with the optimum feed blend should give chromium recoveries of around 93%. The slightly improved recovery in the plasma furnace is attributed to the rapid dissolution and reaction of the fine chromite in the fluid slag and good slag/metal separation.

Low chromium recoveries of 80-85% in the SAF referred to by Barcza (1) and Maske (41) in comparisons of plasma and SAF operations are generally only true for S. African practice, where SAF slag MgO/Al_2O_3 ratios of <1.0 are used to enhance slag resistivity to increase furnace productivity at the expense of chromium recovery.

8.1.6 Energy Consumption

Whilst the trial data is too variable to form any definitive conclusions, the average gross energy consumption was 6.9MWh/t of alloy at an average chromite feed rate of 0.14t/h. The large scatter of data is a result of the metal and slag hold up in the furnace and the consequent difficulties in allocating products from one tap with the feed and energy consumed during that tap.

The plasma furnace average gross energy consumption of 6.9MWh/t of alloy is much higher than the 4.0–4.5MWh/t of alloy associated with a typical commercial operation. This was due in part to the small scale of operation, the use of chromite containing 10% moisture and the carbothermic reduction of SiO_2 and MgO from the slag. Theoretical calculations suggest that completely drying the feed should decrease the gross energy consumption by up to 1.2MWh/t of alloy, assuming all the moisture charged to the furnace undergoes the water gas reaction. Adjusting the operating temperature and using a peripheral charging pattern to minimize the carbothermic reduction of MgO and SiO_2 from the slag should further decrease the gross energy consumption by 0.4MWh/t. Increasing the chromite feed rate from the 0.14t/h achieved during the trial to around 1.0t/h should increase the thermal efficiency of the system and decrease the gross energy consumption by up to 1.1MWh/t alloy, assuming the furnace energy losses remain fairly constant at 0.16MW. In a commercial scale transferred arc plasma furnace operation using dry feed, energy consumptions of 4.5MWh/t of alloy should be possible.

The projected commercial scale plasma furnace energy consumption of 4.5MWh/t of alloy (8.5MWh/t Cr) is significantly greater than the conventional SAF energy consumption of about 4.0MWh/t (8.0MWh/t Cr) because there is no counter-current heat exchange between the hot furnace gases and the charge, and the energy losses from the open melt and plasma arc to the furnace roof and sidewalls. The energy consumption in the SAF can be reduced to about 2.3MWh/t of alloy (4.4MWh/t Cr) using Showa Denko process (38), where the feed is pre-heated and pre-reduced. To be competitive with the SAF, the plasma furnace energy consumption must be reduced by sidewall peripheral charging to encourage feed banks and the potential energy contained in the exhaust gases may be utilized by pre-heating and pre-reducting the chromite. Figure 53 illustrates the energy utilization in the Outokumpu and Showa Denko systems. To maintain the plasma furnace advantage of using chromite fines directly, Curr (136) suggests the hypothetical process route using fluidized-bed pre-heating and pre-reduction shown in Figure 54. In the first two stages, the chromite ore fines are pre-heated to about 1000K and 1400K respectively, depending upon the sintering characteristics of the ore. In the third fluidized-bed, the chromium oxide is 40% reduced at 1600K.

The energy and reducing gas required for the pre-reduction stage are provided by the exhaust gases from the furnace supplemented by combusting coal with preheated oxygen enriched air. Energy for the preheating stages was provided totally by the CO rich gases from the preduction stage. Only the first two stages have been demonstrated in a fluidized-bed and further research is required to determine the operating conditions for the reduction stage.

Because of the good melting characteristics of the plasma furnace, fully reduced chromite concentrates or pellets from a rotary kiln or rotary hearth could be charged directly to the plasma furnace for melting to separate the gangue components. The SAF cannot accept material that is more than 70% metallized because of difficulties of control and power input associated with the conductive charge. Nippon steel (40) are currently evaluating a similar approach using the electric arc furnace as the melting unit.

8.2 STEELPLANT DUST SMELTING IN THE TRANSFERRED ARC/OPEN BATH REACTOR

8.2.1 Raw Materials

The as-received dusts were blended with coal and smelted in the plasma furnace without any major processing problems other than excessive feed carry over with the exhaust gases.

The limited number of Tremorfa dust analyses indicates that some variation in dust analyses can be expected, particularly CaO, ZnO and halogens. Any increase in the CaO content of the dust above about 10% will require the addition of silica flux to maintain the slag liquidus temperature at 1700K. Increases in the ZnO or Fe_2O_3 content of the dust must be accompanied by an increase in the reductant addition. Variations in the halogen content can lead to excessive dross formation in the zinc condenser.

8.2.2 Furnace Operating Mode

Totally reducing conditions must be used for smelting alloy steel dusts to maximize the the recovery of the alloy elements to a ferroalloy for recycling.

Less reducing conditions were preferred for the "selective" reduction of ZnO from carbon steel dusts, leaving the majority of the iron oxides in the slag because the energy and reductant consumptions are marginally less than total reduction, the ZnO baghouse dust product is purer and the exhaust gas volume is smaller. If zinc is to be condensed directly from the exhaust gas, a greater degree of reduction is required to minimize the carbon dioxide in the exhaust gases and prevent the back reaction with the zinc vapour, forming ZnO.

The trials have demonstrated that transferred arc plasma furnace can be easily operated under a variety of Redox potentials simply by altering the reductant addition to the feed blend. The Scandust plasma furnace is less flexible because the coke in the furnace shaft determines the redox potential. Flame reactors and other fossil fuel fired processes rely on combustion of carbon for both the energy generation and the production of a reducing gas, restricting the operational flexibility.

8.2.3 Metal Product Analysis

The total reduction of the alloy steel dust produced a ferroalloy containing 58-68% Fe, 17-22% Cr, 5-7% Ni, 2.0-2.5% Mo, 4-6% C, 0-4% Si, 0.04-0.1% S and 0.05-0.075% P. The carbon and silicon contents of the alloy were similar to the levels experienced in charge grade ferroalloys and should not be a problem when recycling the alloy to the EAF. The sulphur and phosphorus contents of the alloy were higher than the 0.03% maximum usually placed on stainless steel raw materials, however as the recycled alloy only represents about 1% of the EAF charge, no problems are envisaged provided the recovered alloy is not concentrated into a small number of taps.

The small amount of metal produced from the reduction of carbon steel dust contained 95-97% Fe, 0.5-3% C, 0.1-0.7% S, 0.2-0.75% P and 0.5-1.0% Cu. The majority of the S, P and Cu in the steelplant dust reported to the metal phase, exceeding the 0.03% maximum for basic scrap. It is very difficult to reduce the Cu and P levels in the metal, but the S content may be reduced by using a basic slag. It is not economically viable to totally reduce EAF dust to recover the iron units as well as the ZnO/Zn because the value of the poor quality iron will not offset the additional energy and reductant requirements.

8.2.4 Slag Analysis

The slag analysis was consistent with the dust analysis, flux and reductant additions. In totally reduced slags, the metal oxides of interest were almost completely reduced to produce a non-toxic slag containing about 30% CaO, 30% SiO_2, 10% MgO, 10% Al_2O_3, etc. These slags were fluid and easy to tap at 1700K. Selectively reduced slags had a larger composition range, from 10-50% FeO, <1% ZnO, <0.2% PbO, <0.2% CdO and 0.5-2.0% Cr_2O_3, depending on the steelplant dust analysis and coal addition. The % ZnO in the slag agreed reasonably well with the model predictions but the "FeO" was quite variable, probably because relatively minor variations in the slag temperature and coal addition have a large effect on the amount of "FeO" reduced.

On tapping the selectively reduced slags, thick clouds of white ZnO fume were often experienced, even though no carbonaceous reductant was present. Quarm (95) noticed a similar effect when ladles of slag were emptied in slag fuming furnaces and suggested that the "FeO" in the slag reduced the ZnO, liberating zinc vapour which burns at the slag surface.

All the slags tested passed the EPTox test, but several selectively reduced slags produced undesirably high levels of Cr in the leachate. Further work is required to correlate the Cr_2O_3 content of the dust, the degree of reduction, the slag analysis and the EPtox test leachate results.

8.2.5 Baghouse Dust Product Analysis

The maximum ZnO content in the baghouse dust was limited to about 75% by dilution with other volatile species from the steelplant dust, including PbO, CdO, K_2O, Na_2O, Cl and F and gangue oxides carried over with the exhaust gases. The following table (137) presents the baghouse dust analysis and typical commercial ZnO specifications. The baghouse dust is unsuitable for use as a feed material for a smelter or electrolytic refinery without pretreatment to remove the halogens, lead and gangue materials.

ZnO PRODUCT SPECIFICATIONS

OXIDE	BAGHOUSE DUST	SMELTER FEED	ELECTROLYTIC REFINERY	RUBBER GRADE
%	%	%	%	%
ZnO	70-80	>65.0	>92.0	>99.0
PbO	5-10	<2.0	> 0.5	< 0.1
CdO	1- 2	<0.3	> 0.3	< 0.02
Cr_2O_3	0- 1		<1ppm	
F^-	5-10	<1.0	<0.03	
Cl^-	5-10	<1.0	<0.01	

The Cl^- and F^- in the baghouse dust can cause condenser dross formation if the ZnO is used as a pyrometallurgical smelter feed or cell polarization problems in electrolytic zinc recovery. The majority the halogens can be removed from the steelplant dust or the ZnO product by leaching in a caustic solution (77) or calcining at 1300K (80). The limited trial data suggests that a proportion of the fluoride in the dust can be retained in the furnace slag by operating with CaO rich slags. Zinc smelters (78, 82, 83) also report an increased fluorine retention with CaO rich slags, but they limit the fluorine in the raw materials to <1%. There is no apparent way of retaining the chlorine in the slag because the stable chloride compounds all have high vapour pressures at the plasma furnace operating temperature.

An examination of the gangue content of the baghouse dust suggests that 5-10% of the steelplant dust was carried out of the plasma furnace with the exhaust gases, contaminating the ZnO product. If the dust settling rate and exhaust gas velocities in the furnace are calculated for <5micron dust particles, then all of the dust should be carried out of the furnace with the exhaust gases. The fact that the majority of the dust did reach the slag surface indicates that the dust coalesces and enters the furnace in discrete slugs, and indeed this is a characteristic of the screw conveyors used to transport the dust to the furnace feed ports. Agglomerated green-balled dust showed no significant improvement in product quality, probably because the pellets shattered on entering the hot furnace environment.

The baghouse dust produced from selective reduction contained lower levels of impurities than totally reduced dusts because the smaller exhaust gas volume entrained less dust and there was less reduction of gangue oxides to volatile species such as Mg, SiO, etc. The sudden increase in the iron oxide content of the baghouse dust as the carbon addition approaches the stoichiometric requirement suggests that volatile iron species are being produced and this operating area should be avoided if a pure ZnO/Zn product is required.

8.2.6 The Feasiblity of Direct Zinc Condensation from the Plasma Furnace Exhaust Gases

Zinc splash condensers have been successfully operated for many years on vertical retorts using hot briquetted zinc calcine feed (80,128). Attempts to incorporate steel plant dusts in the feed materials of the vertical retort resulted in condenser dross formation if the halogen content of the feed exceeded 1%.

Scandust (24) originally operated their plasma furnace with zinc splash condensers but changed to a lead spray condenser system to overcome halide dross formation and Zn-Fe alloy buildup due to iron carry over with the exhaust gases. The dust carry over in the Scandust plant will be high because of the large exhaust gas volume associated with the totally reducing conditions and the large volume of gas injected through the plasma torches. Total reduction also increases the iron carry-over with the exhaust gases.

The ZnO baghouse dust composition produced from the transferred arc/open bath smelting trials suggests that zinc condensation using a zinc splash condenser will be technically difficult unless the halogen, iron, gangue oxides and CO_2 in the exhaust gas stream entering the condenser are minimized. Steelplant dusts containing >50% iron oxide should be avoided because the iron oxide carry over with the exhaust gases will be excessive. Selective reduction of the dust minimizes the exhaust gas volume, the particulate matter entrainment and "iron" volatilization. Basic slags should be used to retain fluorine in the furnace slag, but dusts containing >1-2% halogens should be avoided as they may generate excessive quantities of halide drosses in the condenser.

Selective reduction generates a small carbon dioxide content in the exhaust gases which may back react with zinc vapour to form ZnO unless the quenching rate in the condenser is extremely rapid. The back reaction can be reduced by using a lead splash condenser where the lead solvent lowers the activity of the zinc, but the large condenser and cooling launder size and the environmental problems associated with the recirculating lead stream make the system impractical for a small plasma furnace operation.

Dust carry over, halogens and CO_2 in the exhaust stream entering the ondenser can be avoided by operating a two stage melting-smelting process. In the first stage, dust is melted in an oxidizing atmosphere to volalitize the halogens, alkalies and lead and produce a zinc oxide rich slag. The slag flows into a separate second stage vessel where the ZnO in the slag is reduced with carbon, aluminium or ferrosilicon, liberating a zinc vapour free of halogens and particulate matter.' Aluminium or ferrosilicon is the preferred reductant because it eliminates CO and CO_2 production, leaving a relatively pure zinc vapour for simple condensation without any back reaction or condenser dross problems.

8.3 TRANSFERRED ARC PLASMA/OPEN BATH REACTOR DESIGN AND OPERATION

8.3.1 The Plasma Torch

The Tetronics' water-cooled transferred arc plasma torch was demonstrated at powers up to 1.0MW during the trials. The torch life was initially limited by burnout of the nozzle and cathode due to insufficient water-cooling and erosion of the nozzle front face. The torch life was improved in later trials to around 70 hours by installing larger water pumps and redesigning the torch water passages. As will be seen in section 8.4, the power available from the torch limits the smelting rate and the economies of scale, therefore efforts to scale up and improve the reliablity of the water-cooled plasma torch must continue. Transferred arc plasma torches have been demonstrated at 5.0MW (27), and higher power inputs can be achieved by using multiple torches, but the equipment becomes complicated and expensive. The DC graphite electrode is an alternative to the water-cooled plasma torch for open bath reactors requiring power inputs of more than 5MW.

Graphite electrode availablity is high and predictable, thermal efficiencies are high because there is no water-cooling requirement, the capital costs and operating costs are only marginally more than the water-cooled electrode and scale up is only limited by the size of available electrodes.

8.3.2 The Furnace Design

The "rule of thumb" furnace power density of 0.75MW/m² of hearth area is slightly too high for the plasma furnace used in the testwork. Although high reaction rates and good heat transfer permitted short residence times to be achieved, the feed carry-over with the exhaust gases and the corrosion of the magnesia refractories at the slag line were severe. To reduce sidewall corrosion, the furnace diameter could be increased, the feed ports should be relocated around the furnace periphery to encourage the formation of feed banks and water-cooled panels could be used at the slag line to promote a frozen slag lining. The heat loss to the water-cooled panel will be appreciable, but it can be offset by operating at higher powers and throughputs, which reduces the gross energy consumption per tonne of product.

At the arc length of 0.3-0.5m, 71% of plasma energy was transferred to the melt. Plasma arc radiation losses and refractory damage to the upper furnace sidewall refractories were minimal, but there was some localized melting of the roof refractories, probably by radiation from the melt rather than from the plasma arc. It may be beneficial to increase the 1.5m melt to centre roof dimension in an attempt reduce the roof refractory damage. The energy transfer efficiencies and refractory wear profiles are similar to those found by Stewart (9) and Szekely (13) for transferred arc/open bath systems.

Blockages of the horizontal exhaust duct by slag splash and particulate matter dropout may be reduced by moving the exhaust port into the furnace roof. Delays due to feed system blockages can be overcome by more robust equipment and mass flow design. The estimated medium term commercial plant availablity is 90% provided refractory wear can be avoided.

The use of plasma arcs do not necessarily enable high temperatures, high power densities and high processing rate to be achieved as claimed in the literature (14-18). The melt temperature is limited by refractory containment, minimization of energy consumption and the avoidance of gangue oxide reduction. The power density and processing rate are determined by conventional reactor design, refractory containment and heat and mass transfer considerations. The plasma furnace operation was responsive and flexible because of the low thermal and mass inertia, and the independent power input and feed rate.

8.4 AN ECONOMIC EVALUATION OF THE TRANSFERRED ARC/OPEN BATH REACTOR

The economics of smelting chromite and steelplant dusts in the plasma furnace are calculated for comparison with existing commercial processes. The data used were extrapolated from the trials or taken from current unit prices. All costs are calculated for smelting 1tonne of raw material (chromite or steelplant dust). The production costs are approximate because of the simplified approach and lack of accurate operating and capital cost data, but the relative cost differences between the plasma furnace and alternative technologies should reflect the economic potential of each process.

8.4.1 Ferrochrome Production Costs

Table 23 presents the lowest "credible" cost of producing charge grade ferrochrome in a 2.0MW and 20MW plasma furnace in the UK. Although the Tetronics plasma torch has not been demonstrated at more than 2.0MW, Voest-Alpine have operated four 5.0MW torches in a steel scrap melting furnace and Middleburg Steel and Alloy operate a 12MVA DC carbon arc furnace for chromite smelting, so there is scope for scale up. The capital costs of a 2.0MW and 20MW plasma facility are approximately £2.5m and £15m respectively and include:

- Feed handling and blending system.
- Furnace and refractories.
- Plasma torch, controls and power supply.
- Exhaust gas handling and cleaning.
- Alloy and slag handling.

A delivered chromite concentrate price of £70/t is used to represent the cost of a freely available chromite. For comparison, the fob cost of Stillwater chromite concentrate is about $74/t (£40/t), Transvaal 44% Cr_2O_3 concentrates cost $40-60/t (£22-32/t) before surcharges and Greek and Turkish 48% Cr_2O_3 concentrates cost $115-120/t (£62-65/t)(131). Anthracite costing approximately £50/t is used as the reductant. The total energy consumption of 2.06MWh/t of chromite (6.4MWh/t Cr) is extrapolated from the trial data assuming a dry concentrate and a feed rate of >1.0 t/hour of chromite. A UK energy cost of £26/MWh is used. Argon consumption in the plasma torch is 7.5m^3/hour at 2.0MW, costing £0.75/m^3. The plasma torch maintenance cost of £2/MWh is based on materials and manpower to refurbish the cathode and nozzle tip after 70 hours of operation at £300 per rebuild. The 2MW plasma furnace refractory costs are based on four major rebuilds per year, costing £8k per rebuild, ie £32k/year. Supplies, including consumable items such as tapping lances, taphole clay, safety equipment, spares, etc, were calculated at 2% of the annual capital cost. The plasma furnace manning consists of 15 and 40 men for the 2MW and 20MW furnaces respectively, for feed preparation, furnace operation, tapping, product disposal, routine maintenance and product handling, at a UK labour cost of £15k/man year. A chromium recovery of 93% was assumed in the plasma furnace, compared to 87% in the SAF. No allowance is made for site charges, insurances, taxes, working capital, etc.

The lowest credible costs of producing ferrochrome in the 2.0MW and 20MW plasma furnace are about £795 and £643/t Cr respectively. The selling price of charge grade ferrochrome during 1985-7 has been static at around $0.4/lb Cr or £586/t Cr (at $1.5:£1). Thus it has not been economically viable to smelt chromite in a plasma furnace in the UK. The recent boom in stainless steel production (1988) has driven the cost of charge grade ferrochrome from $0.4/lb Cr to $0.60/lb (£775/t Cr) in Europe and $0.65/lb (£840/t Cr) in the USA. If the high ferrochrome price and shortage of supply is a long term feature of the economy, then the establishment of a 20MW plasma ferrochrome smelter in the UK might be viable. However, the upturn in demand has brought new capacity on stream which will probably reduce the present shortages, with a consequent drop in the selling price. A 50kt/y smelter is planned in Turkey, a 60kt/y smelter has been commissioned in Sweden and S. Africa has expansion projects totalling 120kt/y.

Ferrochrome Production Cost Sensitivity Analysis

The sensitivity of the ferrochrome production cost to changes in the major variables is seen from the following discussion:

FURNACE RATING

Furnace power	2MW	20MW
Production cost, £/t Cr	795	643

Increasing the furnace capacity from 2MW to 20MW with a concomitant increase in the plant capital cost from £2.5m to £15m and an increase in the manpower requirement, decreases the production costs from £795 to about £643/t of contained chromium. Whilst a small plasma furnace is not viable under the present economic conditions, a 20MW furnace would be marginally profitable.

CHROMITE COST

2MW furnace			
Chromite, £/t	90	70	50
Production cost, £/t Cr	857	795	732

20MW furnace			
Chromite, £/t	90	70	50
Production cost, £/t Cr	706	643	581

Chromite price has a major effect on the ferrochrome price, enabling producers with cheap indigenous concentrates to maintain low production costs.

ELECTRICITY COST

2MW furnace			
Electricity cost, £/MWh	16	26	36
Production cost, £/t Cr	730	795	859

20MW furnace			
Electricity cost, £/MWh	16	26	36
Production cost, £/t Cr	581	643	706

The energy cost is very variable thoughout the world, from £26/MWh in the UK and Japan to less than £20/MWh in France, Canada and Sweden.

ELECTRICITY CONSUMPTION

2MW furnace			
MWh/t chromite	1.06	1.56	2.06
Production cost, £/t Cr	703	749	795

20MW			
MWh/t chromite	1.06	1.56	2.06
Production cost, £/t Cr	561	602	643

Reducing the energy consumption in the plasma furnace by pre-heating/pre-reduction, etc decreases the production costs considerably.

Ferrochrome Production Costs In Commercial Operations

Tables 1 and 2 present the estimated ferrochrome production costs in a 20MW Outokumpu SAF, a DC graphite electrode furnace (MS&A) and the SKF plasma furnace, all located in the UK. In summary:-

2MW transferred arc plasma	£795/t Cr
20MW transferred arc plasma	£643/t Cr
20MW SAF	£690/t Cr
12MW DC arc	£663/t Cr
SKF plasma arc	£676/t Cr

The ferrochrome production costs in the 20MW transferred arc plasma furnace are marginally less than the SAF because the savings associated with using fine chromite and coal, and the greater chromium recovery offset the lower energy consumption of the SAF. For the plasma furnace to gain acceptance as a viable alternative to the established SAF technology, it must demonstrate reliable high power operation and show a significant reduction in production costs. This will only be achieved in a large plasma furnace equipped with a DC graphite electrode using pre-heated and pre-reduced chromite concentrates to decrease the energy consumption.

Table 1 shows that the estimated production costs plus delivery of S. African ferrochrome to European market is approximately £482/t Cr, much lower than any of the projected furnace operating costs in the UK. Very few operations around the world can compete with S. Africa because of cheap energy, labour and raw materials and the weak Rand.

The major trend of the 1980's has been the establishment of new ferrochrome capacity in the chromite producing countries where chromite, energy and manpower costs are low, resulting in many ferrochrome smelter closures in the non-chromite producing countries of the industrialized world. New plants have been installed in S. Africa, Turkey, Finland and Greece and major closures have taken place in the USA, Japan, Sweden and Germany. In the USA, the sole remaining ferrochrome producer is kept in business to maintain the strategic metals stockpile because of the doubt about ferrochrome supply from S. Africa, Zimbabwe and the USSR who supply over 80% of the industrialized world.

8.4.2 The Economics of Alloy Steel Dust Smelting

The cost of smelting alloy steel dust on the steel mill site is calculated in a similar manner to the chromite smelting costs: The major capital equipment items are similar to the chromite plant except that the storage bunkers and baghouse are smaller. 0.28t anthracite/t dust is required for the carbothermic reduction of the alloy oxides. The total energy consumption for smelting the dust is 1.8MWh/t of dust, including the thermodynamic smelting energy requirement and energy losses from the furnace, pumps and fans. The value of the ferroalloy produced from smelting the alloy steel dust can either be calculated using the equivalent ferroalloy price or a scrap price. Credit can only be given for the Mo content of the ferroalloy if it is recycled back to a Mo bearing heat (ASTM 316), which is assumed to be the case. In this evaluation, the value of the ferroalloy produced is calculated using ferroalloy prices quoted on the LME. The metal recoveries from the dust to the ferroalloy were:- Cr 84.8%, Ni 94% and Mo 86%. Table 24 shows that the lowest credible cost of smelting alloy steel dusts in a 2.0MW plasma furnace is approximately £152/t of dust. The recovered ferroalloy is worth approximatey £455/t of dust smelted, giving a nett gain of £303/t dust or £2.65m/year.

Alloy Steel Dust Treatment Cost Sensitivity

The predicted revenue from from treating alloy steel dust is particularly sensitive to dust analysis, recovery to the ferroalloy and alloy price, ie:

DUST ANALYSIS

% NiO in dust	2.5	3.5	4.5
Revenue, £/t dust	236.0	303.0	369.0
% MoO_3 in dust	0.8	1.8	2.8
Revenue, £/t dust	234.0	303.0	372.0
% Cr_2O_3 in dust	10.6	15.6	20.6
Revenue, £/t dust	234.0	303.0	372.0

FERROALLOY PRICE

Ni price, £k/t	6.0	9.0	12.0
Revenue, £/t dust	225.0	303.0	380.0
Mo price, £k/t	9.0	12.0	15.0
Revenue, £/t dust	272.0	303.0	334.0
Cr price, £k/t	0.62	0.72	0.82
Revenue, £/t dust	225.0	303.0	380.0

ELECTRICITY COST

Electricity cost, £/MWh	16.0	26.0	36.0
Revenue, £/t dust	321.0	303.0	284.0

ELECTRICITY CONSUMPTION

MWh/t dust	1.64	1.84	2.04
Revenue, £/t dust	308.0	303.0	297.0

CAPITAL COST

Cost, £m	1.5	2.0	2.5
Revenue, £/t dust	316.0	303.0	291.0

The nickel content of the dust, recovery of nickel from the dust to the ferroalloy and the price of nickel are the biggest factors affecting the revenue. Nickel prices have shot up from $6k to a record $19k/t during 1988 because of increased demand from stainless steel producers, a strike by mine workers at Western Mining's Kambalda mine in Australia (the world's third largest nickel mine) and the unrest around the Le Nickel mine in New Caledonia. The nickel price is expected to reach $25k/t in 1988 (133).

The plasma facility benefits from any increases in nickel prices, but even if the nickel price returns to the 1987 level of $6k/t, the plasma plant still makes an annual profit of around £0.9m. The price of molybdenum has less of an effect on plant profitablity because of the smaller quantities of Mo involved. Electricity costs and consumption have relatively little effect on revenue. Any economies of scale brought about by building a large furnace to treat large quantities of dust would be offset by the high dust transport costs from the geographically dispersed melting shops. Under the present market conditions, plasma processing of alloy steel dust to recover a ferroalloy for recycling is a profitable operation.

Alloy Steel Dust Treatment Costs Using Alternative Technologies

Scandust (138) are treating alloy steel dust in a plasma powered shaft furnace and the estimated processing costs are presented in Table 6. The processing costs are about £170/t of dust, slightly higher than the transferred arc plasma furnace. The high energy consumption and capital costs are offset by the lower Swedish energy costs and the sale of hot water to the local community. In the past, SKF have treated the delivered dust at no cost to the steelplant and kept the ferroalloy produced. More recently, SKF have been making a treatment charge of about £225/t and returning the ferroalloy to the steel company. Scandust has given up treating both EAF and AOD dusts because of the poor economics and zinc condensing problems associated with EAF dusts and is now trying to fully utilize the 50-70kt/y plant capacity treating only AOD dust. As there are only an estimated 40-50kt/y of alloy steel dust arising in Europe, it is unlikely that the plant will operate near its design capacity, with a consequent increase in costs.

The regional rotary hearth/submerged arc furnace plant of Inmetco in Pittsburgh, USA charges $320/t (£190/t) to treat the alloy steel dust from Allegheny-Ludlum, J&L and other small producers in the area and returns the ferroalloy product to the steelmaker. This cost compares favourably with the plasma furnace treatment cost of £180/t.

8.4.3 EAF Dust Treatment Costs

Table 25 shows that the estimated costs of treating a typical EAF dust containing 30% ZnO, 2% PbO and 30% Fe_2O_3 in a 2.0MW plasma furnace to produce an enriched ZnO product or a condensed zinc metal. The capital cost of a 2.0MW plasma facility for the production of ZnO or zinc metal will be approximately £2.0m. For the production of an enriched zinc oxide, the furnace can be operated in the selective reduction mode, consuming 0.15t of anthracite/t of dust and 1.4MWh of electrical energy/t of dust including the thermodynamic smelting energy, furnace energy losses and pumps, fans, etc. For the direct condensation of zinc metal from the plasma furnace exhaust gas stream the furnace should be operated under more reducing conditions, consuming about 0.25t of anthracite/t of dust and 1.6MWh/t of dust. The plasma furnace manning consists of 15 men for feed preparation, furnace operation, tapping, zinc condenser operation, product disposal and routine maintenance. The recoveries of ZnO and PbO to the ZnO baghouse dust product were assumed to be 97.5% and the recoveries of Zn and Pb to the condensed zinc alloy were 80%. In the UK, where the dusts are not classified as hazardous wastes and disposal costs are only about £10/t, plasma dust treatment is not generally an economically viable alternative to dumping unless the zinc content of the dust is high. In the USA, where dumping costs at hazardous landfill sites vary between £40-£100/t, then a dust treatment charge can be levied to offset the operating costs.

EAF Dust Treatment Cost Sensitivity

Because of the limited value in the products obtained from treating EAF dusts, the treatment costs/charges are very sensitive to the product type, the scale of operation, the dust analysis, energy costs, plant capital costs, etc. An indication of sensitivity of the treatment costs can be obtained from the following matrix and Figures 55 and 56.

DUST ANALYSIS

(2MW furnace, £26/MWh, 1.4MWh/t dust, £500/t zinc)

ZnO product;

%ZnO in dust	20	30	40
Treatment cost, £/t dust	-83	-64	-44

Zn product;

%ZnO in dust	20	30	40
Treatment cost, £/t dust	-55	-23	+ 8

The cost of selectively reducing an EAF dust containing 30% ZnO in a 2.0MW plasma furnace to produce a ZnO product is approximately £123/t of dust, the credit from the zinc oxide product is about £59/t of dust, which gives a nett cost of £64/t of dust. The cost of totally reducing the same dust to produce zinc metal is about £145/t of dust, but the credit from the condensed zinc metal is £119/t of dust, giving a nett cost of £23/t of dust. The condensation of zinc metal is, therefore, the favoured route, not only because the costs are less, but the product is easier sell.

ZINC PRICE

(30% ZnO in dust, 2MW furnace, £26/MWh, 1.4MWh/t dust)

ZnO product;

Zinc price, £/t	700	500	300
Treatment cost, £/t dust	-40	-64	-87

Zn product;

Zinc price, £/t	700	500	300
Treatment cost, £/t dust	+15	-23	-61

The price of zinc has a significant and unpredictable impact on the treatment costs. The price of zinc has been very volatile, varying from $700/t (£390/t) in 1986 to $1.35k/t (£750) in 1988. The upturn in the demand for galvanized steel, the strike at Cominco, heavy Chinese buying and smelters stockpiling zinc all contributed to the recent increases in price.

FURNACE CAPACITY

(30% ZnO in dust, furnace, £26/MWh, 1.4MWh/t dust, £500/t of zinc)

ZnO product;

Furnace power, MW	1	2	3
Treatment cost, £/t dust	-79	-64	-41

Zn product;

Furnace power, MW	1	2	3
Treatment cost, £/t dust	-62	-23	+2

ELECTRICITY PRICE

(30% ZnO in dust, 2MW furnace, £500/t zinc, 1.4MWh/t dust)

ZnO product;

Electricity price, £/MWh	36	26	16
Treatment cost, £/t dust	-78	-66	-50

Zn product;

Electricity price, £/MWh	36	26	16
Treatment cost, £/t dust	-39	-23	-7

Because the plasma furnace relies totally on electrical energy, the electricity cost has an impact on the treatment costs.

ELECTRICITY CONSUMPTION

(30% ZnO in dust, 2MW furnace, £500/t zinc, £26/MWh)

ZnO product;

Energy consumption, MWh/t dust	1.2	1.4	1.6
Treatment cost, £/t dust	-57	-64	-69

Zn product;

Energy consumption, MWh/t dust	1.4	1.6	1.8
Treatment cost, £/t dust	-17	-23	-29

The difference in energy costs between the selective reduction and total reduction modes is relatively small and should not unduly influence the choice between the two routes.

The least cost process in all cases is the production of metallic zinc rather than ZnO, because of the higher value of the product. The production of zinc metal also reduces product transportation costs, reduces product liablity and has a ready market. Dust treatment costs obviously decrease as the % ZnO in the dust increases to defray the processing cost, indeed the zinc condensation route will breakeven treating dusts containing >40% ZnO if the zinc price exceeds £500/t.

EAF Dust Treatment Costs Using Alternative Technologies

The plasma furnace will only be economically viable if it can compete with the alternative treatment processes discussed in section 4 and presented in Table 4, ie:

PROCESS	PROCESSING COST £/t dust	TREATMENT CHARGE £/t
Rotary kiln (USA)	44	44
HTR (Japan)	8	39
Scandust (Sweden)	57	65
ZCA Flame reactor (USA)	-	120
Hydrometallurgical (USA)	-	117
Chemical stabilization (USA)	36	75

The rotary kiln technology is the cheapest demonstrated technology against which the plasma furnace must compete. Plasma technology is competitive if the steelplant dust contains more than 20% ZnO, zinc metal is the product, the zinc metal can be sold for >£500/t and the dust is treated on the steelplant site to avoid transport charges. Plasma technology is most applicable to the USA because steelplant dusts are a listed environmental hazard and currently cost up to £100/t to dispose of. The USA also imports over 70% of its slab zinc, smelter capacity having decreased to the level of domestic mine output.

8.5 AN ASSESSMENT OF THE USE OF PLASMA PROCESSES IN PYROMETALLURGY

The pyrometallurgical extraction, heating and refining of most metals takes place at temperatures ranging from 1273 to 1773K. In this temperature range, energy to raise the product temperatures and for the thermodynamic decomposition of the raw materials is most economically provided by the combustion of fossil fuels. When the operating temperature exceeds 1773K, the use of electrical energy in the form of open arcs, submerged arcs, plasma arcs and resistive heating become the most efficient heating processes. Most of the plasma applications are expected to occur when temperatures in excess of 1773K are required. Reported plasma arc advantages include:-

- high temperatures
- high power densities
- fast reaction rates
- low thermal inertia
- improved process control
- improved metallurgical recoveries
- fine raw materials can be processed
- low exhaust gas volumes
- no contamination from the energy source
- simple, cheap reactor design

Care should be taken when assessing plasma applications in pyrometallurgy because the literature often reports the advantages of plasma arcs without fully examining the integration of the plasma generator with the process or the process economics, eg

- reaction temperatures are limited by refractory containment, energy consumption and unwanted reduction reactions
- power densities are limited by the reaction kinetics
- low thermal inertia reactors require accurate control
- the reactor design is based on conventional mass and energy cosiderations
- the power available from water-cooled plasma torches is limited to 5MW
- plasma systems are less energy efficient than conventional SAF

Plasma processes are evaluated under the following categories:

- reduction/smelting using the transferred arc/open bath reactor
- reduction/smelting using the non-transferred arc/shaft furnace
- blast furnace air superheating using the non-transferred arc plasma system
- melting operations using the transferred arc plasma system
- heating operations using the transferred arc plasma system
- recycling

Reduction/Smelting using the Transferred Arc/Open Bath Reactor

Plasma smelting of the oxides of Al, Mg, Ti, Si, V, Cr, P, Mn, etc has received considerable interest because of the high temperatures and low oxygen potentials that are attainable. With the exception of Mn, this energy cannot be economically supplied by the combustion of fossil fuel, therefore, the majority of ferroalloys are smelted in electric processes. The trials have demonstrated that transferred arc plasma/open bath reactor has some advantages over conventional electric furnaces:

- Fine ores can be smelted without agglomeration in the open bath reactor because it is not necessary for a fixed porous bed of feed to be maintained to allow the process gases to escape. Reaction rates are fast with the small particle size and the degree of reduction will be higher for a given residence time. No commercial reactors attempt "in-flight" reduction or take advantage of the more reactive species that might be generated in the high temperature plasma arc.

- Coal fines that are compatible with the process chemistry can be used instead of expensive metallurgical coke. Coal is preferred to coke fines because a high chemical reactivity is required to take advantage of the fast reaction rates and low residence times in the plasma furnace. The consumption of coal will be higher in the plasma furnace than the SAF because there is no pre-reduction of the feed with the exhaust gases and only the fixed carbon in the coal takes part in the reduction reactions.

- The Redox potential is readily controlled in the sealed plasma furnace in the absence of carbon electrodes, excess coke or products of combustion.

- The power input to the plasma furnace is independent of the physical properties of the raw materials or the slag phase, giving a flexible furnace operation, improved control and enabling a wider range of slag chemistries to be used.

- Metallurgical recovery in the plasma furnace is slightly better than the SAF, but it is difficult to make a direct comparison because the SAF often uses slag chemistries aimed at maximizing furnace productivity rather than metallurgical recovery.

- Thermal and mass inertia in the plasma reactor are low, giving good process control and response times. However, accurate feed rate and power input control are essential because there is no buffer of solid charge to absorb feedrate or power input deviations.

Although plasma reactors use cheaper raw materials and achieve good metallurgical recoveries, a number of inherent problems must be solved before plasma processing becomes economically attractive for smelting applications:

- The maximum power available from a water-cooled transferred arc plasma torch is about 5MW, limiting the economies of scale and making many processes uneconomic compared to the SAF. The plasma torch can be replaced with a DC graphite electrode, increasing the power input to 20-30MW. The return electrode will ultimately restrict the power available from DC plasma furnace.

- The plasma furnace energy consumption is generally higher than the SAF because the process gases leave the furnace at close to the reaction temperature and little of the enthalpy or chemical energy is recovered. Pre-heating and pre-reduction of the raw materials could recover some of the exhaust gas energy and reduce the electrical energy requirement of the process. Radiation and convection losses from the transferred arc and the open bath to the unprotected roof and sidewalls are high, unless the sidewalls can be kept covered with a layer of feed.

- The high temperatures available in plasma systems cannot be utilized because of refractory containment and gangue oxide reduction problems. Open bath plasma reactors in particular will suffer from sidewall refractory wear by slag corrosion and convective heat transfer from the high temperature arc flare unless a bank of feed material is maintained around the furnace sidewalls by peripheral feeding. Water-cooled panels can be used to promote a frozen slag lining, but at the expense of higher energy losses. However, the simple furnace design, easy accessibility and low inventory of materials reduce the time and cost of repairs.

- Unless carefully controlled, the high plasma arc temperatures and power densities can promote unwanted carbothermic reduction reactions which consume energy and reductant, and contaminate the products. SiO_2, MgO, Al_2O_3, CaO etc are all carbothermically reduced at temperatures above 2300K. Further work is required to produce a more even heating of the melt by moving the arc, gas bubbling, magnetic stirring etc. The problems of local overheating in the conventional SAF or blast furnace are less apparent because the burden in the shaft will condense and recycle most of volatilized species.

- The concept of very high power densities and productivities in small plasma reactors is not practical because of the kinetic limitations of feed materials melting and reacting in the molten bath, the small melt size requires frequent taps and the high gas volumes and velocities entrain excessive amounts of feed material. Reactor design is determined by conventional mass and energy transport criteria.

- The high temperature and enthalpy inputs available from plasma systems have not been utilized for the highly endothermic reactions such as the carbothermic reduction of MgO or Al_2O_3 because the ancillary condensing equipment has not been developed and the product tends to be contaminated with volatilized gangue materials.

Reduction/Smelting using the Non-Transferred Arc/Shaft Furnace Reactor

Smelting using the non-transferred arc/shaft reactor shares many of the advantages of the transferred arc plasma system, including the abilitity to process fine raw materials, fast reaction rates, independent power input and feed rate, low thermal inertia and improved metal recoveries. There are two major differences between the transferred arc/open bath reactor and the non-transferred arc/shaft furnace (SKF furnace), namely the presence of burden material and the use of the non-transferred arc torch.

- The presence of burden (usually a coke bed which is slowly consumed and replaced) acts as an inefficient particulate filter. Higher power densities can be used because the energy is dissipated by a large volume of process gas, the coke bed protects the sidewalls from radiation and convection from the melt and the arc, and any unwanted volatile species that form can be captured and returned to the bath by the coke column.

- The presence of excess coke prevents any control over the oxygen potential or the possible reactions between the burden material and the feed materials that are injected into the reaction zone.

- The energy consumption is generally higher than the conventional SAF because the process gases together with the large mass of gas used in the arc heaters leave the furnace at close to the reaction temperature. Because the rate of descent of the coke burden is intentionally slow, there is little heat recovery from the exhaust gases. The large surface area of the shaft is extensively water-cooled and both the anode and cathode of the plasma torch require water cooling.

- The exhaust gas volume from the non-transferred arc plasma process will be high because recycled process gas is injected into the torch to transfer the electrical energy to the charge.

Blast Furnace Air Superheating using the Non-transferred Arc Plasma System

Non-transferred arc plasma torches have been fitted to the tuyeres of blast furnaces to superheat the air blast in order to reduce the consumption of metallurgical coke. Coal fines and oil can also be injected into the plasma raceway to achieve further coke economies. The economic benefits of using plasma to superheat air depends on the cost of electrical energy compared to metallurgical coke, therefore, the use of plasma energy in blast furnaces is only feasible in countries where electrical energy is very cheap.

Melting Operations using the Transferred Arc Plasma System

Water-cooled transferred arc plasma torches have been used for steel scrap melting by Linde (26) and Voest-Alpine (27). Both companies reported higher alloy recoveries by melting in the sealed furnace under an inert atmosphere, but the process was abandoned after concluding it was uneconomic compared to the conventional 3-phase AC arc furnace because of the limited power available from the water-cooled torches, the high plasma torch and bottom electrode costs, and the increased melting time. Transferred arc water-cooled electrodes may be more appropriate for melting high alloy steels where increased alloy recoveries are important, although improved recoveries may also be possible in the conventional AC arc furnace if attention is paid to sealing the furnace and operating under an inert gas atmosphere.

DC graphite electrode furnaces capable of delivering up to 60 MW (33) are used for scrap melting. A decrease in graphite electrode consumption and some savings in energy and refractory consumption compared to the AC steelmaking arc furnace are claimed. The bottom electrode life limits the furnace power input and furnace size such that the DC furnace will suitable for small melt shops but is unlikely to replace with the AC furnace for bulk steelmaking.

Water-cooled transferred-arc plasma torches are in regular use for remelting super-alloy scrap in water-cooled hearths and moulds to obtain high purity, inclusion free alloys. The cost of plasma melting is higher than vacuum arc melting or vacuum induction melting, but the increased product quality and value offsets the cost difference.

Plasma remelting is applicable when the alloy has a high value, the property and chemistry specifications are demanding, the alloy is reactive and low levels of inclusions are required.

Heating Operations using the Transferred Arc Plasma System

Water-cooled transferred arc plasma torches are being used to heat steel in tundishes to compensate for the temperature drop during processing, to accurately control the steel casting temperature and to enable the steelmaking furnace tapping temperature to be reduced. This application is ideal for plasma because the power requirements are low, there is no electrode contamination and the plasma torch can easily be retrofitted to most tundishes.

DC graphite plasma electrodes are used for ladle heating because the directional arc reduces refractory damage, especially if it can be buried in slag. Ladle heating using water-cooled torches will be less satisfactory because of the limited power available and refractory damage from the exposed plasma arc.

Recycling Waste Materials

The transferred and non-transferred arc plasma reactors have applications in the recycling of wastes, particularly steelplant baghouse dusts because the feed material can be processed directly to produce a non-toxic slag and the contained ZnO, Cr_2O_3, NiO and MoO_3 values can be recovered to a condensed zinc metal and a ferroalloy to offset the treatment costs. The redox potential in the transferred arc/open bath reactor can be readily adjusted to reduce only the ZnO in the steelplant dust, improving the product quality and minimizing the exhaust gas volume, energy and reductant consumptions. Alternatively, all the alloy oxides can be reduced and recovered to a ferroalloy

The transferred arc plasma furnace is also used for recovering Platinum group metals from spent automobile catalyst in a small, high temperature furnace operating under closely controlled reducing conditions.

Summary

Plasma smelting will be most cost effective where the technical advantages of plasma processes can be utilized, energy is cheap and a small furnace producing a high value material is required. Figure 57 shows the approximate relationship between the value of the product and the minimum power input required for its economic recovery. Superimposed on the curve are the power outputs available from the available plasma devices. High value materials such as platinum group metals are produced in small quantities and should be economically recoverable in a small plasma furnace. Medium value materials such as nickel, cobalt, molybdenum, niobium, ferroalloys and superalloys that are produced in 2-40 MW furnaces may be produced in a plasma furnace if advantage can be taken of a cheaper feed or reductant or an improved metal recovery can be achieved. Low value materials, including some of the ferroalloys, iron and steel are produced on a much larger scale and at a far lower cost than can be achieved in existing plasma furnaces. Smelting residues and steelplant dusts that contain valuable zinc, lead, chromium, nickel and molybdenum is attractive because environmental pressures are providing additional financial incentives.

The most likely short term plasma applications are: the treatment of wastes that are an environmental concern, the recovery of chromium, nickel and molybdenum from steelplant dusts, the production of ferroalloys from concentrates, the recycling of alloy and specialist scrap materials, the heating of steel in tundishes and alloy remelting. Non-transferred arc torches will be used for air blast superheating in countries with cheap energy. DC graphite electrodes will be used for steel melting and ferroalloy smelting.

The development of more powerful plasma torches and the utilization of the potential energy in the reactor exhaust gases by coupling the plasma reactor to a preheater/prereduction unit is required to reduce the operating costs of the present generation of plasma processes.

9.0 CONCLUSIONS AND RECOMMENDATIONS

An evaluation of plasma systems in pyrometallurgy and a series of plasma smelting trials were carried out to determine potential advantages and applications of plasma systems. It is important to consider the total plasma process rather than just the plasma generator when evaluating the processes because some of the potential advantages of plasma generators are constrained by the process.

Fine chromite concentrates and steelplant dusts were successfully smelted with coal and sand flux in the transferred arc plasma/open bath reactor. There was very little carry over of feed material with the exhaust gases from the chromite concentrates, but upto 20% of the fine steelplant dusts were carried out of the reactor.

Fine coal rather than lumpy coke was used as the reductant. 0.31t of coal/t chromite was required in the plasma furnace compared to <0.28t/t in the SAF because there was no pre-reduction of the chromite.

Metallurgical recoveries were slightly higher than conventional processes because of the greater flexiblity in slag chemistry and the improved process control. 91% of the Cr in the chromite was recovered to the ferroalloy and 85-95% of Cr, Ni, Mo and Zn were recovered from the steelplant dusts.

The redox potential and melt temperature were easy to control because the power input, reductant and feed rate were independent. ZnO could be selectively reduced from the steelplant dusts, leaving the FeO in the slag. Alternatively, the dusts could be totally reduced to recover the Fe, Cr, Mo etc to a ferroalloy.

The energy consumption in the plasma furnace was higher than the SAF because there was no utilization of the exhaust gases for pre-heating or pre-reduction. The gross energy consumption in the plasma furnace trials was 6.7MWh/t of ferrochrome, suggesting a commercial energy consumption of 4.5MWh/t of ferrochrome, compared to 4.0MWh/t of ferrochrome in the SAF.

The power available from water-cooled plasma torches is about 5MW, limiting the scale of operation and the process economics. The production of ferrochrome in a 1.0MW plasma furnace was not economic compared to the SAF, but projected production costs in a 20MW plasma furnace will be similar to the SAF. Power inputs of 20MW are best achieved using the DC graphite electrode.

The design principles of the transferred arc/open bath reactor are similar to the conventional steelmaking arc furnace. Little advantage can be taken of high plasma temperatures, enthalpies and energy densities because of refractory wear, reaction kinetics, feed carry over with the exhaust gases and the liquid product capacity of the reactor. Unwanted reduction of SiO_2 and MgO occurred if elevated reaction temperatures were used.

Charge grade ferrochrome was produced from chromite concentrates containing 38% Cr_2O_3. 0.31t of coal/t chromite, 0.16t silica flux/t chromite coal were used with a melt temperature of 1900K. Chromium recovery to the alloy was 91-93%. The recovery of chromium increased with increasing silica and magnesia/alumina ratio in the slag. Furnace availability was 93%.

Alloy steel dust was smelted with coal to produce a Cr-Ni-Mo-Fe alloy suitable for recycling to the EAF. Alloy recoveries were: Cr 85%, Ni 94%, Mo 86% and the energy consumption was 1.7MWh/t of dust. The smelting of AOD dust in a 2.0MW furnace generates a profit of about £265/t of dust smelted, depending on the dust composition and ferroalloy prices.

EAF dust was smelted with coal to produce a non-toxic slag and an impure ZnO baghouse dust. The selective reduction of the ZnO from the dust, leaving the FeO unreduced in the slag, was the preferred operating mode because of the lower smelting energy and coal consumption, improved product purity and decreased waste gas volume. The product quality from feeding green balled dust was not significantly different from treating as-received dust. The treatment of EAF dust to recover an enriched ZnO product is not a profitable operation unless a treatment fee of >£90/t of dust can be charged. The profit/loss is very sensitive to the % ZnO in the dust, energy costs, scale of operation and product quality.

Direct zinc condensation from the exhaust gas stream will be difficult unless the particulate matter carry over and the halogen content of the gases entering the condenser can be reduced. Zinc condensation should be pursued because the enhanced value of the product allows a reduced treatment fee of around £50/t of dust to be charged, making the process competitive with alternative technologies.

It is unlikely that plasma processes will replace existing large scale conventional technologies, such as ironmaking, steelmaking and bulk ferroalloys until high power plasma torches are developed. The advantages of plasma may be better utilized in smaller scale operations producing high-intrinsic value materials (Au, Pt), those requiring elevated reaction temperatures (Cr, Si, Ti, Al, Mg) or those that cannot be treated easily by conventional technologies (steelplant dusts).

RECOMMENDATIONS FOR FURTHER WORK

Further chromite smelting trials should be conducted to confirm the optimum slag chemistry for chromium recovery to the ferroalloy, particularly the magnesia/alumina ratio and the silica content. Lime based slags should be investigated to determine whether a higher value low phosphorus product can be obtained. Pre-heating and pre-reduction of the chromite concentrate should be developed to reduce the smelting energy consumption and operating costs.

Direct condensation of zinc should be investigated to reduce EAF treatment costs. The reduction of feed carry over and halogen volatilization remains the major problem to be overcome. A two stage melting/smelting route should be evaluated.

Plasma torch development aimed at longer electrode life, cheaper electrode materials and higher powers should continue. The DC transferred arc graphite electrode system should be evaluated and compared to the DC water-cooled transferred arc plasma torch for the smelting of ores and dusts as well as the heating and melting of steel because the graphite electrode system can be scaled up to larger power inputs, it is less complicated, more thermally efficient and may be cheaper to operate.

APPENDIX 1 MASS AND ENERGY BALANCE MODEL

A simple mass and energy balance model was written for the BBC Master series micro computer using Computer Concepts' INTERSHEET spreadsheet package.

The dust, flux and reductant analyses are entered in the columns B, C and D.

A preliminary estimate of the weight of flux and reductant (as a % of the dust weight) are entered in columns E and F.

The degree of reduction of the oxide to the metal phase is entered in column H and the degree of reduction of the oxide to a vapour phase is entered in column L. The degree of reduction is calculated by substituting the CO_2/CO ratio, temperature and activity coefficient values into the Free Energy equations 26, 28, 30 and 32 derived in sections 3 and 4 manipulating the degree of reduction in column H until the mass % of metal oxide remaining in the slag calculated from the Free Energy equations coincides with the values given in column T.

$$\log P_{CO_2} - \log P_{CO} = -9312/T + 3.69 - \log P_{Zn} + \log \gamma ZnO + \log mass\%\ ZnO \qquad \text{eqn 26}$$

$$\log P_{CO_2} - \log P_{CO} = 2277/T - 1.985 + \log aFeO - \log aFe \qquad \text{eqn 28}$$

$$\log P_{CO_2} - \log P_{CO} = -5437/T - 0.64 + 1/3 \log aCr_2O_3 - 2/3 \log aCr \qquad \text{eqn 30}$$

$$\log P_{CO_2} - \log P_{PCO} = 3101/T + 1.09 - \log P_{Pb} + \log aPbO \qquad \text{eqn 32}$$

As a first approximation, experimental data can be entered into columns H and L eg, during the total reduction of steelplant dusts, the degree of reduction of Fe_2O_3, Cr_2O_3, NiO, MoO_3 etc to metal will approach 99% and the degree of reduction of ZnO, PbO etc to the vapour phase will approach 99.9%.

The CO_2/CO ratio is entered in column P.

The reaction temperature is entered in column V.

The programme will then calculate:-

The mass of metal produced, total column J.

The metal analysis, column K.

The gas analysis, column R.

The mass of slag produced, total column S.

The slag analysis, column T

The energy requirement, total column Y.

The carbon requirement, column Y.

The coal requirement, column Y.

On completing the initial calculation, the slag analysis given in column T should be inspected and the flux addition rate in column E changed until the required slag composition is obtained. The calculated coal addition given in column Y should be re-entered into column F and the programme rerun to obtain the final mass and energy balance.

Total and selective reduction of dusts can be compared by changing the CO_2/CO ratio in column P and the degree of reduction in columns H and L. The programme will recalculate the reductant, flux and energy consumptions and the metal, slag and gas analyses and masses.

```
 ¦.........A_________B_________C_________D_________E_________F_________G_________H_________I_________J_________K_____L
 1¦TOTAL REDUCTION OF TREMORFA DUST
 2¦
 3¦OXIDE   ORE       FLUX      COAL      FLUX      COAL      TOTAL     DEGREE    MASS      MASS      METAL     DEGREE
 4¦        Anal.     Anal.     Anal.     Addn.     Addn.     Mass      Of        Of        Of        Anal.     Of redn
 5¦        %         %         %         % Of      % Of      Of        Redn.     Oxide     METAL Or  %         to gas
 6¦                                      Ore       Ore       Oxide     To        Reduced   Lower
 7¦                                                          Charged   Metal     To metal  Oxide
 8¦SIO2    3.60      98.00     2.00      0.00      18.00     39.60     0.00      0.00      0.00      0.00      0.00
 9¦CaO     4.80      0.00      0.00                          48.00     0.00      0.00      0.00      0.00      0.00
10¦MgO     2.30      0.00      1.00                          24.80     0.00      0.00      0.00      0.00      0.00
11¦MnO     5.00      0.00      0.00                          50.00     0.00      0.00      0.00      0.00      0.00
12¦Al2O3   0.90      0.00      2.00                          12.60     0.00      0.00      0.00      0.00      0.00
13¦Fe2O3   33.00     0.00      1.00                          331.80    100.00    331.80    298.62    0.00      0.00
14¦FeO     0.00      0.00      0.00                          298.62    99.97     298.55    232.02    93.46     0.00
15¦Cr2O3   0.20      0.00      0.00                          2.00      0.00      0.00      0.00      0.00      0.00
16¦ZnO     35.40     0.00      0.00                          354.00    0.00      0.00      0.00      0.00      99.99
17¦K2O     1.30      0.00      0.00                          13.00     0.00      0.00      0.00      0.00      99.99
18¦P2O5    0.40      0.00      0.00                          4.00      0.00      0.00      0.00      0.00      0.00
19¦F       1.00      0.00      0.00                          10.00     0.00      0.00      0.00      0.00      0.00
20¦Pb3O4   4.00      0.00      0.00                          40.00     0.00      0.00      0.00      0.00      99.00
21¦CdO     0.09      0.00      0.00                          0.90      0.00      0.00      0.00      0.00      99.00
22¦S       0.52      0.00      1.00                          7.00      0.00      0.00      0.00      0.00      2.00
23¦NiO     0.00      0.00      0.00                          0.00      0.00      0.00      0.00      0.00      0.00
24¦MOO3    0.00      0.00      0.00                          0.00      0.00      0.00      0.00      0.00      0.00
25¦H2O     0.00      0.00      0.00                          0.00      0.00      0.00      0.00      0.00      100.00
26¦H2      0.00      0.00      5.00                          9.00      0.00      0.00      0.00      0.00      100.00
27¦O2      0.00      0.00      2.00                          3.60      0.00      0.00      0.00      0.00      100.00
28¦C       0.00      0.00      82.00                         147.60    0.00      0.00      16.24     6.54      0.00
29¦CO2     0.00      0.00      0.00                          0.00      0.00      0.00      0.00      0.00      0.00
30¦CO      0.00      0.00      0.00                          0.00      0.00      0.00      0.00      0.00      0.00
31¦total=  92.51     98.00     96.00     0.00                1097.90             630.35    248.26    100.00
```

```
 ¦.........A_________M_____N_________O_____P_____Q______R_____S_____T_________U_________V_________W________X__________Y
 1¦TOTAL REDU
 2¦
 3¦OXIDE      MASS  MASS of  CARBON CO2/CO  MOLES   GAS   MASS   SLAG      TEMP  ENTHALPY HEAT          HEAT      TOTAL
 4¦          oxide  metal    Addn.        OF GAS ANALYSIS OXIDE  ANAL      .K             Of            Of        Energy
 5¦        reduced  to gas                      mole % IN SLAG   %                        Reaction      Fusion
 6¦         to gas                                      kg
 7¦
 8¦SIO2    0.00           0.00      0.00 0.0010   0.00   0.00  39.60  19.96   1723.00     16.17     0.00     1.72      17.89
 9¦CaO     0.00           0.00      0.00          0.00   0.00  48.00  24.20               15.22     0.00    10.29      25.50
10¦MgO     0.00           0.00      0.00          0.00   0.00  24.80  12.50               10.29     0.00    11.47      21.76
11¦MnO     0.00           0.00      0.00          0.00   0.00  50.00  25.20               12.95     0.00     9.15      22.10
12¦Al2O3   0.00           0.00      0.00          0.00   0.00  12.60   6.35                5.08     0.00     3.17       8.26
13¦Fe2O3   0.00           0.00     24.95          0.00   0.00   0.00   0.00              122.91   145.53    31.11     299.54
14¦FeO     0.00           0.00     49.76          0.00   0.00   0.07   0.04                0.00   262.79     0.00     262.79
15¦Cr2O3   0.00           0.00      0.00          0.00   0.00   2.00   1.01                0.56     0.00     0.05       0.61
16¦ZnO     353.96       284.05     52.44          4.37  20.11   0.04   0.02               77.94   480.69    72.11     630.74
17¦K2O     13.00         10.79      1.66          0.28   1.27   0.00   0.00                4.01    12.00     0.00      16.01
18¦P2O5    0.00           0.00      0.00          0.00   0.00   4.00   2.02                0.49     0.00     0.00       0.49
19¦F       0.00           0.00      0.00          0.00   0.00  10.00   5.04                6.77     0.00     0.00       6.77
20¦Pb3O4   39.60         37.00      3.70          0.18   0.82   0.40   0.20                4.90     9.92     0.47      15.29
21¦CdO     0.89           0.78      0.08          0.01   0.03   0.01   0.00                0.13     0.59     0.00       0.71
22¦S       0.14           0.14      0.00          0.00   0.02   6.86   3.46                1.53     0.29     0.00       1.82
23¦NiO     0.00           0.00      0.00          0.00   0.00   0.00   0.00                0.00     0.00     0.00       0.00
24¦MOO3    0.00           0.00      0.00          0.00   0.00   0.00   0.00                0.00     0.00     0.00       0.00
25¦H2O     0.00           0.00      0.00          0.00   0.00   0.00   0.00                0.00     0.00     0.00       0.00
26¦H2      9.00           9.00      0.00 0.0000   4.50  20.70   0.00   0.00               47.01     0.00     0.00      47.01
27¦O2      3.60           3.60      2.70 0.0000   0.11   0.52   0.00   0.00                0.10     0.00     0.00       0.10
28¦C       0.00           0.00      0.00          0.00          0.00   0.00               86.10    36.45     0.00     122.55
29¦CO2     0.00           0.00     12.30          0.01   0.06   0.00   0.00                0.00    -1.16     0.00      -1.16
30¦CO      0.00           0.00     12.30         12.27  56.47   0.00   0.00                0.00  -343.67     0.00    -343.67
31¦total=  420.19       345.35    135.28         21.73 100.00 198.38 100.00              412.16   603.42   139.54    1155.12
32¦                                     CARBON  147.44                0.00                     ENERGY    kWh/t Dust  1341.22
33¦                                                                                            CARBON    kg/t Dust    147.44
34¦                                                                                            COAL      kg/t Dust    179.80
35¦                                                                                            GAS VOLUME  m3/hour    486.85
```

!.........	A	B	C	D	E	F	G	H	I	J	K	L
1	SELECTIVE REDUCTION OF TREMORFA DUST											
2												
3	OXIDE	ORE	FLUX	COAL	FLUX	COAL	TOTAL	DEGREE	MASS	MASS	METAL	DEGREE
4		Anal.	Anal.	Anal.	Addn.	Addn.	Mass	Of	Of	Of	Anal.	Of redn
5		%	%	%	% Of	% Of	Of	Redn.	Oxide	METAL Or	%	to gas
6					Ore	Ore	Oxide	To	Reduced	Lower		
7							Charged	Metal	To metal	Oxide		
8	SIO2	3.60	98.00	2.00	0.00	9.50	37.90	0.00	0.00	0.00	0.00	0.00
9	CaO	4.80	0.00	0.00			48.00	0.00	0.00	0.00	0.00	0.00
10	MgO	2.30	0.00	1.00			23.95	0.00	0.00	0.00	0.00	0.00
11	MnO	5.00	0.00	0.00			50.00	0.00	0.00	0.00	0.00	0.00
12	Al2O3	0.90	0.00	2.00			10.90	0.00	0.00	0.00	0.00	0.00
13	Fe2O3	33.00	0.00	1.00			330.95	100.00	330.95	297.86	0.00	0.00
14	FeO	0.00	0.00	0.00			297.86	0.00	0.00	0.00	0.00	0.00
15	Cr2O3	0.20	0.00	0.00			2.00	0.00	0.00	0.00	0.00	0.00
16	ZnO	35.40	0.00	0.00			354.00	0.00	0.00	0.00	0.00	96.30
17	K2O	1.30	0.00	0.00			13.00	0.00	0.00	0.00	0.00	99.00
18	P2O5	0.40	0.00	0.00			4.00	0.00	0.00	0.00	0.00	0.00
19	F	1.00	0.00	0.00			10.00	0.00	0.00	0.00	0.00	0.00
20	Pb3O4	4.00	0.00	0.00			40.00	0.00	0.00	0.00	0.00	99.00
21	CdO	0.09	0.00	0.00			0.90	0.00	0.00	0.00	0.00	99.00
22	S	0.52	0.00	1.00			6.15	0.00	0.00	0.00	0.00	2.00
23	NiO	0.00	0.00	0.00			0.00	0.00	0.00	0.00	0.00	0.00
24	MOO3	0.00	0.00	0.00			0.00	0.00	0.00	0.00	0.00	0.00
25	H2O	0.00	0.00	0.00			0.00	0.00	0.00	0.00	0.00	100.00
26	H2	0.00	0.00	5.00			4.75	0.00	0.00	0.00	0.00	100.00
27	O2	0.00	0.00	2.00			1.90	0.00	0.00	0.00	0.00	100.00
28	C	0.00	0.00	82.00			77.90	0.00	0.00	0.00	0.00	0.00
29	CO2	0.00	0.00	0.00			0.00	0.00	0.00	0.00	0.00	0.00
30	CO	0.00	0.00	0.00			0.00	0.00	0.00	0.00	0.00	0.00
31	total=	92.51	98.00	96.00	0.00		1016.30		330.95	0.10	0.00	

!.........	A	M	N	O	P	Q	R	S	T	U	V	W	X	Y
1	SELECTIVE													
2														
3	OXIDE	MASS	MASS of	CARBON	CO2/CO	MOLES	GAS	MASS	SLAG	TEMP	ENTHALPY	HEAT	HEAT	TOTAL
4		oxide	metal	Addn.		OF GAS	ANALYSIS	OXIDE	ANAL	.K		Of	Of	Energy
5		reduced	to gas				mole %	IN SLAG	%			Reaction	Fusion	
6		to gas						kg						
7														
8	SIO2	0.00	0.00	0.00	0.1700	0.00	0.00	37.90	7.50	1723.00	15.48	0.00	1.64	17.12
9	CaO	0.00	0.00	0.00		0.00	0.00	48.00	9.50		15.22	0.00	10.29	25.50
10	MgO	0.00	0.00	0.00		0.00	0.00	23.95	4.74		9.94	0.00	11.08	21.02
11	MnO	0.00	0.00	0.00		0.00	0.00	50.00	9.90		12.95	0.00	9.15	22.10
12	Al2O3	0.00	0.00	0.00		0.00	0.00	10.90	2.16		4.40	0.00	2.75	7.14
13	Fe2O3	0.00	0.00	24.88		0.00	0.00	0.00	0.00		122.59	145.15	31.03	298.77
14	FeO	0.00	0.00	0.00		0.00	0.00	297.86	58.95		0.00	0.00	0.00	0.00
15	Cr2O3	0.00	0.00	0.00		0.00	0.00	2.00	0.40		0.56	0.00	0.05	0.61
16	ZnO	340.90	273.56	50.50		4.21	29.98	13.10	2.59		77.94	462.95	72.11	613.00
17	K2O	12.87	10.68	1.64		0.27	1.95	0.13	0.03		4.01	11.88	0.00	15.89
18	P2O5	0.00	0.00	0.00		0.00	0.00	4.00	0.79		0.49	0.00	0.00	0.49
19	F	0.00	0.00	0.00		0.00	0.00	10.00	1.98		6.77	0.00	0.00	6.77
20	Pb3O4	39.60	37.00	3.70		0.18	1.27	0.40	0.08		4.90	9.92	0.47	15.29
21	CdO	0.89	0.78	0.08		0.01	0.04	0.01	0.00		0.13	0.59	0.00	0.71
22	S	0.12	0.12	0.00		0.00	0.03	6.03	1.19		1.35	0.25	0.00	1.60
23	NiO	0.00	0.00	0.00		0.00	0.00	0.00	0.00		0.00	0.00	0.00	0.00
24	MOO3	0.00	0.00	0.00		0.00	0.00	0.00	0.00		0.00	0.00	0.00	0.00
25	H2O	0.00	0.00	0.00		0.00	0.00	0.00	0.00		0.00	0.00	0.00	0.00
26	H2	4.75	4.75	0.00	0.0000	2.37	16.92	0.00	0.00		24.81	0.00	0.00	24.81
27	O2	1.90	1.90	1.42	0.0000	0.06	0.42	0.00	0.00		0.05	0.00	0.00	0.05
28	C	0.00	0.00	0.00		0.00		0.00	0.00		45.44	36.45	0.00	81.89
29	CO2	0.00	0.00	7.48		0.95	6.76	0.00	0.00		0.00	-89.93	0.00	-89.93
30	CO	0.00	0.00	7.48		5.58	39.75	0.00	0.00		0.00	-156.22	0.00	-156.22
31	total=	401.04	328.79	82.24		13.63	97.13	504.27	99.80		347.02	421.05	138.57	906.64
32					CARBON	78.33			0.00			ENERGY	kWh/t Dust	1052.71
33												CARBON	kg/t Dust	78.33
34												COAL	kg/t Dust	95.53
35												GAS VOLUME	m3/hour	305.39

```
B8    3.6
C8    98
D8    2
E8    0
F8    11
G8    (B8+(C8*E8/100)+(D8*F8/100))*10
H8    0
I8    G8*H8/100
J8    I8*(28/60)
K8    100*(J8/J31)
L8    0
M8    G8*L8/100
N8    M8*28/60
O8    (I8+M8)*24/60
P8    .001
Q8    N8/28
R8    Q8*100/Q31
S8    G8-I8-M8
T8    100*S8/S31
U8    1900
V8    24.5*G8/60
W8    (I8+M8)*217.6/60
X8    2.6*G8/60
Y8    V8+W8+X8
B9    4.8
C9    0
D9    0
G9    (B9+(C9*E8/100)+(D9*F8/100))*10
H9    0
I9    G9*H9/100
J9    I9*(40/56)
K9    100*(J9/J31)
L9    0
M9    G9*L9/100
N9    M9*40/56
O9    (I9+M9)*12/56
Q9    N9/40
R9    Q9*100/Q31
S9    G9-I9-M9
T9    100*S9/S31
V9    (-4050+(11.67*U8)+0.54E-3*(U8*U8)+(1.56E5/U8))*G9/56000
W9    (I9+M9)*151.6/56
X9    12*G9/56
Y9    V9+W9+X9
B10   2.3
C10   0
D10   1
G10   (B10+(C10*E8/100)+(D10*F8/100))*10
H10   0
I10   G10*H10/100
J10   I10*(24/40)
K10   100*(J10/J31)
L10   0
M10   G10*L10/100
```

```
N10   M10*24/40
O10   (I10+M10)*12/40
Q10   N10/24
R10   Q10*100/Q31
S10   G10-I10-M10
T10   100*S10/S31
V10   (-3609+(10.18*U8)+0.87E-3*(U8*U8)+(1.48E5/U8))*G10/40000
W10   (I10+M10)*143.7/40
X10   18.5*G10/40
Y10   V10+W10+X10
B11   5
C11   0
D11   0
G11   (B11+(C11*E8/100)+(D11*F8/100))*10
H11   0
I11   G11*H11/100
J11   I11*(55/71)
K11   100*(J11/J31)
L11   0
M11   G11*L11/100
N11   M11*55/71
O11   (I11+M11)*92/71
Q11   N11/55
R11   Q11*100/Q31
S11   G11-I11-M11
T11   100*S11/S31
V11   (-3690+(11.11*U8)+0.97E-3*(U8*U8)+(0.88E5/U8))*G11/71000
W11   (I11+M11)*92/71
X11   13*G11/71
Y11   V11+W11+X11
B12   .9
C12   0
D12   2
G12   (B12+(C12*E8/100)+(D12*F8/100))*10
H12   0
I12   G12*H12/100
J12   I12*(54/102)
K12   100*(J12/J31)
L12   0
M12   G12*L12/100
N12   M12*54/102
O12   (I12+M12)*36/102
Q12   N12/54
R12   Q12*100/Q31
S12   G12-I12-M12
T12   100*S12/S31
V12   (-11155+(27.43*U8)+1.53E-3*(U8*U8)+(8.47E5/U8))*G12/102000
W12   (I12+M12)*400.9/102
X12   25.7*G12/102
Y12   V12+W12+X12
B13   33
C13   0
D13   1
G13   (B13+(C13*E8/100)+(D13*F8/100))*10
```

```
H13   100
I13   G13*H13/100
J13   I13*(144/160)
K13   0
L13   0
M13   G13*L13/100
N13   M13*112/160
O13   (I13+M13)*12/159.6
Q13   N13/56
R13   Q13*100/Q31
S13   G13-I13-M13
T13   100*S13/S31
V13   (-9020+(23.49*U8)+9.3E-3*(U8*U8)+(3.55E5/U8))*G13/160000
W13   (I13+M13)*70/159.6
X13   15*G13/160
Y13   V13+W13+X13
B14   0
C14   0
D14   0
G14   (B14+(C14*E8/100)+(D14*F8/100)+(J13/10))*10
H14   0
I14   G14*H14/100
J14   I14*(55.8/71.8)
K14   100*(J14/J31)
L14   0
M14   G14*L14/100
N14   M14*56/72
O14   (I14+M14)*12/72
Q14   N14/56
R14   Q14*100/Q31
S14   G14-I14-M14
T14   100*S14/S31
V14   (-3790+(11.66*U8)+1E-3*(U8*U8)+(0.67E5/U8))*(G14-J13)/72000
W14   (I14+M14)*63.2/71.8
X14   (B14+(C14*E14/100)+(D14*F14/100))*75/71.8
Y14   V14+W14+X14
B15   .2
C15   0
D15   0
G15   (B15+(C15*E8/100)+(D15*F8/100))*10
H15   0
I15   G15*H15/100
J15   I15*(104/152)
K15   100*(J15/J31)
L15   0
M15   G15*L15/100
N15   M15*104/152
O15   (I15+M15)*36/152
Q15   N15/52
R15   Q15*100/Q31
S15   G15-I15-M15
T15   100*S15/S31
V15   (-9760+(28.53*U8)+1.10E-3*(U8*U8)+(3.74E5/U8))*G15/154000
W15   (I15+M15)*270/152
X15   4.2*G15/154
```

```
Y15   V15+W15+X15
B16   35.4
C16   0
D16   0
G16   (B16+(C16*E8/100)+(D16*F8/100))*10
H16   0
I16   G16*H16/100
J16   0
K16   100*(J16/J31)
L16   99
M16   G16*L16/100
N16   M16*65/81
O16   (I16+M16)*12/81
Q16   N16/65
R16   Q16*100/Q31
S16   G16-I16-M16
T16   100*S16/S31
V16   (-4280+(11.71*U8)+0.61E-3*(U8*U8)+(2.18E5/U8))*G16/81000
W16   (I16+M16)*110/81
X16   16.5*G16/81
Y16   V16+W16+X16
B17   1.3
C17   0
D17   0
G17   (B17+(C17*E8/100)+(D17*F8/100))*10
H17   0
I17   G17*H17/100
J17   0
K17   100*(J17/J31)
L17   99
M17   G17*L17/100
N17   M17*78/94
O17   (I17+M17)*12/94
Q17   N17/39
R17   Q17*100/Q31
S17   G17-I17-M17
T17   100*S17/S31
V17   29*G17/94
W17   (I17+M17)*86.8/94
X17   0
Y17   V17+W17+X17
B18   .4
C18   0
D18   0
G18   (B18+(C18*E8/100)+(D18*F8/100))*10
H18   0
I18   G18*H18/100
J18   I18*(62/142)
K18   100*(J18/J31)
L18   0
M18   G18*L18/100
N18   M18*62/142
O18   (I18+M18)*60/142
Q18   N18/31
R18   Q18*100/Q31
```

```
S18   G18-I18-M18
T18   100*S18/S31
V18   (-9795+(16.75*U8)+5.4E-3*(U8*U8))/2*(G18/142000)
W18   (I18+M18)*356.6/142
X18   0
Y18   V18+W18+X18
B19   1
C19   0
D19   0
G19   (B19+(C19*E8/100)+(D19*F8/100))*10
H19   0
I19   G19*H19/100
J19   I19*18.9
K19   100*(J19/J31)
L19   0
M19   G19*L19/100
N19   M19*18.9/18.9
O19   (I19+M19)*0/18.9
Q19   N19/18.9
R19   Q19*100/Q31
S19   G19-I19-M19
T19   100*S19/S31
V19   12.8*G19/18.9
W19   (I19+M19)*18.66/18.9
X19   0
Y19   V19+W19+X19
B20   4
C20   0
D20   0
G20   (B20+(C20*E8/100)+(D20*F8/100))*10
H20   0
I20   G20*H20/100
J20   0
K20   100*(J20/J31)
L20   99
M20   G20*L20/100
N20   M20*640/685
O20   (I20+M20)*64/685.6
Q20   N20/207
R20   Q20*100/Q31
S20   G20-I20-M20
T20   100*S20/S31
V20   84*G20/685.6
W20   (I20+M20)*171.77/685.6
X20   8*G20/685.6
Y20   V20+W20+X20
B21   .09
C21   0
D21   0
G21   (B21+(C21*E8/100)+(D21*F8/100))*10
H21   0
I21   G21*H21/100
J21   0
K21   100*(J21/J31)
```

```
L21   99
M21   G21*L21/100
N21   M21*112/128
O21   (I21+M21)*12/128
Q21   N21/128
R21   Q21*100/Q31
S21   G21-I21-M21
T21   100*S21/S31
V21   18.0*G21/128
W21   (I21+M21)*84.5/128
X21   0
Y21   V21+W21+X21
B22   .52
C22   0
D22   1
G22   (B22+(C22*E8/100)+(D22*F8/100))*10
H22   0
I22   G22*H22/100
J22   I22
K22   100*(J22/J31)
L22   2
M22   G22*L22/100
N22   M22*32/32
O22   (I22+M22)*0/32
Q22   N22/32
R22   Q22*100/Q31
S22   G22-I22-M22
T22   100*S22/S31
V22   7*G22/32
W22   (I22+M22)*66.2/32
X22   0
Y22   V22+W22+X22
B23   0
C23   0
D23   0
G23   (B23+(C23*E8/100)+(D23*F8/100))*10
H23   0
I23   G23*H23/100
J23   I23*58.7/74.7
K23   100*(J23/J31)
L23   0
M23   G23*L23/100
N23   M23*58.7/74.7
O23   (I23+M23)*12/74.7
Q23   N23/58.7
R23   Q23*100/Q31
S23   G23-I23-M23
T23   100*S23/S31
V23   (1122-(4.99*U8)+18.79E-3*(U8*U8)-(3.89E5/U8))*G23/74700
W23   (I23+M23)*57.5/74.7
X23   0
Y23   V23+W23+X23
B24   0
C24   0
```

```
D24   0
G24   (B24+(C24*E8/100)+(D24*F8/100))*10
H24   0
I24   G24*H24/100
J24   I24*95.9/143.9
K24   100*(J24/J31)
L24   0
M24   G24*L24/100
N24   M24*95.9/143.9
O24   (I24+M24)*36/143.9
Q24   N24/95.9
R24   Q24*100/Q31
S24   G24-I24-M24
T24   100*S24/S31
V24   (-7480+(20.07*U8)+2.95E-3*(U8*U8)+(3.68E5/U8))*G23/143900
W24   (I24+M24)*180.3/143.9
X24   12.54*G24/143.9
Y24   V24+W24+X24
B25   0
C25   0
D25   0
G25   (B25+(C25*E8/100)+(D25*F8/100))*10
H25   0
I25   G25*H25/100
J25   I25*(2/18)
K25   100*(J25/J31)
L25   100
M25   G25*L25/100
N25   M25*2/18
O25   (I25+M25)*12/18
Q25   N25/2
R25   Q25*100/Q31
S25   G25-I25-M25
T25   100*S25/S31
V25   (8280+(7.17*U8)+1.28E-3*(U8*U8)-(0.08E5/U8))*G25/18000
W25   (I25+M25)*60.5/18
X25   9.7*G25/18
Y25   V25+W25+X25
B26   0
C26   0
D26   5
G26   (B26+(C26*E8/100)+(D26*F8/100))*10
H26   0
I26   G26*H26/100
J26   I26*(2/2)
K26   100*(J26/J31)
L26   100
M26   G26*L26/100
N26   M26*2/2
O26   (I26+M26)*0/2
P26   0
Q26   N26/2
R26   Q26*100/Q31
S26   G26-I26-M26
T26   100*S26/S31
```

```
V26   (-1939+(6.52*U8)+0.39E-3*(U8*U8)-(0.12E5/U8))*G26/2E3
W26   (I26+M26)*0/2
X26   0*G26/2
Y26   V26+W26+X26
B27   0
C27   0
D27   2
G27   (B27+(C27*E8/100)+(D27*F8/100))*10
H27   0
I27   G27*H27/100
J27   I27*(32/32)
K27   100*(J27/J31)
L27   100
M27   G27*L27/100
N27   M27*32/32
O27   (I27+M27)*24/32
P27   0
Q27   N27/32
R27   Q27*100/Q31
S27   G27-I27-M27
T27   100*S27/S31
V27   (-2313+(1*U8)+0.5E-3*(U8*U8)+(0.4E5/U8))*G27/32E3
W27   (I27+M27)*0/32
X27   0*G27/32
Y27   V27+W27+X27
B28   0
C28   0
D28   82
G28   (B28+(C28*E8/100)+(D28*F8/100))*10
H28   0
I28   0
J28   0.07*SUM(J8:J12,J14:J15,J16:J22)
K28   100*(J28/J31)
L28   0
M28   G28*L28/100
N28   0
O28   0
Q28   0
S28   0
T28   0
V28   7*G28/12
W28   O27*1.35
X28   0
Y28   V28+W28+X28
B29   0
C29   00
D29   0
G29   (B29+(C29*E8/100)+(D29*F8/100))*10
H29   0
I29   G29*H29/100
J29   0
K29   100*(J29/J31)
L29   0
M29   G29*L29/100
```

```
N29   0
O29   SUM(O8:O29)/12
Q29   O29*P8/(1+(2*P8))
R29   Q29*100/Q31
S29   G29-I29-M29
T29   0
V29   0
W29   -Q29*94.8
X29   0
Y29   V29+W29+X29
B30   0
C30   0
D30   0
G30   (B30+(C30*E8/100)+(D30*F8/100))*10
H30   0
I30   G30*H30/100
J30   0
K30   100*(J30/J31)
L30   0
M30   0
N30   0
O30   SUM(O8:O29)/12
Q30   O30/(1+(2*P8))
R30   Q30*100/Q31
S30   G30-I30-M30
T30   0
V30   0
W30   -Q30*28
X30   0
Y30   V30+W30+X30
B31   SUM(B8:B30)
C31   SUM(C8:C30)
D31   SUM(D8:D30)
E31   0
G31   SUM(G8:G13,G15:G30)
I31   SUM(I8:I30)
J31   IF(SUM(J8:J12,J14:J15,J16:J30)>0,SUM(J8:J12,J14:J15,J16:J30),0.1)
K31   SUM(K8:K30)
M31   SUM(M8:M30)
N31   SUM(N9:N30)
O31   SUM(O8:O28)
Q31   IF(SUM(Q8:Q30)>0,SUM(Q8:Q30),0.1)
R31   SUM(R8:R30)
S31   IF(SUM(S8:S30)>0,SUM(S8:S30),0.1)
T31   SUM(T8:T30)
V31   SUM(V8:V30)
W31   SUM(W8:W30)
X31   SUM(X8:X30)
Y31   SUM(Y8:Y30)
Q32   12*(Q29+Q30)
T32   0
Y32   Y31*4.18/3.6
Y33   Q32
Y34   Q32*100/D28
Y35   Q31*22.4
```

REFERENCES

1 Maske K.U., PhD Thesis, University of Minnesota, April 1984.
2 Drellishak K.S., PhD Thesis, Northwestern University, Evanston IL, 1963.
3 Szekely J., Mc Kelliget J., Choudary M. Ironmaking & Steelmaking, vol 4, pp169-179.
4 IUPAC sub-commission on plasma chemistry: Pure and Applied Chemistry 54, 1221, 1982.
5 Fauchais P. et al, ISPC, 1987, pp 1856.
6 Pfender E., Pure and Applied Chemistry, vol 52, 1980, pp 1773-1800.
7 Eckert E.R.G. and Pfender E., Advances In Heat Transfer 4, Acedemic Press, New York, 1967.
8 Finkelburg W., J.Applied Physics, 20, 1949, pp 468-474.
9 Stewart J., Proc MINTEK 50, Santon, S.Africa, 1984.
10 Bowman B., Elektowaeme International, vol 30, 1972, No B2, pp 87-93.
11 Stenkvist S.E., Bowman B., Plasma Technology In Metallurgical Processing. ISS 1987, pp 103-109.
12 Blackburn T.R., 8th International Conference on Gas Discharges, Oxford, Sept 1985, pp 1-4, Leeds Univ. Press.
13 Szekely J., Ushio M., Chang C.W. Iron and Steelmaking, vol 8, No 6, 1981, pp 279-286.
14 Hamblyn S.M.L., Min. Sci. Eng. vol 9, No 3, July 1977.
15 Sayce I.G., Inst. Min. Met.1972, pp 241-272.
16 Barcza N.A., Stewart A.B., Infacon 1983.
17 Plasma Technology In Metallurgical Processing, ISS, 1987.
18 Barcza N.A., Curr T.R., Maske K.U., Int. Conf. Min. Metall. 1985, pp 709-740.
19 Kunze, H.G., 4th Arc Furnace Meeting, Budapest, Sept. 1985, pp 815-841.
20 Essmann, H., Grunberg, D. Stahl und Eisen, vol 103, No 3, 1983, pp 49-53.
21 Butel M., SFPO, Societe Francaise des Thermiciens, June, 1988.
22 Ponghis N., Vidal R., Poos A., Proc. 38th Annual Iron Making Conf. AIME Iron and Steel Soc. Detroit, 1979, vol 38, pp 224-229.
23 Dighne S.V. et al, Westinghouse brochure, Westinghouse, Pittsburgh PA, 1985.
24 Herlitz H. et al, AIME Electric Arc Furnace Conf. Proc. vol 45, 1987, pp 81-93.
25 Gladisch H., Hydrocarbon Processes and Petroleum Refining, vol 41, June 1962, pp 159-164.
26 McCollough R.J., Journal of Metals, vol 14, No 12, Dec. 1962, pp 906-911.
27 Voest Alpine Plasma Plant, Metals Bulletin Monthly, June, 1983, pp 45-48.
28 Bebber H.J. Proc MINTEK 50, Santon, S. Africa, 1984.
29 Fujware T., Daido Steel, Nagoya, Japan, 1983.

30 Nippon Steel Corporation, ISPC 8. Tokyo, Sept. 1987, pp 2247-2252.
31 Saville J., Texasgulf Brochure, Anniston, Al.
32 Steinkvist S.E., Proc MINTEK 50, Santon, S. Africa, 1984.
33 US Dept. of Energy and Electrical Power Research Institute, EPRI EM-5445, project 2787-2, Oct. 1987.
34 Bengstsson E., Widel B. ISS of AIME, vol 8, No 10, Oct. 1981, pp 30-34.
35 Bainbridge R., South African Patent 68/7766, 1968.
36 Robiette A., Electric Smelting Processes, Griffin, 1973.
37 Hokkanen P., et al. ILAFA Ferro-alloy Congress, Acapulco, 1978.
38 O'Shaughnessy, D.P., et al. South African Inst. Min. Metall, April 1980.
39 Pickles C.A., McLean A., Alcock B., Segsworth R.S., Advances in Extractive Metallurgy, Inst. Min. Met. 1977, pp 69-87.
40 Smith R.B. and Corbett M.J., AIME. 7th Process Technology Conf. Toronto 1988.
41 Barcza N., et al, 29th Electric Furnace Conf. 1971, vol 29, pp 88-93.
42 Downing J., Geochimica and Cosmochimica Acta, vol 39, 1975, pp 853-856.
43 Urquart R., Min. Sci. Eng. vol 14, No 4, Oct. 1972.
44 Wederpohl A., Proc MINTEK 50, Santon, S. Africa, 1984.
45 Muan A., Proc MINTEK 50, Santon, S. Africa, 1984.
46 Fukagawa S., Shimoda T. Trans. ISS Japan, vol 27, 1987, pp 609-617.
47 Kadarmetov K.N. S Nauchn-Tekhn. Tr Nauch-Issled., Inst. Met. Chelyabinsk Sovnakhoza.
48 Kouroki S., Morita K., Sano N. Proc MINTEK 50, Santon, S. Africa, 1984.
49 Barmin L.N., Izv. Vyssh. Ucheb Zabed Chern Meta, vol 11, No 8, 1968, pp 20-23.
50 Sevinc N., Elliott J.F., Ironmaking and Steelmaking, vol 13, 1976, pp 268.
51 Suzuki M., Mori I., Ito T., Tetsu-to-Hagane, vol 65, 1979, pp 1131.
52 Fruehan R.J., Met. Trans. B, vol 8B, 1977, pp 429.
53 Kawakami M., et al, Proc. Shenyang Int. Symp. on Smelting Reduction, 1986, China.
54 Lisniak S., Evseev N.F., Sb Nauch. Tekhn. tr. Cheliab. No 3, 1961 pp 12-20.
55 Griffing N.R., Forgeng W.D., Healy G.W., Trans. Metall. Soc. AIME, vol 224 1962, pp 148-159.
56 Kubaschewski O., Alcock C.B., Metallurgical Thermochemistry, 5th Ed. Pergamon Press, New York, N.Y.
57 Healy G.W., Trans. ISS. Dec 1987, pp 51-59.
58 Rowley D.H., Legg D.M., 35th Electric Furnace Conf. Chigaco, 1977.
59 Dresler W., Can. Inst. Met. vol 79, No 893, Sept. 1986, pp 98-105.
60 Thomas P.R., SME-AIME Annual Meeting, Los Angeles, Ca. Feb. 1984.

61 Hamakos G. Personnal communication with Hellenic Ferroalloys.
62 Downing J., Electric Furnace Conf. Proc. vol 29, 1971, pp 93.
63 Chipman J., J.I.S.I. vol 180. 1955, pp 97-106.
64 Nakamura Y., et al, Tetsu-to-Hagane, vol 64, 1978, pp 402-410.
65 Osborn E.F., Muan A., American Ceram. Soc. 1964, pp 246.
66 Johnston G.H., Proc. Infacon '74.
67 Machin J.S., Yee T.B., Hanna D.L., J. Amer. Ceram. Soc. vol 51, 1954, pp 682-687.
68 Lyutikov R.A., Tyslev L.M., Russian Met. Mining, 1963 pp 129.
69 Rennie M.S., et al, J. S. African Inst. Min. Metall. Aug 1972.
70 McCoy C.M., Philbrook W.O., Trans. Metall. Soc. AIME. April 1958, pp 226-235.
71 Higley K.W., Fukabayashi H.H., U.S. Bureau of Mines, 4th Waste Utilization Sym. Chigaco, Illinois, May 1984.
72 Lu K., Proc. of Hamilton Sym. MacMaster University, Ontario, 1974.
73 Keyser N.H., Porter J.R., et al, Sym. of Iron and Steel Pollution Abatement Technology, 1981, Chigaco, Illinois.
74 Fosnatch D.R., Sym. of Iron and Steel Pollution Abatement Technology, Chigaco, 1979.
75 MacRae D.R., "Electric Arc Furnace Dust, Disposal, Recycle and Recovery" Report No 85-2, Centre For Metals Production, May 1985.
76 Harris C.F., et al. Lead-Tin-Zinc '80, Proc. of World Sym. on Metallurgy and Environmental Control, TMS-AIME, Feb, 1980, pp 247-260.
77 Bounds C.O., J. of Metals, Aug. 1983, pp 30-36.
78 Freshcorn D., Personal communication, St Joe Minerals Corp. Monaca, PA. USA.
79 Krishnan E.R., Environmental progress, Aug 1983, vol. 2, pp 184-187.
80 Maczek H., Kola R., J. of Metals, Jan, 1980, pp 53-58.
81 Yatsukami T., et al, AIME. Electric Steelmaking Conf. 1981.
82 Ojima Y., Ishikawa Y., Yasukawa M., TMS paper a84-26, 1984.
83 Pargeter J.K., Proc. 44th Electric Arc Furnace Conf. Dec. 1986.
84 Pusateri J., Proc. 44th Electric Arc Furnace Conf. Dec. 1986.
85 Lynn J.D., Sym. of Iron and Steel Pollution Abatement Technology, 1983, Chigaco, Illinois.
86 Metius G., Proc. 44th Electric Arc Furnace Conf. Dec. 1986.
87 Kemner W., et al, US EPA report 68-02-4048.
88 Askins C.W., Schochet R.A., Sym. of Iron and Steel Pollution Abatement Technology, 1984, Cleveland, Ohio, USA.

89 Evans L.G., Proc. 44th Electric Arc Furnace Conf. Dec. 1986.
90 Frenay J., Proc. 44th Electric Arc Furnace Conf. Dec. 1986.
91 Conner J.R., US Patent 3,837,872.
92 Bell R.C., Turner G.H., Peters E., J. of Metals, vol 7, 1955, pp 472-477.
93 Kellogg H.H., Trans. AIME, 1967, vol 239, pp 1439-1449.
94 Grant R.J., Barnett L.J., Australian IMM. Melbourne, 1975, pp 247-265.
95 Quarm T.A.A., Trans. AIME. 1980, vol 89, pp 139-144.
96 Richards G.G., Brimacombe J.K., Troop G.W., Trans. Met. B Sept. 1985, vol 163, pp. 513-549.
97 Sannikov Y., Russian Metallurgy No.2, 1978, pp. 36-40.
98 Yakovenko A., Łakernik M., Tsvetnye Metally. 16. vol 11, 1975, pp 31-33.
99 Roa Y.K., El Rahaiby S.K., Met. Trans. B, vol 16B, Sept 1985, pp 465-475.
100 Bell R.C., Turner G.H. and Peters E., J. of Metals, 7, 1955, pp 472-477.
101 Okunev A.I. and BovyKin V.S., Doklady Akad. Nauk. SSSR. 112, 1957, pp 77-79.
102 Lebed B.V., Smirnov V.I. and Kirov S.M., Doklady Akad. Nauk. SSSR. 147, (1), 1962, pp 159-161.
103 Davenport W.G., Masters Thesis University of British Columbia, 1960.
104 Reyes R.A., Gaskell D.R. AIME. Annual Meeting, Atlanta, 1983.
105 Ashuma K., Goto S., Ogawa O.. J. Fac. Eng. Univ. Tokyo Ser. A. No. 5 (1), 1967, pp. 54-55.
106 Richards A.W., Thorne D.F., Physical Chemistry of Process Metallurgy, Part 1, Ed. St Pierre, Interscience Publishers, New York. 1961 pp 277-292.
107 Filipovska N.J., Bell H.B., IMM. 1978, pp c94-98.
108 Levin I.K., Lakernik M.M., Tsvet. Met. 39, (12), 1966, pp 30-35.
109 Taylor C.R., Chipman J., Trans. AIME, 1943, vol 159, pp 228.
110 Hadrys H.G., Frohberg M.G., Elliott J.F., Metall. Trans. 1 1970 No.7 pp 1867-1874.
111 Wellbeloved D.B., Finn C.W.P., Mintek Report No. M8, Randburg, S Africa, May 1982.
112 Richardson F.D., Pillay T.C.D., Trans. IMM, 66, 1957, pp 309-330.
113 Meyer H.W., Nolan J.B., Richardson F.D., Trans. IMM, 75 1966, pp C121-C122.
114 Kozakevitch P., Rev. Met. vol 51, 1954, pp 569-587.
115 Physical Chemistry of Process Metallurgy, Part 1, Ed. St. Piere, Interscience Publishers, New York. 1961 pp. 109.
116 Baldwin B.G., J.I.S.I. 1957, Vol. 186, pp 388.
117 Osborn E.F., Devries R.C., Gee K.H., Trans. Amer. Inst. Min. Engrs. 1954, vol. 200, pp.33.
118 Machin J.S., Yee T.B., Hanna D.L., J. Amer. Ceram. Soc. 1954, vol 51, pp. 569.

119 Turkdogan E.T., Bills P.M., Trans. Ceram. Soc. 1960, vol 39, pp 682-687.
120 Bodnar L., et al. Advances In Extractive Metallurgy, London 1977, pp. 35-38.
121 Rontgen P., Winterhanger H., Kammel R., Erxmetall, 13, vol. 8, 1960, pp 363-373.
122 Kaira G.H., Togumi., Marchant G. Met. Soc. CIM Annual Volume, Montreal 1977, pp 156-160.
123 Williams P., Sunderland B., Briggs G., Trans. Inst. Min Metall. Sect C. 92, June 1983.
124 Fukutake T., et al, Australia/Japan Extractive Met. Sym 1980 Aust. Inst. Min. Met.
125 Dietzel A., Merker L., IV Int. Congress on Glass, 1957, Paris, Federation Des Chambres Syndicates de l'Industrie du Verre.
126 Schwerdtfeger K., Klein K., Proc. Int. Sym. on Electroslag Remelting Processes, ISI. Japan, 1973, pp 81.
127 Shinmei K., et al. Can. Met. 1983.
128 Torigoe T., Met. Review of MMIJ. vol 1, No.2, 1984, pp 109-124.
129 Plansee Tungsten. Private communication. Plansee, Austria.
130 Kreith F., Principles of Heat Transfer, 3rd Ed. Harper and Row.
131 Hewitt G.F., Heat Transfer, 1978, Toronto, Canada, vol 6, pp 143-171.
132 Doroshchuk V.E., et al, Thermal Engineeering, vol 22, No 12, pp 77-80.
133 Horiike H., Kuriyama M., Morita H., Nuclear Technology, 1982, vol 2, pp 637-647.
134 Schaefer J.W., Jack J., NASA Technical note D-1214, Washington, 1962.
135 Wallein, J., Private communication.
136 Herlitz H., AIME. Electric Furnace Conf. Proc. vol 45. 1987, pp 81-93.
137 Unger T.W., AIME. Electric Furnace Conf. Proc. vol 44. 1986, pp 413-417.
138 Mining Annual Review, 1987, pp 64.
139 Financial Times, March 24, 1988.

TABLE 1 FERROCHROME PRODUCTION COSTS IN THE SAF

SPECIFICATION	UNIT		
Material		Chromite	Chromite
Furnace type		OUTOKUMPU	OUTOKUMPU
Location		UK	S. Africa
Power	MW	20.00	20.00
Energy Consumption	MWh/t chromite	1.52	1.60
Capacity	t/h chromite	13.16	12.50
Scheduled time	h/y	8760.00	8760.00
Availablity	%	90.00	90.00
Operating time	h/y	7884.00	7884.00
Processing rate	t chromite/y	103736.84	98550.00
Processing rate	t chromite/h	11.84	11.25
Labour	Men	75.00	75.00
Labour cost	£/y	15000.00	10000.00
MATERIAL ANALYSIS		%	%
Cr2O3		53.00	48.00
Fe2O3		17.00	22.00
TOTAL CAPITAL COST	£m	30.00	30.00
ANNUAL CAPITAL COST	£/t chromite	289.19	304.41

OPERATING COSTS	UNIT	UNIT COST	QUANTITY	£/t ORE	UNIT COST	QUANTITY	£/t ORE
Chromite	t	70.00	1.00	70.00	10.00	1.00	10.00
Agglomeration	t	20.00	1.00	20.00	15.00	1.00	15.00
Coke	t	70.00	0.17	11.90	50.00	0.17	8.50
Coal	t	50.00	0.00	0.00	50.00	0.00	0.00
Sand	t	5.00	0.11	0.55	5.00	0.11	0.55
Alumina	t	50.00	0.06	3.00	50.00	0.00	0.00
Electricity	MWh	26.00	1.52	39.52	15.00	1.52	22.80
Electrodes	£/t	250.00	0.01	1.50	250.00	0.01	3.12
Refractories	£/t	1.00	0.60	0.60	1.00	0.60	0.60
Supplies	£/t	1.00	2.00	2.00	1.00	2.00	2.00
Direct labour	man h	10.84	1.30	14.11	7.61	1.37	10.43
Gas credit	£/t	-8.66	0.00	0.00	0.00	1.00	0.00
TOTAL OPERATING COST				163.18			73.00
CAPITAL CHARGE/ROI	%	20.00	289.19	57.84	20.00	304.41	60.88
PROCESSING COST, £/t chromite				221.02			133.88
T chromium/t chromite				0.32			0.30
PROCESSING COST, £/t chromium				690.69			452.31
DELIVERY, £/t chromium				0.00			30.00
TOTAL				690.69			482.31

TABLE 2 FERROCHROME PRODUCTION COSTS IN PLASMA PROCESSES

SPECIFICATION	UNIT						
Material				Chromite			Chromite
Furnace type				MS&A			SKF Plasma
Location				UK			UK
Power	MW			12.00			48.00
Energy Consumption	MWh/t chromite			2.00			2.25
Capacity	t/h chromite			6.00			21.33
Scheduled time	h/y			8760.00			8760.00
Availablity	%			90.00			90.00
Operating time	h/y			7884.00			7884.00
Processing rate	t chromite/y			47304.00			168192.00
Processing rate	t chromite/h			5.40			19.20
Labour	Men			40.00			75.00
Labour cost	£/y			15000.00			15000.00
MATERIAL ANALYSIS							%
Cr2O3				53.00			53.00
Fe2O3				17.00			17.00
TOTAL CAPITAL COST	£m			10.00			50.00
ANNUAL CAPITAL COST	£/t chromite			211.40			297.28
OPERATING COSTS	UNIT	UNIT COST	QUANTITY		UNIT COST	QUANTITY	£/t ORE
Chromite	t	70.00	1.00	70.00	70.00	1.00	70.00
Agglomeration	t	0.00	1.00	0.00	0.00	1.00	0.00
Coke	t	70.00	0.00	0.00	70.00	0.08	5.60
Coal	t	50.00	0.28	14.00	50.00	0.22	11.00
Sand	t	5.00	0.11	0.55	5.00	0.11	0.55
Alumina	t	50.00	0.06	0.00	50.00	0.06	3.00
Electricity	MWh	26.00	2.00	52.00	26.00	2.20	57.20
Electrodes	£/t	1500.00	0.01	15.00	600.00	0.01	7.50
Refractories	£/t	1.50	1.00	1.50	1.50	1.00	1.50
Supplies	£/t	211.40	0.02	4.23	297.28	0.02	5.95
Direct labour	man h	7.69	1.65	12.68	7.69	0.87	6.69
Gas credit	£/t	0.00	0.00	0.00	-12.00	1.00	-12.00
TOTAL OPERATING COST				169.96			156.98
CAPITAL CHARGE/ROI	%	20.00	211.40	42.28	20.00	297.28	59.46
PROCESSING COST, £/t chromite				212.24			216.44
T chromium/t chromite				0.32			0.32
PROCESSING COST, £/t chromium				663.26			676.38

TABLE 3 STEELPLANT DUST ANALYSES

STEEL	INLAND	ARMCO	LTV	EMPIRE	CHAPARRA	FLORIDA	TIMKEN	LUKENS	AAUBURN	LTV
COMPANY	STEEL	BUTLER	CHIGACO	DETROIT		STEEL				CLEVELAND
COUNTRY	USA	USA	USA	USA	USA	USA	USA	USA	USA	USA
ANALYSIS %										
ZnO	6.50	12.50	18.70	18.70	23.20	30.00	30.00	33.00	35.60	37.40
Fe2O3	62.90	64.30	61.40	34.30	61.00	28.30	36.70	41.00	33.70	50.00
PbO	2.60	0.40	2.40	1.10	2.80	4.03	4.30	2.10	6.00	0.70
CdO	0.05	0.05	0.00	0.01	0.10	0.07	0.20	0.05	0.14	0.02
CuO	0.13	0.19	0.00	0.14	0.36	0.34	0.50	0.25	0.21	0.11
MgO	3.50	5.00	3.00	1.70	3.80	3.10	5.20	6.70	2.50	3.70
MnO	7.00	6.50	5.90	2.58	4.90	3.20	8.40	4.90	4.50	4.40
NiO	0.03	1.90	0.00	0.04	0.10	0.03	0.30	0.09	0.04	0.10
Cr2O3	0.26	5.90	0.00	4.40	0.60	0.23	0.60	0.41	0.37	0.09
MoO3	0.00	0.00	0.00	0.00	0.00	0.00	0.00	0.00	0.00	0.00
Al2O3	0.42	1.00	1.30	1.40	1.95	4.58	1.00	1.60	0.34	1.00
CaO	8.40	5.00	4.50	39.20	16.74	10.23	11.20	14.00	3.70	2.40
SiO2	2.80	8.00	2.90	3.20	4.15	6.03	4.40	3.40	2.40	4.30
K2O	1.00	0.00	0.72	0.90	0.71	0.80	0.66	nd	1.20	0.84
P2O5	0.10	0.07	0.10	0.40	nd	0.53	0.11	nd	0.02	nd
Na2O	0.89	nd	nd	nd	1.89	4.91	1.90	nd	0.60	nd
Cl	0.60	nd	nd	3.60	nd	2.99	nd	0.26	1.00	nd
F	1.00	nd	nd	nd	nd	0.01	nd	nd	0.92	nd
S	0.58	0.50		nd	0.77	0.38	0.33	0.07	0.33	0.50
TOTAL %	98.76	111.31	100.92	111.67	123.07	99.76	105.80	107.83	93.57	105.56
T dust/y	75000.00	10000.00	18000.00	7000.00	19200.00	14000.00	11500.00	8000.00	5000.00	16000.00
DUMPING COST, $/t	70.00	120.00	67.00	82.00	90.00	75.00	95.00	50.00	120.00	75.00

STEEL	SMACC	MANCH	SHEER	IRISH	TEMPLE	TREMORFA	THYSSEN	KRUPP	AVESTA	DAGEFORS
COMPANY	BSC	STEEL	NESS	STEEL	BSC	ALLIED				
COUNTRY	UK	UK	UK	UK	UK	UK	GERMANY	GERMANY	SWEDEN	SWEDEN
ANALYSIS %										
ZnO	7.00	23.40	21.80	32.10	13.80	35.00	2.40	0.70	1.80	nd
Fe2O3	41.80	28.80	28.50	29.50	60.00	33.30	45.00	51.80	24.20	38.50
PbO	1.70	3.60	1.00	6.40	2.10	4.00	0.45	nd	0.65	2.80
CdO	0.18	nd	0.08	nd	0.02	0.10	nd	nd	nd	nd
CuO	0.50	nd	nd	nd	nd	nd	nd	nd	nd	nd
MgO	3.50	2.90	1.50	1.40	2.10	2.30	nd	nd	nd	nd
MnO	6.50	2.90	2.70	2.50	5.40	5.00	5.00	nd	4.50	1.60
NiO	3.50	<0.2	<0.2	<0.2	<0.2	<0.2	2.00	2.90	4.20	3.30
MoO3	1.80	<0.2	<0.2	0.2	<0.2	<0.2	0.60	nd	0.60	0.45
Cr2O3	15.60	0.20	0.20	0.20	0.30	0.20	19.00	14.20	8.90	12.50
Al2O3	0.50	0.60	1.00	1.10	0.60	0.90	nd	nd	nd	nd
CaO	6.80	24.40	10.30	6.00	5.50	4.80	8.00	18.20	37.90	7.00
SiO2	8.30	2.50	3.50	3.00	2.80	3.60	7.00	nd	6.00	6.20
K2O	0.70	nd	2.40	1.40	1.30	1.30	nd	nd	nd	nd
P2O5	0.20	nd	0.50	0.30	0.20	0.40	nd	nd	nd	nd
Na2O	0.60	nd	nd	nd	nd	nd	nd	nd	nd	nd
Cl	0.49	nd	nd	4.16	nd	3.36	nd	nd	nd	nd
F	0.85	nd	nd	0.10	nd	0.09	nd	nd	nd	nd
S	0.21	0.40	0.93	nd	0.52	nd	nd	nd	nd	nd
H2O	1.00	1.00	8.00	7.00	1.00	1.00	nd	nd	nd	nd
TOTAL %	97.89	90.07	74.41	83.90	94.64	90.80	89.45	89.50	88.75	72.35
t dust/y	6000.00	8000.00	20000.00	6000.00	5000.00	6000.00	4000.00	4000.00	5000.00	5000.00

TABLE 4 EAF DUST TREATMENT COSTS IN REGIONAL PROCESSES

SPECIFICATION	UNITS							
PROCESS				WAELZ KILN		HTR KILN		SCANDUST
Material				EAF dust		EAF dust		EAF dust
Location				USA		Japan		Sweden
Capacity	t/y			76500.00		76500.00		76500.00
Operating days	d/y			300.00		300.00		300.00
Availablity	%			95.00		95.00		95.00
Operating time	h/y			6840.00		6840.00		6840.00
Processing rate	t/h			11.18		11.18		11.18
MATERIAL ANALYSIS				%		%		%
Fe203				30.00		30.00		30.00
ZnO				30.00		30.00		30.00
PbO				3.25		2.00		2.00
TOTAL CAPITAL COST	£m			17.33		10.00		26.60
ANNUAL CAPITAL COST	£/annual t			226.54		130.72		347.71
OPERATING COSTS	UNIT	UNIT COST	QUANTITY	£/t ORE	QUANTITY	£/t ORE	QUANTITY	£/t ORE
Fume	t	0.00	1.00	0.00	1.00	0.00	1.00	1.00
Coal	t	44.40	0.00	0.00	0.04	1.78	0.14	6.22
Coke	t	66.00	0.00	0.00	0.07	4.62	0.05	3.30
Coke breeze	t	44.40	0.40	17.76	0.00	0.00	0.00	0.00
Sand	t	11.10	0.18	2.00	0.00	0.00	0.08	0.89
Fuel oil	t	100.00	0.00	0.00	0.06	5.90	0.00	0.00
Electricity	MWh	26.66	0.05	1.33	0.04	1.07	2.10	55.99
Binder	t	148.00	0.00	0.00	0.02	2.96	0.00	0.00
Plasma torch	£/h	3.00	0.00	0.00	0.09	0.27	2.30	6.90
Graphite electrode	t	250.00	0.00	0.00	0.00	0.00	0.00	0.00
Refractories	t	1481.00	0.00	2.07	0.00	1.78	0.00	2.07
Supplies	t	4.00	1.45	5.80	0.80	3.20	2.18	8.72
Direct labour	man h	10.00	1.11	11.10	1.10	11.00	1.50	15.00
Maintenance labour	man h	10.00	1.10	11.00	0.65	6.50	1.74	17.40
TOTAL OPERATING COST	£/t dust			51.06		39.07		117.48
DUMPING COST	t	10.00	0.50	5.00	0.50	5.00	0.50	5.00
CAPITAL CHARGE/ROI	%	20.00	226.54	45.31	130.72	26.14	347.71	69.54
CREDITS	UNIT	UNIT COST	% RECOVERY	VALUE	% RECOVERY	VALUE	% RECOVERY	VALUE
Fe	t	50.00	0.00	0.00	0.00	0.00	90.00	9.45
Zn	t	500.00	0.00	0.00	0.00	0.00	90.00	108.33
Pb	t	250.00	0.00	0.00	0.00	0.00	0.00	0.00
ZnO	t	225.00	85.00	57.37	91.00	61.42	10.00	6.75
Process gas								10.00
TOTAL CREDIT	£/t dust			57.37		61.42		134.53
TOTAL GAIN (COST)	£/t dust			-44.00		-8.79		-57.49

TABLE 5 EAF DUST TREATMENT COSTS IN ON-SITE PROCESSES .

SPECIFICATION	UNITS					
PROCESS				FIXATION		REYCLE
Material				EAF dust		EAF dust
Location				USA		USA
Capacity	t/y			5443.00		5443.00
Operating days	d/y			300.00		300.00
Availablity	%			95.00		95.00
Operating time	h/y			6840.00		6840.00
Processing rate	t/h			0.80		0.80
MATERIAL ANALYSIS				%		%
Fe2O3				30.00		30.00
ZnO				30.00		30.00
PbO				3.25		2.00
TOTAL CAPITAL COST	£m			0.33		0.40
ANNUAL CAPITAL COST	£/annual t			60.63		73.49
OPERATING COSTS	UNIT	UNIT COST	QUANTITY	£/t ORE	QUANTITY	£/t ORE
Fume	t	0.00	1.00	0.00	1.00	0.00
Coal	t	44.40	0.00	0.00	0.00	0.00
Coke	t	66.00	0.00	0.00	0.00	0.00
Coke breeze	t	44.40	0.00	0.00	0.00	0.00
Sand	t	11.10	0.00	0.00	0.00	0.00
lime	t	51.00	0.10	5.10	0.00	0.00
Electricity	MWh	26.60	0.00	0.00	0.80	21.28
Binder	t	148.00	0.00	0.00	0.02	2.96
Plasma torch	£/h	0.00	0.00	0.00	0.00	0.00
Graphite electrode	t	250.00	0.00	0.00	0.00	0.00
Refractories	t	1481.00	0.00	0.00	0.00	0.00
Supplies	t	4.00	0.38	1.52	0.47	1.88
Direct labour	man h	10.00	0.55	5.50	0.55	5.50
Maintenance labour	man h	10.00	0.31	3.10	0.37	3.70
TOTAL OPERATING COST	£/t dust			15.22		35.32
DUMPING COST	t	7.40	1.20	8.88	0.50	3.70
CAPITAL CHARGE/ROI	%	20.00	60.63	12.13	73.49	14.70
CREDITS	UNIT	UNIT COST	% RECOVERY	VALUE	% RECOVERY	VALUE
Fe	t	50.00	0.00	0.00	0.00	0.00
Zn	t	500.00	0.00	0.00	0.00	0.00
Pb	t	250.00	0.00	0.00	0.00	0.00
ZnO	t	225.00	0.00	0.00	95.00	64.12
Process gas						
TOTAL CREDIT	£/t dust			0.00		64.12
TOTAL GAIN (COST)	£/t dust			-36.23		10.41

TABLE 6 AOD DUST TREATMENT COSTS IN THE SCANDUST FURNACE

SPECIFICATION	UNIT	
Material		AOD dust
Furnace type		SKF
Location		SWEDEN
Power	MW	24.00
Energy consumption	MWh/t	2.10
Capacity	t/h	11.43
Scheduled time	h/y	8400.00
Availablity	%	80.00
Operating time	h/y	6720.00
Processing rate	t/y	76800.00
Processing rate	t/h	9.14
Labour	Men	60.00
Labour cost	£/y	20000.00

MATERIAL ANALYSIS	%
Cr_2O_3	15.60
NiO	3.50
MoO_3	1.80
Fe_2O_3	41.80
ZnO	7.00

TOTAL CAPITAL COST	£M	26.60
ANNUAL CAPITAL COST	£/annual t	346.35

OPERATING COSTS	UNIT	UNIT COST £	QUANTITY	£/t ORE
Fume	t	0.00	1.00	0.00
Coal	t	50.00	0.23	11.50
Coke	t	70.00	0.05	3.30
Sand	t	5.00	0.08	0.40
Electricity	MWh	26.00	2.10	54.60
Argon	m3	0.75	0.00	0.00
Plasma torch	£/h	2.00	2.30	4.60
Graphite electrode	£/t		0.00	0.00
Refractories	£/t	4.20	0.50	2.10
Supplies	£/t	346.35	0.02	6.93
Direct labour	£/man h	15.62	1.52	23.80
Gas credit	£/t	12.00	-1.00	-12.00
TOTAL OPERATING COST	£/t			95.23
DUMPING COST	t	10.00	0.50	5.00
CAPITAL CHARGE	%	20.00	346.35	69.27

CREDITS	UNIT	UNIT COST £	% RECOVERY	VALUE
Cr	t	720.00	84.80	65.17
Ni	t	9000.00	94.00	232.93
Mo	t	12000.00	86.00	123.84
Fe	t	70.00	97.00	19.87
Zn	t	500.00	0.00	0.00
Pb	t	250.00	0.00	0.00
ZnO	t	200.00	97.50	0.00
TOTAL CREDIT	£/t			441.81
TOTAL GAIN (COST)	£/t			272.31

TABLE 7 CHROMITE RAW MATERIALS

	CHROMITE	COAL	SAND	LIME
ANALYSIS %				
ZnO	0.00	0.00	0.00	0.00
Fe_2O_3	24.20	1.00	1.00	0.20
PbO	0.00	0.00	0.00	0.00
CdO	0.00	0.00	0.00	0.00
CuO	0.00	0.00	0.00	0.00
MgO	15.40	1.00	0.00	0.20
MnO	0.00	0.00	0.00	0.20
NiO	0.00	0.00	0.00	0.00
MoO_3	0.00	0.00	0.00	0.00
Cr_2O_3	38.20	0.00	0.00	0.00
Al_2O_3	14.70	0.00	0.00	0.20
CaO	0.50	0.00	1.00	96.00
SiO_2	7.10	2.00	98.00	2.50
K_2O	0.00	0.00	0.00	0.00
P_2O_5	0.10	0.20	0.00	0.10
Na_2O	0.00	0.00	0.00	0.00
Cl	0.00	0.00	0.00	
F	0.00	0.00	0.00	
S	0.03	1.00	0.00	0.50
C	0.00	82.00	0.00	0.00
H_2	0.00	8.00	0.00	0.00
H_2O	10.00	1.00	0.00	0.00

TABLE 8 CHROMITE SMELTING PRODUCT ANALYSES - BSC

TAP No	A/1	A/2	A/3	A/4	A/5	A/6	A/7	A/8	A/9	A/10	A/11	A/12	A/12	A/13	A/14	A/15	A/16	A/17	A/18	A/19	A/20	A/21
FEED BLEND																						
% COAL ADDITION	31.00	31.00	31.00	31.00	31.00	31.00	31.00	31.00	31.00	31.00	31.00	31.00	31.00	31.00	31.00	31.00	31.00	29.00	29.00	27.00	27.00	24.50
% SAND ADDITION	14.00	14.00	14.00	16.20	16.20	16.20	16.20	16.20	16.20	16.20	16.20	16.20	16.20	14.00	14.00	18.50	18.50	18.50	18.50	18.50	18.50	18.50
% LIME ADDITION	4.00	4.00	4.00	4.00	4.00	4.00	4.00	4.00	4.00	5.00	5.00	5.00	5.00	5.00	5.00	5.00	5.00	5.00	5.00	5.00	5.00	5.00
CHROMITE WEIGHT, t	0.94	0.72	0.05	0.88	0.60	0.89	0.60	0.62	0.67	0.15	0.82	0.87	0.87	0.62	0.81	0.26	0.61	0.94	0.95	0.82	0.79	1.35
METAL WEIGHT, t	0.32	0.07	0.20	0.02	0.72	0.21	0.20	0.34	0.55	0.00	0.00	0.34	0.34	0.21	0.15	0.27	0.67	0.51	0.17	0.78	0.34	0.53
METAL ANALYSIS																						
% Si	0.67	nd	1.17	nd	4.00	2.08	3.36	4.00	2.12			nd	nd	4.00	nd	nd	4.68	1.68	2.32	0.28	1.36	0.68
% Mn	0.41	nd	0.40	nd	0.60	0.52	0.44	0.62	0.54			nd	nd	0.44	nd	nd	0.54	0.32	0.32	0.16	0.28	0.32
% Fe	86.00	nd	77.00	nd	34.40	35.60	35.34	35.00	35.00			nd	nd	37.60	nd	nd	36.50	39.70	41.10	40.60	34.20	38.60
% Cr	9.69	nd	17.50	nd	54.10	54.40	53.60	53.20	54.80			nd	nd	52.00	nd	nd	51.70	51.50	49.60	51.60	57.20	53.20
% C	2.09	nd	3.00	nd	6.89	7.32	7.20	7.03	7.27			nd	nd	5.80	nd	nd	6.46	6.70	6.58	7.21	6.81	7.13
% S	0.09	nd	0.10	nd	0.04	0.04	0.03	0.03	0.03			nd	nd	0.03	nd	nd	0.03	0.05	0.05	0.08	0.05	0.04
% P	0.06	nd	0.06	nd	0.03	0.04	0.03	0.03	0.03			nd	nd	0.04	nd	nd	0.04	0.04	0.04	0.04	0.03	0.03
SLAG WEIGHT, t	0.50	0.01	0.31	0.32	0.23	0.66	0.27	0.15	0.98	0.38	0.40	0.39	0.39	0.29	0.00	0.31	1.02	0.56	0.63	0.51	0.45	0.71
SLAG ANALYSIS																						
% CaO	6.60	nd	7.90	6.60	6.20	6.90	6.40	6.00	5.50	3.90	6.00	6.00	6.00	5.40	6.60	7.00	6.30	6.10	6.20	6.40	6.80	6.50
% SiO2	35.70	nd	29.10	29.00	29.10	33.00	30.50	26.40	28.30	29.10	36.10	31.90	31.90	23.10	28.80	26.50	28.80	35.70	33.60	38.60	36.70	35.00
% MgO	25.40	nd	30.50	28.40	27.50	31.80	29.80	33.90	37.00	37.50	25.90	22.50	22.50	25.00	25.30	24.50	31.60	26.20	27.20	21.30	26.30	22.90
% Al2O3	25.90	nd	28.00	27.80	28.80	24.00	26.80	28.60	24.30	22.40	25.20	23.90	23.90	33.90	29.60	30.30	28.00	25.10	24.80	21.50	25.50	23.70
% Fe2O3	1.10	nd	1.50	2.50	2.53	1.70	2.40	1.60	1.20	1.70	1.20	5.10	5.10	5.30	4.20	4.40	1.40	1.80	2.80	3.10	1.00	2.90
% Cr2O3	3.30	nd	2.10	5.10	5.70	2.20	3.30	2.70	3.50	3.70	4.10	9.30	9.30	7.70	6.10	7.60	3.10	4.40	5.10	8.10	2.60	7.70
B.H. DUST WEIGHT, t			0.13									0.22	0.22									0.50
B.H. DUST ANALYSIS																						
% CaO			4.50									4.50	4.50									4.50
% SiO2			25.70									24.80	24.80									30.80
% MgO			41.00									39.30	39.30									41.00
% Al2O3			4.10									3.10	3.10									3.30
% Fe2O3			4.70									4.70	4.70									4.70
% Cr2O3			4.60									3.90	3.90									4.20

TABLE 9 CHROMITE SMELTING PRODUCT ANALYSES - LSM

TAP No	A/1	A/2	A/3	A/4	A/5	A/6	A/7	A/8	A/9	A/10	A/11	A/12	A/13	A/14	A/15	A/16	A/17	A/18	A/19	A/20	A/21
FEED BLEND																					
% COAL ADDITION	31.00	31.00	31.00	31.00	31.00	31.00	31.00	31.00	31.00	31.00	31.00	31.00	31.00	31.00	31.00	31.00	29.00	29.00	27.00	27.00	24.50
% SAND ADDITION	14.00	14.00	14.00	16.20	16.20	16.20	16.20	16.20	16.20	16.20	16.20	16.20	14.00	14.00	18.50	18.50	18.50	18.50	18.50	18.50	18.50
% LIME ADDITION	4.00	4.00	4.00	4.00	4.00	4.00	4.00	4.00	4.00	5.00	5.00	5.00	5.00	5.00	5.00	5.00	5.00	5.00	5.00	5.00	5.00
METAL ANALYSIS																					
% Si	5.10	0.67	1.22	nd	1.80	2.33	3.19	3.90	2.08	nd	nd	2.00	4.00	nd	6.80	4.90	2.10	2.80	0.60	0.60	1.10
% Mn	nd	nd	nd	nd	nd	nd	nd	nd	nd	nd	nd	nd	nd	nd	nd	nd	nd	nd	nd	nd	nd
% Fe	nd	nd	nd	nd	nd	nd	nd	nd	nd	nd	nd	nd	nd	nd	nd	nd	nd	nd	nd	nd	nd
% Cr	40.20	9.10	13.90	nd	51.50	49.20	51.20	51.20	52.50	nd	nd	50.10	47.70	nd	49.50	50.00	49.10	47.60	51.70	53.10	48.30
% C	4.70	2.10	3.03	nd	6.87	7.53	7.29	7.29	7.44	nd	nd	7.55	6.20	nd	5.82	6.50	6.69	6.68	7.08	6.71	6.68
% S	nd	nd	nd	nd	nd	nd	nd	nd	nd	nd	nd	nd	nd	nd	nd	nd	nd	nd	nd	nd	nd
% P	nd	nd	nd	nd	nd	nd	nd	nd	nd	nd	nd	nd	nd	nd	nd	nd	nd	nd	nd	nd	nd
SLAG ANALYSIS																					
% CaO	6.52	nd	7.80	6.65	6.40	7.10	6.08	5.95	5.52	3.82	6.05	6.01	5.51	6.62	7.05	6.25	6.12	6.22	6.41	6.91	6.48
% SiO2	35.78	nd	28.63	29.62	29.03	33.71	29.23	26.69	28.39	29.38	36.54	32.42	24.60	29.17	27.31	28.89	35.58	34.03	38.38	36.88	34.67
% MgO	23.49	nd	29.95	28.48	27.53	32.67	27.47	32.04	34.25	34.39	24.28	23.17	25.39	25.40	24.69	31.37	25.77	26.93	21.68	26.10	23.35
% Al203	26.15	nd	28.80	28.30	27.90	24.64	26.90	28.90	24.80	22.70	25.66	24.40	33.70	30.00	30.50	27.90	25.26	25.14	21.64	25.76	23.75
% Fe203	1.39	nd	1.12	1.85	2.67	0.90	4.72	1.65	1.03	2.17	1.20	4.85	4.57	3.89	3.91	1.79	1.98	2.85	3.05	0.79	3.38
% Cr203	2.88	nd	1.80	4.79	4.96	1.27	5.13	2.96	3.28	3.95	3.46	9.53	7.08	6.05	7.02	3.69	4.39	4.93	7.92	2.38	8.72

TABLE 10 CHROMITE SMELTING MASS BALANCE

RECOVERY OF OXIDES TO THE CONDENSED PHASES

OXIDE	METAL %	SLAG %	B.H. DUST %	ACCOUNTABLITY %
Cr2O3	91.40	8.20	0.70	100.30
Fe2O3	90.90	6.10	1.23	98.23
CaO		86.30	5.90	92.20
SiO2	8.30	84.40	7.11	99.80
MgO		124.00	16.70	140.00
Al2O3		117.00	1.46	178.00

PRODUCT RATIOS

ALLOY/CHROMITE	0.41
SLAG/CHROMITE	0.61
B.H. DUST/CHROMITE	0.06

TABLE 11 CHROMITE SMELTING OPERATIONAL RESULTS

TAP No	A/1	A/2	A/3	A/4	A/5	A/6	A/7	A/8	A/9	A/10	A/11	A/12	A/13	A/14	A/15	A/16	A/17	A/18	A/19	A/20	A/21
TAP TEMPERATURE, K	1923	1923	1873	1873	1973	1773	1923	1953	1723	1843	1723	1823	1703	1703	1873	1973	1843	1873	1713	1803	1723
TAP TO TAP TIME, hrs	11.00	5.96	1.00	7.50	5.10	5.46	3.70	4.50	7.58	3.38	5.36	4.26	3.58	4.40	2.18	4.05	5.23	7.41	6.33	4.10	4.00
FEED ON TIME, hrs	8.28	5.96	1.00	6.53	4.10	5.34	3.70	4.11	7.48	2.96	5.03	4.26	3.58	4.26	2.18	3.96	5.23	6.82	6.08	4.10	4.00
PLASMA ON TIME, hrs	8.28	5.96	1.00	6.53	4.10	5.34	3.70	4.11	7.48	2.99	5.03	4.26	3.58	4.26	2.18	3.96	5.23	6.82	6.08	4.10	4.00
ENERGY CONSUMED, MWh	3.33	2.19	0.26	2.03	2.31	2.11	1.72	1.97	2.63	0.63	2.40	2.06	1.81	2.13	1.00	1.99	2.68	3.08	2.97	1.88	4.72
FURNACE LOSSES, MW	0.14	0.14	0.14	0.14	0.14	0.14	0.14	0.15	0.16	0.16	0.16	0.16	0.16	0.16	0.16	0.17	0.17	0.17	0.18	0.18	0.18
ORE FEED RATE, t/hr	0.09	0.12	0.05	0.12	0.12	0.16	0.16	0.14	0.09	0.04	0.15	0.20	0.17	0.18	0.12	0.15	0.18	0.13	0.13	0.19	0.34
POWER INPUT, MW	0.30	0.37	0.26	0.27	0.45	0.39	0.46	0.44	0.35	0.19	0.45	0.48	0.51	0.48	0.46	0.49	0.51	0.42	0.47	0.46	1.18
GROSS ENERGY, MWh/t alloy	10.50	30.83	1.25	0.00	3.20	10.25	8.50	5.79	4.74	0.00	0.00	0.00	8.64	0.00	3.73	2.97	5.29	18.57	3.83	5.45	8.89
NETT ENERGY, MWh/t alloy	5.65	19.08	0.57	0.00	2.21	6.54	5.94	3.81	2.52	82.06	0.00	0.00	5.86	0.00	2.40	1.94	3.54	10.98	2.36	3.31	7.53
FEED AVAILABLITY, %	75.27	100.00	100.00	87.11	80.39	97.80	100.00	91.33	98.68	87.57	93.84	100.00	100.00	96.82	100.00	97.78	100.00	92.04	96.05	100.00	100.00
PLASMA AVAILABLITY, %	75.27	100.00	100.00	87.07	80.39	97.80	100.00	91.33	98.68	88.34	93.84	100.00	100.00	96.82	100.00	97.78	100.00	92.04	96.05	100.00	100.00
ALLOY/CHROMITE	0.34	0.10	3.92	0.02	1.21	0.23	0.33	0.55	0.83	0.01	0.00	0.39	0.34	0.18	1.04	1.09	0.54	0.18	0.95	0.44	0.39
SLAG/CHROMITE	0.53	0.02	5.88	0.36	0.39	0.74	0.45	0.25	1.47	2.55	0.48	0.45	0.46	0.00	1.20	1.67	0.60	0.67	0.63	0.56	0.52
B.H. DUST/CHROMITE	0.00	0.00	2.56	0.00	0.00	0.00	0.00	0.00	0.00	0.00	0.00	0.25	0.00	0.00	0.00	0.00	0.00	0.00	0.00	0.00	0.37

TABLE 12 FURNACE COOLING LOSSES

WATER COOLING LOSSES

ITEM	WATER INLET TEMPERATURE K	WATER OUTLET TEMPERATURE K	WATER FLOW m3/s	ENERGY LOSS kW
Torch nozzle	311.80	301.00	0.00110	50.00
Torch cathode	307.10	301.00	0.00017	5.00
Torch jacket	308.60	301.00	0.00012	4.00
Torch bearing	299.60	293.00	0.00012	3.00
Head plate	298.70	293.00	0.00012	3.00
Furnace roof	302.00	299.00	0.00443	55.00
Sidewall sprays	302.00	299.00	0.00100	85.00
Total				205.00

CONVECTION LOSSES

	AREA m2	TEMPERATURE K	ENERGY LOSS PER UNIT AREA W/m2	ENERGY LOSS kW
Sidewalls	5.00	473.00	2000.00	10.00
Bottom	2.00	413.00	1200.00	2.40
Exhaust	0.90	573.00	6000.00	5.40
Total				17.40

TOTAL LOSSES				222.00

TABLE 13 EAF DUST RAW MATERIALS ANALYSES

	AOD	SHEERNESS	IRISH	TEMPLEBO'	TREMORFA	COAL	SAND
ANALYSIS %							
ZnO	7.00	21.80	32.10	13.80	35.40	0.00	0.00
Fe_2O_3	41.80	28.50	29.50	60.00	33.30	1.00	1.00
PbO	1.70	1.00	6.40	2.10	4.00	0.00	0.00
CdO	0.18	0.08	0.08	0.02	0.10	0.00	0.00
CuO	0.50	nd	nd	nd	nd	0.00	0.00
MgO	3.50	1.50	1.40	2.10	2.30	1.00	0.00
MnO	6.50	2.70	2.50	5.40	5.00	0.00	0.00
NiO	3.50	<0.2	<0.2	<0.2	<0.2	0.00	0.00
MoO_3	1.80	<0.2	0.2	<0.2	<0.2	0.00	0.00
Cr_2O_3	15.60	0.20	0.20	0.30	0.20	0.00	0.00
Al_2O_3	0.50	1.00	1.10	0.60	0.90	0.00	0.00
CaO	6.80	10.30	6.00	5.50	4.80	0.00	1.00
SiO_2	8.30	3.50	3.00	2.80	3.60	2.00	98.00
K_2O	0.70	2.40	1.40	1.30	1.30	0.00	0.00
P_2O_5	0.20	0.50	0.30	0.20	0.40	0.20	0.00
Na_2O	0.60	1.10	1.00	1.10	1.30	0.00	0.00
Cl	0.49	0.90	4.16	0.80	3.36	0.00	0.00
F	0.85	0.10	0.10	0.40	0.09	0.00	0.00
S	0.21	0.93	nd	0.52	nd	1.00	0.00
C	0.30	nd	nd	nd	nd	82.00	0.00
H_2	0.00	0.00	0.00	0.00	0.00	8.00	0.00
H_2O	1.00	8.00	7.00	1.00	1.00	1.00	0.00

TABLE 14 TREMORFA DUST ANALYSES

ANALYSIS %								
ZnO	35.40	34.60	35.00	33.50	31.10	31.70	39.50	38.80
Fe2O3	33.30	35.00	36.00	35.40	37.40	37.40	26.90	30.60
PbO	4.00	3.50	3.10	3.10	3.00	2.90	3.70	3.60
CdO	0.10	0.16	0.15	0.14	0.10	0.10	0.10	0.10
MgO	2.30	1.90	2.20	2.60	2.40	2.70	2.40	1.70
MnO	5.00	5.00	4.80	5.40	5.40	5.30	4.70	4.70
NiO	<0.2	<0.2	<0.2	<0.2	<0.2	<0.2	<0.2	<0.2
MoO3	<0.2	<0.2	<0.2	<0.2	<0.2	<0.2	<0.2	<0.2
Cr2O3	0.20	0.20	0.20	0.20	0.20	0.30	<0.2	0.20
Al2O3	0.90	0.80	1.00	0.80	0.80	0.80	0.80	0.90
CaO	4.80	4.80	5.40	5.40	5.40	5.50	4.60	5.00
SiO2	3.60	3.60	3.40	3.60	3.50	3.50	3.30	3.20
K2O	1.30	1.00	1.00	0.90	0.90	0.90	1.50	1.30
P2O5	0.40	0.45	0.50	0.50	0.50	0.50	0.40	0.50
Na2O	nd	1.36	1.30	1.31	1.30	1.30	1.90	1.78
Cl	3.36	3.21	3.30	3.35	3.30	3.30	4.14	3.80
F	0.09	0.07	0.08	3.38	0.10	0.10	0.10	0.07

TABLE 15 AOD DUST SMELTING PRODUCT ANALYSES

TAP No	B/1	B/2	B/3	B/4	B/5	B/6	B/7	B/8	B/9	B/10
DUST SOURCE	AOD	AOD	AOD	AOD	AOD	AOD	AOD	AOD	AOD	AOD
DUST FORM	DUST	DUST	DUST	DUST	DUST	DUST	DUST	PELLET	PELLET	PELLET
FEED BLEND										
% COAL ADDITION	28.00	28.00	28.00	28.00	28.00	28.00	28.00	28.00	28.00	28.00
% SAND ADDITION	0.00	0.00	0.00	0.00	0.00	0.00	0.00	0.00	0.00	0.00
DUST WEIGHT, t	1.33	1.06	1.38	0.90	0.60	0.89	0.15	0.75	0.60	1.00
METAL WEIGHT, t	0.21	0.45	0.26	0.15	0.54	0.44	0.01	0.67	0.07	0.45
METAL ANALYSIS										
% Si	0.02	0.02	0.15	0.42	0.30	0.24	2.50	3.60	0.09	2.80
% Mn	1.80	2.60	3.20	3.90	4.10	4.55	1.30	4.50	1.40	4.10
% Fe	69.80	63.80	61.30	58.30	58.70	58.20	89.00	59.40	65.80	61.90
% Cr	16.80	19.70	19.90	22.30	22.60	21.60	4.50	19.10	18.60	17.70
% Ni	4.83	5.77	6.74	6.04	5.36	5.96	1.30	5.85	6.12	5.91
% Mo	1.93	2.31	2.45	2.39	2.34	2.35	0.60	2.35	2.50	2.25
% C	4.00	5.20	5.50	5.90	6.03	6.45	0.18	4.43	4.64	4.59
% S	0.17	0.09	0.07	0.06	0.06	0.05	0.00	0.05	0.10	0.04
% P	0.07	0.06	0.06	0.06	0.05	0.05	0.02	0.06	0.06	0.05
% Cu	0.52	0.61	0.66	0.56	0.47	0.53	0.03	0.62	0.66	0.59
SLAG WEIGHT, t	0.14	0.12	0.17	0.18	0.16	0.27	0.01	0.30	0.14	0.13
SLAG ANALYSIS										
% CaO	21.50	23.00	25.90	28.10	28.40	27.40	34.70	20.40	20.30	24.30
% SiO_2	31.60	30.80	37.30	35.20	29.10	32.60	35.80	40.90	37.10	45.40
% MgO	11.30	10.10	11.90	10.20	8.90	9.10	5.80	11.70	10.60	11.20
% Al_2O_3	6.30	4.10	4.30	14.30	25.50	16.20	22.30	7.60	3.70	10.50
% MnO	17.40	16.10	15.00	9.20	5.70	9.20	0.60	10.30	17.40	6.40
% Fe_2O_3	2.00	7.60	1.60	0.90	0.90	2.10	1.30	4.70	3.40	0.90
% Cr_2O_3	8.80	7.30	3.60	1.40	1.00	2.60	0.40	4.70	7.10	1.10
% NiO	0.10	0.10	0.10	0.10	0.10	0.10	0.10	0.10	0.10	0.10
% MoO_3	0.10	0.10	0.10	0.10	0.10	0.10	0.10	0.10	0.10	0.10
% ZnO	<0.2	<0.2	<0.2	<0.2	<0.2	<0.2	<0.2	<0.2	<0.2	<0.2
% PbO	<0.2	<0.2	<0.2	<0.2	<0.2	<0.2	<0.2	<0.2	<0.2	<0.2
% CdO	<0.2	<0.2	<0.2	<0.2	<0.2	<0.2	<0.2	<0.2	<0.2	<0.2
% S	0.87	0.92	0.87	0.78	0.76	0.68	0.26	0.47	0.63	0.63
% P_2O_5	<0.2	<0.2	<0.2	<0.2	<0.2	<0.2	<0.2	<0.2	<0.2	<0.2
% K_2O	<0.2	<0.2	<0.2	<0.2	<0.2	<0.2	<0.2	<0.2	<0.2	<0.2
B.H. DUST WEIGHT, t	0.17	0.07	0.14	0.01	0.06	0.14	0.01	0.03	0.01	0.54
B.H. DUST ANALYSIS										
% CaO	1.30	1.80	4.60	4.70	6.20	7.10	nd	7.50	nd	5.20
% SiO_2	2.50	2.90	4.10	3.90	3.90	4.90	nd	5.60	nd	10.70
% MgO	2.00	2.80	6.30	6.20	8.90	9.00	nd	10.10	nd	11.00
% Al_2O_3	0.60	0.20	1.70	1.80	2.90	5.60	nd	7.70	nd	3.50
% MnO	4.90	4.90	5.90	5.60	5.60	6.40	nd	7.00	nd	6.10
% Fe_2O_3	16.90	5.90	5.10	6.80	5.70	5.40	nd	5.70	nd	4.80
% Cr_2O_3	1.50	1.20	1.20	1.20	1.00	1.40	nd	1.50	nd	1.10
% ZnO	33.20	53.60	46.60	44.00	43.00	47.60	nd	34.00	nd	35.00
% PbO	4.70	5.70	5.30	4.60	5.20	5.00	nd	5.00	nd	5.20
% CdO	0.87	0.93	0.78	0.75	0.69	0.70	nd	0.70	nd	0.72
% S	1.21	0.93	0.89	0.94	0.77	0.82	nd	0.73	nd	0.73
% P_2O_5	<0.2	<0.2	<0.2	<0.2	<0.2	<0.2	nd	<0.2	nd	<0.2
% Cl	0.87	0.93	0.78	0.75	0.69	0.70	nd	0.70	nd	0.72
% F	nd	nd	nd	nd	nd	nd	nd	nd	nd	nd
% Na_2O	nd	nd	nd	nd	nd	nd	nd	nd	nd	nd
% K_2O	2.60	2.80	2.70	2.20	2.50	2.40	nd	2.20	nd	2.40

TABLE 16 EAF DUST SMELTING PRODUCT ANALYSES

TAP No	C/1	C/2	C/3	C/4	C/5	C/6	C/7	C/8	C/9	C/10	C/11	C/12	C/13	C/14	C/15	C/16	C/17	C/18	C/19	C/20	C/21
DUST SOURCE	SHEER	SHEER	SHEER	SHEER	SHEER	SHEER	SHEER	SHEER	SHEER	SHEER	SHEER	SHEER	SHEER	SHEER	SHEER	SHEER	IRISH	IRISH	IRISH	IRISH	IRISH
DUST FORM	PELLET	PELLET	PELLET	PELLET	PELLET	PELLET	PELLET	PELLET	PELLET	PELLET	PELLET	DUST	DUST	DUST	DUST	DUST	PELLET	PELLET	PELLET	PELLET	PELLET
FEED BLEND																					
% COAL ADDITION	21.00	21.00	21.00	21.00	21.50	21.50	21.50	21.50	21.50	20.00	17.50	12.50	21.50	21.50	22.50	23.70	25.00	23.75	23.75	25.60	26.25
% SAND ADDITION	4.00	4.00	4.00	4.00	7.50	7.50	7.50	10.50	10.00	10.00	10.00	10.00	10.00	10.00	5.00	10.00	10.00	7.50	7.50	7.50	7.50
DUST WEIGHT, t	1.20	1.20	0.80	1.20	1.20	1.20	0.80	0.80	0.80	0.80	0.80	0.80	0.40	0.80	0.80	0.80	0.80	0.40	0.80	0.80	0.40
METAL WEIGHT, t	0.00	0.14	0.11	0.10	0.07	0.34	0.00	0.32	0.21	0.12	0.17	0.08	0.07	0.17	0.00	0.00	0.00	0.00	0.00	0.00	0.00
METAL ANALYSIS																					
% Si		nd	nd	nd	nd	nd		nd	0.71	nd	nd	nd	nd	nd							3.10
% Mn		nd	nd	nd	nd	nd		nd	0.41	nd	nd	nd	nd	nd							3.30
% Fe		nd	nd	nd	nd	nd		nd	96.40	nd	nd	nd	nd	nd							89.00
% Cr		nd	nd	nd	nd	nd		nd	0.38	nd	nd	nd	nd	nd							0.80
% C		nd	nd	nd	nd	nd		nd	1.39	nd	nd	nd	nd	nd							3.40
% S		nd	nd	nd	nd	nd		nd	0.62	nd	nd	nd	nd	nd							0.03
% P		nd	nd	nd	nd	nd		nd	nd	nd	nd	nd	nd	nd							nd
% Cu		nd	nd	nd	nd	nd		nd	nd	nd	nd	nd	nd	nd							nd
SLAG WEIGHT, t	0.11	0.27	0.15	0.27	0.11	0.57	0.22	0.34	0.27	0.25	0.32	0.32	0.20	0.19	0.29	0.19	0.14	0.11	0.03	0.06	0.06
SLAG ANALYSIS																					
% CaO	18.50	32.20	30.00	28.80	21.60	23.90	24.30	21.80	20.90	26.30	25.50	21.00	21.80	23.50	24.10	35.60	33.10	29.40	24.70	32.70	32.70
% SiO2	16.90	31.30	28.10	41.60	32.00	31.90	33.40	39.40	41.50	35.70	38.30	33.50	38.40	41.10	38.40	37.30	42.50	42.20	32.90	41.00	41.00
% MgO	7.70	14.70	18.20	17.50	15.20	18.20	12.90	21.80	18.10	16.40	17.70	27.60	21.20	13.60	17.80	17.70	16.00	14.40	27.40	9.20	9.20
% Al2O3	3.50	5.20	4.20	5.80	3.60	3.40	3.20	2.90	2.80	3.60	4.30	4.30	3.60	3.80	3.60	7.80	5.50	5.20	6.80	12.00	12.00
% MnO	7.80	10.30	10.90	4.50	10.50	10.10	10.50	8.50	8.70	9.60	8.50	7.20	8.40	8.40	7.80	0.80	2.20	5.50	3.20	2.90	2.90
% Fe2O3	42.80	4.10	4.30	1.00	7.90	4.30	13.10	5.20	7.10	6.70	5.40	5.60	5.40	8.20	7.60	0.50	0.30	2.90	4.40	1.40	1.40
% Cr2O3	5.50	2.30	4.00	0.90	9.20	4.70	2.10	0.60	0.90	1.10	0.90	0.70	1.00	1.20	0.60	0.20	0.20	0.20	0.30	0.20	0.20
% ZnO	0.10	0.10	0.10	0.10	0.10	0.10	0.10	0.10	0.10	0.10	0.10	0.10	0.10	0.10	0.10	0.10	0.10	0.10	0.10	0.10	0.10
% PbO	0.10	0.10	0.10	0.10	0.10	0.10	0.10	0.10	0.10	0.10	0.10	0.10	0.10	0.10	0.10	0.10	0.10	0.10	0.10	0.10	0.10
% CdO	0.10	0.10	0.10	0.10	0.10	0.10	0.10	0.10	0.10	0.10	0.10	0.10	0.10	0.10	0.10	0.10	0.10	0.10	0.10	0.10	0.10
% P205	0.50	<0.2	<0.2	<0.2	0.20	0.50	0.90	<0.2	<0.2	0.40	<0.2	<0.2	<0.2	<0.2	<0.2	<0.2	<0.2	<0.2	<0.2	<0.20	<0.2
% K20	<0.2	<0.2	<0.2	<0.2	<0.2	<0.2	<0.2	<0.2	<0.2	<0.2	<0.2	<0.2	<0.2	<0.2	<0.2	<0.2	<0.2	<0.2	<0.2	<0.20	<0.2
B.H. DUST WEIGHT, t	0.28	0.09	0.03	0.08	0.32	0.17	0.18	0.12	0.02	0.09	0.01	0.02	1.57	0.24	0.08	0.10	0.15	0.14	0.16	0.24	0.27
B.H. DUST ANALYSIS																					
% CaO	0.60	0.70	nd	0.40	0.60	0.50	0.50	0.50	0.60	0.50	nd	nd	0.50	0.60	0.70	1.60	1.40	1.30	1.20	1.00	2.20
% SiO2	1.10	0.80	nd	0.40	2.70	1.20	1.50	1.00	2.70	1.30	nd	nd	1.00	1.10	1.00	4.70	3.10	3.40	3.80	3.70	2.80
% MgO	0.50	0.80	nd	0.40	1.40	0.80	1.10	0.80	1.30	0.80	nd	nd	0.80	0.60	0.80	5.10	2.80	3.50	2.60	2.20	2.20
% Al2O3	0.30	0.50	nd	<0.2	<0.2	<0.2	<0.2	<0.2	<0.2	<0.2	nd	nd	<0.2	<0.2	<0.2	0.30	0.30	0.20	0.30	0.20	0.20
% MnO	0.60	1.00	nd	1.00	1.70	1.10	1.20	1.00	1.60	1.10	nd	nd	0.80	0.70	0.70	2.00	1.40	1.60	1.60	1.40	1.40
% Fe2O3	5.90	8.30	nd	2.50	3.00	3.00	3.40	3.20	3.60	3.40	nd	nd	3.60	4.10	3.90	4.60	5.30	4.80	4.40	3.80	7.20
% Cr2O3	0.30	0.30	nd	0.20	0.20	0.20	0.20	0.20	0.20	0.20	nd	nd	0.20	0.20	0.20	0.20	0.20	0.20	0.20	0.20	0.60
% ZnO	51.40	53.00	nd	71.00	66.50	68.00	68.00	70.00	64.50	66.00	nd	nd	68.80	67.70	68.90	59.60	62.00	62.20	57.10	59.10	53.30
% PbO	7.20	7.00	nd	8.80	8.20	8.40	8.10	8.20	7.70	8.10	nd	nd	8.50	9.20	8.70	7.70	7.90	8.00	9.20	9.90	9.20
% CdO	nd	nd	nd	nd	nd	nd	nd	nd	nd	nd	nd	nd	nd	1.00	nd	nd	nd	nd	nd	0.90	nd
% P205	<0.2	<0.2	nd	<0.2	<0.2	<0.2	<0.2	<0.2	<0.2	<0.2	nd	nd	<0.2	<0.2	<0.2	<0.2	<0.2	<0.2	<0.2	<0.20	<0.2
% Cl	nd	nd	nd	nd	nd	nd	nd	5.35	nd	nd	nd	nd	nd	5.10	nd	nd	nd	nd	nd	6.57	nd
% F	nd	nd	nd	nd	nd	nd	nd	0.22	nd	nd	nd	nd	nd	0.31	nd	nd	nd	nd	nd	0.18	nd
% Na20	nd	nd	nd	nd	nd	nd	nd	2.45	nd	nd	nd	nd	nd	2.30	nd	nd	nd	nd	nd	3.05	nd
% K20	2.20	2.00	nd	2.50	2.40	2.40	2.40	2.50	2.20	2.20	nd	nd	2.40	2.40	2.30	2.10	2.00	2.10	3.00	3.40	52.10

TABLE 17 EAF DUST SMELTING PRODUCT ANALYSES

TAP No	D/22	D/23	D/24	D/25	D/26	D/27	D/28	D/29	D/30	D/31	D/32	D/33	D/34	D/35	D/36	D/37	D/38	D/39	D/40	D/41	D/42	D/43	D/44	D/45	D/46	D/47	D/48
DUST SOURCE	TEMPL	TEMPL	TEMPL	TEMPL	TEMPL	TEMPL	TEMPL	TEMPL	TEMPL	TEMPL	TEMPL	TEMPL	TEMPL	TEMPL	TREM	TREM	TREM	TREM	TREM	IRISH	IRISH	IRISH	IRISH	IRISH	IRISH	IRISH	IRISH
DUST FORM	DUST	DUST	DUST	DUST	DUST	DUST	DUST	DUST	DUST	DUST	DUST	DUST	DUST	DUST	DUST	DUST	DUST	DUST	DUST	PELLET	PELLET	PELLET	PELLET	PELLET	PELLET	PELLET	PELLET
FEED BLEND																											
% COAL ADDITION	10.50	10.50	10.50	15.00	15.00	20.00	20.00	20.00	25.00	25.00	25.00	25.00	10.00	10.00	10.00	10.00	15.00	20.00	25.00	14.00	14.00	14.00	22.00	18.00	18.00	22.00	22.00
% SAND ADDITION	3.00	3.00	3.00	3.00	3.00	3.00	3.00	3.00	3.00	3.00	3.00	3.00	3.00	3.00	3.00	3.00	3.00	3.00	3.00	3.00	3.00	3.00	3.00	3.00	3.00	3.00	3.00
DUST WEIGHT,t	0.80	0.40	0.40	0.80	0.80	0.80	0.80	0.80	0.80	0.40	0.40	0.80	0.80	0.80	0.80	0.80	0.80	0.40	0.80	0.40	0.80	0.40	0.80	0.40	0.80	0.80	0.80
METAL WEIGHT, t	0.00	0.00	0.00	0.34	0.31	0.90	0.30	0.53	0.00	0.40	0.36	0.39	0.30	0.00	0.00	0.00	0.00	0.16	0.43	0.27	0.27	0.08	0.00	0.12	0.16	0.03	0.08
METAL ANALYSIS																											
% Si				nd	nd	<0.20	nd	nd		nd	1.54	nd	nd					nd	<0.20	nd	nd	nd		nd	<0.20	nd	nd
% Mn				nd	nd	0.39	nd	nd		nd	0.97	nd	nd					nd	0.39	nd	nd	nd		nd	0.24	nd	nd
% Fe				nd	nd	97.57	nd	nd		nd	96.00	nd	nd					nd	97.32	nd	nd	nd		nd	97.00	nd	nd
% Cr				nd	nd	0.17	nd	nd		nd	0.40	nd	nd					nd	0.16	nd	nd	nd		nd	0.22	nd	nd
% C				nd	nd	0.53	nd	nd		nd	1.54	nd	nd					nd	0.68	nd	nd	nd		nd	0.40	nd	nd
% S				nd	nd	0.44	nd	nd		nd	0.26	nd	nd					nd	0.37	nd	nd	nd		nd	0.73	nd	nd
% P				nd	nd	0.08	nd	nd		nd	0.18	nd	nd					nd	0.13	nd	nd	nd		nd	0.18	nd	nd
% Cu				nd	nd	0.69	nd	nd		nd	0.54	nd	nd					nd	0.82	nd	nd	nd		nd	1.01	nd	nd
							nd	nd																			
SLAG WEIGHT,t	0.15	0.17	0.33	0.27	0.27	0.10	0.18	0.06	0.24	0.06	0.16	0.15	0.00	0.39	0.36	0.42	0.27	0.17	0.16	0.12	0.15	0.10	0.14	0.15	0.11	0.22	0.18
SLAG ANALYSIS																											
% CaO	13.20	11.80	11.20	13.30	15.40	23.20	19.40	25.20	23.90	22.30	23.00	24.90		16.10	13.80	12.10	11.30	13.40	23.90	27.00	27.30	24.30	21.20	27.80	24.20	25.50	23.20
% SiO2	19.10	14.50	13.20	15.10	17.20	27.20	23.40	28.20	26.00	24.60	26.50	27.00		17.50	16.70	15.50	14.50	17.80	30.00	28.90	27.90	26.00	22.60	28.80	24.80	26.40	25.00
% MgO	10.60	7.70	6.20	7.60	7.50	14.10	9.70	13.50	18.00	17.00	17.60	13.50		8.50	6.70	5.70	6.50	7.80	14.50	11.90	12.10	15.30	15.20	15.40	18.70	22.20	15.00
% Al2O3	1.90	1.60	1.50	2.00	2.50	7.10	4.20	4.70	8.40	11.20	5.90	4.90		3.20	2.80	2.60	4.30	4.40	6.60	6.50	5.70	5.40	4.80	6.20	6.60	7.30	5.70
% MnO	15.50	12.70	11.10	12.40	14.00	20.10	18.80	22.10	18.50	18.40	21.00	22.10		16.80	13.60	11.70	11.00	13.30	20.10	19.50	14.70	12.20	9.60	11.40	11.00	10.30	10.20
% Fe2O3	38.00	51.20	58.50	50.80	43.60	6.20	23.60	4.10	3.00	4.80	5.10	5.10		37.00	46.60	53.90	53.80	44.20	3.80	3.80	8.90	15.30	24.00	8.20	11.20	5.60	18.80
% Cr2O3	2.00	1.40	1.00	1.20	1.10	0.60	0.90	0.50	0.40	0.50	0.60	0.50		1.30	0.90	0.70	0.70	0.80	0.40	0.80	0.90	1.00	1.00	0.60	1.20	0.90	1.60
% ZnO	<0.20	<0.20	0.40	0.30	<0.20	<0.20	<0.20	<0.20	<0.20	<0.20	<0.20	<0.20		0.40	0.80	1.00	1.10	0.30	0.20	0.20	0.30	0.20	0.30	0.20	0.20	0.20	0.40
% PbO	<0.20	<0.20	0.02	<0.20	0.02	<0.20	<0.20	0.01	<0.20	<0.20	0.01	<0.20		<0.20	0.20	0.20	0.20	0.20	0.20	0.20	0.20	0.20	0.20	0.20	0.20	0.20	0.20
% CdO	<0.20	<0.20	<0.002	<0.20	<0.002	<0.20	<0.20	<0.002	<0.20	<0.20	<0.002	<0.20		<0.20	0.20	0.20	0.20	0.20	0.20	0.20	0.20	0.20	0.20	0.20	0.20	0.20	0.20
% P2O5	1.50	1.00	0.80	0.70	0.70	<0.20	0.90	<0.20	<0.20	<0.20	<0.20	<0.20		0.80	0.80	0.80	0.70	0.90	<0.20	0.40	0.80	0.70	1.10	0.70	0.70	0.30	0.90
% K2O	<0.20	<0.20	0.20	<0.20	<0.20	<0.20	<0.20	<0.20	<0.20	<0.20	<0.20	<0.20		<0.20	<0.20	<0.20	<0.20	<0.20	<0.20	<0.20	<0.20	<0.20	<0.20	<0.20	<0.20	<0.20	<0.20
% F	nd	nd	nd	nd	nd	nd	nd	nd	nd	nd	nd	nd		nd	0.14	nd	nd	nd	0.12	nd	nd	nd	nd	nd	nd	nd	nd
B.H. DUST WEIGHT, t	0.00	0.00	0.00	0.24	0.08	0.18	0.08	0.19	0.11	0.11	0.11	0.10	0.11	0.01	0.16	0.17	0.35	0.15	0.23	0.16	0.19	0.20	0.60	0.12	0.27	0.20	0.21
B.H. DUST ANALYSIS																											
% CaO				0.30	0.20	0.20	0.20	0.20	0.50	0.40	0.30	0.30	0.20		0.20	0.20	0.20	0.20	0.20	0.20	0.20	0.20	0.30	0.20	0.30	0.30	0.20
% SiO2				0.60	0.40	0.40	0.40	0.40	1.00	0.60	0.50	0.50	0.40		0.20	0.20	0.40	0.30	0.20	0.20	0.20	0.20	0.30	0.30	0.40	0.30	0.20
% MgO				0.20	0.20	0.20	0.20	0.30	0.90	0.50	0.50	0.20	0.20		0.20	<0.20	<0.20	<0.20	<0.20	<0.20	<0.20	<0.20	0.20	<0.20	0.60	0.30	0.30
% Al2O3				0.20	0.20	0.20	0.20	0.20	0.20	0.20	0.20	0.20	<0.20		<0.20	<0.20	<0.20	<0.20	<0.20	<0.20	<0.20	<0.20	<0.20	<0.20	<0.20	<0.20	0.20
% MnO				1.40	0.70	0.90	0.90	0.90	2.50	2.60	2.30	2.30	1.50		0.30	0.40	1.10	0.40	0.70	0.60	0.50	0.50	0.50	0.40	0.70	0.60	2.40
% Fe2O3				3.10	3.50	3.70	3.60	3.60	6.20	6.20	6.20	4.80	6.30		1.70	2.00	3.00	1.80	1.50	1.60	1.80	2.30	2.50	2.30	2.20	2.20	2.00
% Cr2O3				<0.20	<0.20	<0.20	<0.20	<0.20	<0.20	<0.20	<0.20	<0.20	<0.20		<0.20	<0.20	<0.20	<0.20	<0.20	<0.20	<0.20	<0.20	<0.20	<0.20	<0.20	<0.20	<0.20
% ZnO				66.10	68.90	68.20	69.80	69.50	61.00	62.40	62.60	65.70	65.20		71.20	70.50	67.50	73.80	73.90	71.90	69.70	68.40	67.90	67.60	66.20	66.30	67.50
% PbO				10.30	10.20	9.80	9.50	9.60	9.60	9.10	9.90	9.30	9.70		9.60	9.90	9.80	8.40	8.50	9.70	10.20	10.70	10.60	10.90	11.20	11.10	11.50
% CdO				nd	nd	nd	nd	0.10	nd	nd	nd	nd	0.10		nd	nd	nd	nd	nd	nd	nd	nd	nd	nd	nd	nd	nd
% P2O5				0.20	<0.20	<0.20	<0.20	<0.20	<0.20	<0.20	<0.20	<0.20	<0.20		<0.20	<0.20	<0.20	<0.20	<0.20	<0.20	<0.20	<0.20	<0.20	<0.20	<0.20	<0.20	<0.20
% Cl				nd	nd	nd	nd	nd	nd	nd	nd	nd	nd		nd	nd	nd	nd	nd	nd	nd	nd	nd	nd	nd	nd	nd
% F				nd	nd	nd	nd	nd	nd	nd	nd	nd	nd		nd	nd	nd	nd	nd	nd	nd	nd	nd	nd	nd	nd	nd
% K2O				5.90	5.70	5.70	5.70	5.70	5.60	5.70	5.10	5.70	5.80		4.20	4.30	5.00	3.20	3.00	3.70	4.20	4.60	4.50	4.40	4.40	4.40	4.40

TABLE 18 EXTRACTION PROCEDURE TOXICITY TEST (EP Tox Test)

TAP No	D/24	D/25	D/26	D/27	D/28	D/32	D/37	D/41	D/43	D/46
DUST ANALYSIS										
% ZnO	13.80	13.80	13.80	13.80	13.80	35.00	32.10	32.10	32.10	32.10
% Fe_2O_3	60.00	60.00	60.00	60.00	60.00	33.30	29.50	29.50	29.50	29.50
% Cr_2O_3	0.30	0.30	0.30	0.30	0.30	0.20	0.20	0.20	0.20	0.20
% PbO	2.10	2.10	2.10	2.10	2.10	4.00	2.10	2.10	2.10	2.10
% CdO	0.02	0.02	0.02	0.02	0.02	0.10	0.10	0.10	0.10	0.10
SLAG ANALYSES										
% ZnO	0.40	0.30	<0.2	0.20	0.20	0.20	1.00	0.20	0.20	0.20
% Fe_2O_3	58.50	50.80	43.60	6.20	23.60	5.10	53.90	3.80	15.30	11.20
% Cr_2O_3	1.00	1.20	1.10	0.60	0.90	0.60	0.70	0.80	1.00	1.20
% PbO	0.02	<0.20	<0.20	<0.20	<0.20	<0.20	<0.20	<0.20	<0.20	<0.20
% CdO	0.00	<0.01	<0.01	<0.01	<0.01	<0.01	<0.01	<0.01	<0.01	<0.01
EPTT LEACHATE										
Pb, ppm	<0.10	<0.10	<0.10	<0.10	<0.10	<0.10	<0.10	<0.10	<0.10	<0.10
Cd, ppm	<0.02	<0.02	<0.02	<0.02	<0.02	<0.02	<0.02	<0.02	<0.02	<0.02
Cr, ppm	<0.02	1.00	0.06	0.13	0.19	<0.05	<0.05	<0.05	<0.05	<0.05
LEACHATE LIMIT										
Pb, ppm	0.30									
Cd, ppm	0.06									
Cr, ppm	0.30									

TABLE 19 DISTRIBUTION OF OXIDES BETWEEN THE CONDENSED PHASES

TRIAL A CHROMITE

OXIDE	METAL	SLAG	CYCLONE	BAGHOUSE	TOTAL
	%	%	%	%	%
SiO2	10.00	81.80		6.80	98.60
MgO	0.00	121.80		16.54	138.34
Fe2O3	111.80	5.93		1.17	118.90
Cr2O3	89.20	8.36		0.52	98.08

TRIAL B AOD DUST

OXIDE	METAL	SLAG	CYCLONE	BAGHOUSE	TOTAL
	%	%	%	%	%
SiO2	8.50	44.70		10.42	63.62
CaO	0.00	58.61		12.24	70.85
Fe2O3	90.70	1.13		4.16	95.99
Cr2O3	84.80	4.50		2.56	91.86
MoO3	86.00	ND		ND	86.00
NiO	94.00	ND		ND	94.00
ZnO	0.00	0.00		86.29	86.29
PbO	0.00	0.00		45.92	45.92

TRIAL C SHEERNESS AND IRISH STEEEL DUST

OXIDE	METAL	SLAG	CYCLONE	BAGHOUSE	TOTAL
	%	%	%	%	%
SiO2	3.29	78.15	0.79	6.97	89.20
CaO	0.00	62.30	0.50	4.76	67.56
Fe2O3	59.30	4.18	0.90	4.95	69.33
Cr2O3	77.47	232.89	4.74	37.61	352.71
ZnO	0.00	0.10	9.17	89.43	98.70
PbO	0.00	0.10	17.26	204.82	222.18

TRIAL D TEMPLEBOROUGH, TREMORFA AND IRISH STEEL DUSTS

OXIDE	METAL	SLAG	CYCLONE	BAGHOUSE	TOTAL
	%	%	%	%	%
SiO2	0.20	90.68	0.78	1.68	93.34
CaO	0.00	87.52	1.00	1.27	89.79
Fe2O3	87.05	18.14	1.22	1.67	108.08
Cr2O3	41.29	102.16	3.23	20.99	167.67
ZnO	0.00	0.50	10.47	79.14	90.11
PbO	0.00	1.55	5.93	73.70	81.18

TABLE 20 AOD DUST SMELTING OPERATIONAL RESULTS

TAP No	B/1	B/2	B/3	B/4	B/5	B/6	B/7	B/8	B/9	B/10
DUST SOURCE	AOD	AOD	AOD	AOD	AOD	AOD	AOD	AOD	AOD	AOD
DUST FORM	DUST	DUST	DUST	DUST	DUST	DUST	DUST	PELLETS	PELLETS	PELLETS
FEED BLEND										
% COAL ADDITION	28.00	28.00	28.00	28.00	28.00	28.00	28.00	28.00	28.00	28.00
% SAND ADDITION	0.00	0.00	0.00	0.00	0.00	0.00	0.00	0.00	0.00	0.00
TAP TEMPERATURE, K	1783	1773	1773	1783	1793	1793	1873	1843	1923	1833
TAP TO TAP TIME, hrs	5.50	3.10	4.00	2.66	4.25	3.36	9.50	3.15	3.30	5.00
FEED ON TIME, hrs	5.00	3.00	3.50	2.06	1.65	3.36	5.35	3.05	2.55	3.25
PLASMA ON TIME, hrs	5.50	3.10	4.00	2.50	2.75	3.36	5.50	3.15	3.30	4.00
ENERGY CONSUMED, MWh	2.99	2.22	2.82	1.95	1.57	2.24	1.50	1.08	1.85	2.65
MASS FED, t	1.70	1.30	1.80	1.20	0.75	1.00	0.15	1.00	0.77	1.50
FURNACE LOSSES, MW	0.23	0.23	0.23	0.23	0.23	0.23	0.23	0.23	0.23	0.23
DUST FEED RATE, t/hr	0.24	0.34	0.34	0.34	0.14	0.27	0.02	0.56	0.18	0.20
POWER INPUT, MW	0.54	0.72	0.71	0.73	0.37	0.67	0.30	0.80	0.56	0.53
GROSS ENERGY, MWh/t	2.24	2.09	2.05	2.16	2.62	2.51	10.00	1.44	3.08	2.64
NETT ENERGY, MWh/t	1.30	1.42	1.38	1.48	0.99	1.64	2.30	1.03	1.82	1.50
FEED AVAILABLITY, %	90.91	96.77	87.50	77.44	38.82	100.00	56.32	96.83	77.27	65.00
PLASMA AVAILABLITY, %	100.00	100.00	100.00	93.98	64.71	100.00	57.89	100.00	100.00	80.00

TABLE 21 EAF DUST SMELTING OPERATIONAL RESULTS

TAP No	C/1	C/2	C/3	C/4	C/5	C/6	C/7	C/8	C/9	C/10	C/11	C/12	C/13	C/14	C/15	C/16	C/17	C/18	C/19	C/20	C/21
DUST SOURCE	SHEER	SHEER	SHEER	SHEER	SHEER	SHEER	SHEER	SHEER	SHEER	SHEER	SHEER	SHEER	SHEER	SHEER	SHEER	SHEER	IRISH	IRISH	IRISH	IRISH	IRISH
DUST FORM	PELLET	PELLET	PELLET	PELLET	PELLET	PELLET	PELLET	PELLET	PELLET	PELLET	PELLET	DUST	DUST	DUST	DUST	DUST	PELLET	PELLET	PELLET	PELLET	PELLET
FEED BLEND																					
% COAL ADDITION	21.00	21.00	21.00	21.00	21.50	21.50	21.50	21.50	21.50	20.00	17.50	12.50	21.50	21.50	22.50	23.70	25.00	23.75	23.75	25.60	26.25
% SAND ADDITION	4.00	4.00	4.00	4.00	7.50	7.50	7.50	10.50	10.00	10.00	10.00	10.00	10.00	10.00	5.00	10.00	10.00	7.50	7.50	7.50	7.50
TAP TEMPERATURE, K	1763	1885	1853	1823	1805	1779	1723	1743	1863	1761	1893	1843	1803	1813	1868	1947	1833	1883	1838	1730	1750
TAP TO TAP TIME, hrs	5.00	7.70	5.66	9.70	5.60	6.73	4.16	4.16	5.00	5.63	4.20	6.82	3.40	5.93	3.53	7.43	3.04	3.41	2.11	3.36	3.88
FEED ON TIME, hrs	4.20	3.80	2.80	3.90	4.20	4.50	3.10	3.00	3.00	3.70	3.20	3.30	1.90	2.60	2.80	3.10	1.50	2.90	1.60	1.90	1.00
PLASMA ON TIME, hrs	4.80	5.50	5.30	7.50	5.50	5.40	3.50	3.80	3.90	4.50	3.70	6.00	3.20	5.70	3.35	6.20	2.70	3.40	2.11	2.46	3.00
ENERGY CONSUMED, MWh	3.00	3.51	2.47	4.22	2.56	2.94	2.08	2.33	2.45	2.56	2.35	3.48	1.49	2.40	2.17	3.40	1.65	1.85	1.46	1.80	1.98
DUST FED, t	1.20	1.20	0.80	1.20	1.20	1.20	0.80	0.80	0.80	0.80	0.80	0.80	0.40	0.80	0.80	0.80	0.80	0.80	0.80	0.80	0.40
FURNACE LOSSES, MW	0.23	0.23	0.23	0.23	0.23	0.23	0.23	0.23	0.23	0.23	0.23	0.23	0.23	0.23	0.23	0.23	0.23	0.23	0.23	0.23	0.23
DUST FEED RATE, t/hr	0.24	0.16	0.14	0.12	0.21	0.18	0.19	0.19	0.16	0.14	0.19	0.12	0.12	0.13	0.23	0.11	0.26	0.12	0.38	0.24	0.10
POWER INPUT, MW	0.60	0.46	0.44	0.44	0.46	0.44	0.50	0.56	0.49	0.45	0.56	0.51	0.44	0.40	0.61	0.46	0.54	0.54	0.69	0.54	0.51
GROSS ENERGY, MWh/t	2.50	2.92	3.09	3.52	2.13	2.45	2.60	2.91	3.06	3.20	2.94	4.35	3.73	3.00	2.71	4.25	2.06	4.62	1.82	2.25	4.95
NETT ENERGY, MWh/t	1.54	1.45	1.46	1.66	1.06	1.16	1.40	1.72	1.63	1.58	1.73	2.39	1.77	1.30	1.70	2.11	1.19	2.66	1.22	1.28	2.72
FEED AVAILABLITY, %	84.00	49.35	49.47	40.21	75.00	66.86	74.52	72.12	60.00	65.72	76.19	48.39	55.88	43.84	79.32	41.72	49.34	85.04	75.83	56.55	25.77
PLASMA AVAILABLITY,	96.00	71.43	93.64	77.32	98.21	80.24	84.13	91.35	78.00	79.93	88.10	87.98	94.12	96.12	94.90	83.45	88.82	99.71	100.00	73.21	77.32

TABLE 22 EAF DUST SMELTING OPERATIONAL RESULTS

TAP No	D/22	D/23	D/24	D/25	D/26	D/27	D/28	D/29	D/30	D/31	D/32	D/33	D/34	D/35
DUST SOURCE	TEMPL	TEMPL	TEMPL	TEMPL	TEMPL	TEMPL	TEMPL	TEMPL	TEMPL	TEMPL	TEMPL	TEMPL	TEMPL	TEMPL
DUST FORM	DUST	DUST	DUST	DUST	DUST	DUST	DUST	DUST	DUST	DUST	DUST	DUST	DUST	DUST
FEED BLEND														
% COAL ADDITION	10.50	10.50	10.50	15.00	15.00	20.00	20.00	20.00	25.00	25.00	25.00	25.00	10.00	10.00
% SAND ADDITION	3.00	3.00	3.00	3.00	3.00	3.00	3.00	3.00	3.00	3.00	3.00	3.00	3.00	3.00
TAP TEMPERATURE, k	1773	1793	1773	1743.00	1723	1773	1773	1791	1793	1822	1743	1753	1748	1793
TAP TO TAP TIME,hrs	5.80	4.67	5.33	3.50	2.67	2.50	3.00	2.83	6.75	1.67	3.75	2.67	2.33	7.10
FEED ON TIME, hrs	3.90	3.00	4.10	2.80	2.50	2.10	2.30	2.83	5.90	1.30	2.70	2.47	2.13	2.90
PLASMA ON TIME, hrs	4.90	3.00	4.10	2.80	2.50	2.50	3.00	2.83	6.65	1.57	2.70	2.47	2.13	4.40
ENERGY CONSUMED, MWh	2.40	1.63	1.96	2.20	1.84	1.18	2.02	2.14	3.04	0.86	2.19	1.93	1.55	2.74
DUST FED, t	0.80	0.40	0.40	0.80	0.80	0.80	0.80	0.80	0.80	0.40	0.40	0.80	0.80	0.80
FURNACE LOSSES, MW	0.27	0.27	0.27	0.27	0.26	0.25	0.24	0.24	0.22	0.25	0.26	0.25	0.22	0.20
DUST FEED RATE, t/hr	0.00	0.00	0.00	0.23	0.00	0.00	0.00	0.00	0.00	0.00	0.00	0.00	0.00	0.00
POWER INPUT, MW	0.41	0.35	0.37	0.63	0.69	0.47	0.67	0.76	0.45	0.51	0.58	0.72	0.67	0.39
GROSS ENERGY, MWh/t	3.00	4.07	4.90	2.75	2.30	1.48	2.52	2.67	3.80	2.15	5.48	2.41	1.94	3.42
NETT ENERGY, MWh/t	1.08	0.98	1.37	1.59	1.43	0.69	1.61	1.83	1.94	1.11	3.04	1.58	1.30	1.65
FEED AVAILABLITY, %	67.24	64.24	76.92	80.00	93.63	84.00	76.67	100.00	87.41	77.84	72.00	92.51	91.42	40.85
PLASMA AVAILABLITY, %	84.48	64.24	76.92	80.00	93.63	100.00	100.00	100.00	98.52	94.01	72.00	92.51	91.42	61.97

TAP No	D/36	D/37	D/38	D/39	D/40	D/41	D/42	D/43	D/44	D/45	D/46	D/47	D/48
DUST SOURCE	TREM	TREM	TREM	TREM	TREM	IRISH	IRISH	IRISH	IRISH	IRISH	IRISH	IRISH	IRISH
DUST FORM	DUST	DUST	DUST	DUST	DUST	PELLET	PELLET	PELLET	PELLET	PELLET	PELLET	PELLET	PELLET
FEED BLEND													
% COAL ADDITION	10.00	10.00	15.00	20.00	25.00	14.00	14.00	14.00	22.00	18.00	18.00	22.00	22.00
% SAND ADDITION	3.00	3.00	3.00	3.00	3.00	3.00	3.00	3.00	3.00	3.00	3.00	3.00	3.00
TAP TEMPERATURE, k	1743	1773	1773	1743	1723	1773	1743	1883	1783	1703	1823	1753	1753
TAP TO TAP TIME,hrs	4.50	7.17	2.10	2.00	2.00	2.10	4.90	2.20	3.10	2.80	3.30	4.00	1.80
FEED ON TIME, hrs	4.20	3.30	2.00	2.00	1.80	2.00	3.30	2.20	2.50	1.00	3.30	2.60	1.80
PLASMA ON TIME, hrs	4.00	4.80	2.10	2.00	1.80	2.10	3.60	2.20	2.50	2.10	3.30	3.50	1.80
ENERGY CONSUMED, MWh	1.99	2.07	1.26	1.63	1.75	1.61	2.54	1.61	1.90	1.40	2.42	2.35	1.34
DUST FED, t	0.80	0.80	0.80	0.40	0.80	0.40	0.80	0.40	0.80	0.40	0.80	0.80	0.80
FURNACE LOSSES, MW	0.23	0.23	0.23	0.23	0.23	0.22	0.22	0.20	0.23	0.23	0.20	0.20	0.20
DUST FEED RATE, t/hr	0.00	0.00	0.00	0.00	0.00	0.00	0.00	0.00	0.00	0.00	0.00	0.00	0.00
POWER INPUT, MW	0.44	0.29	0.60	0.81	0.87	0.77	0.52	0.73	0.61	0.50	0.73	0.59	0.74
GROSS ENERGY, MWh/t	2.49	2.59	1.57	4.07	2.19	4.03	3.18	4.02	2.37	3.49	3.02	2.94	1.67
NETT ENERGY, MWh/t	1.19	0.53	0.97	2.92	1.61	2.88	1.83	2.92	1.48	1.88	2.19	1.94	1.22
FEED AVAILABLITY, %	93.33	46.03	95.24	100.00	90.00	95.24	67.35	100.00	80.65	35.71	100.00	65.00	100.00
PLASMA AVAILABLITY, %	88.89	66.95	100.00	100.00	90.00	100.00	73.47	100.00	80.65	75.00	100.00	87.50	100.00

TABLE 23 FERROCHROME PRODUCTION COSTS IN PLASMA PROCESSES

SPECIFICATION	UNIT		
Material		Chromite	Chromite
Furnace type		Plasma	Plasma
Location		UK	UK
Power	MW	2.00	20.00
Energy Consumption	MWh/t chromite	2.06	2.00
Capacity	t/h chromite	0.97	10.00
Scheduled time	h/y	8760.00	8760.00
Availablity	%	90.00	90.00
Operating time	h/y	7884.00	7884.00
Processing rate	t chromite/y	7654.37	78840.00
Processing rate	t chromite/h	0.87	9.00
Labour	Men	15.00	50.00
Labour cost	£/y	15000.00	15000.00
MATERIAL ANALYSIS			%
Cr2O3		53.00	53.00
Fe2O3		17.00	17.00
TOTAL CAPITAL COST	£m	2.50	15.00
ANNUAL CAPITAL COST	£/t chromite	326.61	190.26

OPERATING COSTS	UNIT	UNIT COST	QUANTITY		UNIT COST	QUANTITY	£/t ORE
Chromite	t	70.00	1.00	70.00	70.00	1.00	70.00
Agglomeration	t	0.00	1.00	0.00	0.00	1.00	0.00
Coke	t	70.00	0.00	0.00	70.00	0.08	5.60
Coal	t	50.00	0.30	15.00	50.00	0.30	15.00
Sand	t	5.00	0.11	0.55	5.00	0.11	0.55
Alumina	t	50.00	0.00	0.00	50.00	0.00	0.00
Electricity	MWh	26.00	2.06	53.56	26.00	2.00	52.00
Electrodes	£/MWh	2.00	2.06	4.12	2.00	2.06	4.12
Argon	m3	0.75	7.72	5.79	0.75	7.72	5.79
Refractories	£/t	4.20	1.00	4.20	1.50	1.00	1.50
Supplies	£/t	326.61	0.02	6.53	190.26	0.02	3.81
Direct labour	man h	7.69	3.82	29.39	7.69	1.24	9.51
Gas credit	£/t	0.00	0.00	0.00	0.00	1.00	0.00
TOTAL OPERATING COST				189.15			167.88
CAPITAL CHARGE/ROI	%	20.00	326.61	65.32	20.00	190.26	38.05
PROCESSING COST, £/t chromite				254.47			205.93
T chromium/t chromite				0.32			0.32
PROCESSING COST, £/t chromium				795.22			643.53

TABLE 24 AOD DUST TREATMENT COSTS IN THE PLASMA FURNACE.

SPECIFICATION	UNIT	
Material		AOD dust
Furnace type		Plasma
Location		UK
Power	MW	2.00
Energy consumption	MWh/t	1.80
Capacity	t/h	1.11
Scheduled time	h/y	8760.00
Availablity	%	90.00
Operating time	h/y	7884.00
Processing rate	t/y	8760.00
Processing rate	t/h	1.00
Labour	Men	15.00
Labour cost	£/y	15000.00

MATERIAL ANALYSIS	%
Cr2O3	15.60
NiO	3.50
MoO3	1.80
Fe2O3	41.80
ZnO	7.00

TOTAL CAPITAL COST	£M	2.00
ANNUAL CAPITAL COST	£/annual	228.31

OPERATING COSTS	UNIT	UNIT COST £	QUANTITY	£/t ORE
Fume	t	0.00	1.00	0.00
Coal	t	50.00	0.28	14.00
Coke	t	70.00	0.00	0.00
Sand	t	5.00	0.00	0.00
Electricity	MWh	26.00	1.84	47.84
Argon	m3	0.75	6.90	5.18
Plasma torch	£/h	2.00	0.90	1.80
Graphite electrode	£/t	-	0.00	0.00
Refractories	£/t	3.65	1.00	3.65
Supplies	£/t	228.31	0.02	4.57
Direct labour	man h	7.69	3.34	25.68
TOTAL OPERATING COST	£/t			102.72
SLAG DUMPING COST	t	10.00	0.50	5.00
CAPITAL CHARGE/ROI	%	20.00	228.31	45.66

CREDITS	UNIT	UNIT COST £	% RECOVERY	VALUE
Cr	t	720.00	84.80	65.17
Ni	t	9000.00	94.00	232.93
Mo	t	12000.00	86.00	123.84
Fe	t	70.00	97.00	19.87
Zn	t	500.00	0.00	0.00
Pb	t	250.00	0.00	0.00
ZnO	t	200.00	97.50	13.65
TOTAL CREDIT	£/t			455.46
TOTAL GAIN (COST)	£/t			302.08

TABLE 25 EAF DUST TREATMENT COSTS IN THE PLASMA FURNACE

SPECIFICATION	UNIT					
Material				EAF		EAF
Furnace type				Plasma		Plasma
Product				ZnO		Zn
Location				UK		UK
Power	MW			2.00		2.00
Energy consumption	MWh/t			1.40		1.60
Capacity	t/h			1.43		1.25
Scheduled time	h/y			8400.00		8400.00
Availablity	%			85.00		85.00
Operating time	h/y			7140.00		7140.00
Processing rate	t/y			10200.00		8925.00
Processing rate	t/h			1.21		1.06
Labour	Men			15.00		15.00
Labour cost	£/y			15000.00		15000.00
MATERIAL ANALYSIS				%		%
Fe2O3				30.00		30.00
ZnO				30.00		30.00
PbO				2.00		2.00
TOTAL CAPITAL COST	£m			2.00		2.00
ANNUAL CAPITAL COST	£/annual t			196.08		224.09
OPERATING COSTS	UNIT	UNIT COST £	QUANTITY	£/t ORE	QUANTITY	£/t ORE
Fume	t	0.00	1.00	0.00	1.00	0.00
Coal	t	50.00	0.13	6.50	0.25	12.50
Sand	t	10.00	0.00	0.00	0.00	0.00
Lime	t	40.00	0.00	0.00	0.00	0.00
Electricity	MWh	26.00	1.40	36.40	1.60	41.60
Argon	m3	7.50	0.52	3.94	0.60	4.50
Plasma torch	£/h	3.00	0.70	2.10	0.80	2.40
Graphite electrode	£/t		0.00	0.00	0.00	0.00
Refractories	£/t	3.14	1.00	3.14	1.00	3.14
Supplies	£/t	196.08	0.02	3.92	0.02	3.92
Direct labour	man h	7.69	2.87	22.06	3.28	25.21
TOTAL OPERATING COST		£/t		78.06		93.27
SLAG DUMPING COST	£/t	10.00	0.50	5.00	0.50	5.00
CAPITAL CHARGE/ROI	%	20.00	196.08	39.22	224.09	44.82
CREDITS	UNIT	UNIT COST £	% RECOVERY	VALUE	% RECOVERY	VALUE
Cr	t	720.00	0.00	0.00	0.00	0.00
Ni	t	9000.00	0.00	0.00	0.00	0.00
Mo	t	12000.00	0.00	0.00	0.00	0.00
Fe	t	50.00	0.00	0.00	95.00	9.98
Zn	t	500.00	0.00	0.00	80.00	96.30
Pb	t	300.00	0.00	0.00	80.00	4.46
ZnO	t	200.00	97.50	58.50	15.00	9.00
TOTAL CREDIT				58.50		119.73
TOTAL GAIN (COST)				-63.77		-23.36

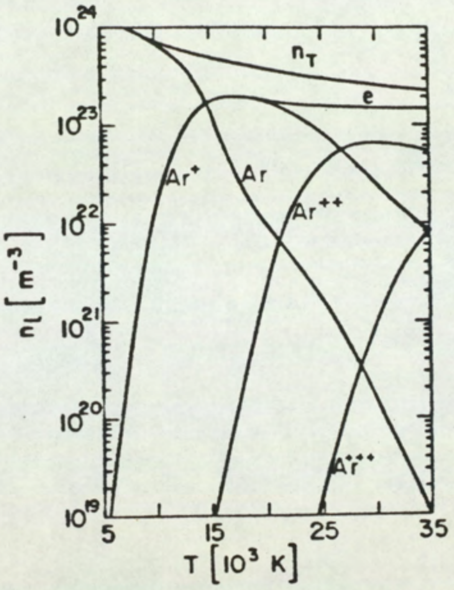

Figure 1 Composition of an argon plasma at atmospheric pressure as a function of temperature

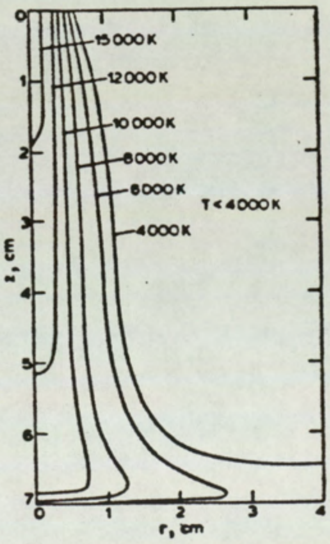

Figure 2 Computed temperature distribution in the plasma arc

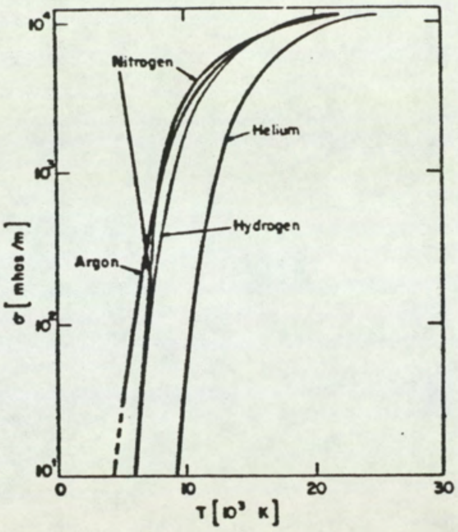

Figure 3 Electrical conductivity of plasma gases at atmospheric pressure as a function of temperature

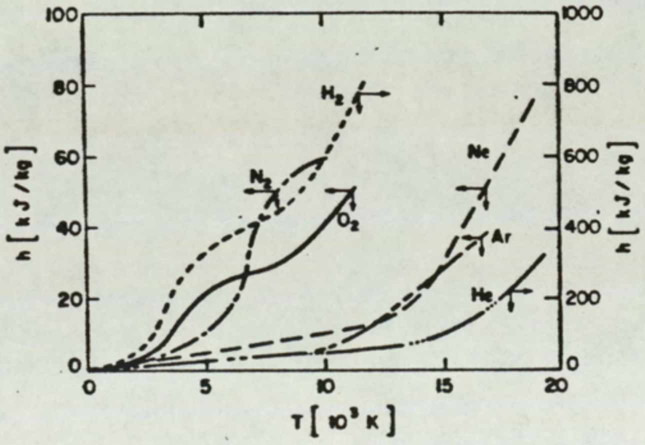

Figure 4 Specific enthalpy of plasma gases at atmospheric pressure as a function of temperature

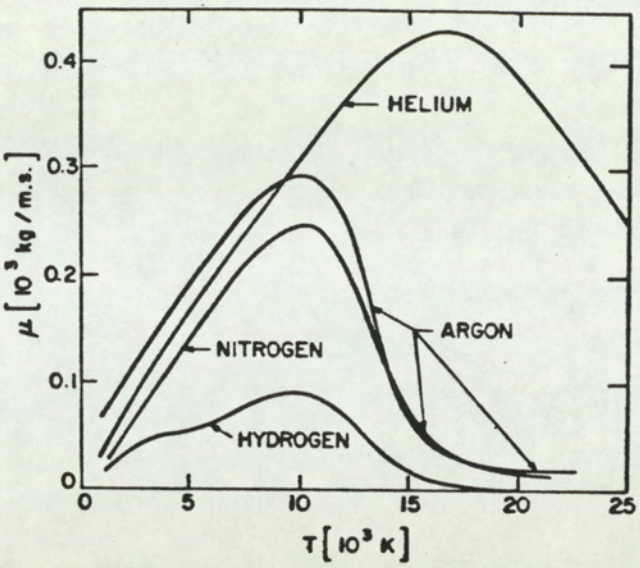

Figure 5 Viscosity of plasma gases at atmospheric pressure as a function of temperature

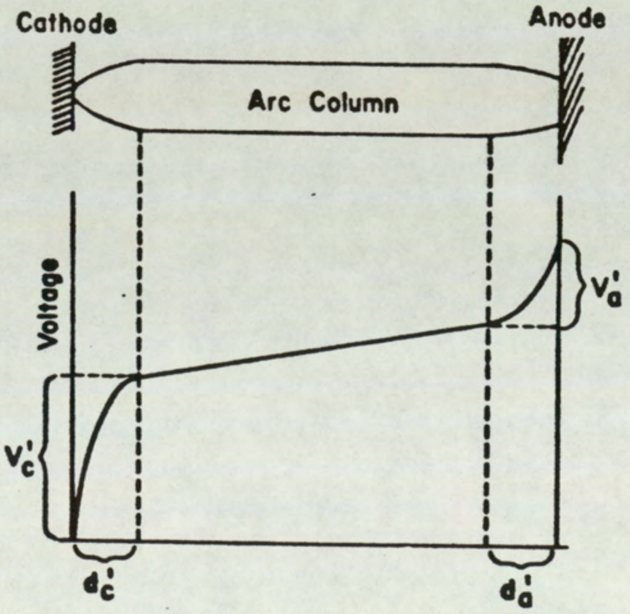

Figure 6 A typical potential distribution along a plasma arc

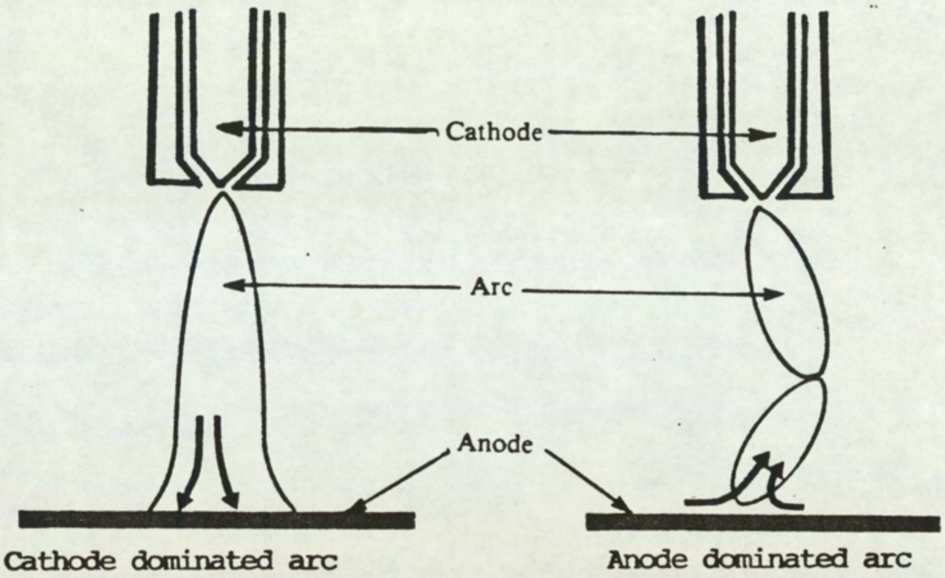

Figure 7 Cathode and anode dominated arcs

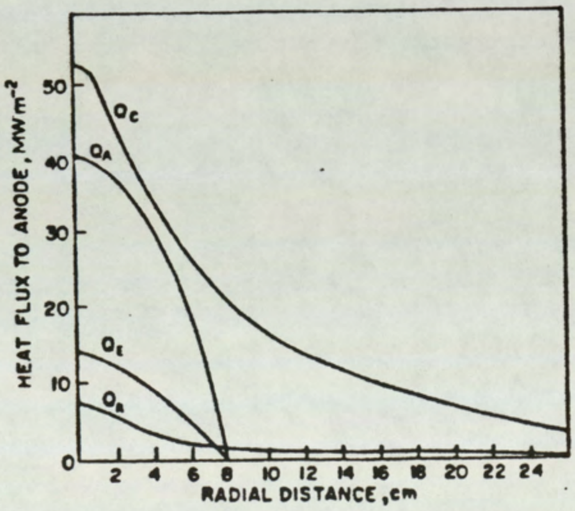

Figure 8 Heat distribution at the anode

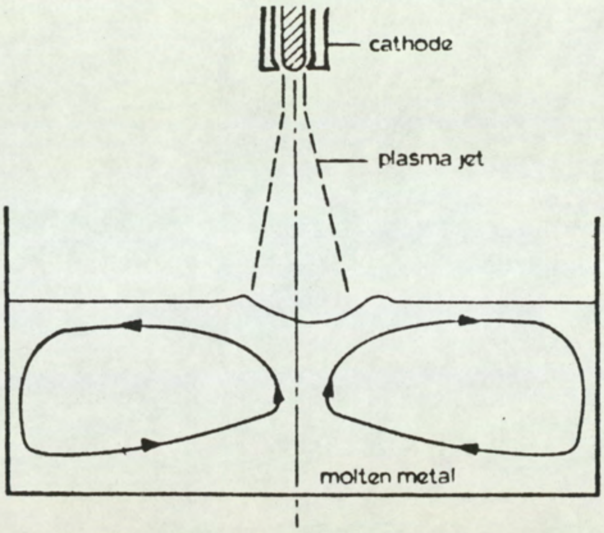

Figure 9 Circulation patterns from plasma arc momentum and thermal gradients

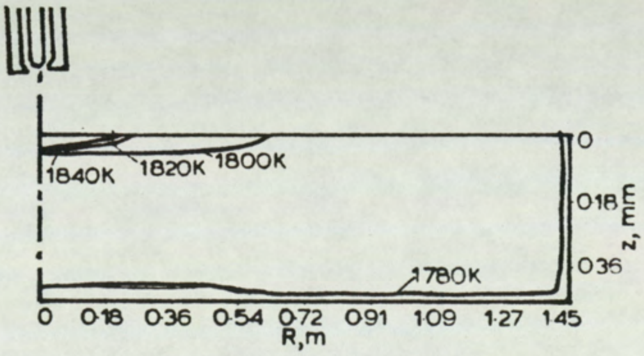

Figure 10 Calculated temperature distribution in a plasma heated steel melt

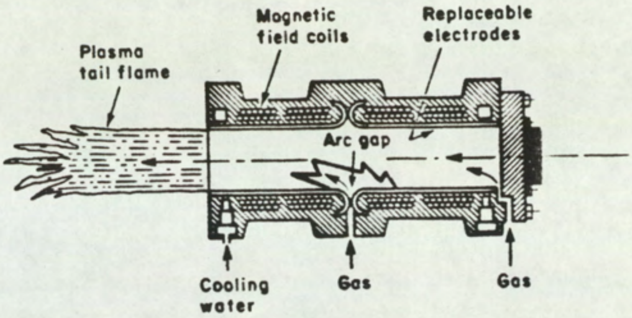

Westinghouse 1.5 MW AC plasma arc heater

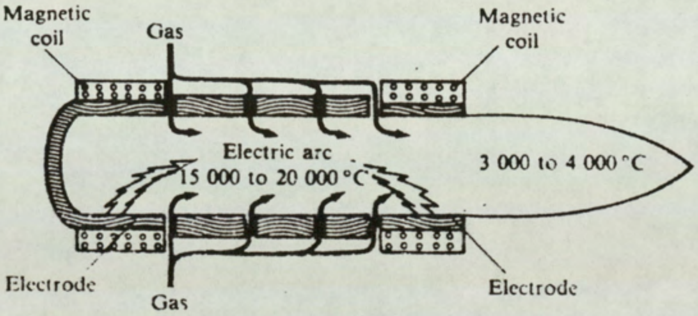

SKF 6 MW DC plasma arc heater

Figure 11 Non-transferred arc plasma torch designs

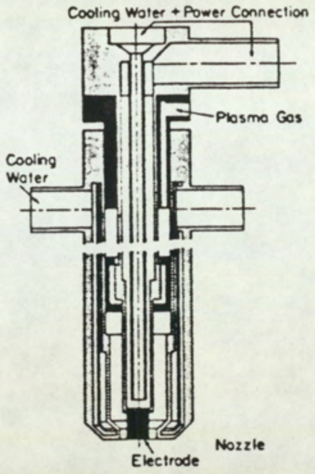

Krupp AC transferred arc plasma torch

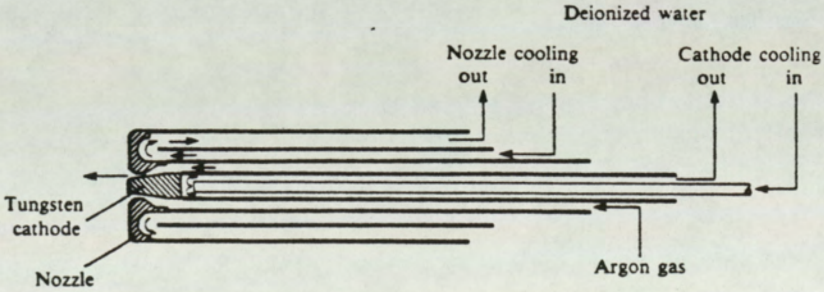

Tetronics DC transferred arc plasma torch

Figure 12 Transferred arc plasma torches

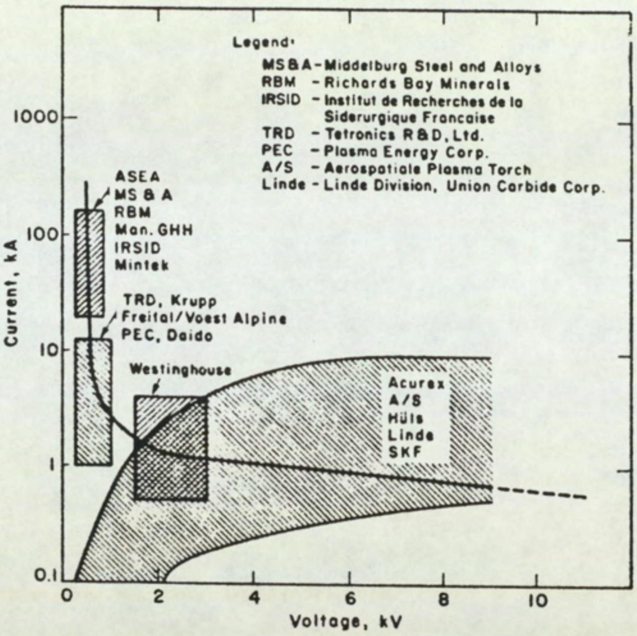

Figure 13 The relationship between current and voltage for various plasma devices

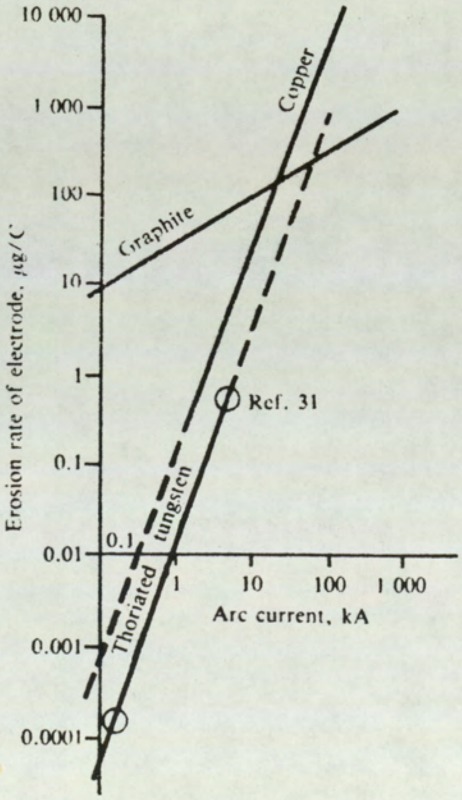

Figure 14 Electrode erosion as a function of arc current

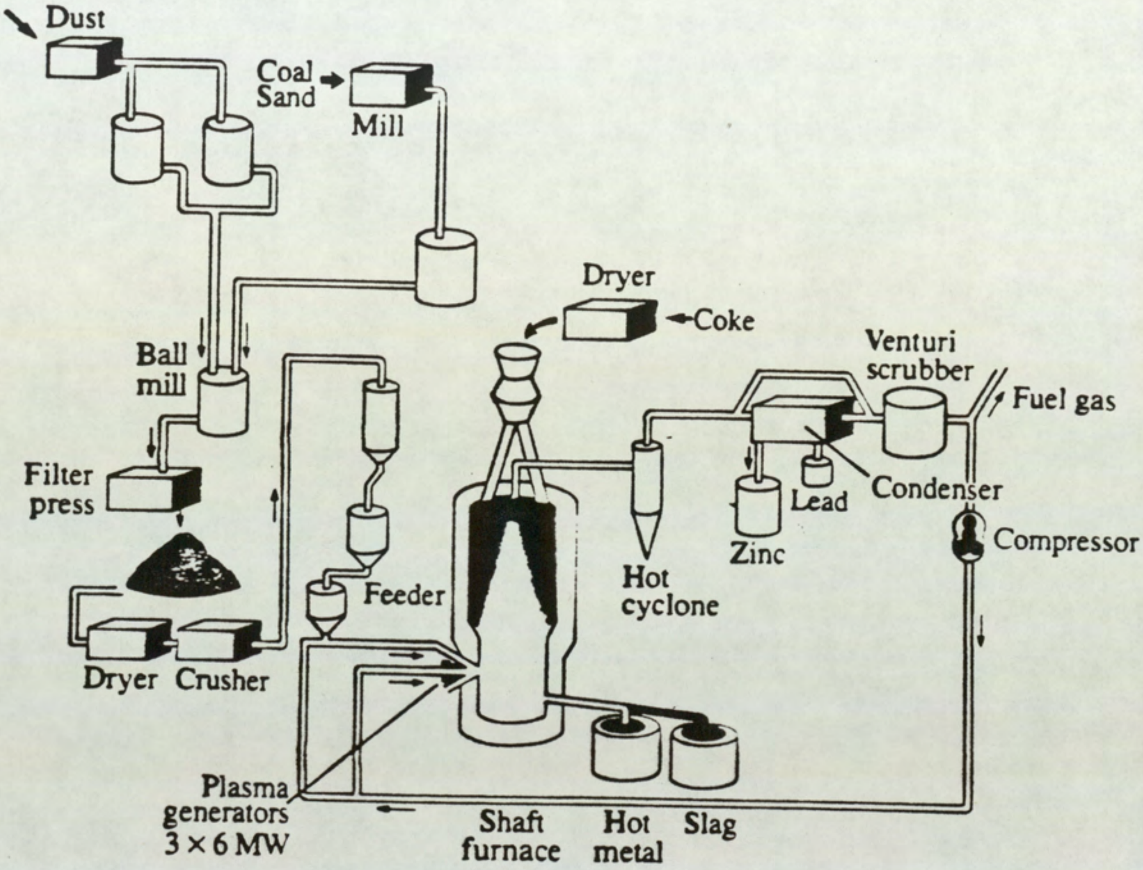

Figure 15 The SKF Scandust process flowsheet

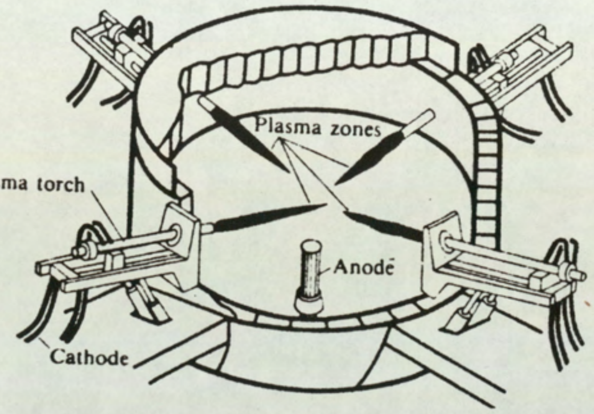

Figure 16 The Voest-Alpine scrap melting furnace

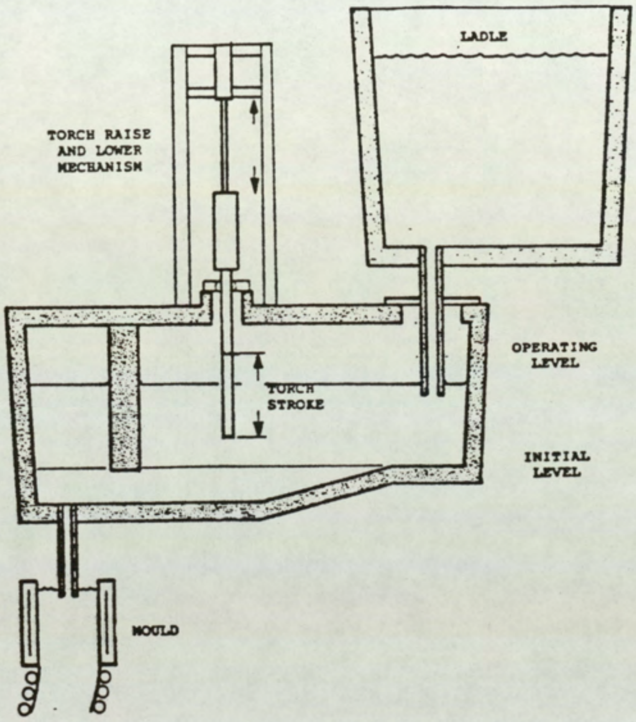

Figure 17 Plasma heating of the continuous caster tundish

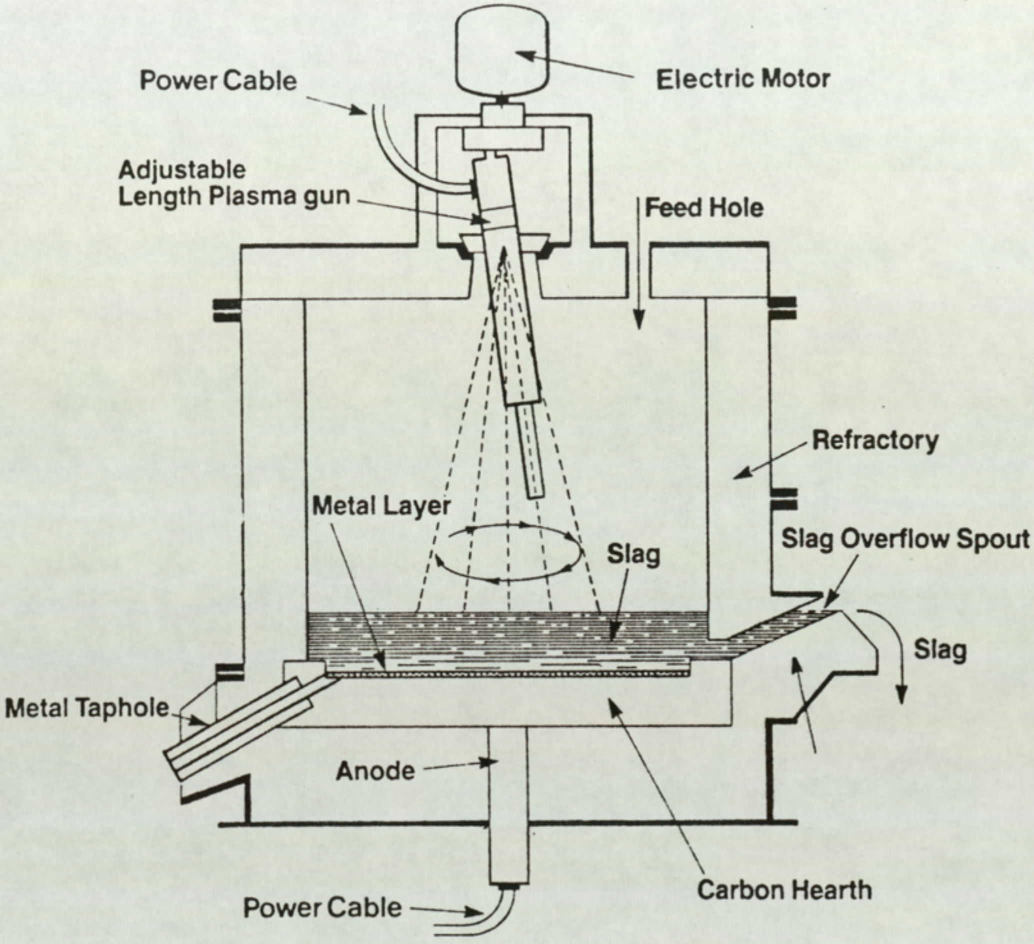

Figure 18 The Texasgulf plasma furnace for recovering platinum group metals from automobile catalysts

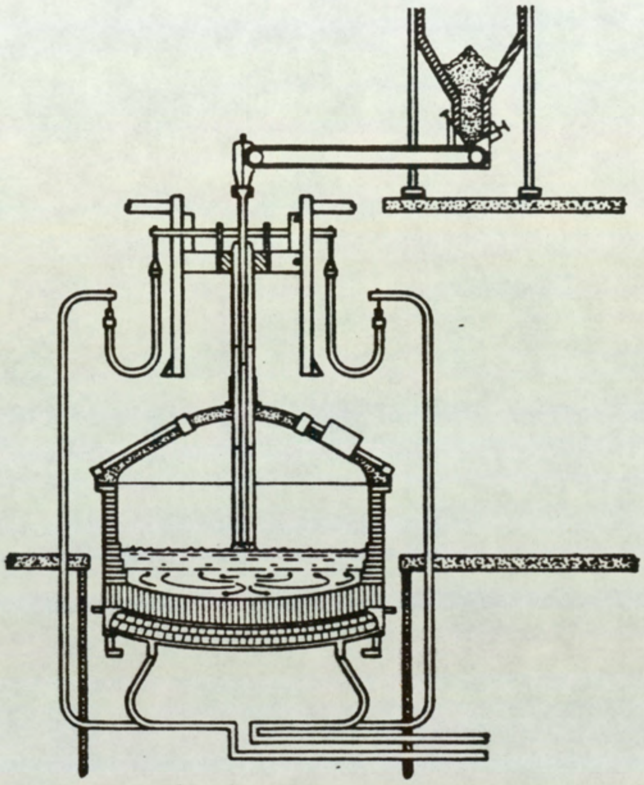

Figure 19 The MS&A DC furnace for the reduction of oxide fines

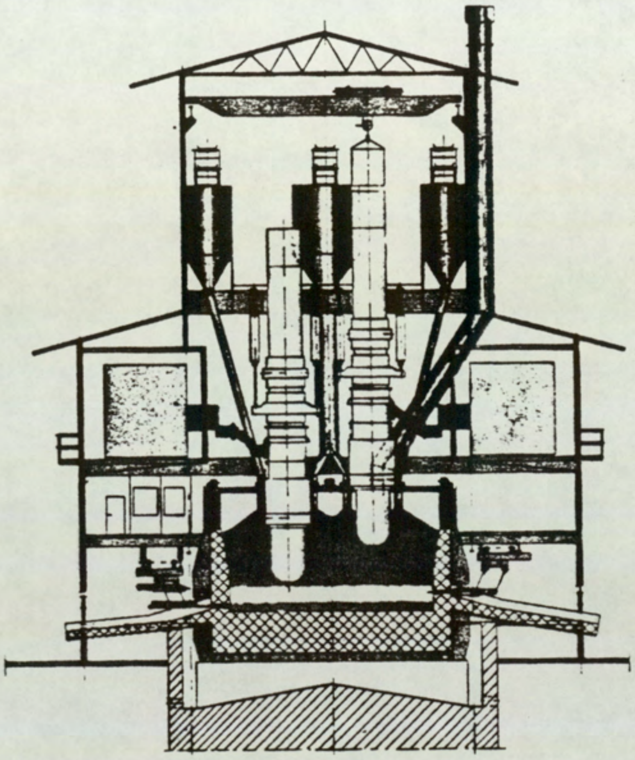

Figure 20 A submerged arc furnace for ferrochrome production

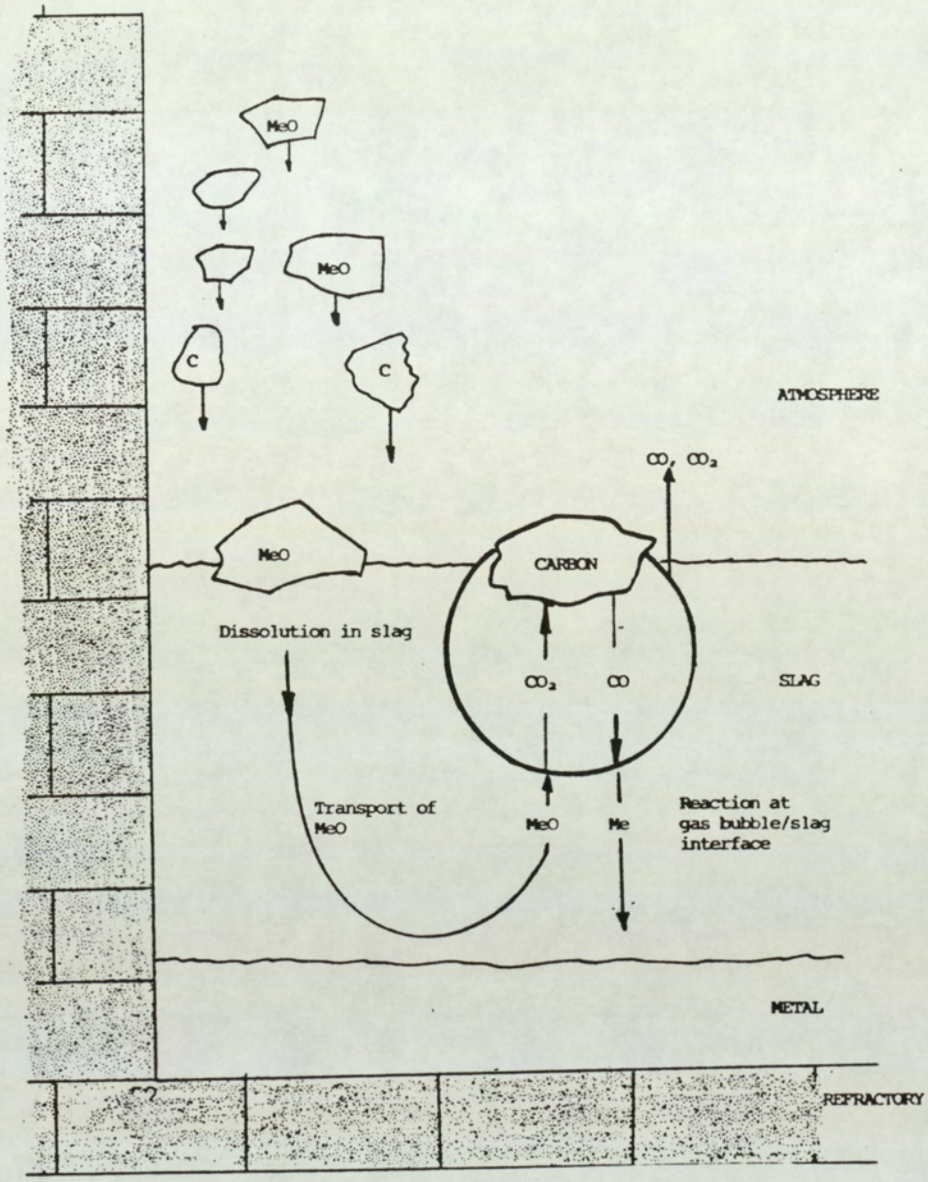

Figure 21 The reaction model

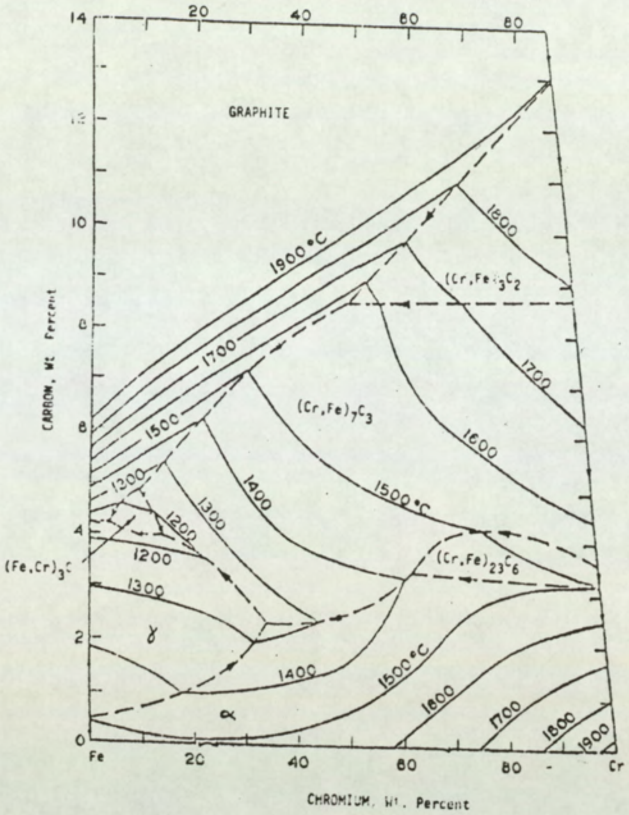

Figure 22 The Cr-Fe-C liquidus temperatures

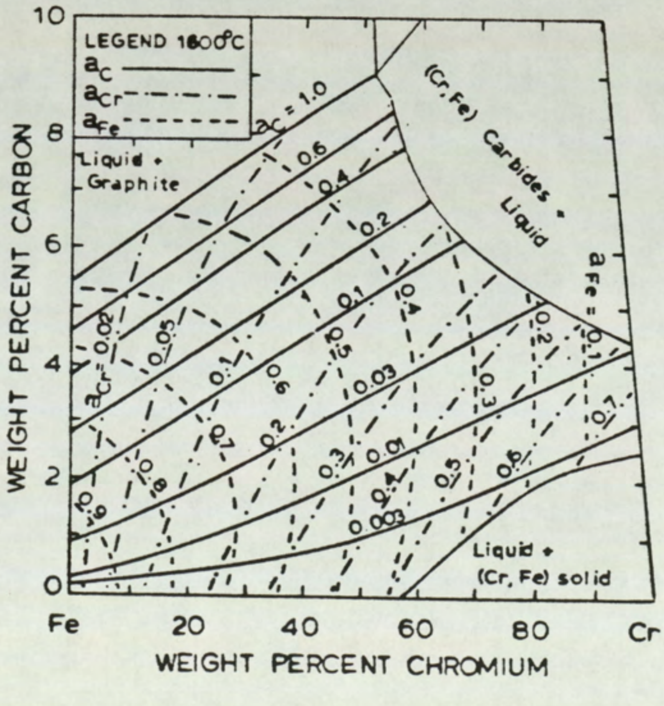

Figure 23 Activities in the Cr-Fe-C system at 1873K

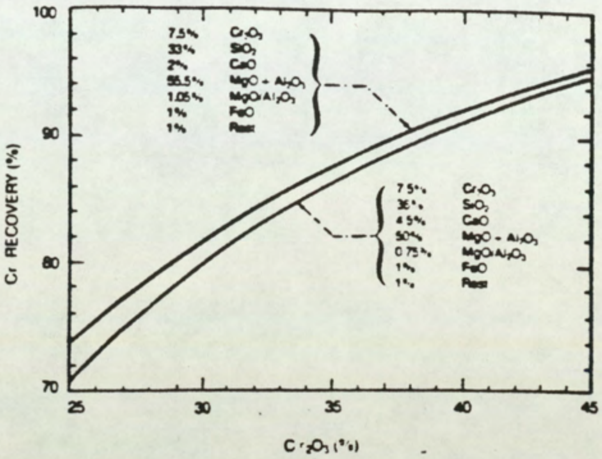

Figure 24 The effect of Cr_2O_3 content in the chromite on Cr recovery for two different MgO/Al_2O_3 ratios

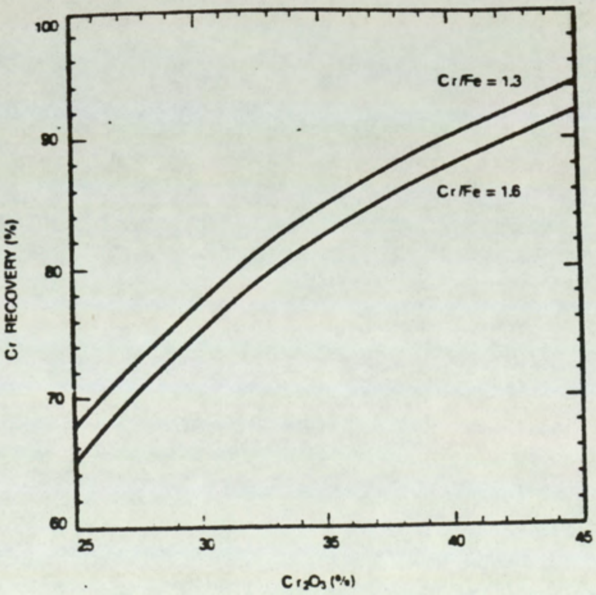

Figure 25 The effect of Cr_2O_3 content in the chromite on Cr recovery for two different Cr/Fe ratios

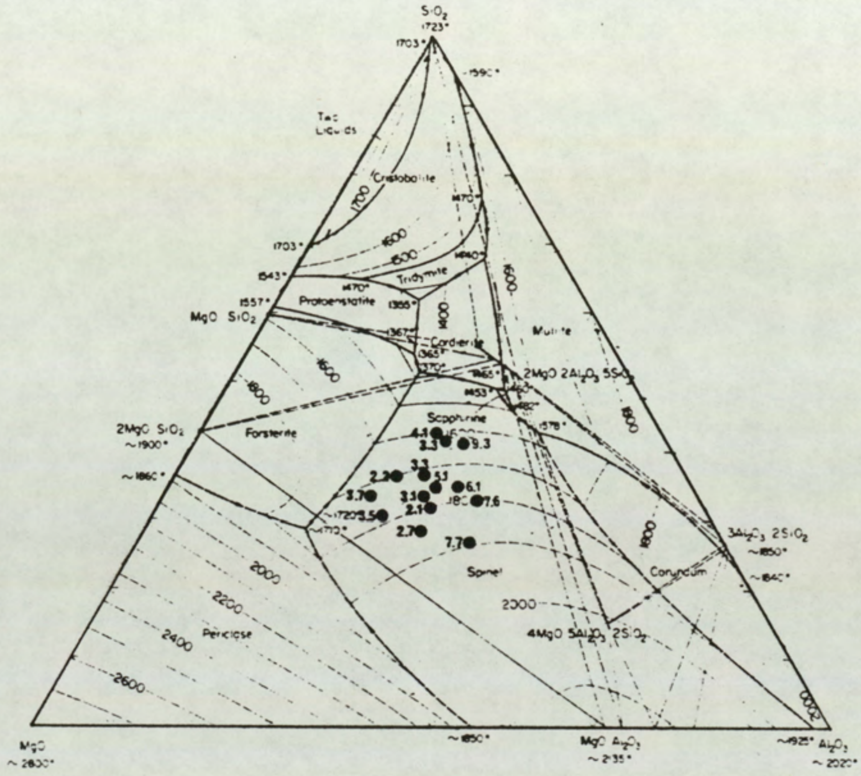

Figure 26 Liquidus temperatures in the system SiO_2-MgO-Al_2O_3

Values next to data points are the Cr_2O_3 content of the slag.

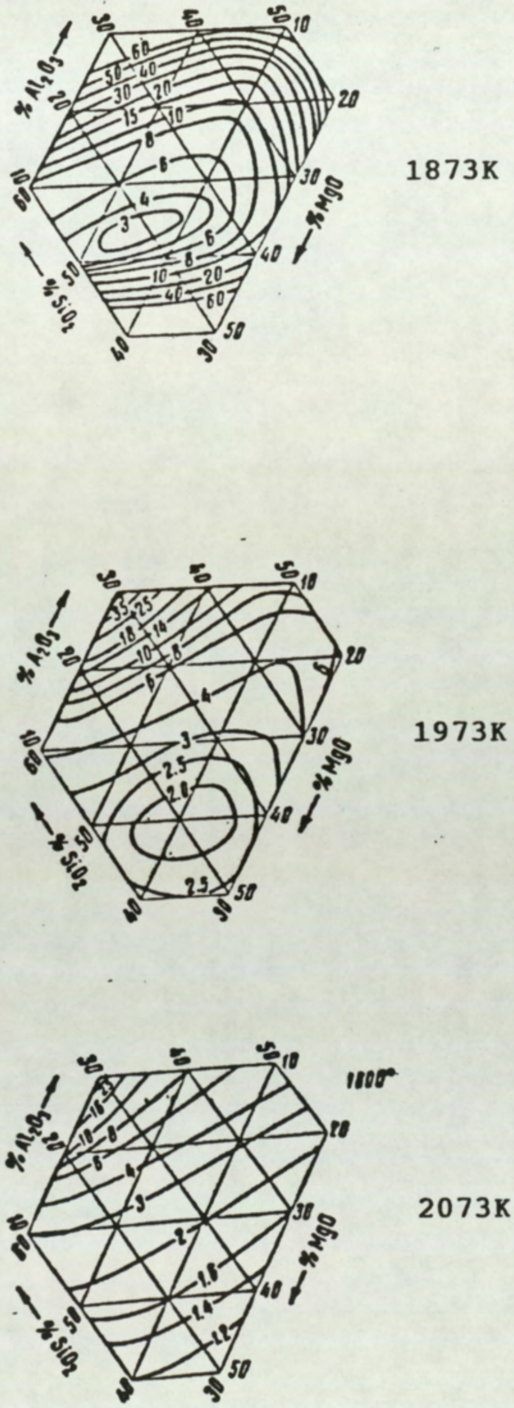

Figure 27 Viscosity (poise) in the system MgO - SiO_2 - Al_2O_3

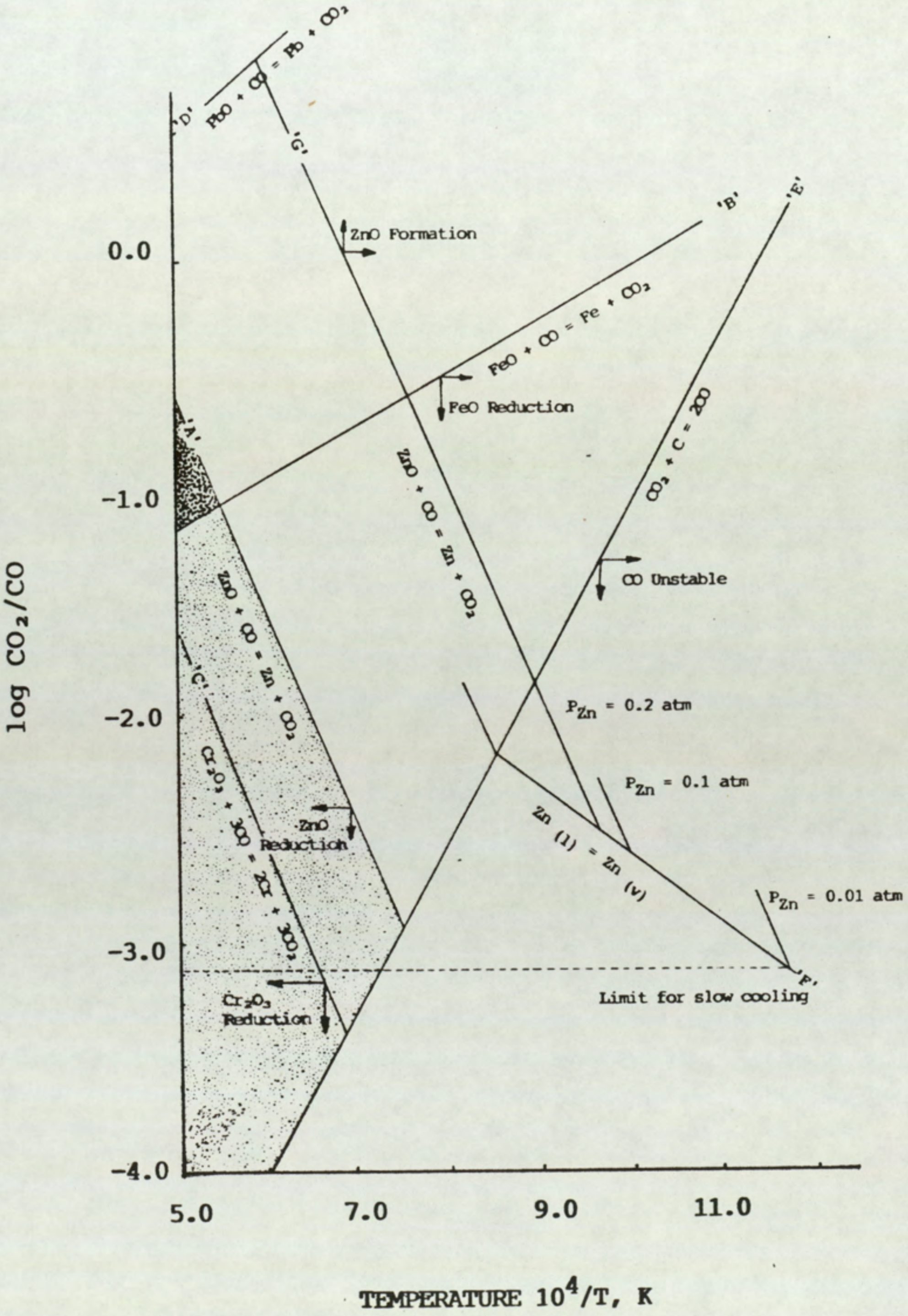

Figure 28 The ZnO – Zn – CO – CO_2 equilibrium diagram

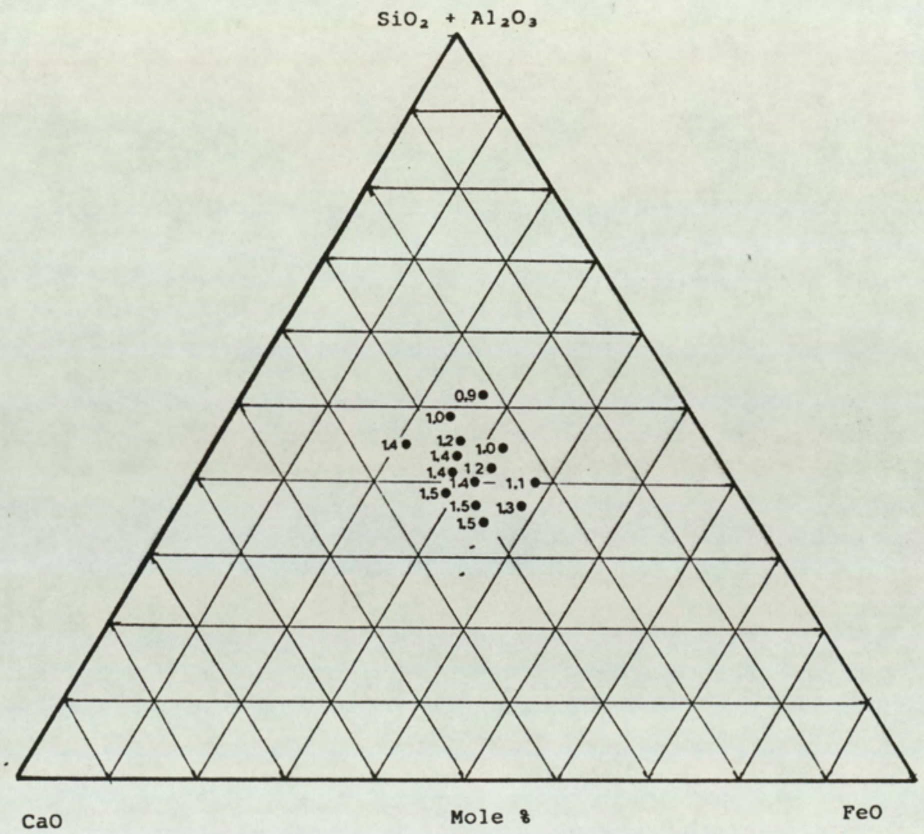

Figure 29a The ZnO activity coeficient in the system $CaO-SiO_2-Al_2O_3-FeO-ZnO$ at 1523K. After Filipovska and Bell

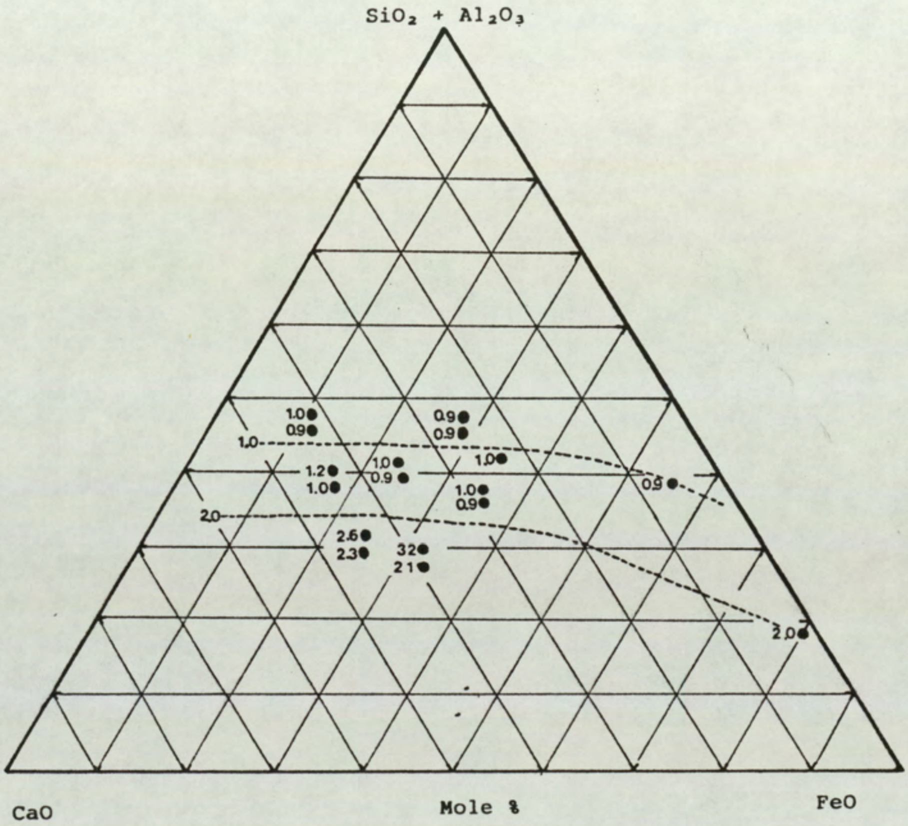

Figure 29b The ZnO activity coefficient in the system $CaO-SiO_2-Al_2O_3-FeO-ZnO$ at 1573K. After Levin et al.

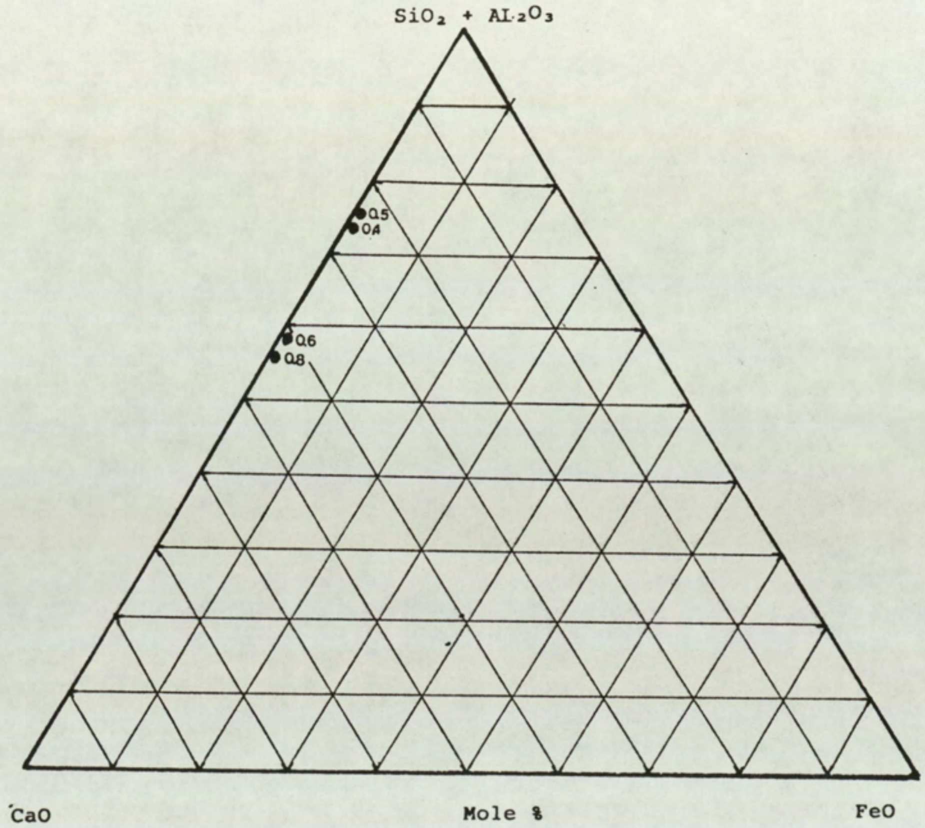

Figure 29c The ZnO activity coefficient in the system $CaO-SiO_2-Al_2O_3-FeO-ZnO$ at 1823K. After Reyes and Gaskell

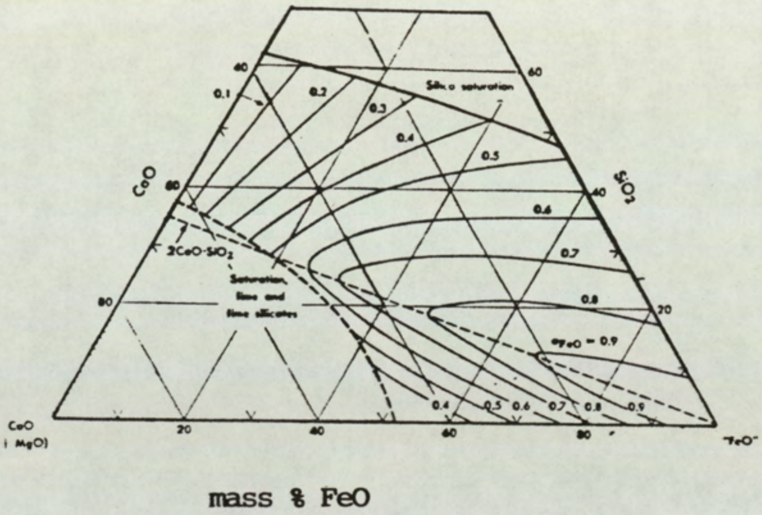

Figure 30 Activity of FeO in the system $FeO-SiO_2-CaO$ at 1873K

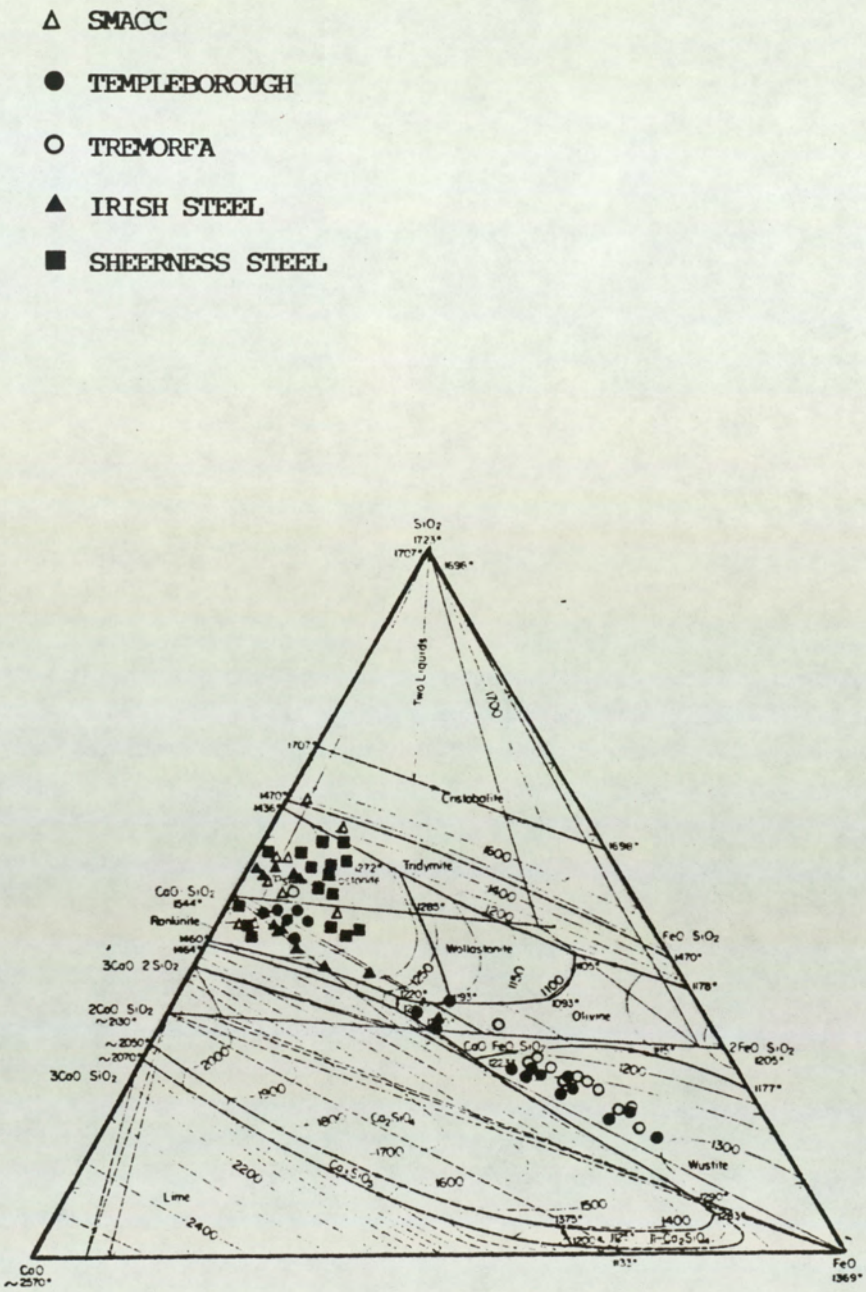

Figure 31 Liquidus temperature in the system SiO_2-CaO-FeO

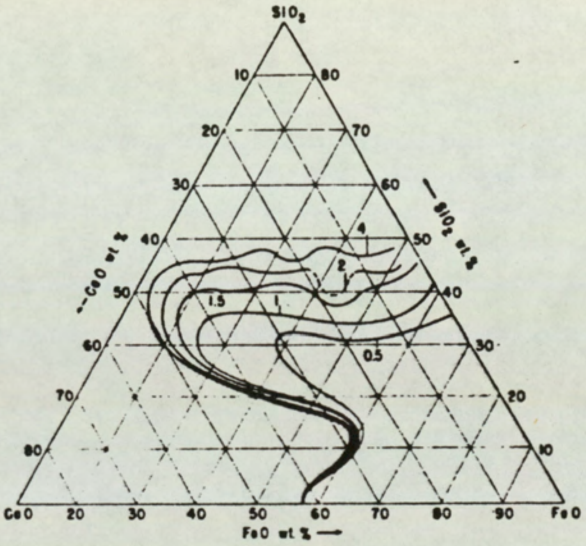

Figure 32 Viscosities in the system FeO-SiO$_2$-CaO at at 10% Al$_2$O$_3$ and 1673K

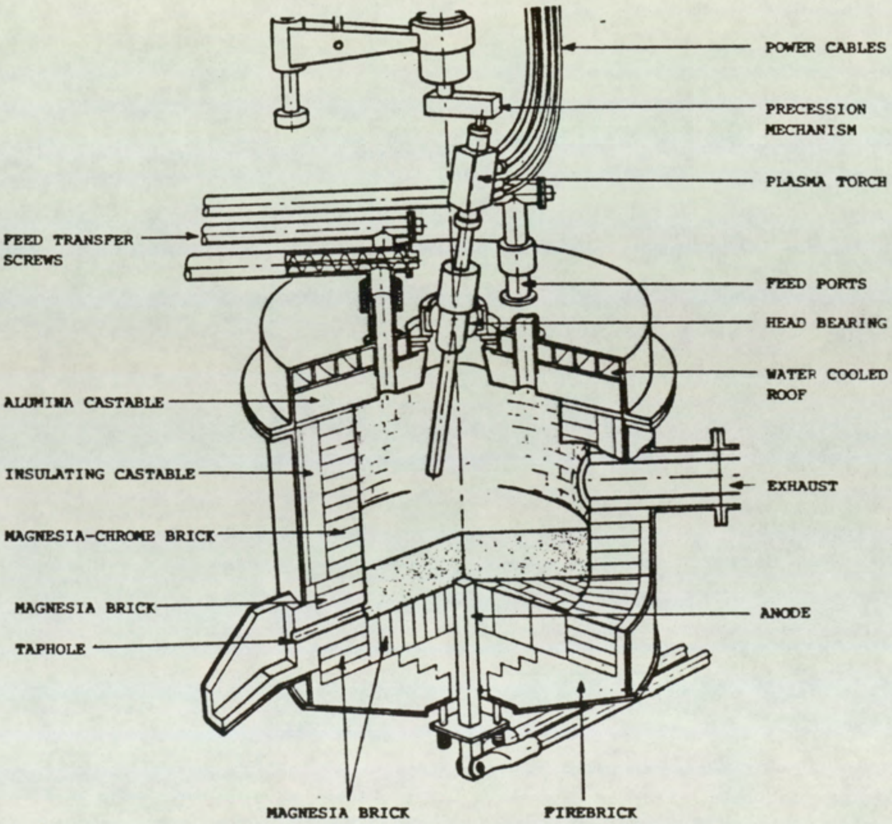

Figure 33 The Plasma Furnace Arrangement

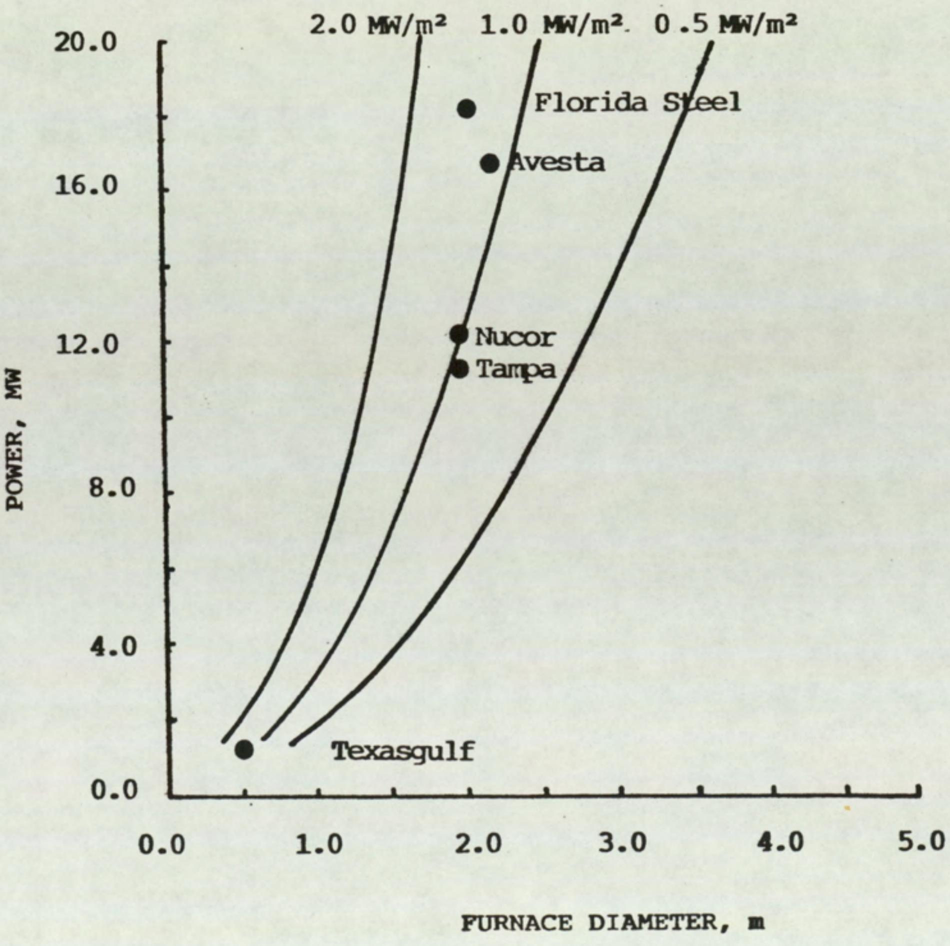

Figure 34 Furnace radius v power input, showing commercial DC furnaces

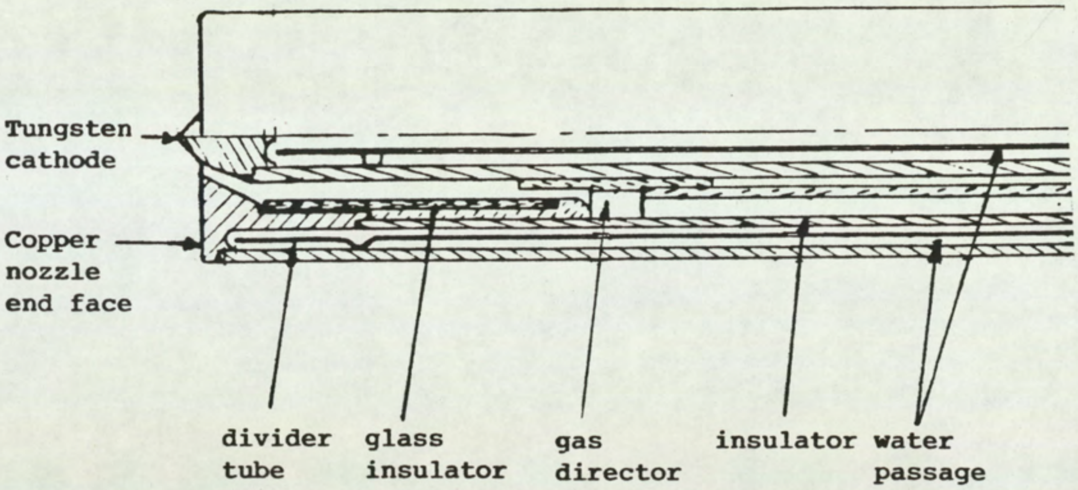

1984 TORCH DESIGN

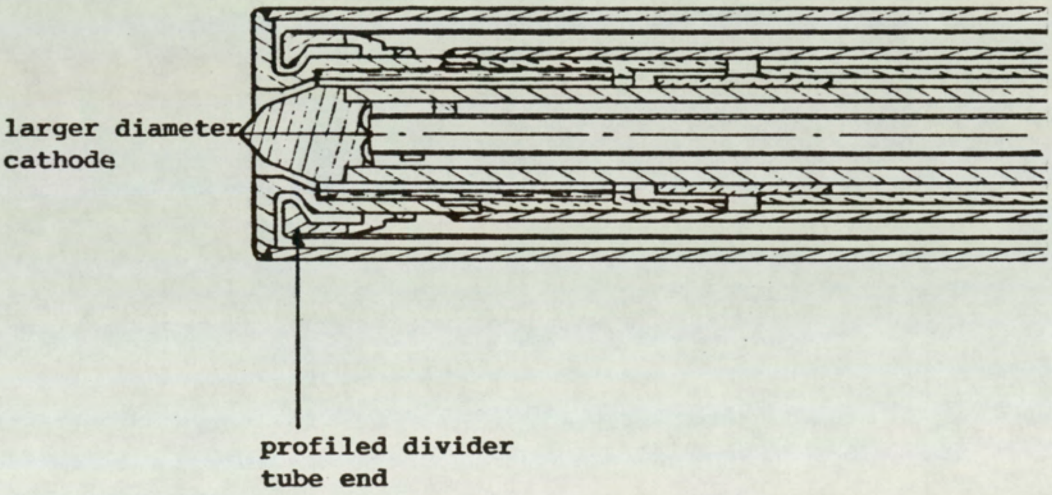

1986 TORCH DESIGN

Figure 35 The plasma torch design

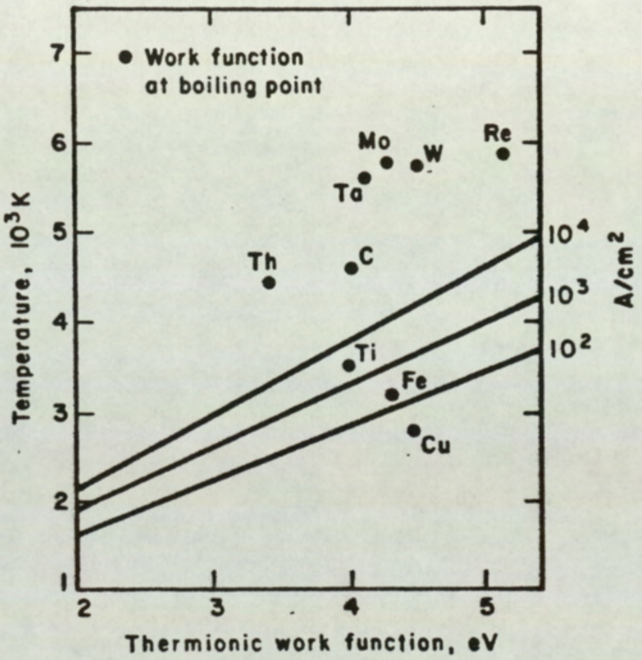

Figure 36 Thermionic work function of cathode materials

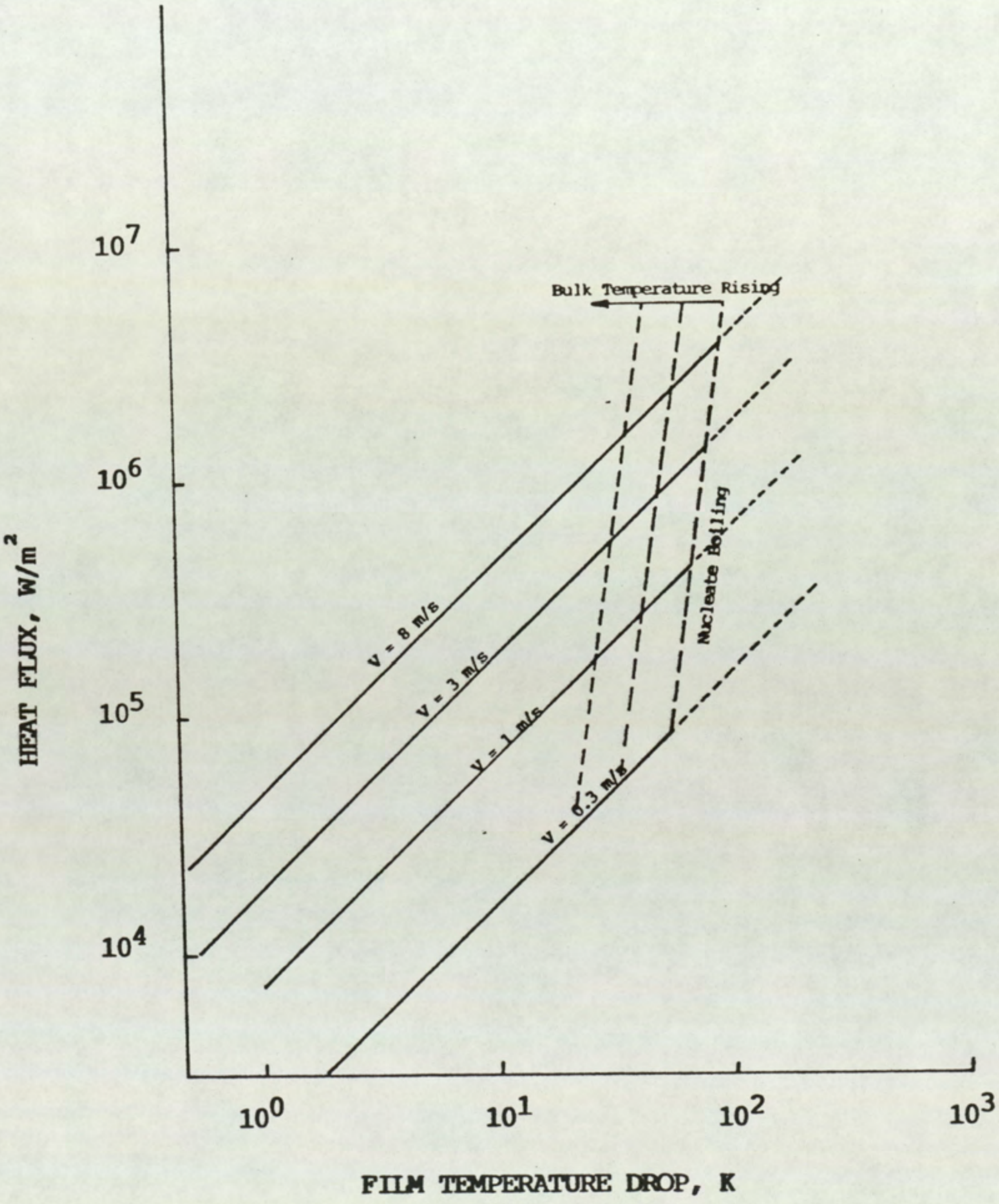

Figure 37 Limits of forced convection cooling

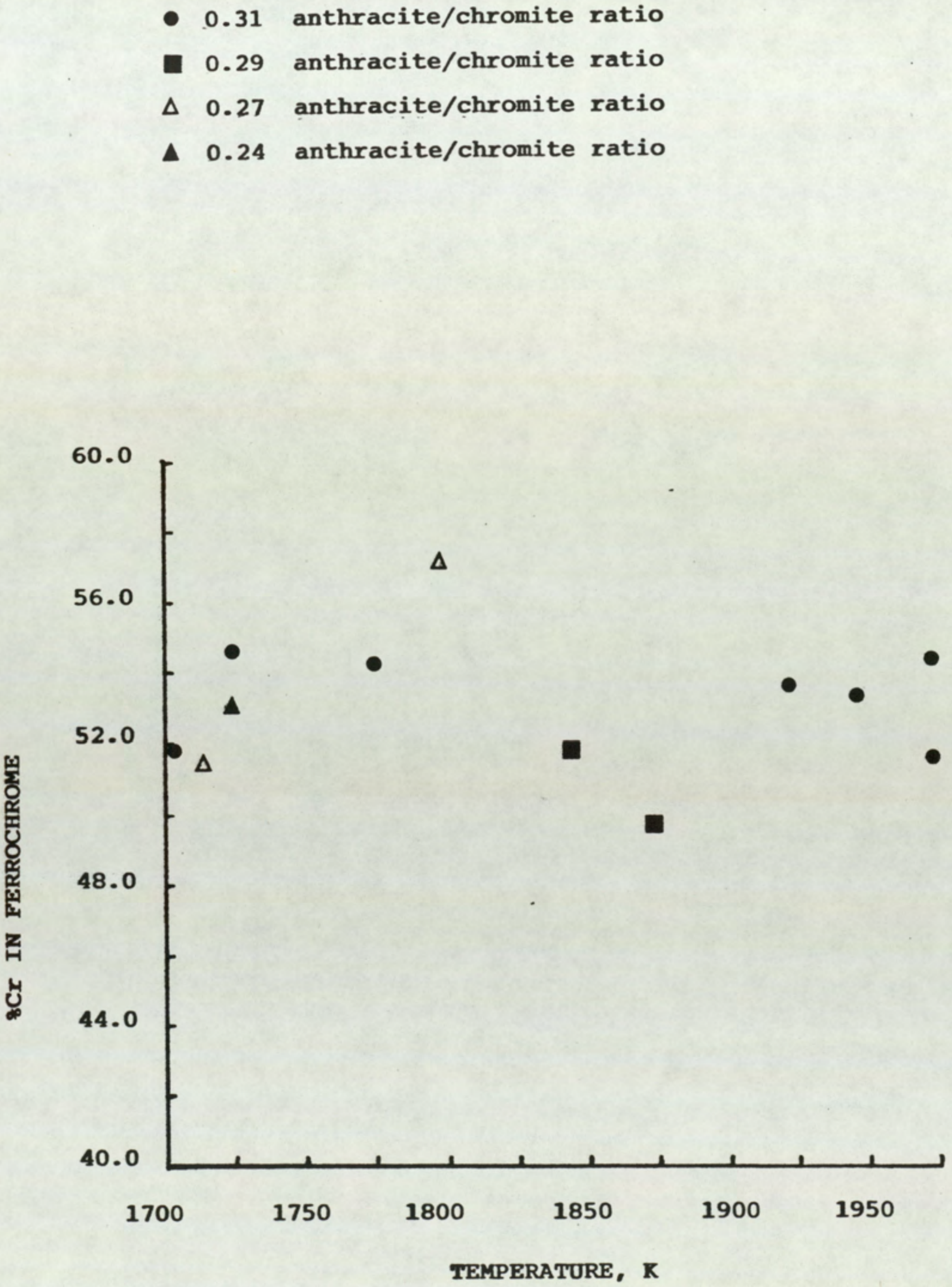

Figure 38 %Cr in ferrochrome v tapping temperature and anthracite/chromite ratio (BSC analyses)

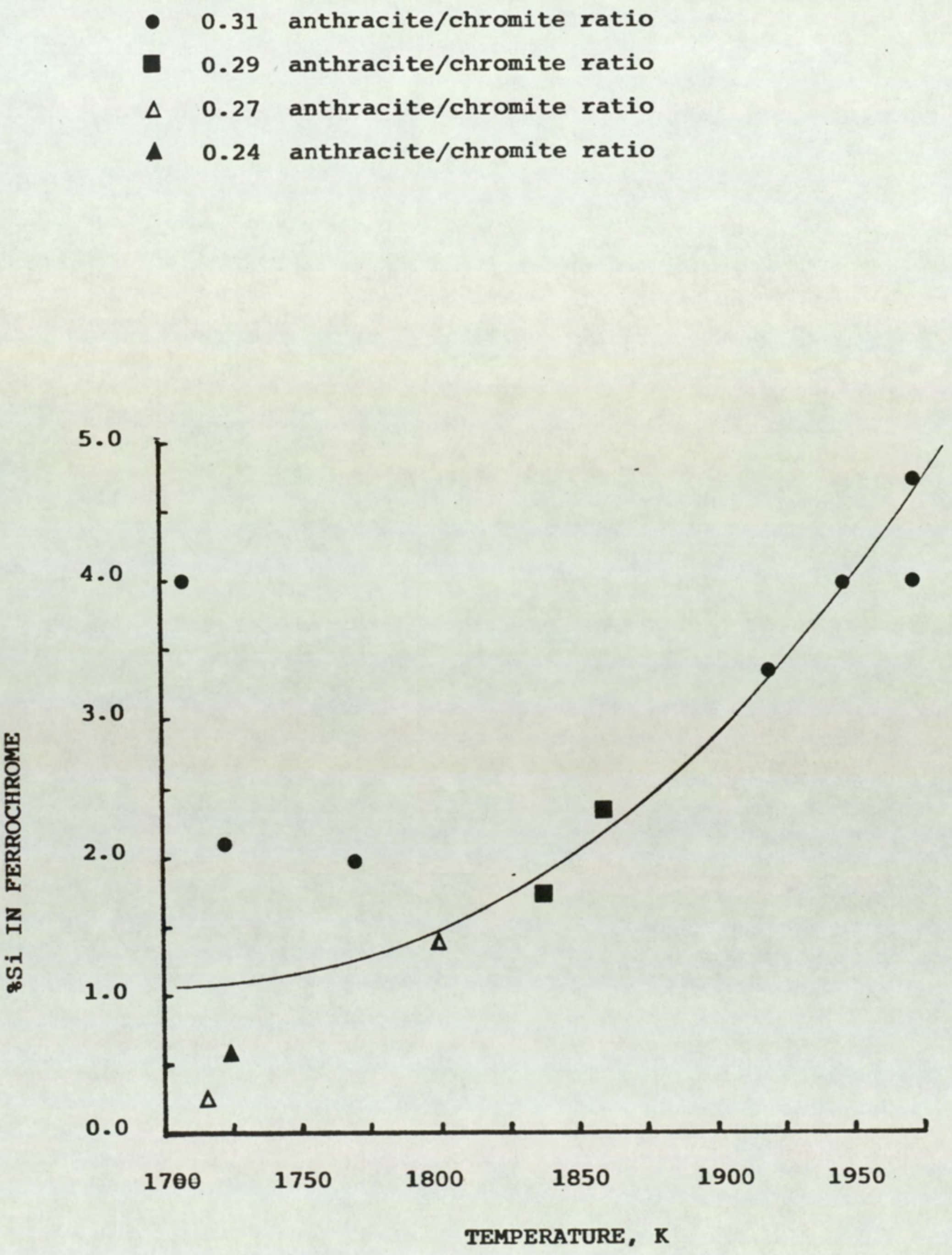

Figure 39 %Si in ferrochrome v tapping temperature and anthracite/chromite ratio (BSC analyses)

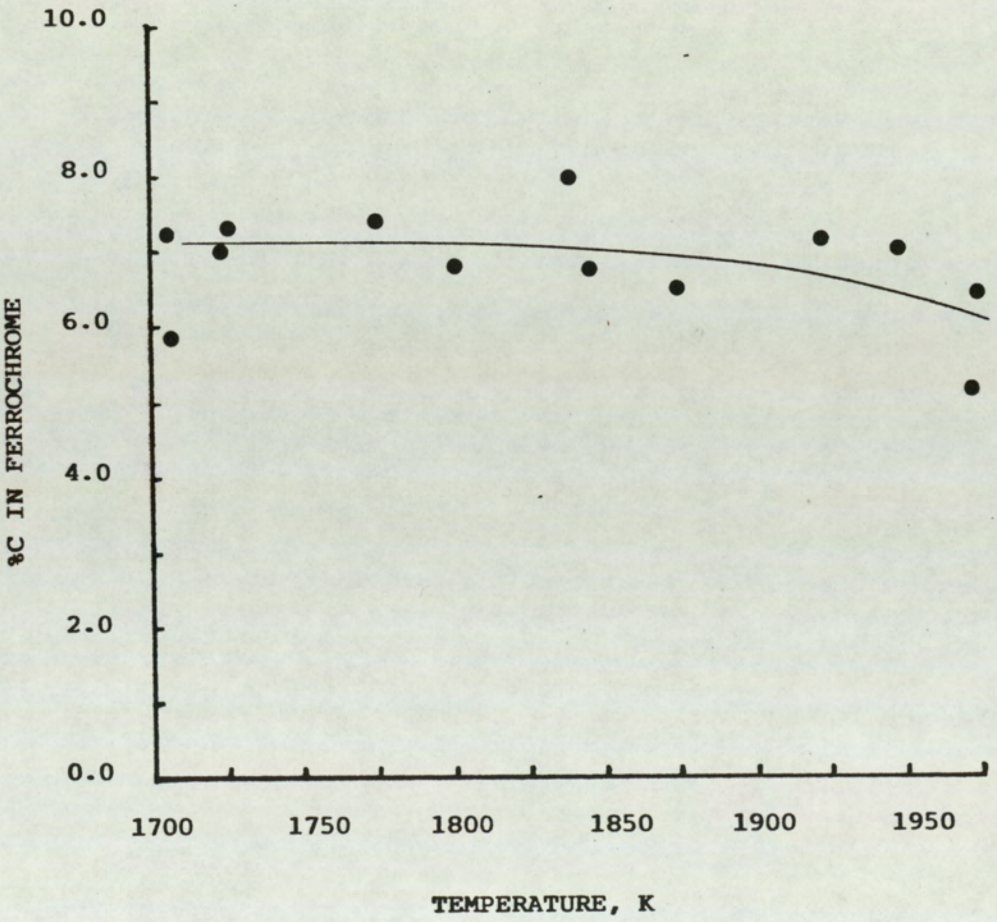

Figure 40 %C in ferrochrome V tapping temperature (BSC analyses)

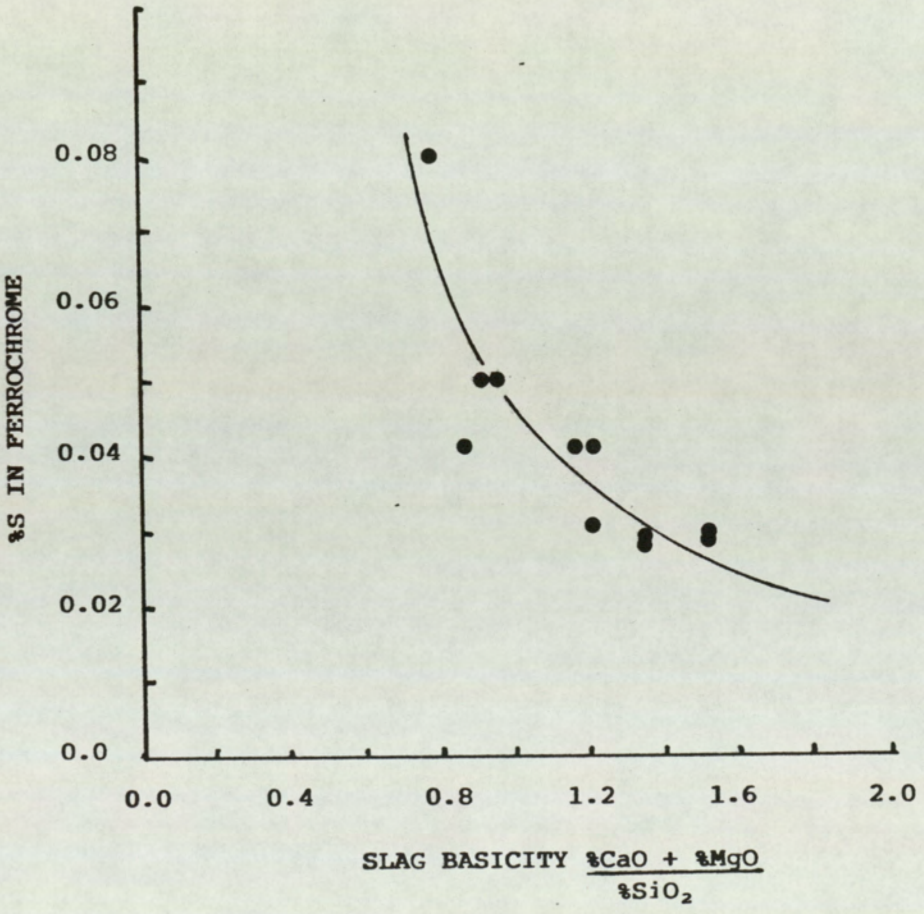

Figure 41 %S in ferrochrome v slag basicity

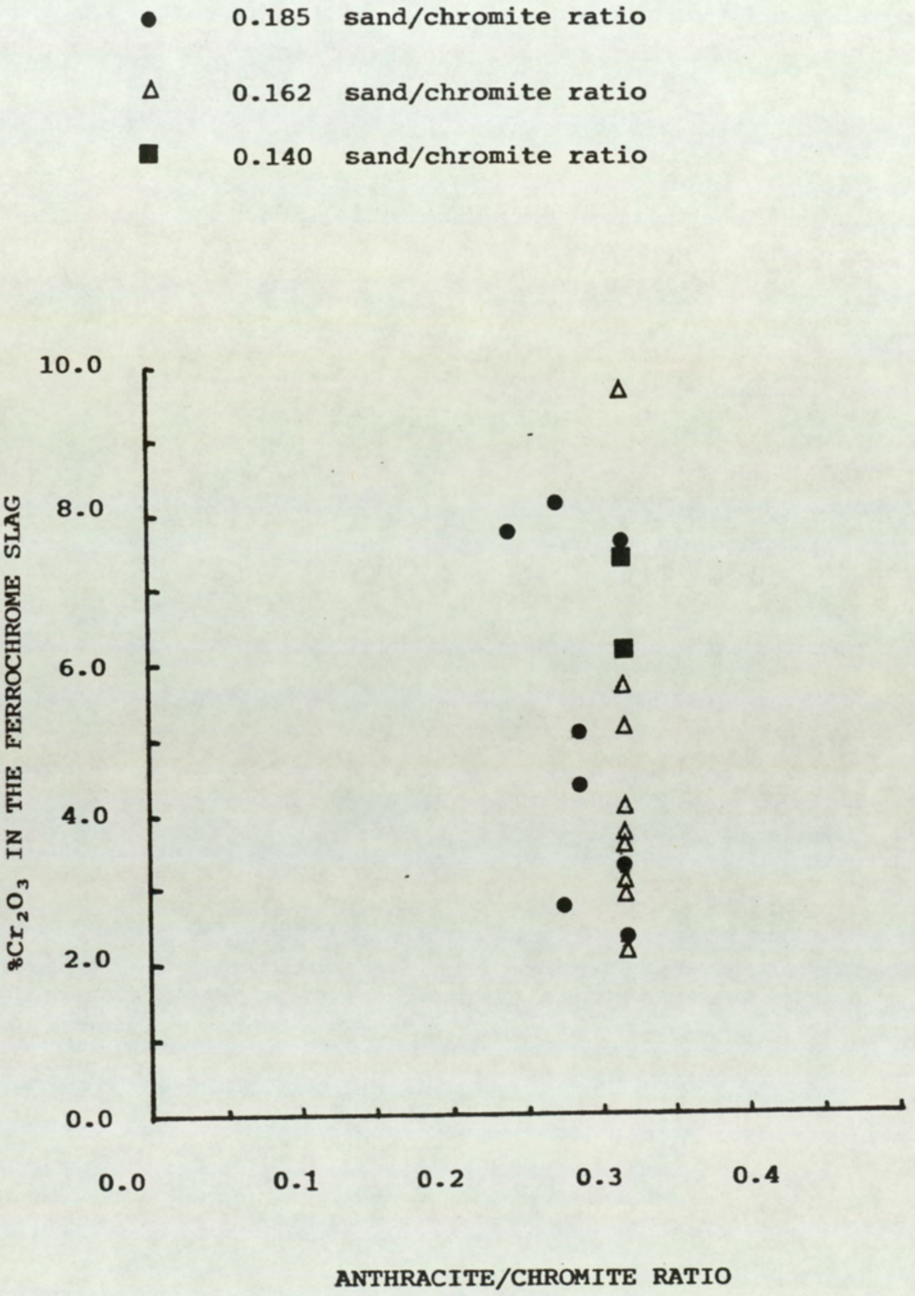

Figure 42 %Cr_2O_3 in the slag v anthracite/chromite ratio and sand/chromite ratio

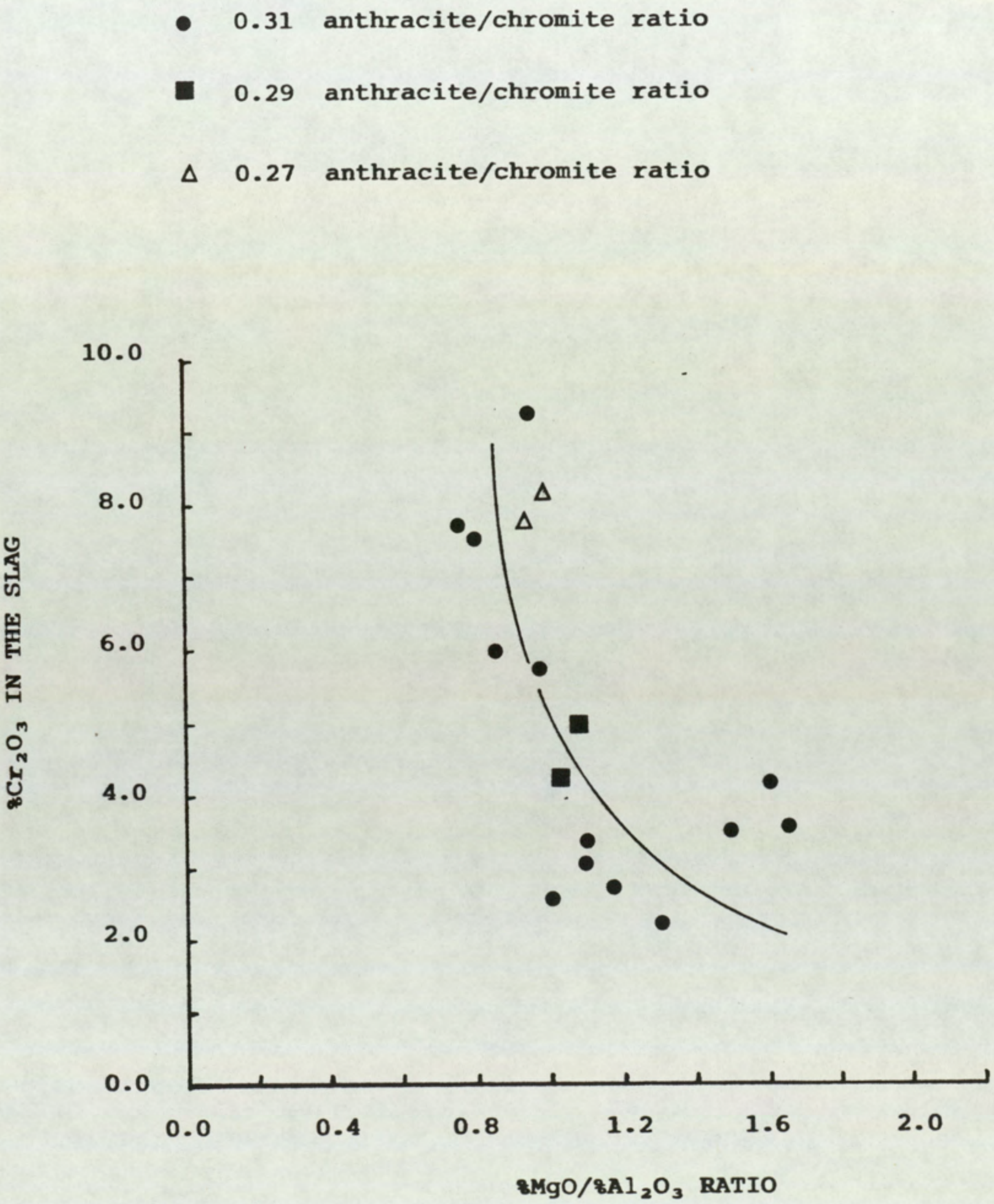

Figure 43 $\%Cr_2O_3$ in the slag v $\%MgO/\%Al_2O_3$

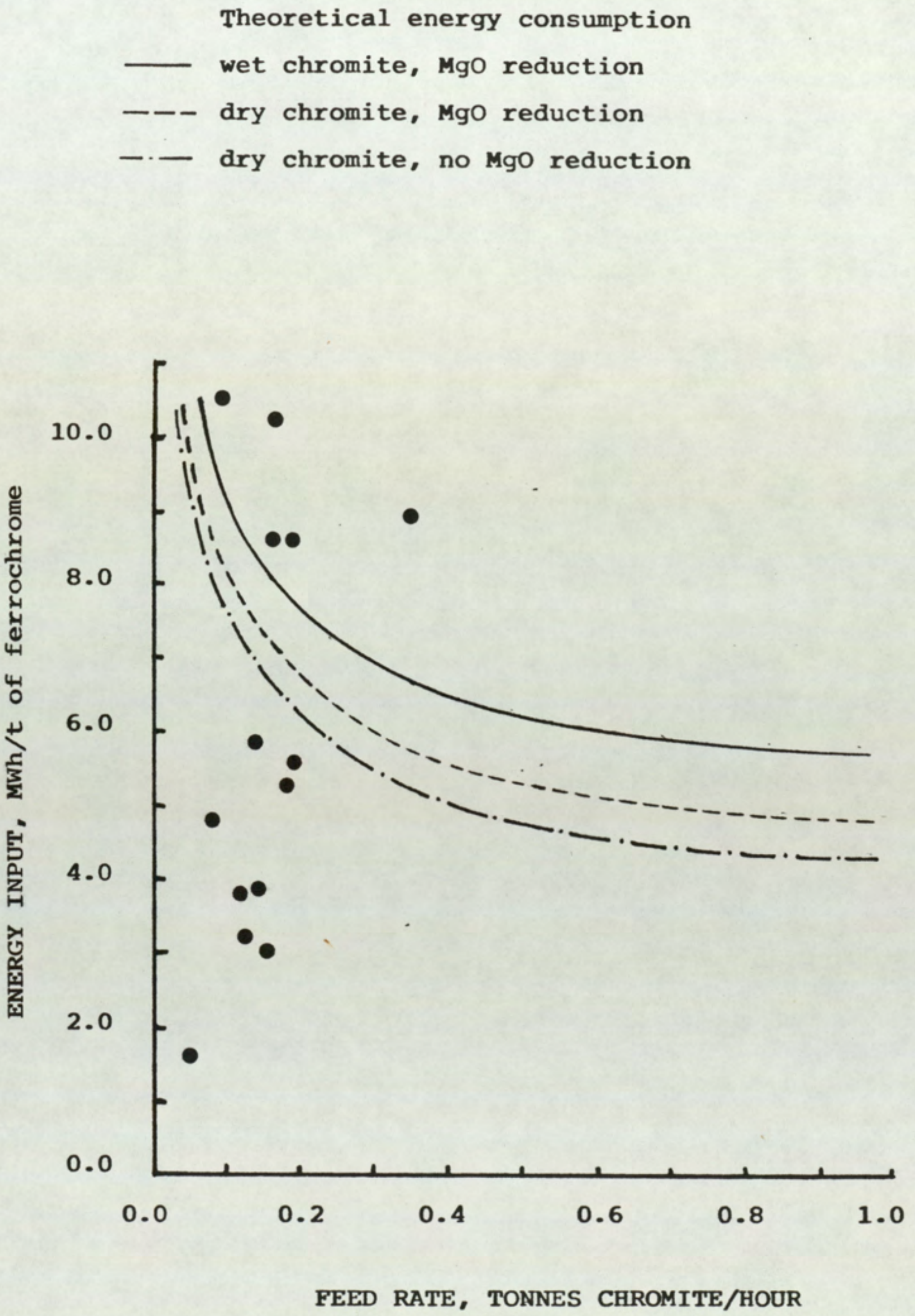

Figure 44 Energy input rate for chromite smelting v chromite feed rate

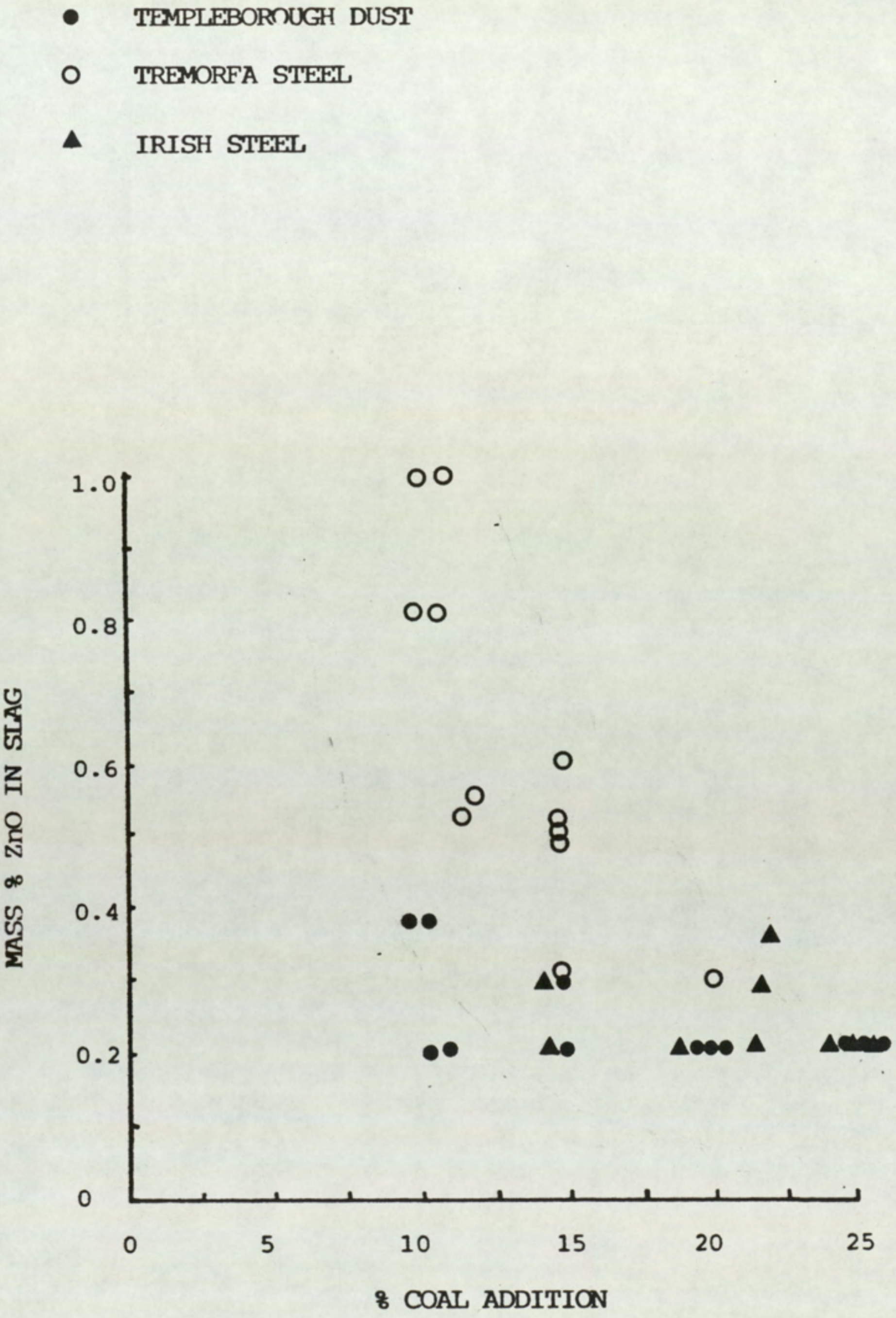

Figure 45 The effect of coal addition rate on %ZnO in the slag

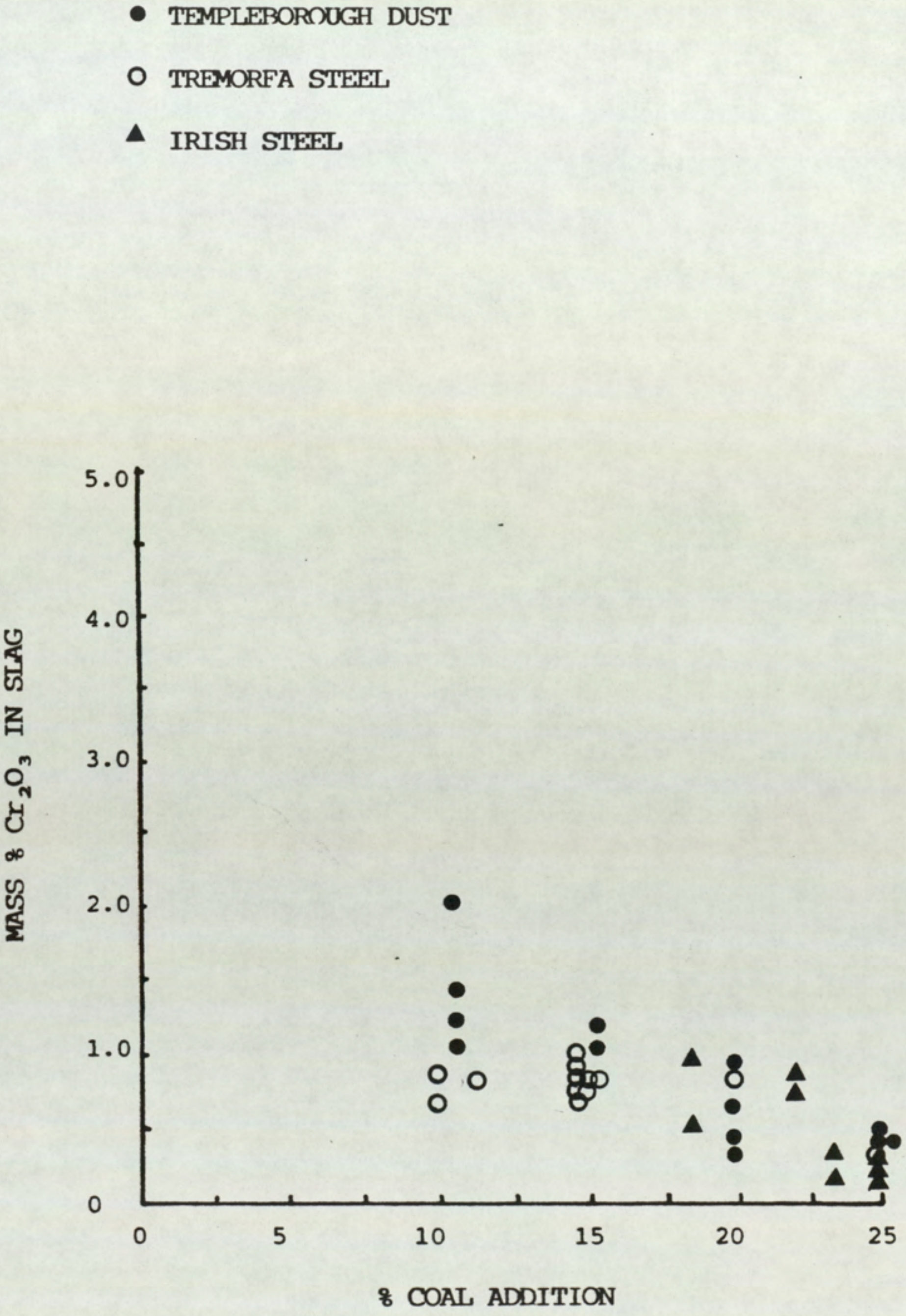

Figure 46 The effect of coal addition rate on the Cr_2O_3 in the slag

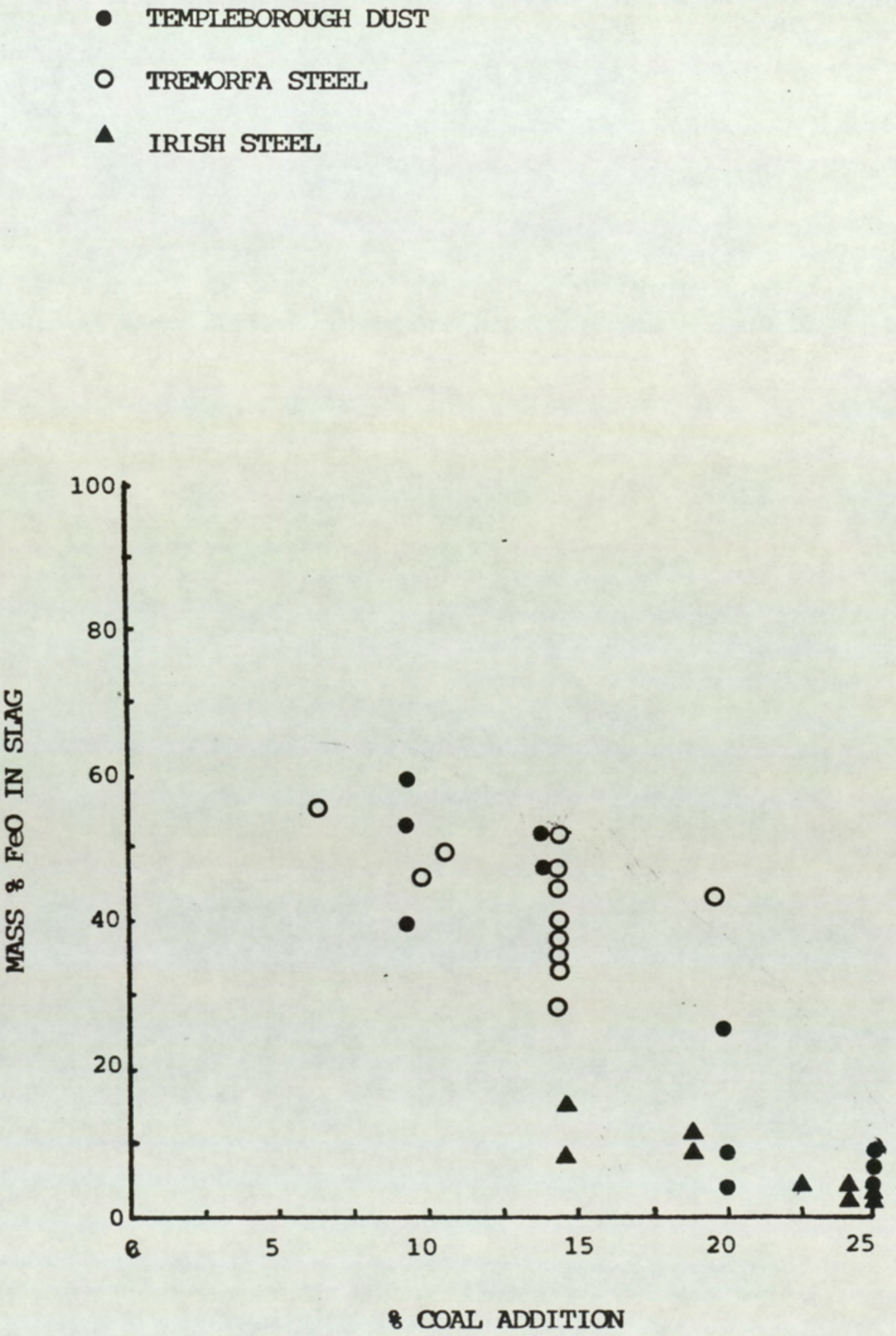

Figure 47 The effect of coal addition rate on FeO in the slag

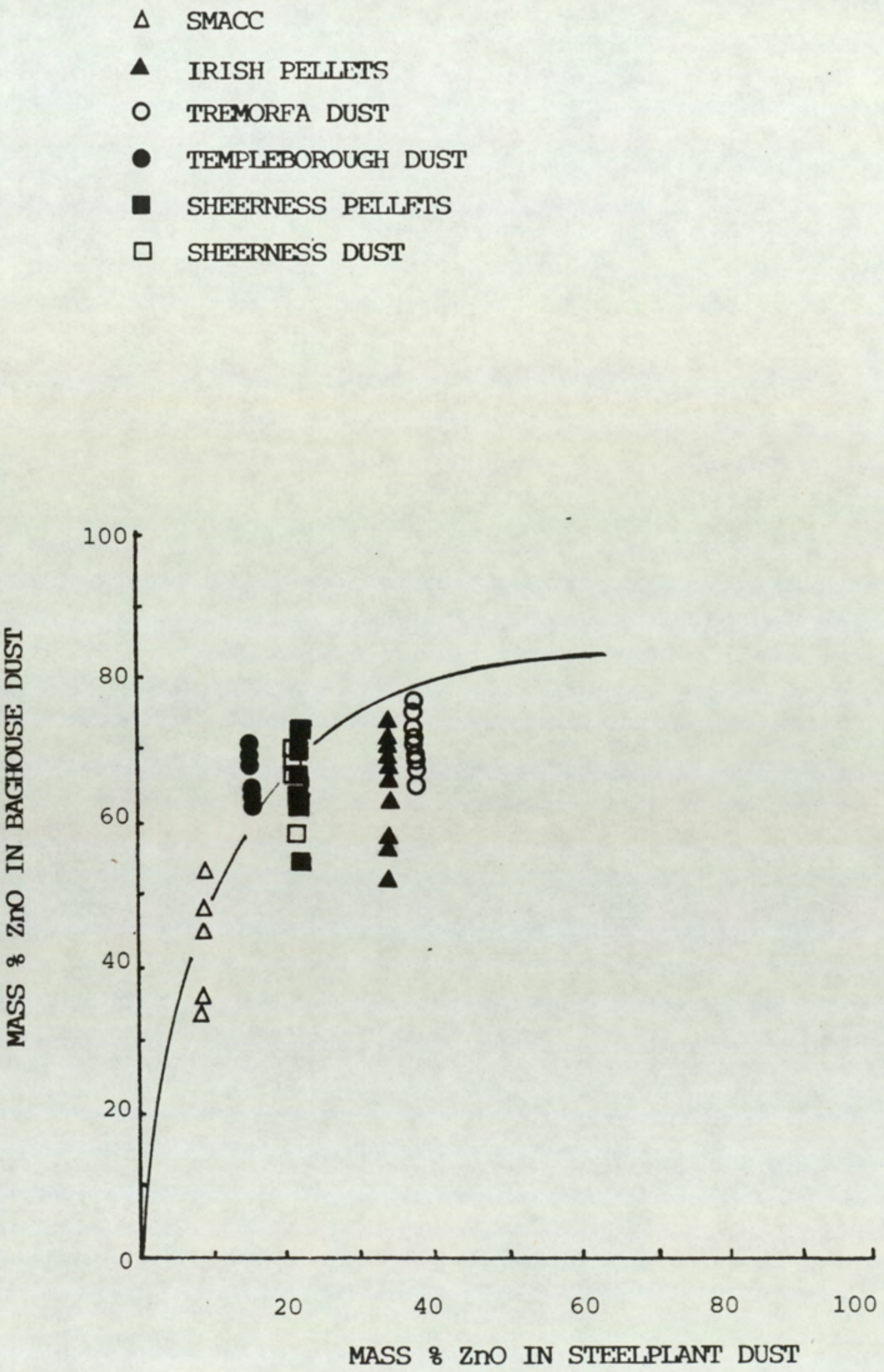

Figure 48 The effect of ZnO in the steelplant dust on ZnO in the baghouse dust

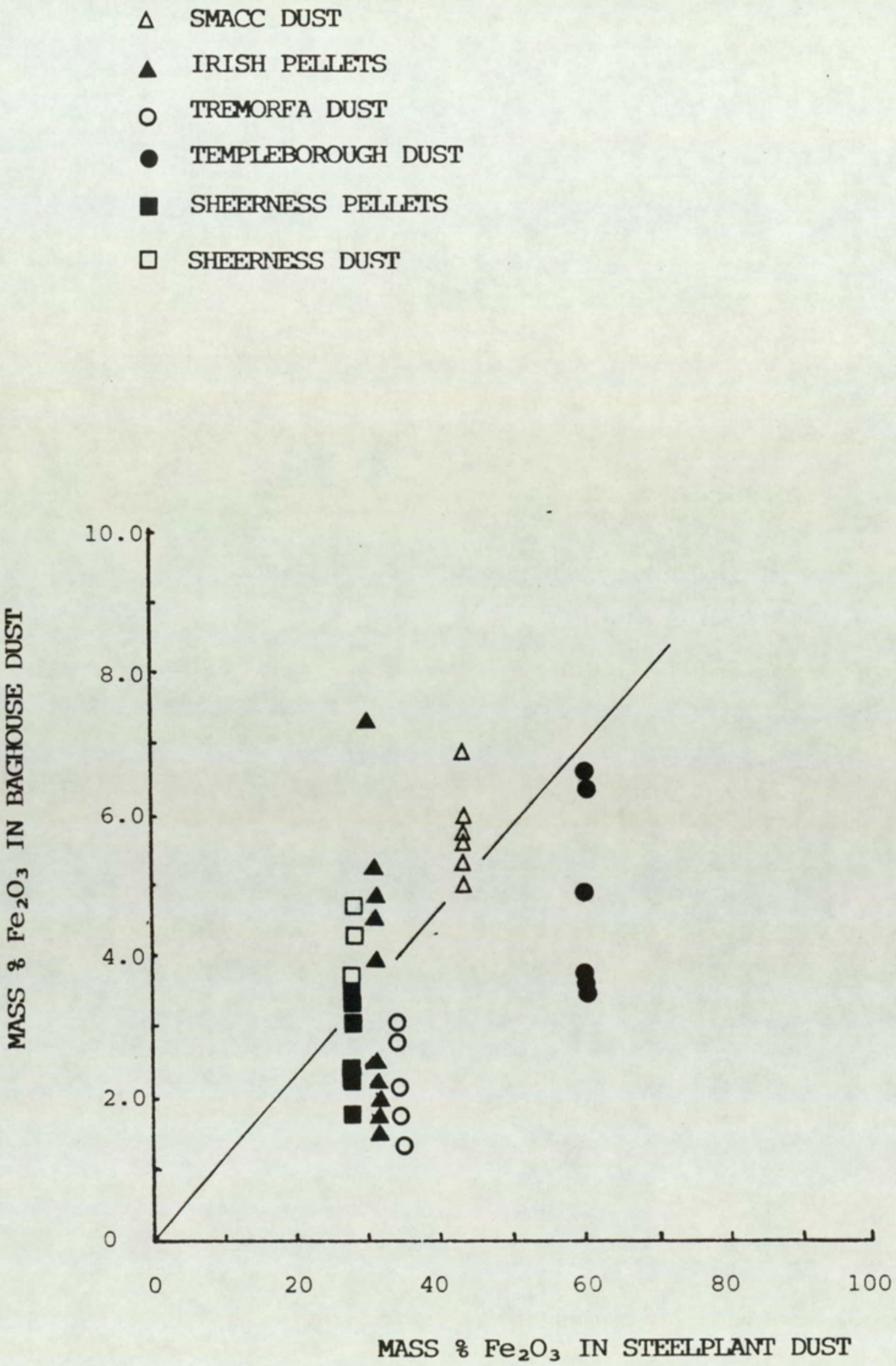

Figure 49 The effect of %Fe_2O_3 in the steelplant dust on the %Fe_2O_3 in the baghouse dust

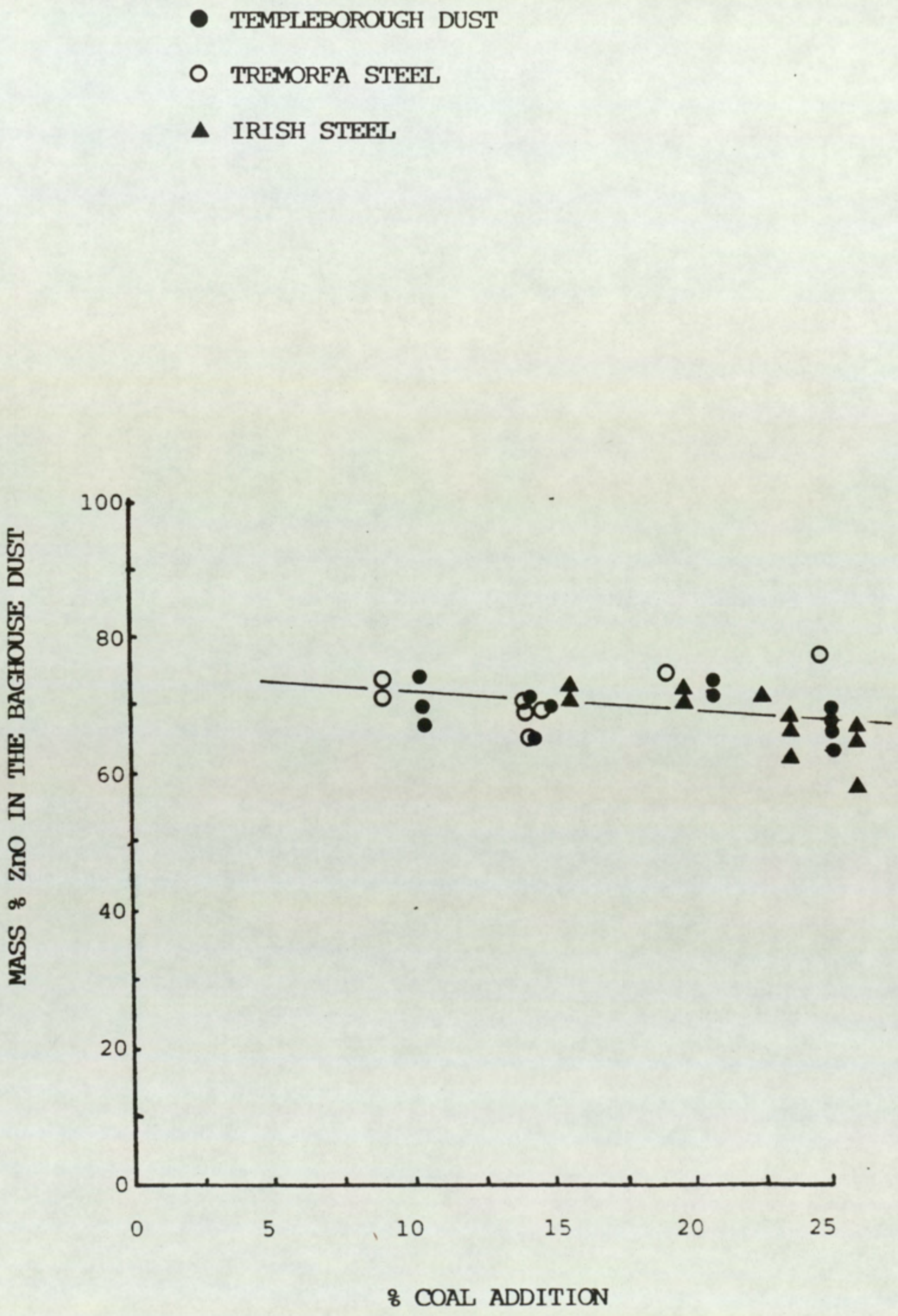

Figure 50 The effect of coal addition rate on the the %ZnO in the baghouse dust

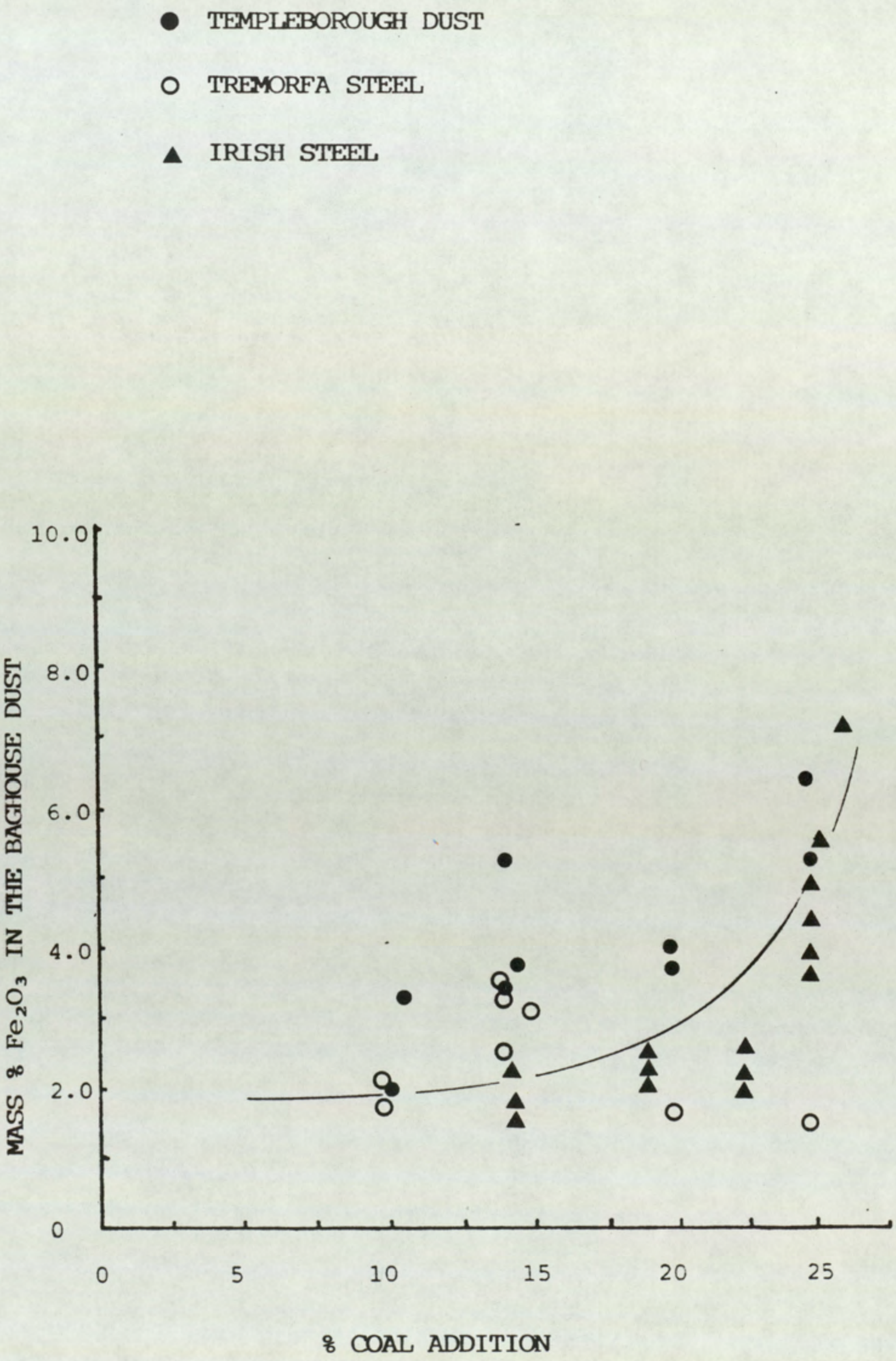

Figure 51 The effect of coal addition rate on the %Fe_2O_3 in the baghouse dust

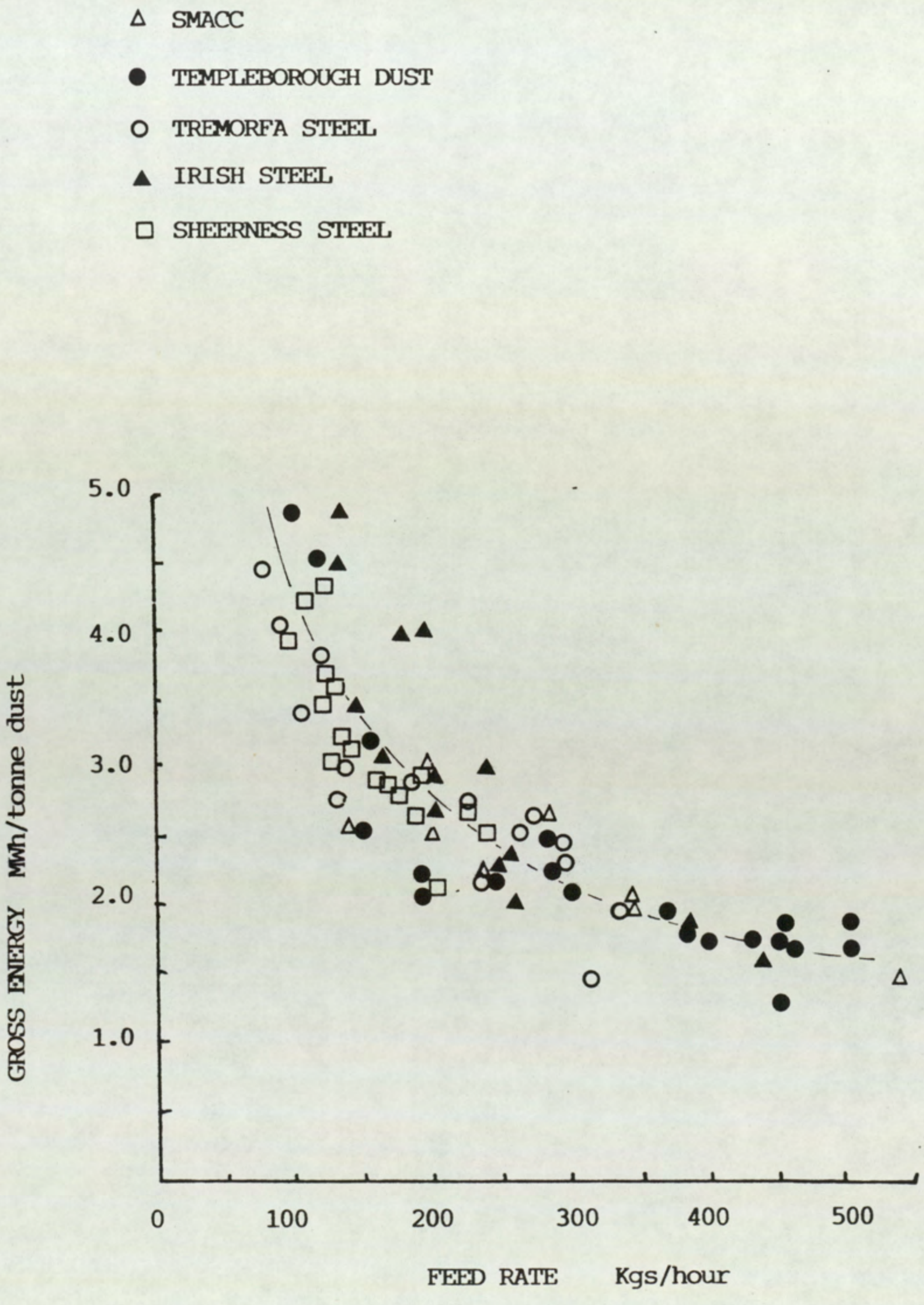

Figure 52 The effect of feed rate on gross energy consumption

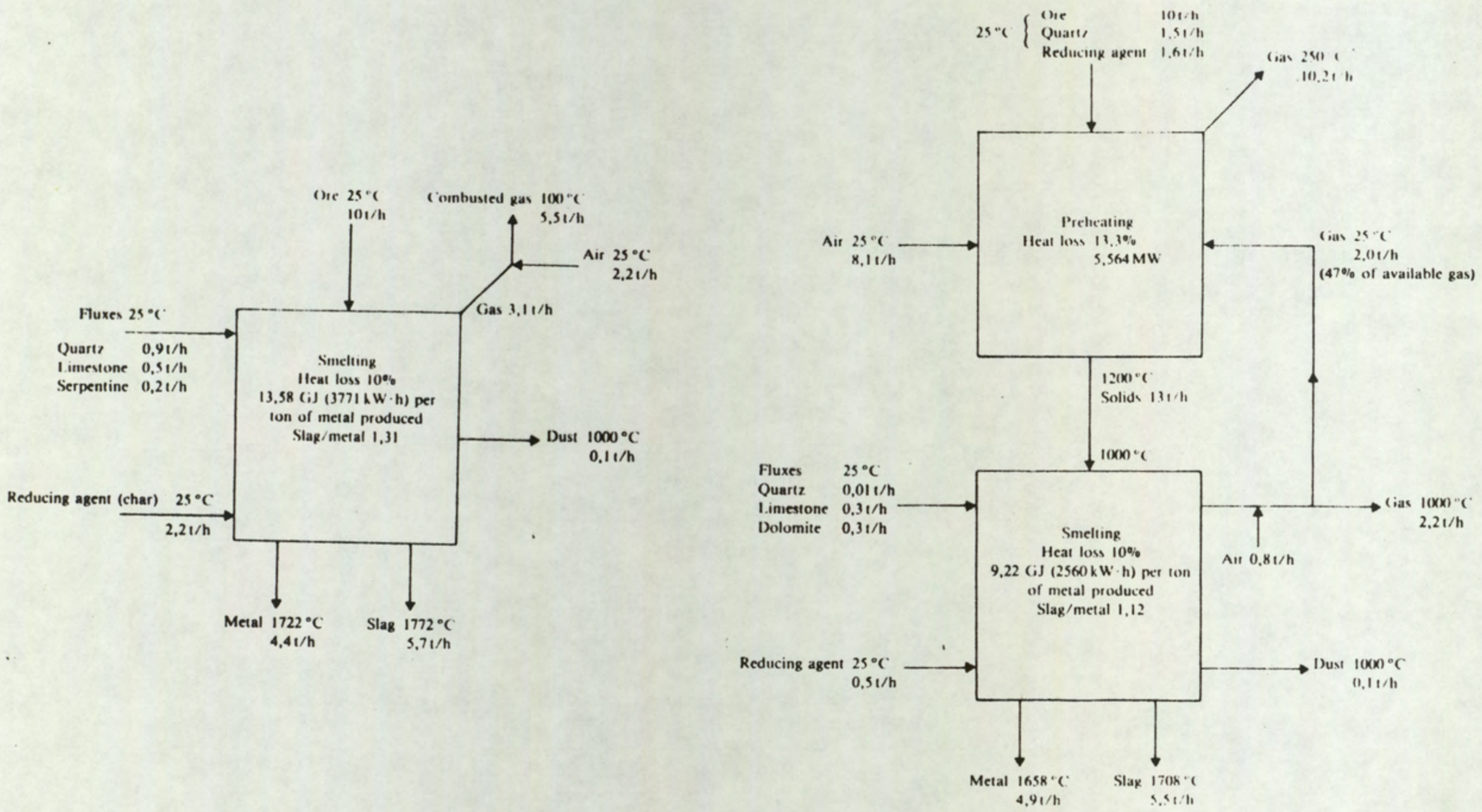

CONVENTIONAL SUBMERGED ARC FURNACE SMELTING

OUTUKUMPU OY SUBMERGED ARC FURNACE SMELTING

Figure 53 A comparison of chromite smelting process routes

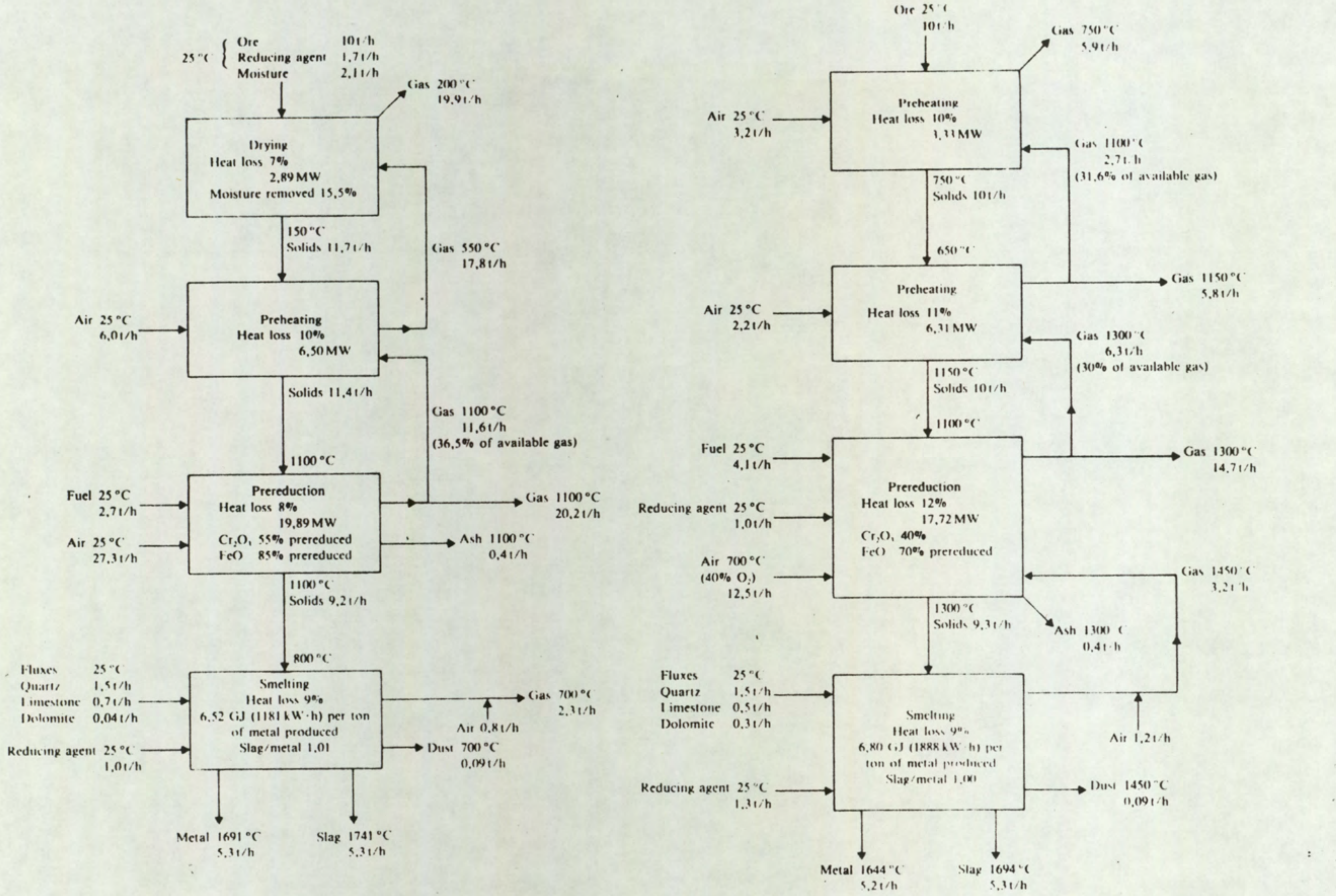

SHOWA DENKO PROCESS ROUTE

PREHEATING/PREREDUCTION/PLASMA SMELTING ROUTE

Figure 54 A comparison of chromite smelting process routes

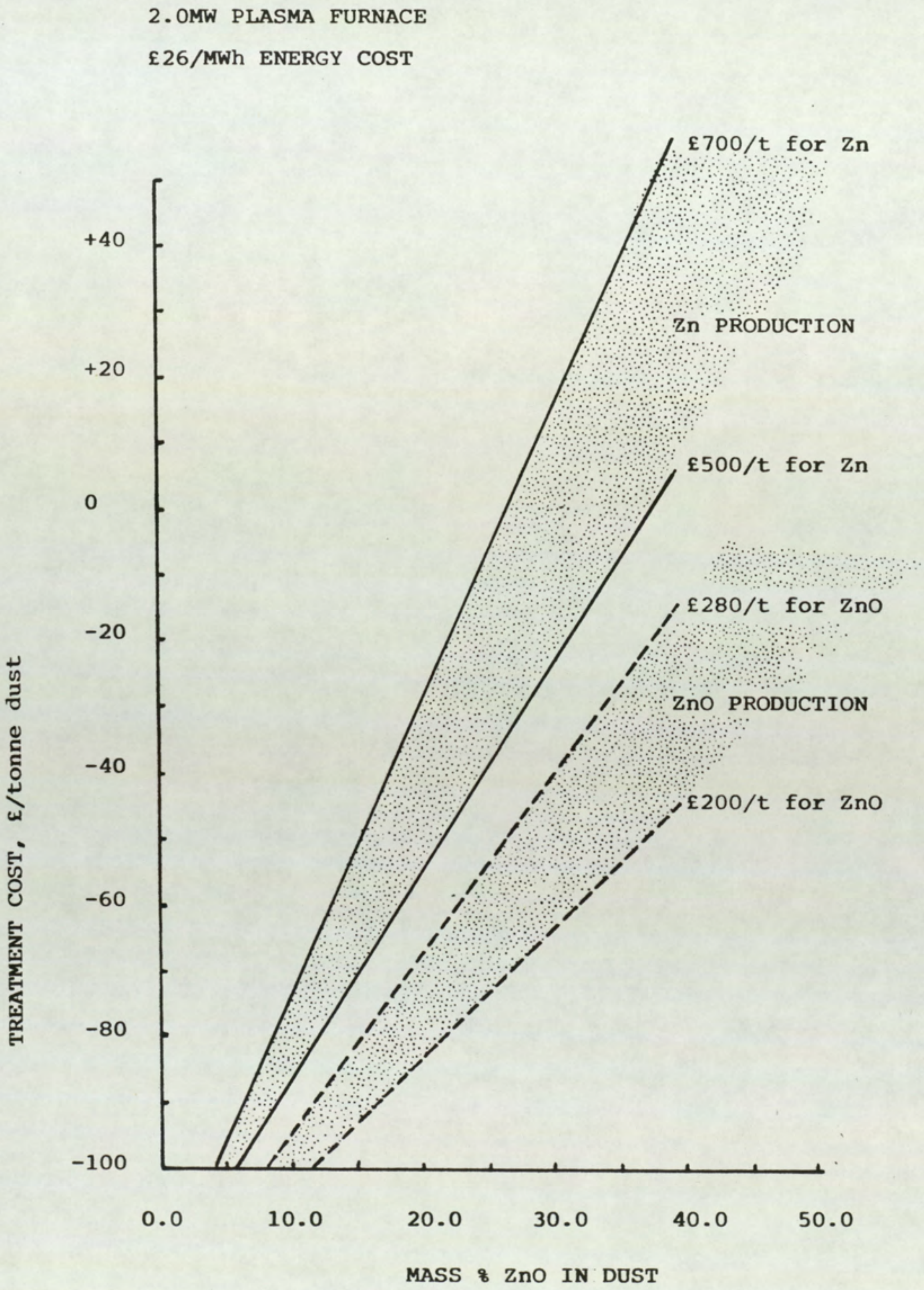

Figure 55 The effect of EAF dust composition on treatment costs for ZnO and Zn products

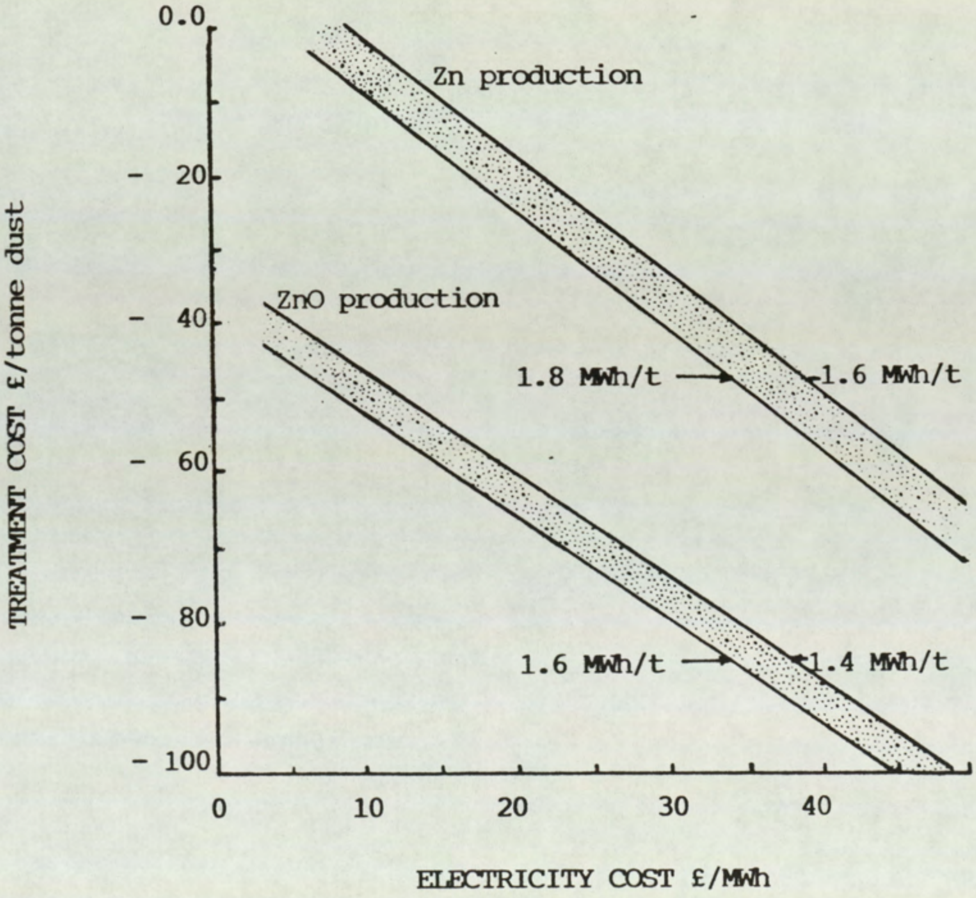

Figure 56 The effect of energy cost on EAF dust treatment costs

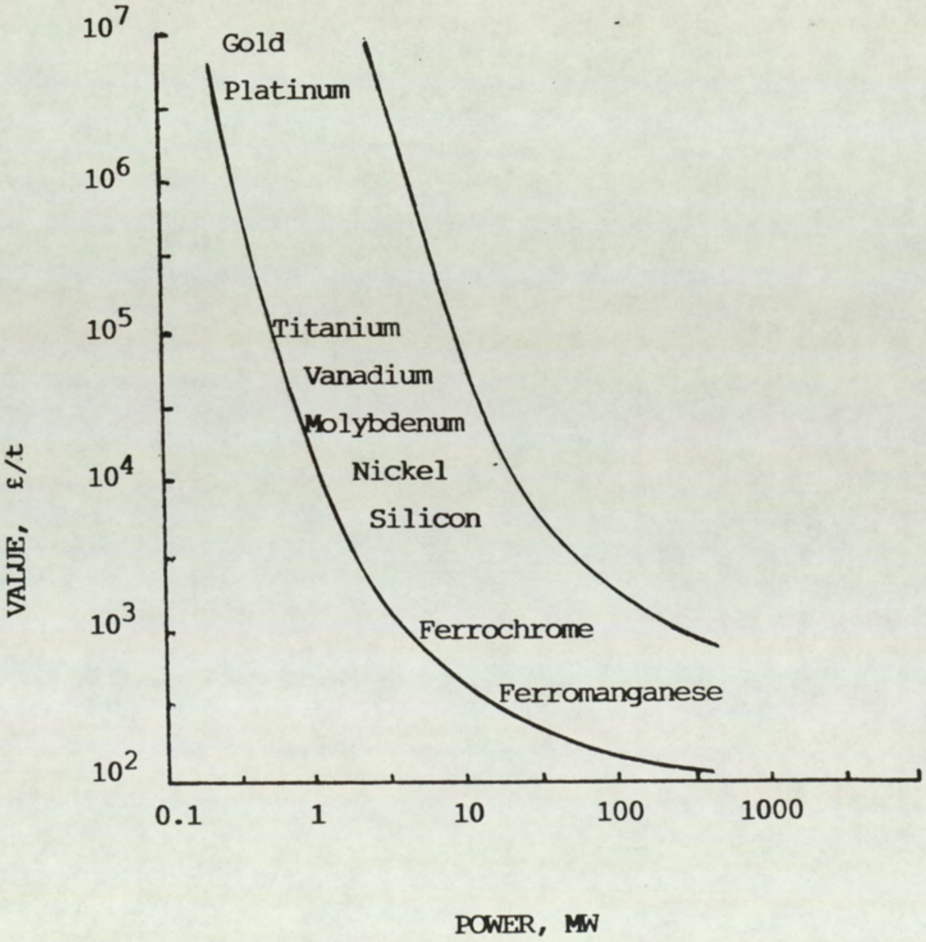

Figure 57 The relationship between power requirements and the approximate value of the materials being processed